Scientific Excellence • Resource Protection & Conservation • Benefits for Canadians
Excellence scientifique • Protection et conservation des ressources • Bénéfices aux Canadiens

Analysis of Physical Oceanographic Data from the Labrador Shelf, Summer 1980

D.B. Fissel and D.D. Lemon

Published by:

Physical and Chemical Sciences Branch
Scotia-Fundy Region
Department of Fisheries and Oceans

Bedford Institute of Oceanography
P.O. Box 1006
Dartmouth, Nova Scotia
Canada B2Y 4A2

1991

Canadian Contractor Report of Hydrography and Ocean Sciences No. 39

Fisheries and Oceans Pêches et Océans

Canada

Canadian Contractor Report of

Hydrography and Ocean Sciences No. 39

March 1991

ANALYSIS OF PHYSICAL OCEANOGRAPHIC DATA FROM THE LABRADOR SHELF, SUMMER 1980

by

D.B. Fissel[1] and D.D. Lemon[2]

Physical and Chemical Sciences
Scotia-Fundy Region
Department of Fisheries and Oceans

Bedford Institute of Oceanography
P.O. Box 1006
Dartmouth, Nova Scotia
Canada B2Y 4A2

[1] Arctic Sciences Ltd.
201 Brownlow Avenue, Suite 59
Dartmouth, Nova Scotia
Canada B3B 1W2

[2] Arctic Sciences Ltd.
1986 Mills Road, R.R. #2
Sidney, British Columbia
Canada V8L 3S1

ACKNOWLEDGEMENTS

The authors would like to thank Dr. J.R. Buckley, formerly of Petro-Canada, who directed all phases of this study. In regard to the data analysis, many discussions with Dr. Buckley were helpful in formulating the analysis approach and in interpreting the results. We also thank Ms. J. Bobbitt, formerly with Nordco Ltd., and Drs. J. Lazier and B. Petrie of the Bedford Institute of Oceanography and Dr. J. Warner of Martec Ltd., for helpful discussions.

Arctic Sciences Ltd. personnel who contributed to this report are: S. Oberski, R. Chave and E.C. Luscombe for computer programming; B. Clarke for preparing the many figures; R. Birch for reviewing a draft version of this report and S. Norton and F. Welsman for word processing.

Publication of this report in the Canadian Report of Hydrography and Ocean Sciences Series was made possible by the support of Dr. S. Prinsenberg of the Bedford Institute of Oceanography. This project was prepared under contract to the Department of Fisheries and Oceans for the sea-ice program at the Bedford Institute of Oceanography, funded by the Federal Panel of Energy Research and Development.

This project was funded by Petro-Canada as part of the Offshore Labrador Biological Studies (OLABS) Program. The program studies were developed by the OLABS Management Committee which is chaired by the Canadian Oil & Gas Lands Administration (COGLA), formerly the Resource Management Branch, Energy Mines & Resources. Other members of the management committee include the Department of Environment, the Department of Fisheries and Oceans of the federal government; the Department of Environment of the Newfoundland provincial government; the Labrador Resources Advisory Council, representing the people of Labrador; and the petroleum industry.

Total Eastcan was operator for the Labrador Group of Companies in 1978 and 1979, and Petro-Canada was the operator in 1980 and 1981. The petroleum industry financed all studies during the course of the program, and the two companies representing the industry managed the study projects. The following companies financed the OLABS Program: AGIP Canada Ltd.; Amerada Minerals Corporation of Canada Ltd.; BP Exploration Canada Ltd.; Canterra Energy Ltd.; Chevron Canada Ltd.; Esso Resources Canada Ltd.; Gulf Canada Resources Inc.; Hudson's Bay Oil & Gas Company Ltd.; Petro-Canada Exploration Inc.; Ranchmen's Resources (1976) Ltd.; Suncor Inc.; Texaco Canada Resources Ltd.; Total Petroleum (North America) Ltd. A complete list of studies conducted under the OLABS Program is available from COGLA: Canadian Oil & Gas Lands Administration, Environmental Protection Branch, Place Vanier, Tower B, 14th Floor, 355 River Road, Ottawa, Ontario, K1A 0E4

Cat. No. Fs97-17/39E ISSN 0711-6748

Correct citation for this publication:

Fissel, D. B. and D. D. Lemon. 1991. Analysis of physical oceanographic data from the Labrador Shelf, summer 1980. Can. Contract. Rep. Hydrogr. Ocean Sci. 39: xviii + 136 pp

TABLE OF CONTENTS

ABSTRACT

Fissel, D. B. and D. D. Lemon. 1991. Analysis of physical oceanographic data from the Labrador Shelf, summer 1980. Can. Contract. Rep. Hydrogr. Ocean Sci. 39: xviii + 136 pp

An extensive, physical oceanographic survey was conducted over the Labrador continental shelf and slope in the summer of 1980. Time series measurements of subsurface currents were obtained simultaneously from 29 Aanderaa RCM-4 and 2 Neil Brown ACM-2 current meters. A pattern of CTD stations was occupied four times during the course of the summer and early autumn.

In this report, the results of three types of time series analysis methods applied to the current meter data are presented. These are: spectral analysis, harmonic (or tidal) analysis and digital filtering. The analysis of the CTD data involved the preparation of vertical and horizontal sections of various water properties and the computation of geostrophic flow fields.

The regional circulation consisted of the two southeastward- flowing cores of the Labrador Current, with the stronger one following the edge of the continental shelf and the other, slightly weaker, located over the seaward half of the marginal trough. Near-surface speeds in the main core averaged 30 to 40 cm/s, with peak speeds near 80 cm/s, while in the inner core, the average was 15 to 20 cm/s with peaks near 50 cm/s. The two cores were separated by a zone of more variable, but not less energetic, currents.

The main core of the Labrador Current is in approximate geostrophic balance and forms the boundary between the relatively warm, saline water of the Labrador Sea and the relatively cold, fresh Shelf Water which occupies the majority of the water column over the shelf and marginal trough. The water in the main current core itself is a mixture of Shelf Water and Labrador Sea Water called Slope Water. Slope Water is also found in the saddles and at the bottom of the marginal trough.

Large variations occurred in the currents at low frequencies (periods of 4 to 7 days or greater). Over the continental slope, marginal trough and the saddles between banks, the largest low frequency variations tended to occur at periods ranging from 7 to 30 days but variations also occurred with periods of 4 to 7 days. Over the banks, the low frequency variations were dominated by clockwise oscillations having periods of 4 to 7 days. The horizontal scale of spatial variability of the currents was less than the minimum spacing between current meter moorings of 35 to 40 km.

Meanders were observed at the shelf break in the main current core and in Cartwright Saddle. These events, with periods of 4 to 7 days, were characterized by an increase in current speed, followed by an increase in temperature and salinity. Such meanders could form warm-cored eddies spun off the inner edge of the main core of the Labrador Current, providing a possible mechanism for transporting Slope Water into the saddles and eventually into the marginal trough.

RÉSUMÉ

Fissel, D. B. and D. D. Lemon. 1991. Analysis of physical oceanographic data from the Labrador Shelf, summer 1980. Can. Contract. Rep. Hydrogr. Ocean Sci. 39: xviii + 136 pp

Au cours de l'été 1980, un vaste levé océanographique a été effectué en vue de l'étude des conditions physiques au-dessus de la plate-forme et de la pente continentale du Labrador. Des mesures de série chronologique des courants de subsurface ont été déterminées silmultanément à partir de 29 courantomètres RCM-4 Aanderaa et de 2 courantomètres ACM-2 Neil Brown. Un réseau de stations CTD a été occupé quatre fois pendant l'été et au début de l'automne.

Le présent rapport fait état des résultats de trois types de méthodes d'analyse de séries chronologiques appliquées aux données courantométriques. Il s'agit des méthodes suivantes : analyse spectrale, analyse harmonique de la marée et filtrage numérique. L'analyse des données CTD a nécessité la préparation de coupes verticales et horizontales pour diverses propriétés de l'eau et le calcul de champs de courants géostrophiques.

La circulation régionale était produite par les deux noyaux du courant du Labrador s'écoulant vers le sud-est, le plus fort des deux siuvant le rebord de la plate-forme continentale, tandis que l'autre, légèrement plus faible, était situé au-dessus de la moitié côté mer de la cuvette marginale. Dans le noyau principal, les vitesses épipélagiques s'établissaient en moyenne à 30 ou 40 cm/s, avec des vitesses de pointe atteignant près de 80 cm/s, pendant que dans le noyau intérieur, la moyenne était de 15 à 20 cm/s avec des pointes de près de 50 cm/s. Les deux noyaux étaient séparés par une zone de courants plus variables, mais non moins énergétiques.

Le noyau principal du courant du Labrador se trouve à peu près en équilibre géostrophique et forme la limite entre les eaux relativement chaudes et salines de la mer du Labrador, d'une part, et les eaux relativement froides et douces de la plate-forme qui occupent d'ailleurs la majeure partie de la colonne d'eau au-dessus de la plate-forme et de la cuvette marginale, d'autre part. Les eaux du noyau du courant principal sont elles-mêmes un mélange d'eau de la plate-forme et d'eau de la mer du Labrador, mélange appelé *eau de pente*. On trouve aussi de l'eau de pente dans les cols et au fond de la cuvette marginale.

De grandes variations se sont produites dans les courants à basses fréquences (périodes de 4 à 7 jours ou plus). Au-dessus de la pente continentale, de la cuvette marginale et des cols entre les bancs, les plus fortes variations de basse fréquence avaient tendance à se produire siuvant des périodes oscillant entre 7 et 30 jours, mais des variations se sont aussi produites dont les périodes se situaient entre 4 et 7 jours. Au-dessus des bancs, les variations de basse fréquence ont été dominées par des oscillations dans le sens des aiguilles d'une montre dont les périodes étaient aussi de 4 à 7 jours. L'échelle horizontale de variabilité spatiale des courants était inférieure à l'espacement minimal entre les ancrages de courantomètres, soit de 35 à 40 km.

Des méandres ont été observés à la rupture de la plate-forme dans le noyau principal du courant ainsi que dans le col Cartwright. Ces phénomènes, ayant des périodes de 4 à 7 jours, étaient caractérisés par une hausse de la vitesse du courant et s'accompagnaient d'une hausse de température et de salinité. De tels méandres pourraient former des remous à noyau chaud à partir de la bordure intérieure du noyau principal du courant du Labrador, fournissant ainsi un mécanisme possible pour le transport de l'eau de pente jusque dans les cols et éventuellement dans la cuvette marginale.

PREFACE

This report was originally distributed as a limited edition in November 1982 as part of the Offshore Labrador Biological Studies (OLABS) Program Report Series. The present report has undergone minor revisions.

LIST OF FIGURES

LIST OF FIGURES, cont...

LIST OF FIGURES, cont...

LIST OF FIGURES, cont...

LIST OF FIGURES, cont...

LIST OF FIGURES, cont...

LIST OF FIGURES, cont...

LIST OF FIGURES, cont...

LIST OF TABLES

LIST OF TABLES, cont...

LIST OF TABLES, cont...

1. INTRODUCTION

During the summer of 1980, an extensive physical oceanographic survey was carried out on the Labrador continental shelf and slope. Data were collected by NORDCO Ltd. (NORDCO, 1981) under contract to Petro-Canada, operator for the Labrador group of companies. Figure 1 shows the location of the study area. The measurements, consisting of 11 current meter moorings and 10 lines of CTD stations, covered the length of the Labrador coastline, from just south of Hudson Strait to the entrance of the Strait of Belle Isle. The bulk of the measurements were concentrated in the south-central portion of the shelf, between Makkovik and Hamilton Banks (for place names see Figure 2).

This report contains the results of an analysis of the data set, which was begun after completion of the basic data processing by NORDCO Ltd. (NORDCO, 1981) was complete. A description of the major features of the mean circulation is given, along with a description of the temporal and spatial variability of the flow, and the properties, distribution and movement of the major water masses in the area. Some processes which may be partly responsible for the observed variability are tentatively identified.

Standard analysis products, such as time series plots, bivariate distributions, tidal analysis and auto- and cross- spectra of the current meter records along with vertical and horizontal sectional plots of water properties are presented in the appendices of this report.

The bathymetry of the Labrador Shelf is unusually complex (Figure 3). The width of the continental shelf decreases from about 160 km at the northern limit of the coast to about 100 km just north of Hamilton Inlet. South of Hamilton Inlet it quickly increases in width to approximately 230 km. The edge of the shelf is marked by the 300 or 400 m isobath, after which the continental slope plunges steeply to abyssal depths. The slope itself is a relatively uniform linear feature over much of its length, with the exception of the portion between Nain and Hamilton Banks, where a series of canyons and spur ridges causes the slope to vary in direction over distances of about 20 kilometres.

The shelf itself, rather than being of uniform depth, is divided into a series of banks by saddles which traverse the shelf. The banks are separated from the coastline by the Labrador Marginal Trough which runs most of the length of the coast. While it is an essentially continuous feature, the trough is not uniform in depth over its length, but is divided into a series of basins up to 700 m deep. The deeper basins usually coincide with the saddles (e.g. Hopedale Saddle and Cartwright Saddle). The banks are generally less than 200 m deep, and are quite flat on top. The saddles connect the basins of the marginal trough with the slope at depths of 400 to 500 m. Some are of relatively simple geometry, such as Hopedale Saddle, while others, in particular Cartwright Saddle, have quite complex forms with medial and transverse ridges and hollows, often 100 m or more in relief.

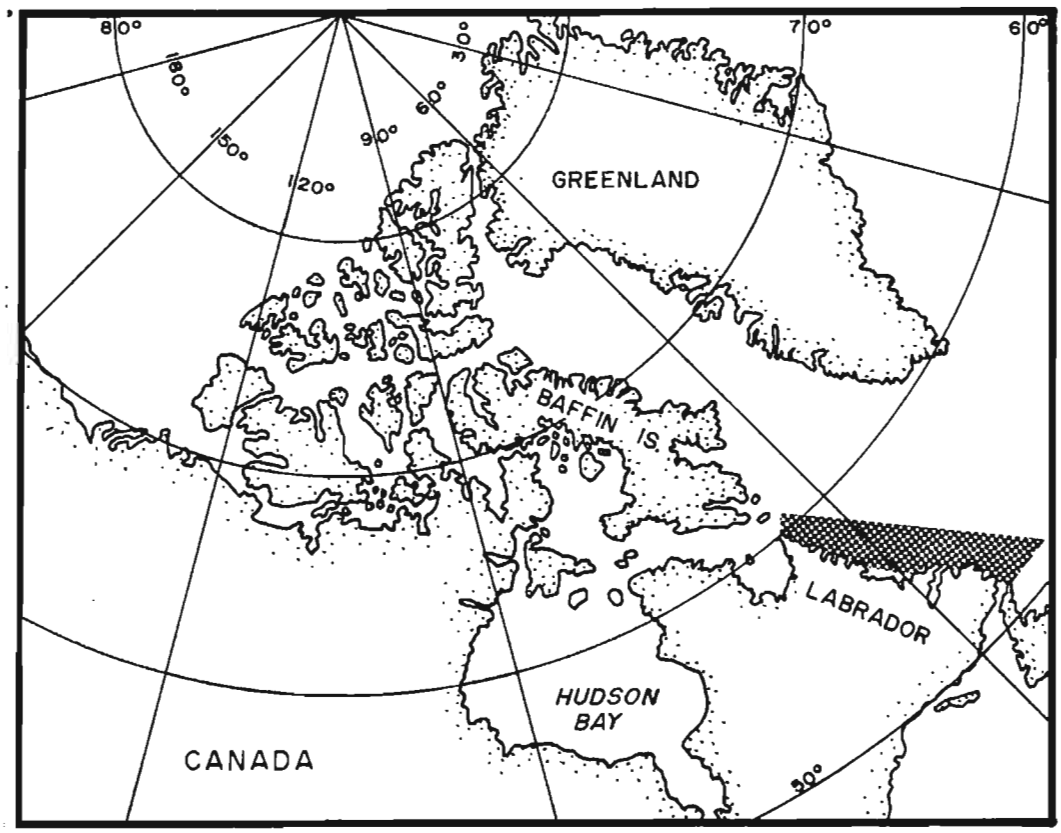

Figure 1: Location of study area.

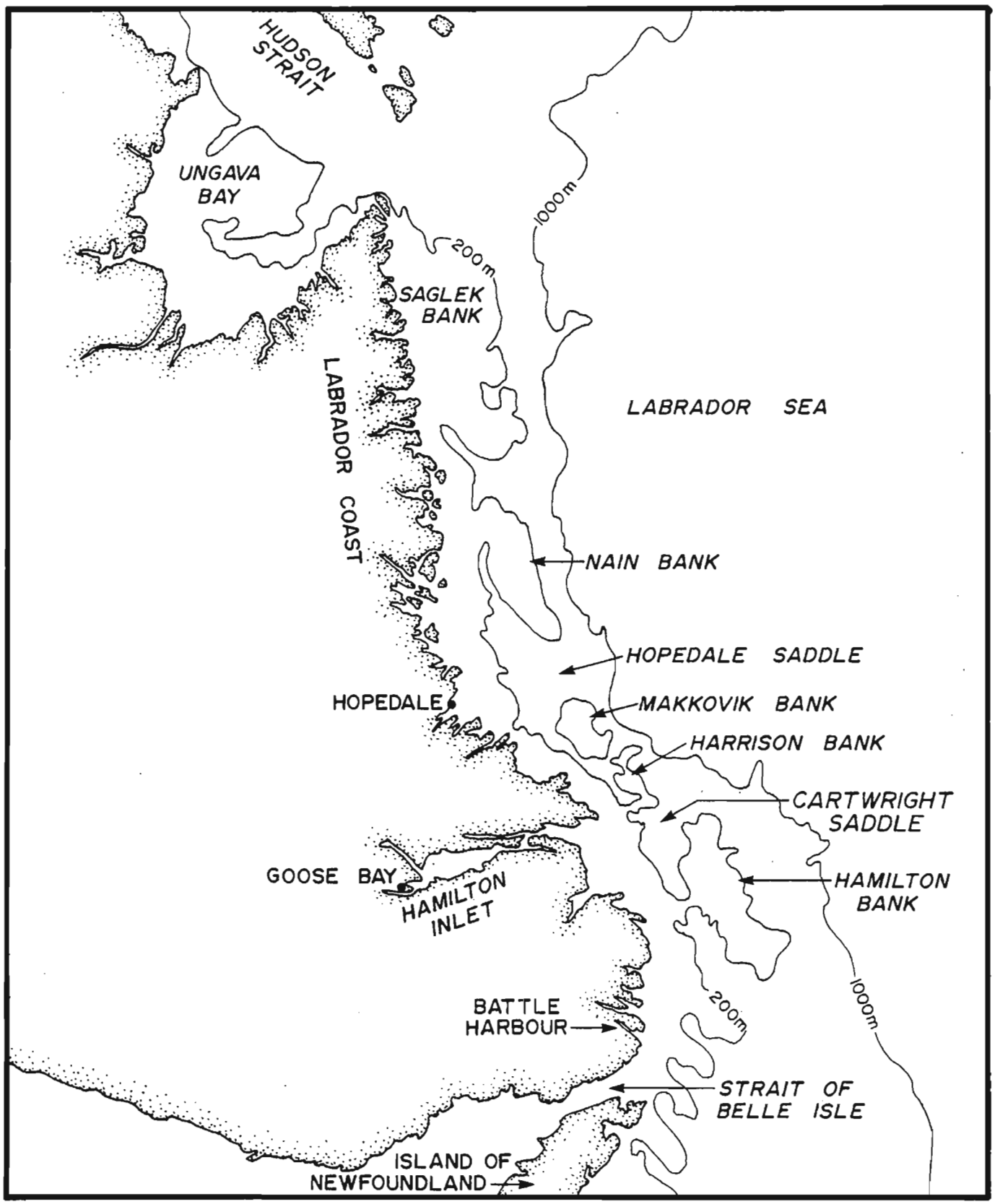

Figure 2: Place names along the Labrador coast.

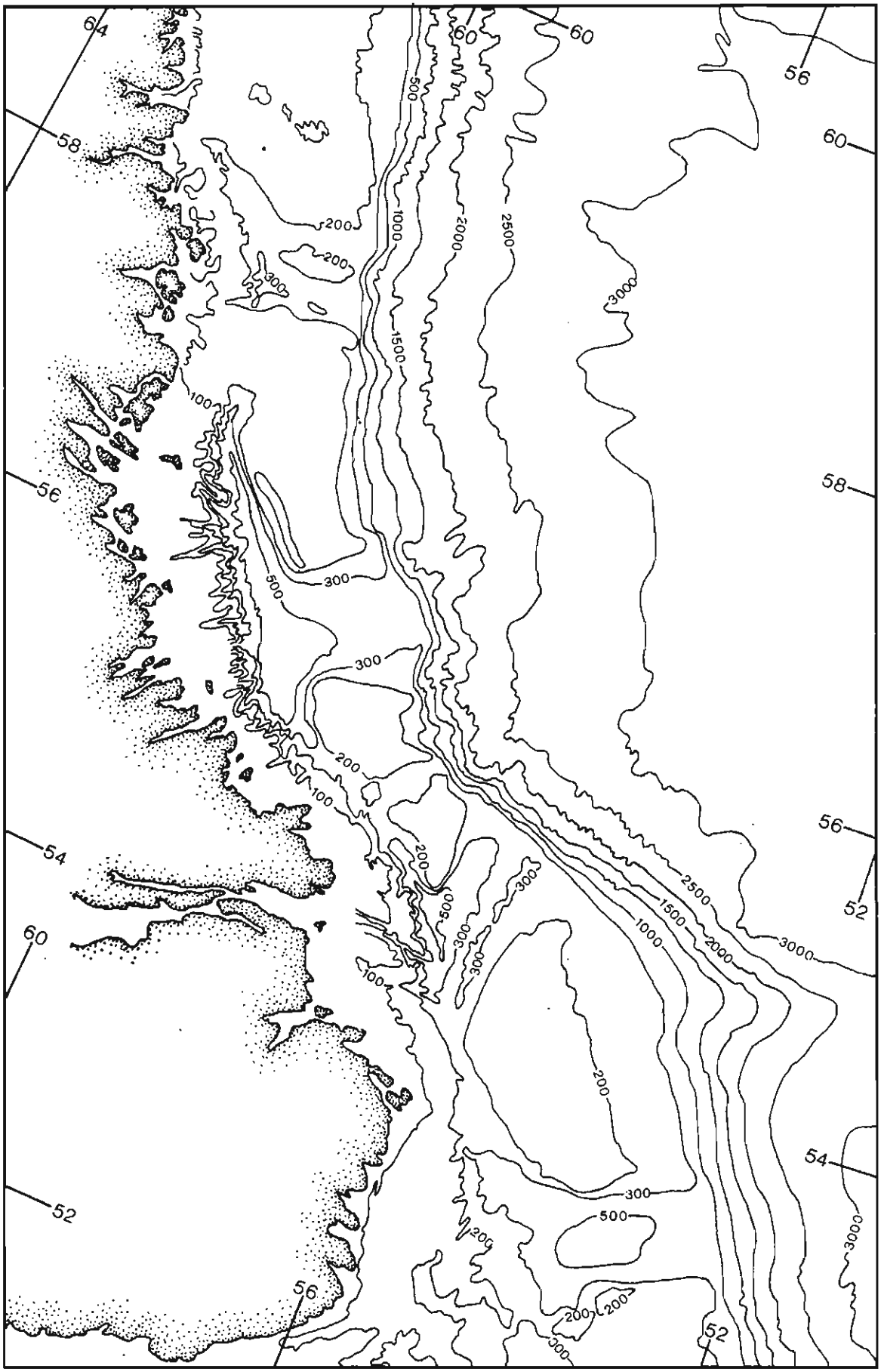

Figure 3: Detailed bathymetry of the Labrador coast

2. HISTORICAL BACKGROUND

Physical oceanographic measurements have been collected off the coast of Labrador from the 1890's to the present. The impetus for collecting these measurements has usually been the support of other scientific and engineering studies. Since 1914, the U.S. Coast Guard has carried out oceanographic surveys as part of its International Ice Patrol service. At about the same time, oceanographic data began to be collected during the course of regional fisheries studies. A large amount of such data was collected under the auspices of the Biological Board of Canada (later the Fisheries Research Board of Canada) and the International Commission for Northwest Atlantic Fisheries (ICNAF, now renamed NAFO, the Northwest Atlantic Fisheries Organization). Since the early 1970's, the search for oil and gas along the Labrador Continental Shelf has resulted in renewed interest in the physical oceanography of the region. The Bedford Institute of Oceanography (BIO), since its establishment in 1962, has been involved in several physical oceanographic studies of the Labrador area. A detailed review of the history of early oceanographic investigations is given in Smith, Soule and Mosby (1937), and Dunbar (1951).

Until the 1970's, oceanographic measurements consisted largely of hydrographic (temperature and salinity) data. From these data, the characteristic properties and spatial distributions of the major water masses could be described with reasonable accuracy during the summer months. In addition, the net circulation could be inferred from the measured internal mass distribution by the dynamic method.

A major contribution to physical oceanographic knowledge of the Labrador Shelf and Sea was provided by Smith, Soule and Mosby (1937). In this report, which in some ways remains the most comprehensive single study of the region, the geostrophic circulation and water mass distributions were described on the basis of hydrographic data collected from the Marion expedition of 1928 and the General Greene cruises of 1931, 1933, 1934 and 1935. The net circulation was southeasterly and dominated by two cores, one located over the inshore portion of the continental shelf in the vicinity of the marginal trough (where it is a recognizable entity) and the other centred over the steepest part of the continental slope (Figure 4).

The origins of the Labrador Current can be traced to three upstream sources. The cold Baffin Current, consisting of outflows from the Arctic Islands and possible remnants of the West Greenland current in northern Baffin Bay, flows southward along the coast of Baffin Island. At the entrance to Hudson Strait, it divides into two branches: one branch intrudes into Hudson Strait, joins with cold outflowing water from Hudson Bay and Foxe Basin and moves to the east out of Hudson Strait on the south side. This outflow rejoins the undeflected branch of the Baffin Current to form the inner or coastal core of the Labrador Current. The other source of the Labrador Current is the West Greenland Current. This flow originates off the southern tip of Greenland as the East Greenland Current and a western branch of the Irminger Current. It flows northward until reaching Davis Strait, whereupon a substantial part of the Current is deflected across the Strait and then flows southward offshore of the Baffin Current. The offshore core of the Labrador Current occurs along the lateral density gradients between the cold, fresher waters of Baffin Current origin and the warmer, saltier waters originating in the West Greenland Current.

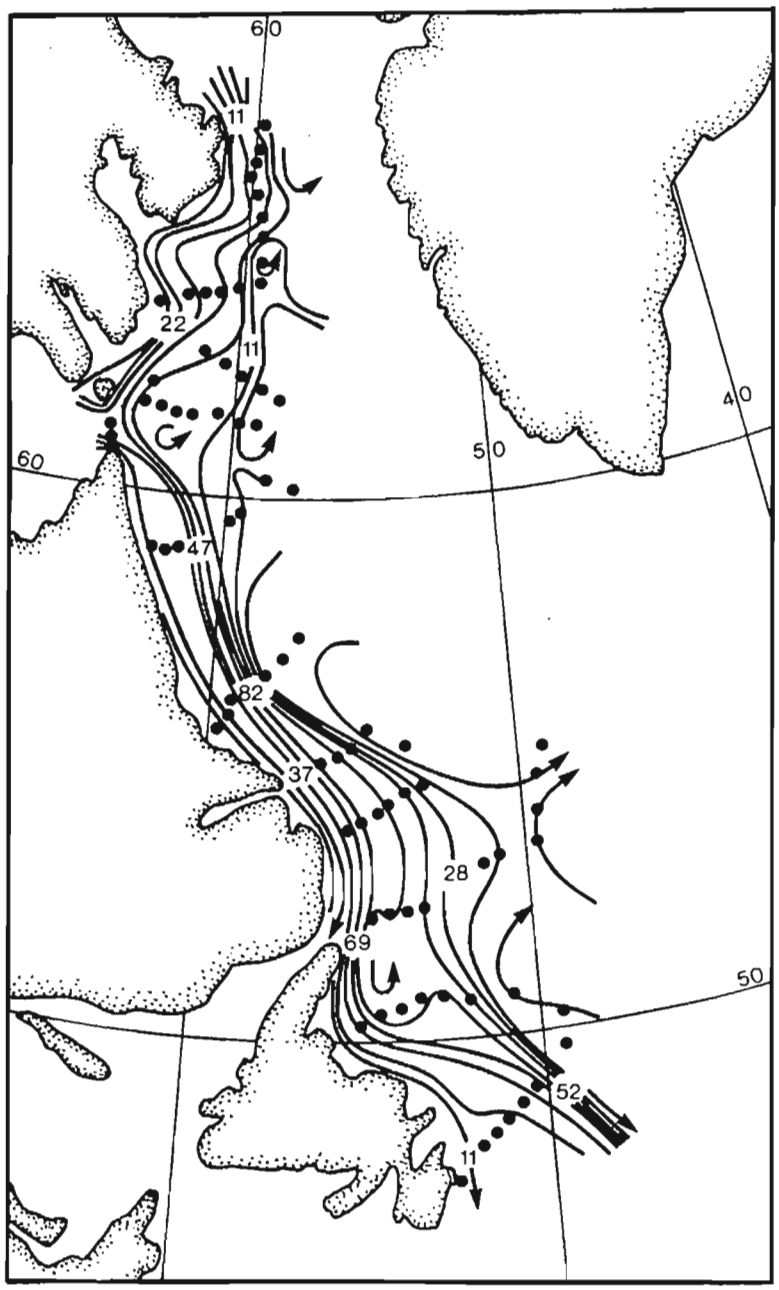

Figure 4: Countours of dynamic height anomaly based on the 1928 data obtained from the Marion (Smith, Soule and Mosby, 1937). The numbers represent the strength of the flows in the current core, in cm/s.

The properties of the source waters of the Labrador Current have been summarized by Dunbar (1951). Their temperature and salinity characteristics are shown in Figure 5. Both the Baffin Current and outflows from Hudson Strait supply Arctic Water to the Labrador coast. This water (the bottom polygon in Figure 5) has low temperatures (0 to -1.8°C) and relatively low salinities (32 to 34.1°/oo). The West Greenland Water (supplied by the West Greenland Current) has temperatures between 1.5 and 7°C, and a fairly wide range of salinities (32 to 35°/oo), the lower salinities being due to coastal influences. Labrador Sea Water has similar temperature properties, but spans a narrower range of salinity (34 to 35°/oo). The water of the Labrador Current, being a mixture of West Greenland and Arctic Water, occupies the region between those two water masses on the temperature-salinity diagram.

While subsequent studies confirmed the description of Smith, Soule and Mosby (1937), they were (until the 1970's) based on hydrographic data alone. This type of data lends itself to descriptions of the general circulation and water mass characteristics, but can provide only very limited information on the temporal variability of the circulation. As well, the large dimensions of the area (over 1000 km from Hudson Strait to the Strait of Belle Isle) caused difficulties in obtaining synoptic hydrographic data. Technological innovations made the collection of extended time series of direct current measurements possible by the beginning of the 1970's. These data, obtained from drillships and subsurface current meter moorings, provided the first information on the shorter term temporal variability of the circulation.

The available moored current meter time series data obtained up to and including 1979 have been compiled (Petro-Canada, 1982). A summary of the results of these measurements is presented in Table 1. In Figure 6, the location of each mooring site is plotted along with the net velocity of the uppermost current meter record in those cases where the measurement depth is less than 300 m. These data indicate that the net flows are stronger over the steepest portion of the continental slope than over the continental shelf or locations further offshore in the deeper parts of the Labrador Sea. At the two stations (G and J) situated over the steeply sloping continental shelf, the net velocity magnitude at 100 m depth was 35 cm/s with the direction of the net flow paralleling the local bathymetry. The flows varied little in direction during the course of the observations. The steadiness factor, computed as the ratio of the magnitude of the net velocity to the mean speed (Ramster et al., 1978) exceeded 90% for both records. At the measurement sites located over the continental shelf, the steadiness factors were markedly lower, ranging from 19 to 55%, indicating a much higher degree of directional variability in the currents. While the magnitudes of the vector mean currents over the continental shelf were much less than those measured over the slope, the reduction of the mean current speeds is less pronounced. At times, strong flows of up to 79 cm/s were observed over the continental shelf.

Prior to the 1980 physical oceanographic study, the available current meter data were irregularly distributed in both space and time. All of the data available on the continental shelf had been obtained in the summer months. Furthermore, these data were collected at locations on the shallow banks of the shelf in water depths of 220 m or less. No time series current meter data were available from either the marginal trough or from the saddles. As for the

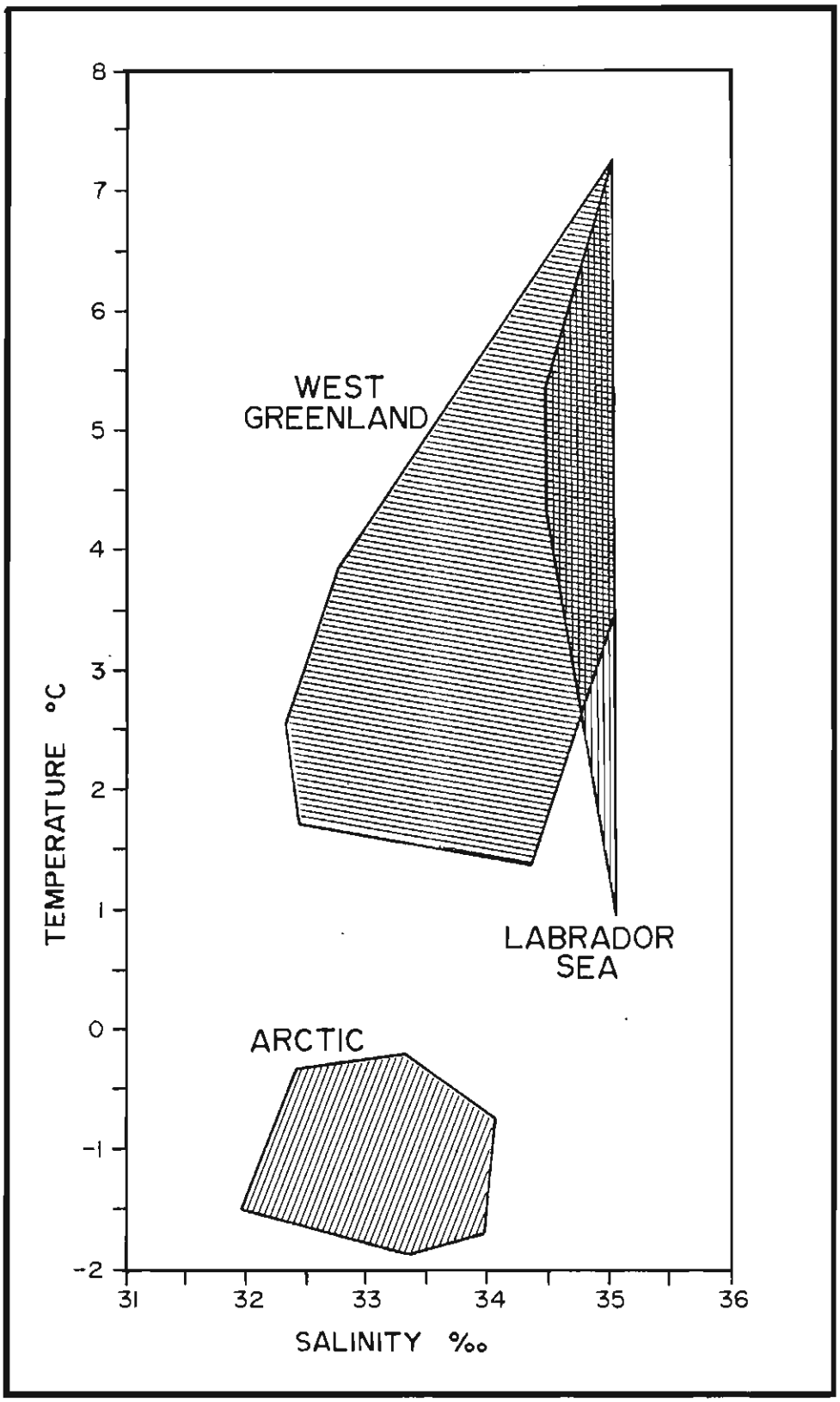

Figure 5: Temperature-salinity characteristics of the Arctic, West Greenland and Labrador Sea water masses (after Dunbar, 1951).

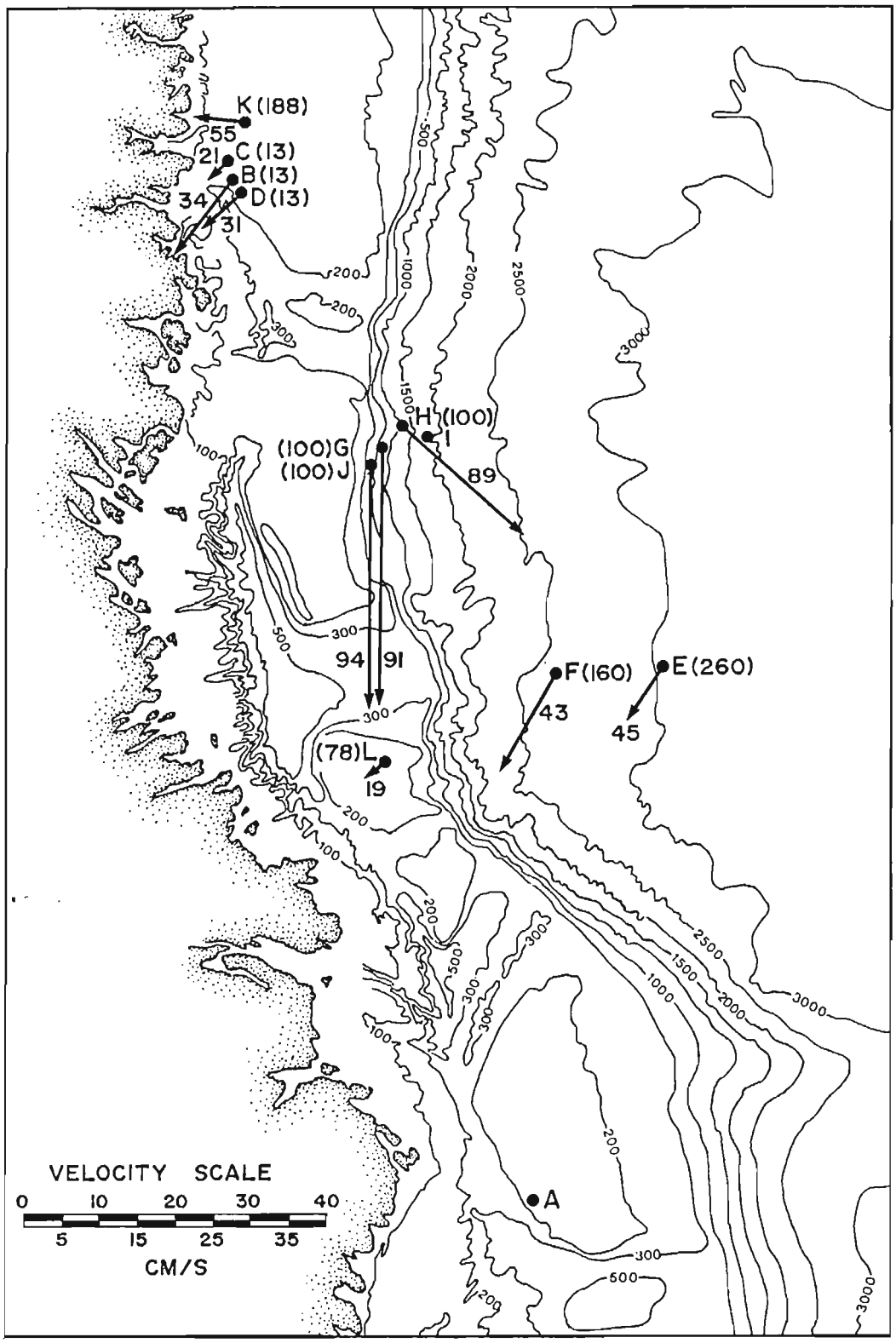

Figure 6: Locations of current meter mooring measurements obtained prior to 1980. The net velocities obtained at depths of 300 m or less are shown, where available, along with the measurement depth (m) (in parentheses) and the steadiness factor.

Table 1

A summary of available current meter data obtained from moorings prior to 1980

STN	LATITUDE	LONGITUDE	TIMES	DAYS	DEPTHS INST. M	DEPTHS WATR M	VELOCITY MAG CM/S	VELOCITY DIR	SPEED B CM/S		MAX SPEED CM/S	SOURCE
A	53 30.0	54 29.0	JUL-AUG 70	14	37	217	-	-	19.0	-	-	(1)
A	53 30.0	54 29.0	JUL-AUG 70	14	81	217	-	-	14.0	-	-	(1)
A	53 30.0	54 29.0	JUL-AUG 70	14	124	217	-	-	19.0	-	-	(1)
B	58 30.0	62 02.0	AUG 72	14	13	200	13.7	193	40.0	34	79.0	(2)
B	58 30.0	62 02.0	AUG 72	14	166	200	8.0	252	20.0	40	27.0	(2)
C	58 37.0	62 10.0	AUG 72	14	13	180	4.1	205	20.0	21	38.0	(2)
C	58 37.0	62 10.0	AUG 72	14	136	180	6.3	200	15.0	42	37.0	(2)
D	58 28.0	61 57.0	AUG 72	14	13	200	9.2	200	30.0	31	75.0	(2)
D	58 28.0	61 57.0	AUG 72	14	155	200	4.6	183	15.0	31	24.0	(2)
E	56 49.0	55 19.0	MAR-APR 76	27	260	3000	8.7	013	20.0	44	45.0	(3)
F	56 33.0	56 22.0	MAR-APR 76	27	160	3000	15.2	188	35.0	43	75.0	(3)
F	56 33.0	56 22.0	MAR-APR 76	27	2500	3000	12.1	201	25.0	48	30.0	(3)
G	57 25.0	59 09.0	OCT'77-JAN'78	95	100	600	35.3	157	39.0	91	94.0	(4)
G	57 25.0	59 09.0	OCT'77-JAN'78	95	250	600	13.8	154	17.0	79	60.0	(4)
G	57 25.0	59 09.0	OCT'77-JAN'78	95	500	600	10.5	147	13.0	83	44.0	(4)
H	57 35.0	59 02.0	OCT'77-JAN'78	95	100	1320	22.3	109	25.0	89	89.0	(4)
H	57 35.0	59 02.0	OCT'77-JAN'78	95	500	1320	11.6	157	13.0	89	37.0	(4)
I	57 35.0	58 44.0	JAN-JUL 78	166	1200	1306	3.6	152	6.0	55	31.0	(4)
J	57 18.0	59 10.0	JAN-JUL 78	166	100	600	33.5	157	36.0	94	86.0	(4)
J	57 18.0	59 10.0	JAN-JUL 78	166	500	600	9.0	173	11.0	79	58.0	(4)
K	58 52.0	62 11.0	AUG-OCT 78	40	188	192	6.6	251	12.0	55	30.0	(5)
L	55 39.0	57 42.0	JUL-AUG 79	9	37	160	-	-	14.0	-	-	(6)
L	55 39.0	57 42.0	JUL-AUG 79	9	78	160	2.7	218	14.0	19	40.0	(6)
L	55 39.0	57 42.0	JUL-AUG 79	9	130	160	2.6	179	12.0	22	40.0	(6)

DATA SOURCES:

(1) SCOBIE (1972)
(2) HOLDEN (1973)
(3) ALLEN (1979)
(4) LAZIER (1979)
(5) MACLAREN MAREX (1980)
(6) NORDCO (1980)

current meter data available from the slope and regions further offshore, all of the available data had been collected in months other than summer, from October to April. In the design of the 1980 program, an attempt was made to redress these disparities in sampling locations for the summer months by obtaining simultaneous current meter data at locations in the marginal trough, saddles and continental slope in addition to sites on the banks.

While a considerable quantity of oceanographic data has been acquired, there remains a paucity of studies describing the dynamics of the oceanic circulation of the Labrador Sea and its continental margin. The circulation and water mass distributions at depth in the Labrador Sea have received some attention (e.g. Lazier, 1973; Swallow and Worthington, 1969). More recently, Allen (1979) has studied the flow variability at the offshore edge of the Labrador Current based on two current meter data sets obtained in water depths of 2600 to 3000 m. Bottom trapped topographic Rossby waves were identified which produced pronounced cross-slope motions at periods between 4 and 8 days. At longer periods (8 to 10 days), the topographic Rossby waves appeared to extend throughout the water column. These waves apparently interacted positively with the baroclinic surface currents which could account for the observed periods of strong steady flows interspersed with periods of weak, highly variable flows. From an analysis of current meter time series data obtained at a single location in the Labrador Current at the edge of the Grand Banks in 490 m of water, Mountain (1980) noted temporal variations with periods of 10 to 16 days and 2 to 4 days. The former variations, at depths of 110 and 380 m, were found to be coherent with the local wind stress. Mountain (1980) suggested that either stable continental shelf waves or baroclinic or barotropic instabilities could account for the shorter period variability.

The 1980 physical oceanographic program significantly extends the existing data base for the regions of the continental shelf and adjoining slope in the summer months. While it is beyond the scope of the present report to provide a detailed dynamical interpretation of these data, the analysis results are presented as a first step in identifying and studying the underlying dynamics of the Labrador Current.

3. DATA COLLECTION

3.1 MOORED CURRENT METER DATA

Measurement Times and Locations

Twenty-nine Aanderaa RCM-4 current meters and two Neil Brown ACM-2 current meters were deployed at the locations shown in Figure 7. A total of 13 subsurface current meter moorings were deployed. Each mooring contained either a single Neil Brown current meter or two or three Aanderaa instruments. Since each Neil Brown mooring was located within 1 km of a mooring containing Aanderaa meters, these Neil Brown data are presented in the remainder of this report as having the same location as the adjacent Aanderaa current meter data.

The subsurface current meter moorings were designed by Arctic Sciences Ltd. NORDCO Ltd. deployed and recovered the moorings and processed the data (NORDCO, 1981). Nine of the mooring sites were located in the vicinity of the south-central portion of the Labrador continental shelf. These were arranged in three lines of three measurement sites each. The innermost mooring on each of these lines (4-1, 5-1 and 7-1) was placed in the inner marginal trough. Stations 4-2 and 4-3 were located on the northern side of Hamilton Bank, with 4-2 on the western flank and 4-3 in the eastern portion. Station 5-2 was located in Cartwright Saddle while station 7-2 was situated on the northern portion of Makkovik Bank. Two of the outermost moorings were located at or near the steep inner portion of the continental slope: station 5-3 was approximately 6 km from the edge of the slope and station 7-3 was located on the slope itself. At this latter site, large ship drift combined with rapidly changing water depths resulted in the current meters being placed about 50 m deeper than originally intended. The remaining two moorings, 9-1 and 10-1, were positioned further north near drilling sites on Nain Bank and Saglek Bank, respectively.

The intended depths of the Aanderaa current meters were at 50 m, 150 m (where depths permitted) and near the bottom. At most sites, the near-bottom instruments were 9 m from the sea floor with the exception of the outermost locations on lines 4, 5 and 7 where the deepest meters were placed 50 m above the bottom. In the upper portion of the water column (at depths of less than 50 m) surface wave induced velocities could seriously bias the speed data from Aanderaa meters. As a result, two Neil Brown current meters were used at shallow depths, 30 and 25 m, at two locations (5-2 and 7-2).

The nine southernmost current meter stations were deployed between July 3 and July 11, 1980 while the remaining two northern moorings were deployed on July 15 (10-1) and July 18 (9-1). Recovery of the moorings commenced on September 11 and by September 16 the equipment at all but four stations (4-3, 5-2, 9- 1 and 10-1) had been recovered. These latter moorings were recovered between September 30 and October 6, 1981. The period of operation for each current meter is illustrated schematically in Figure 8. The longest time series were obtained at stations 5-2 and 4-3 with record lengths of 91 and 87 days. Seventy-five days of data were collected at stations 9-1 and 10-1 while at the remaining sites, the record lengths ranged from 62 to 71 days.

Mooring locations were determined through the ARGOS positioning system used for locating drillships. Positions are believed to be accurate to better than

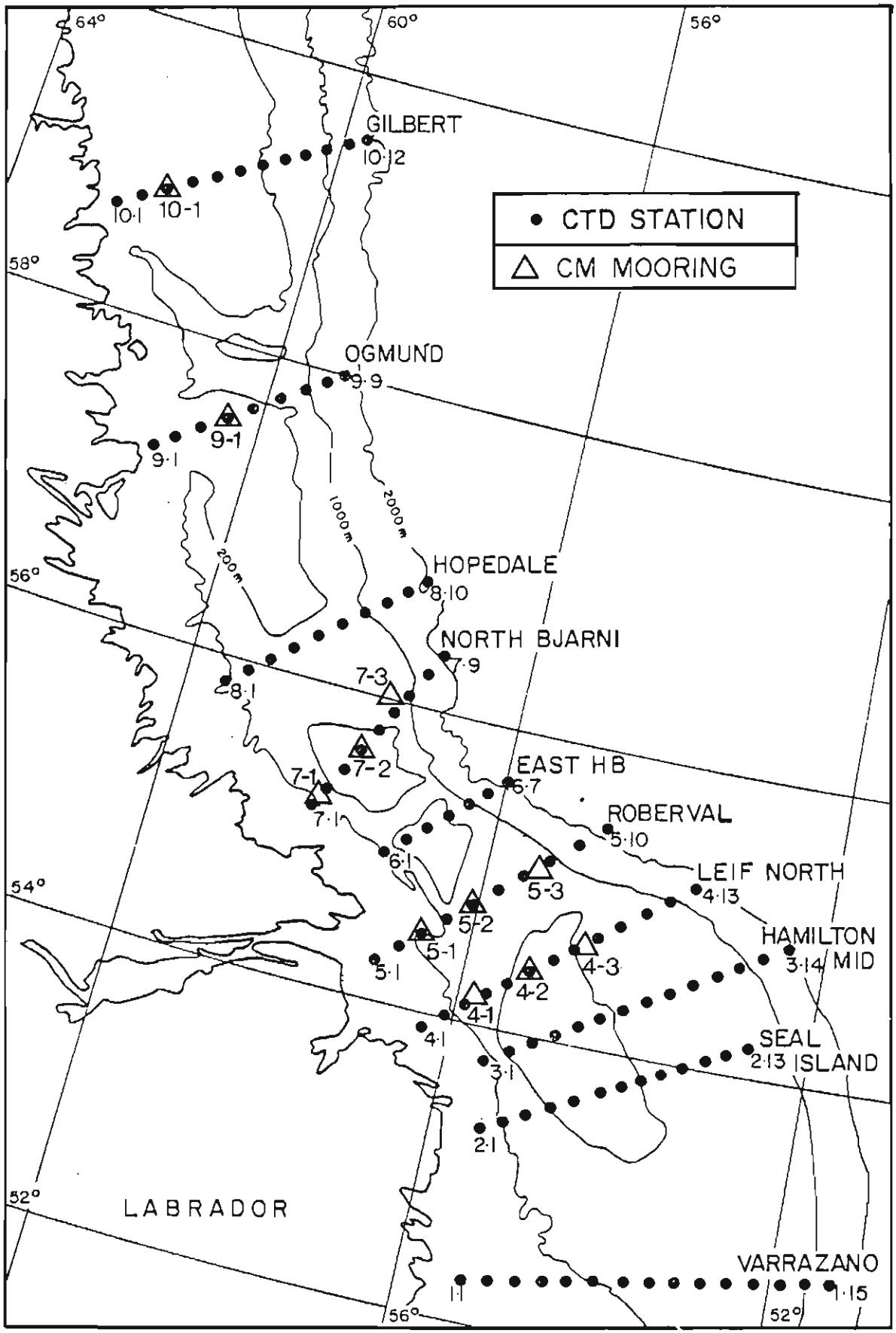

Figure 7: Locations of measurement sites.

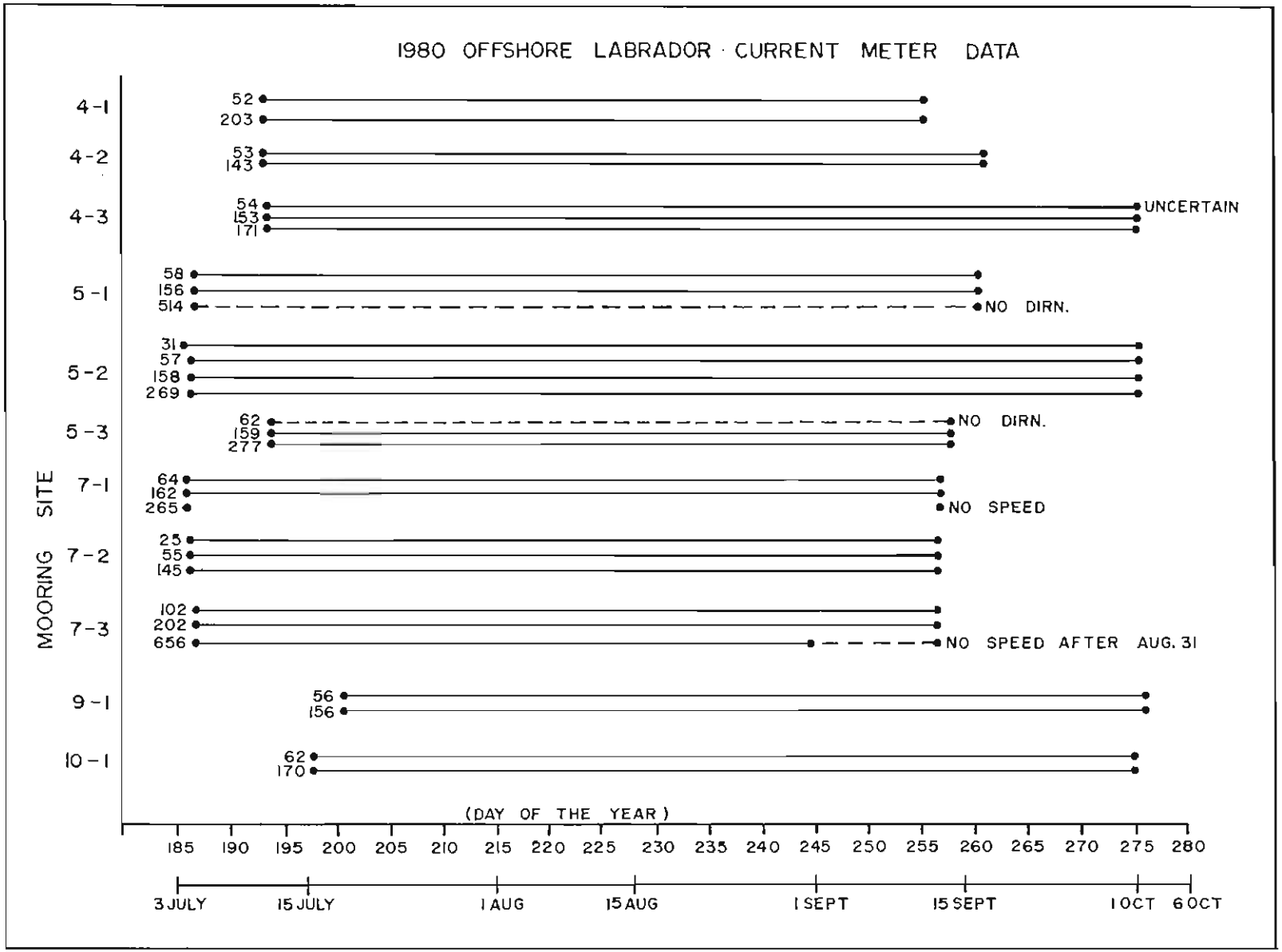

Figure 8: Periods of operation for current meters deployed off the Labrador coast, in the summer of 1980. Numbers to the left of the horizontal lines represent nominal instrument depths in metres.

0.2 km. Instrument depths (Figure 8) were computed from soundings at the time of deployment and the measured length of mooring components. No pressure data were available from the current meters to check the estimated depths.

Current Meter Instrumentation

The Aanderaa RCM-4 meters measured current speed and direction and water temperature and conductivity at 15-minute intervals. The expected accuracies for each measured quantity are given in Table 2. The directional accuracy of the Aanderaa current meters used in the present study has been improved through modifications to the instruments (Fissel and Wilton, 1980).

The Neil Brown current meter employs an acoustic travel time sensor capable of measuring high frequency (to within 1 cycle in 2 seconds) fluctuations in the current. This capability, together with its internal vector averaging of the data, enables the measurement of meaningful currents in the presence of surface wave induced motions (unlike the Aanderaa current meter - McCullough, 1980). Thus, the Neil Brown current meter data collected for this study are believed to be reliable, even though significant wave motions may, at times, have been present at the measurement depths. In addition to the vector averaged velocity recorded once every 2 minutes, the water temperature was also measured at 20-minute intervals.

Table 2

The accuracy and resolution of the Aanderaa RCM-4 and Neil Brown ACM-2 current meters.

Quantity	Range	Accuracy	Resolution
Aanderaa RCM-4			
Speed[a]	2.5 to 200 cm/s	±1 cm/s or ±2% of the actual speed	0.19 cm/s
Direction[b]	0 to 360°	±5°	0.35°
Temperature[b]	-2.5 to 21.5°C	±0.1°C	0.02°C
Conductivity[a]	0 to 70 mmho/cm	---	0.07 mmho/cm
	22 to 64 mmho/cm	---	0.04 mmho/cm
Neil Brown ACM-2			
Velocity[a]	0 to ±250 cm/s	±1 cm/s or ±5%	--
Direction[a]	0 to 360°	±2°	--
Temperature	-2.4 to 36°C	±0.5°C	±0.15°C

[a] Manufacturer's specifications (Aanderaa Instruments Ltd., 1978; Neil Brown Instrument Systems, 1979).

[b] Based on Arctic Sciences Ltd. tests (Fissel and Wilton, 1980; Knight and Fissel, 1981).

Data Processing

The raw current meter data were calibrated and obvious errors were removed following the procedures described in NORDCO (1981). On processing the data, it was discovered that data from some of the instruments were incorrect or suspect. These data sets are (NORDCO, 1981) 4-1/153, 4-3/54, 5-1/514, 5-3/62, and 7- 3/656. (Note that in this report current meter data sets will be identified by the following code: station number/depth in metres.) Data sets 5-1/514 and 5-3/62 had no useable direction data due to, respectively, a broken compass wire and the inadvertent use of a magnetic battery immediately above the compass. The data from 4-1/153 were limited to a highly erratic record of just 20 days and were considered too unreliable for the purposes of this study. The speed data from 7-3/656 ended on August 31, 1980 because of a faulty encoder in the current meter. The data from 4-3/54 contained many spikes which were attributed to use of a magnetic battery about 10 cm from the compass (NORDCO, 1981). Following extensive editing of the data to remove spurious values, a time series was produced.

3.2 CTD DATA

Measurement Times and Locations

The pattern of CTD stations is shown in Figure 7, along with the locations of the current meter moorings. The station lines were oriented perpendicularly to the coast, cutting across the major circulation features. Four occupations of the station pattern were made throughout the summer, one in July, two in August, and the last in October. The times at which the lines were occupied are summarized in Figure 9. In most cases, all stations in the lines were occupied with the occasional exception of the outermost one or two. Detailed listings of the times of occupation and positions for all the stations may be found in NORDCO (1981).

Instrumentation

The data were collected with a Guildline 8706 digital CTD probe and model 87102 control unit. Calibration samples were collected by means of bottles and reversing thermometers attached to the CTD wire. A full description of the data collection and initial calibration and processing may be found in NORDCO (1981).

The CTD data were collected with a Guildline Model 8706 Digital CTD. The manufacturer's specifications for the instrument are listed in Table 3 below.

The instrument was calibrated with water samples taken during the field program and with thermistors and water samples at the Institute of Ocean Sciences after completion of the field program. Differences between the samples and the probe salinities ranged from 0.01°/oo to 0.07°/oo. Correction factors for the conductivity ratio were derived from the comparisons with the bottle samples and the I.O.S. calibration and applied to the data from each cast. Further details of the procedures used, and the calibration corrections applied to each cast may be found in NORDCO (1981).

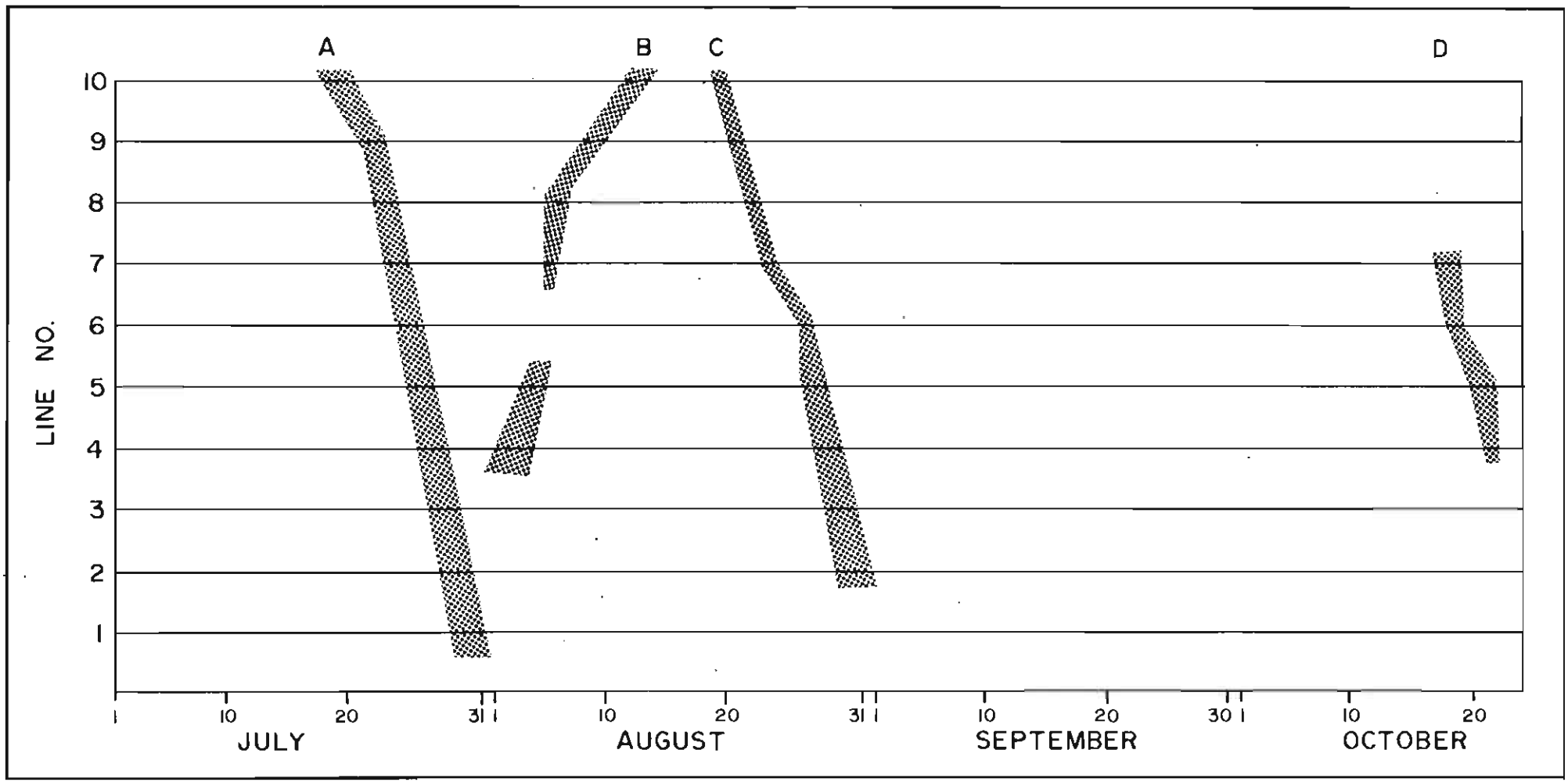

Figure 9: Times of occupations of CTD stations.

Table 3

	Pressure	Temperature	Conductivity[a]
Range	0-1500 dbar	-2°C to +30°C	100 ppm to 40 ppt
Accuracy	±0.15% of full-scale pressure	±0.005°C	±0.005 ppt
Resolution	±0.01% of full-scale pressure	±0.0005°C	±0.001 ppt
Stability	---	±0.002°C/30 days ±0.005°C/6 mos.	±0.002 ppt/6 mos.

[a] expressed as equivalent salinities.

3.3 OTHER DATA

In the course of the analysis of the 1980 physical oceanographic data, other types of data were obtained. These were:

(1) hourly wind data measurements from the drillships Pelican, Neddrill II and Pelerin (Plansearch, 1981a; Plansearch, 1981b; Fenco, 1981);

(2) water level data from the permanent station at Nain, Labrador operated by the Marine Environmental Data Services (MEDS).

The wind data were obtained from the Atmospheric Environment Service (AES) on computer tape in the form of 3-hourly synoptic meteorological data records in the standard World Meteorological Organization (WMO) format. Some additional wind data, from the drillship Pelican, obtained from July 16 to September 11 (Plansearch, 1981b) were not on the AES tape. These data were entered manually from the data report at 3-hour intervals. The times and locations of drillship wind data used in the analysis are provided in Figure 10.

The Nain, Labrador (56°32'N, 61°41'W) hourly water level data were obtained on punched cards from MEDS for the months of July to September, 1980, inclusive. Some data were missing due to a malfunction of the mechanical gauge throughout the month of July and again from August 31 to September 9.

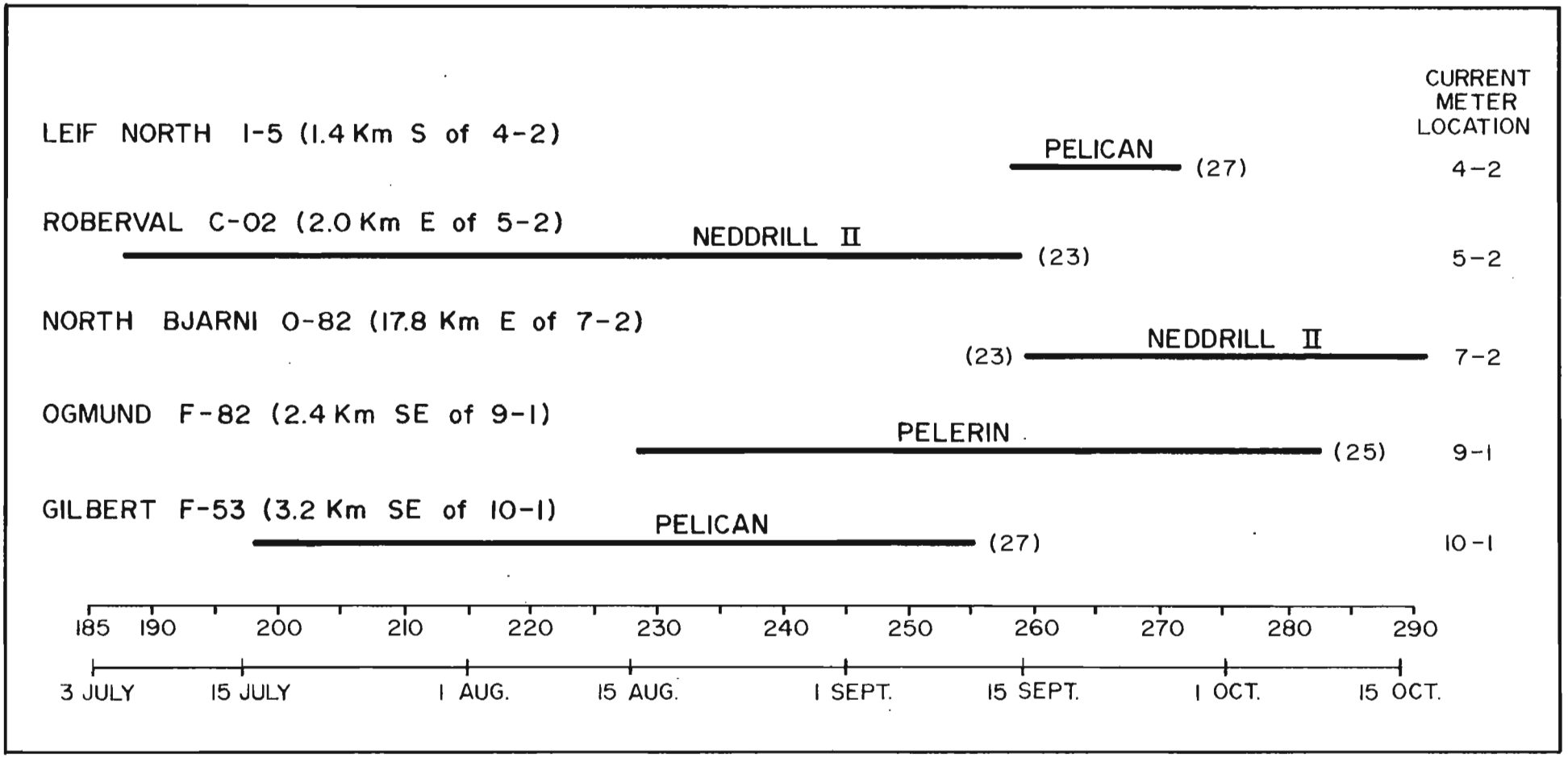

Figure 10: The period of wind measurements obtained at drillships in the summer of 1980. The numbers in parantheses indicate the height of the anemometer in metres above sea level.

4. ANALYSIS TECHNIQUES

4.1 CURRENT METER DATA

Pre-Analysis Data Processing

The current meter data, as received on 9-track computer tapes, were converted to the standard current meter format. The northerly and easterly components of velocity were computed. Salinities were calculated from the temperature and conductivity data using the algorithm of Bennett (1976). Sigma-t values were then computed using Knudsen's formula (Fofonoff, 1962). Standard computer programs provided summary statistics of the data, joint bivariate distributions of speed and direction and time series plots of the temperature and salinity data.

From these standard displays, erroneous or suspect data were identified beyond those described in the data report (NORDCO, 1981). The conductivity values for the data set 4-3/54 were incorrect due to the use of incorrect calibration values. Furthermore, other data sets revealed occasional unusually large or small salinity values (e.g. maximum values in excess of 34.9°/oo in data sets 5-3/62, 5-3/159, 7-2/55, 7-3/202, 7-3/656 and a minimum value of less than 30.9°/oo in data set 10-1/170. Such erroneous salinity values can result from the mismatch of response time of the conductivity and temperature sensors on the Aanderaa current meters. Pending a careful examination of these data, the salinity time series should be used with caution.

In the course of analyzing the currents, some other data sets were identified as suspect. The speed data recorded at 7- 1/265 are questionable, having a very high proportion of zero values (90%). Furthermore, non-zero speeds tend to occur intermittently over periods of a few hours separated by several hours or days of zero speeds. The distribution of the non-zero speeds, being heavily skewed towards values of 6 to 13 cm/s and with few observations (23%) of less than 6 cm/s, appears to be inconsistent with a very low speed current regime. It appears more likely that the rotor on the instrument may have had a very high threshold value, possibly due to problems with the bearings. Whatever the cause, the speed data are considered unreliable for analysis purposes.

The data from 4-3/54 were subjected to additional processing by the field services contractor to remove many spurious values present. in all channels. Subsequent analyses performed on this data set suggested that the velocity data remained unreliable. In particular, the tidal analysis results revealed semi-diurnal activity of only half that measured by the two current meters at greater depths on the same mooring. While it is not possible to positively attribute such anomalous results to an instrument problem, the analysis results for 4-3/54 must be used with caution in view of the greater uncertainties associated with this data set.

For some of the analysis, simultaneous data sets were required. Many of the Aanderaa current meters had not been started on the quarter hour. For example, one current meter had been initialized at 37 minutes after the hour while another had been started at 41 minutes after the hour. A computer program

was written to provide interpolated data at times that were multiples of 15 minutes: (i.e. on the hour, 15, 30 and 45 minutes after the hour).

In some instances data were required at lower sampling frequencies than the original sampling rate. For this purpose, three low-pass moving average filters were used. The 15-minute Aanderaa data were subjected to a filter, designated A(4) A(4) A(5)/(4 X 4 X 5) following the notation of Godin (1972). For the Neil Brown data, the original readings at 2-minute intervals were first averaged in groups of 5 to produce 10-minute samples. These were then subjected to an A(6) A(6) A(7)/(6 X 6 X 7) digital filter. Following the filtering, the values were subsampled on the hour, resulting in hourly time series.

Spectral Analysis

Three types of standard time series analysis techniques were carried out on the current meter data: spectral analysis, harmonic (or tidal) analysis and digital filtering.

The spectral analysis programs used the Fast Fourier Transform algorithm of Singleton (1969) following the methods of Jenkins and Watts (1968). Auto-spectra were computed for vector time series (currents and winds) and scalar time series (temperatures). The time series were first processed to remove the mean value and linear trend of each signal, prior to computing the Fast Fourier Transform values. For the vector time series of currents, the spectral results were represented in two ways: as the computed spectral levels of the southeasterly and southwesterly flow components displayed on a logarithmic frequency axis or as the clockwise and anticlockwise rotary spectral values displayed on a linear frequency axis. In both display formats, the area beneath the spectral curve is proportional to the total variance of the vector current.

In the auto- and cross-spectral analysis, the initial time series was divided into a number of sequential blocks. Spectral values were computed separately for each block; the results for each frequency band were then used to calculate an average spectral level in order to increase the statistical reliability of each spectral estimate (Bendat and Piersol, 1971). The standard deviation about the mean for each band was also computed as an empirical estimate of the variability in spectral levels among the individual blocks.

Current vector spectral values were computed in block record lengths of exactly 14 days. This choice limited the amount of sideband leakage for the four major tidal constituents (M_2, S_2, K_1 and O_1) to less than 0.5%. The total time series data were subdivided into blocks of 14-day records, with the number of blocks varying from four to six.

Cross-spectral values were computed for pairs of current vector time series, current vector with wind vector time series and current component with temperature time series. The cross-spectral results are represented in the form of coherence and phase values. The coherence values, ranging from 0 to 1, represent the fraction of the amplitude of each signal that matches a similar oscillation in the other signal regardless of the phase difference between the two oscillations. The phase difference between the two signals at each

frequency represents the angle in degrees by which the second signal leads the first.

When presenting the coherence values between two quantities, some criterion must be used to decide if the coherence between them is statistically significant. Here we take the significance level to be that value of coherence (Table 4) below which the true random coherence will fall with a given probability (Groves and Hannan, 1968).

Table 4
Coherence values between two time series that exceed random noise at 80, 90 and 95% probability levels.

Number of Blocks	Percentage Significance Levels 80	90	95
3	0.74	0.83	0.88
4	0.64	0.73	0.79
5	0.58	0.66	0.73
6	0.52	0.61	0.67

Harmonic Analysis

The harmonic analysis of the vector currents was performed using the program of Foreman (1978) applied to current meter data sets subsampled at hourly intervals. The harmonic analyses are presented in tidal current ellipse format. In this format, an ellipse is described as representing the sum of two oppositely rotating vectors, oscillating at the frequency of a tidal constituent. The length of the semi-major axis corresponds to the maximum amplitude for the particular tidal constituent while the length of the semi-minor axis represents the minimum amplitude. The inclination angle indicates the angle in degrees counterclockwise between geographical east and the direction of maximum tidal flow.

Digital Filtering

To examine the variability of the currents at particular frequencies of interest, finite impulse recursive digital filters were designed. For the arranged hourly time series data, three filters were used: a low-pass filter eliminating variations with periods of one day or less, and two band-pass filters, centred on the semi- diurnal and inertial frequencies. The transfer functions for these digital filters are shown in Figure 11.

Other digital filters were designed to examine current fluctuations at higher frequencies (f > 10 cycles/day [cpd]. For the 15 minutes Aanderaa data, a high pass digital filter was applied to detect variations at frequencies from 10 to 48 cpd. Two high pass digital filters were constructed for the Neil Brown current meter data: a high pass filter (frequencies of 10 to 72 cpd) applied

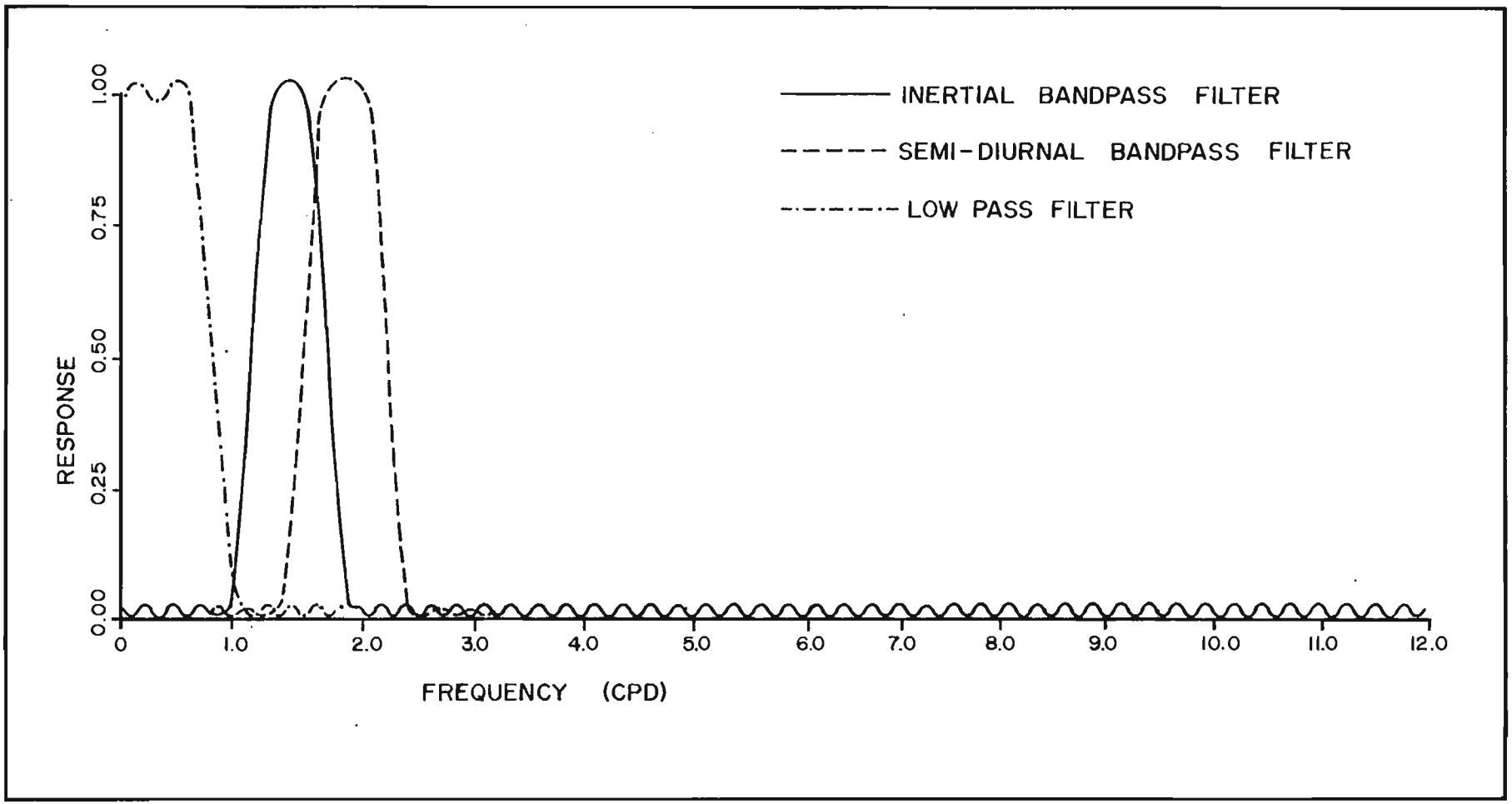

Figure 11: Transfer functions of three digital filters, low pass, inertial and semi-diurnal bandpass, used in the analysis.

to the 10 minute average values and a very high pass filter (75 to 360 cpd) applied to the 2 minute data. Transfer functions for the higher pass digital filters are presented in Figure 12.

4.2 CTD DATA

Pre-Analysis Data Processing

The data were received on 9-track tape as listings of depth, pressure, salinity, temperature, sigma-t (σ_t), conductivity ratio, specific volume anomaly, dynamic height anomaly and sound speed. The data collection and processing techniques used to produce the data set are described in NORDCO (1981). Temperature and salinity profiles were scanned and any obvious spikes were removed. In addition, segments of the data where the CTD probe was moving up instead of down, due to heavy wave conditions, were eliminated.

The edited data were then processed by a program which produced an output file containing records of pressure, temperature, salinity, depth, sigma-t, specific volume anomaly, dynamic height, potential energy and sound velocity at 1-decibar increments. Sigma-t was computed using Knudsen's formula (Fofonoff, 1962). Integrations for the dynamic depths were performed from the surface down, for every listed value.

Vertical and Horizontal Sections

The contents of the output file were used to produce further standard analysis products. Vertical cross-sections of temperature, salinity and sigma-t were produced for each occupation of each line of stations. Two sets were produced: one set displayed data from 25 m to the bottom, with a vertical exaggeration of 250:1 in all examples; the second showed data from the surface to 100 m, with a vertical exaggeration of 1250:1 in all cases. The second set was used for intermediate analysis stages only, and sections from it are presented only where required in the text. Contour intervals of 0.5°C,.0.2°/oo and 0.2 in σ_t were used in both cases.

Horizontal sections of temperature, salinity and σ_t were drawn at 0 and 100 m depth for all four station occupations. Contour intervals of 0.5°C, 0.25o/oo and 0.2 in σ_t were used. The map projection is Lambert Conformal Conic, with standard parallels of 58°N and 54°N. The charts are reproduced at a scale of 1:4,000,000 and are included where required in the text.

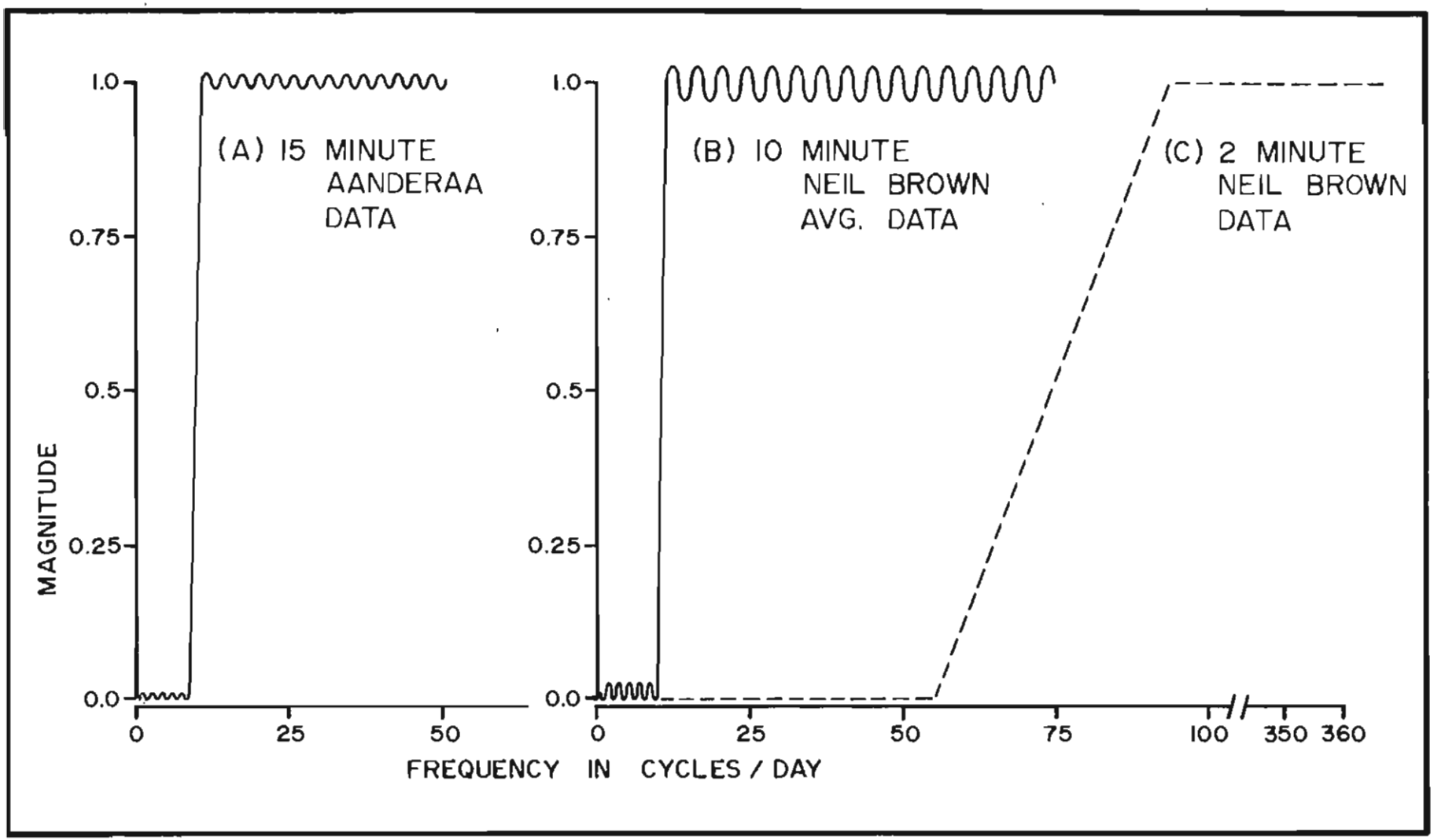

Figure 12: Transfer functions of three high-pass digital filters used in the analysis.

5. RESULTS

5.1 MEAN CIRCULATION

The mean flows derived from the current meter records are displayed as the mean current vectors measured at each mooring for the upper (Figure 13) and lower (Figure 14) portions of the water column. The pattern of flow shown in the upper part of the water column is in general agreement with that found by the earlier measurements described in Section 2. Overall southeasterly flow, parallel to the trend of the coastline, is apparent with the strongest portion of the current concentrated over the continental slope, a weaker mean flow over the marginal trough and mean flows that are weaker yet over the central portion of the shelf. The stronger flow over the continental slope corresponds to the main branch of the Labrador Current, while that in the marginal trough appears to be the inner or coastal branch of the current. The two are separated by a zone of more unsteady, but not necessarily less energetic flow.

At most of the sites in Figures 13 and 14, the mean flow vectors are quite closely aligned with the bathymetric contours. The effect is most apparent on the slope (stations 5-3 and 7-3) and in the marginal trough (stations 4-1, 5-1 and 7-1). At stations on the banks (4-2, 4-3, 7-2 and 9-1), the mean currents follow the general southeasterly trend of the adjoining regions. However, the currents do not seem to exhibit any close coupling to the local bathymetry, which is characterized by relatively small gradients. An exception may be observed at station 10-1, where the mean flow is directed toward the coastline at all depths. Inspection of the detailed bathymetry in Figure 3 will show that this flow is more or less aligned with a shallow trench cutting across Saglek Bank. Whether or not the trench is sufficiently sharp to account for the mean flow direction observed at station 10-1 is not clear.

Table 5 summarizes the positional information for each current meter, as well as the mean speed, mean velocity and steadiness factor for its data record. The steadiness factor, B, is defined as 100 times the ratio of the magnitude of the mean velocity to the mean speed. Ramster et al. (1978) suggest that values of B significantly less than 70% characterize unsteady flows for which the vector mean is not representative of their true nature. Examination of Table 5 shows that the highest steadiness factors are associated with stations 5-3 and 7-3, located in the strong shelf-edge flow. Steadiness factors at stations 4-1, 5-1 and 7-1, while still at or near the 70% significance level, are lower than those at stations 5-3 and 7-3. At station 4-1 the steadiness factor at depth (203 m) is much lower than that at 53 m; it should be remembered, however, that the 203 m instrument was only 9 m above the bottom, and may have been subjected to bottom boundary-layer effects. At stations 4-3, 4-2, 7-2, 9-1 and 10-1, all located on the banks, the values of B indicate significantly unsteady flow at all depths. The steadiness factor at station 5-2 (located in Cartwright Saddle) is also low, but the mean speed is significantly larger than that of the stations on the banks.

Some differences in mean vertical shear are also apparent, in Table 5 and in Figures 13 and 14. Considering the stations with steady flow as a group, the inner stations (4-1, 5-1 and 7- 1) show larger vertical mean shears than do the stations on the continental slope. In general, the stations characterized by

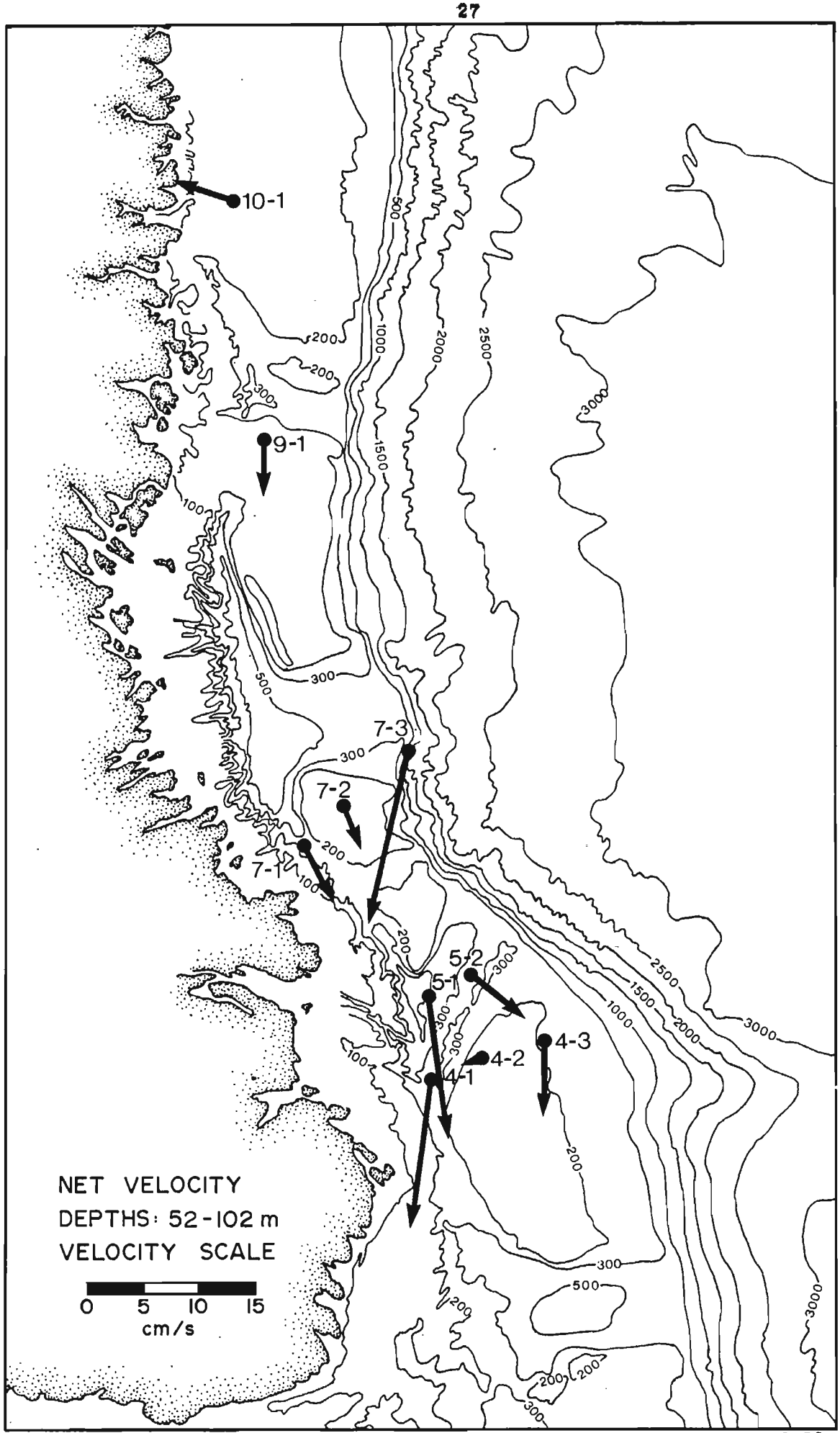

Figure 13: Net velocities from current meter records at depths of 52 to 102 m.

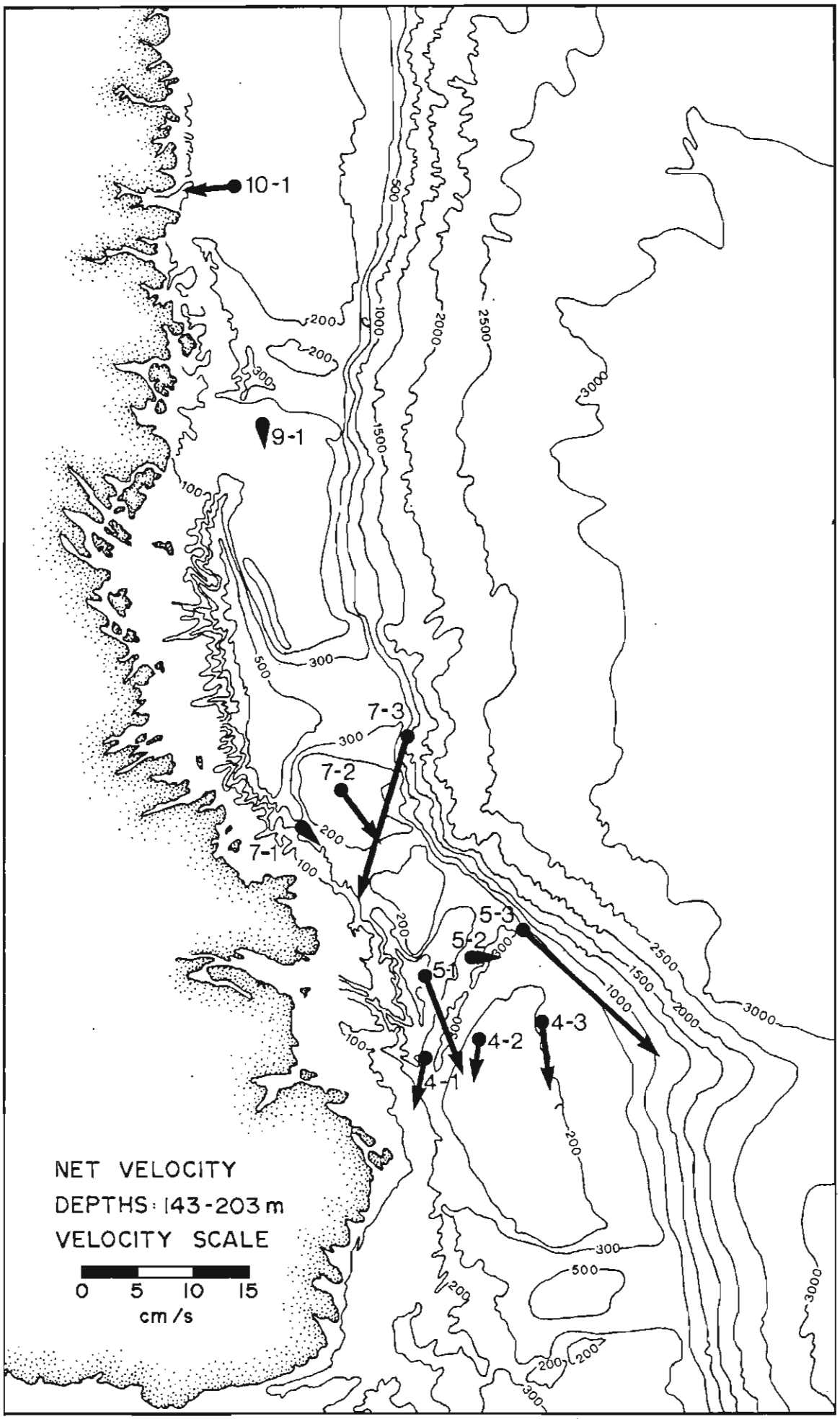

Figure 14: Net velocities from current meter records at depths of 143 to 203 m.

Table 5

A summary of the average current velocity and other parameters for each current meter data set. The steadiness factor B is computed as the ratio of current velocity magnitude to mean speed.

Stn	Latitude	Longitude	Start/Stop Time	No. Days	Depth Inst (m)	Depth Wtr (m)	Vector Mag. cm/s	Vector Dir deg	Mean Spd cm/s	B	Max Spd cm/s
4-1	54 10.0	55 44.0	10/07 11/09	62	52	212	13.3	164	16.3	81	43.5
4-1	54 10.0	55 44.0	10/07 11/09	62	203	212	4.3	164	7.9	54	23.3
4-2	54 25.2	55 15.9	10/07 16/09	67	53	152	1.6	224	10.8	15	37.0
4-2	54 25.2	55 15.9	10/07 16/09	67	143	152	3.5	162	8.0	43	30.4
4-3	54 39.1	54 44.0	11/07 6/10	87	54	220	6.6	157	14.2	47	49.1
4-3	54 39.1	54 44.0	11/07 6/10	87	153	220	5.4	146	9.5	57	38.3
4-3	54 39.1	54 44.0	11/07 6/10	87	171	220	4.8	140	9.1	52	37.7
5-1	54 37.4	56 7.7	6/07 16/09	71	58	523	12.7	150	16.3	78	53.2
5-1	54 37.4	56 7.7	6/07 16/09	71	156	523	9.2	139	12.1	76	42.4
5-1	54 37.4	56 7.7	6/07 16/09	71	514	523	*	*	4.9	*	17.9
5-2	54 51.7	55 47.2	6/07 6/10	92	31	273	6.7	109	23.9	28	86.0
5-2	54 51.4	55 47.9	6/07 6/10	91	57	278	5.9	110	20.5	29	74.3
5-2	54 51.4	55 47.9	6/07 6/10	91	158	278	2.4	68	12.3	19	33.0
5-2	54 51.4	55 47.9	6/07 6/10	91	269	278	3.0	326	9.4	32	28.6
5-3	55 11.0	55 16.1	11/07 13/09	64	62	326	*	*	35.0	*	82.7
5-3	55 11.0	55 16.1	11/07 13/09	64	159	326	17.8	111	19.2	92	57.9
5-3	55 11.0	55 16.1	11/07 13/09	64	277	326	11.5	119	13.8	83	40.9
7-1	55 15.0	58 5.9	3/07 12/09	71	64	274	6.9	126	11.2	62	45.9
7-1	55 15.0	58 5.9	3/07 12/09	71	162	274	2.8	112	8.5	33	40.1
7-1	55 15.0	58 5.9	3/07 12/09	71	265	274	**	**	**	**	**
7-2	55 36.6	57 46.7	4/07 12/09	70	25	154	5.6	139	17.3	33	58.4
7-2	55 36.5	57 47.4	3/07 12/09	70	55	154	4.5	138	14.6	31	47.4
7-2	55 36.5	57 47.4	3/07 12/09	70	145	154	6.1	122	11.8	52	33.4
7-3	56 2.5	57 24.2	4/07 12/09	69	102	706	16.1	171	17.7	91	52.8
7-3	56 2.5	57 24.2	4/07 12/09	69	202	706	14.6	175	16.0	92	45.2
7-3	56 2.5	57 24.2	4/07 31/08	58	656	706	3.4	185	5.6	61	28.8
9-1	57 32.3	60 28.3	18/07 1/10	75	56	165	4.9	154	10.7	45	34.4
9-1	57 32.3	60 28.3	18/07 1/10	75	156	165	1.8	144	7.5	24	24.3
10-1	58 53.3	62 10.3	15/07 30/09	76	62	179	5.4	261	14.0	39	46.7
10-1	58 53.3	62 10.3	15/07 30/09	76	170	179	5.4	243	12.0	45	34.0

---

* No Direction Data

** Suspect Speed Data

more unsteady flows exhibit smaller mean vertical shears than do the stations with steadier flows, with the exception of station 5- 2.

The above comparisons lead to a division of the area's circulation into four categories (see Figure 15):

i) strong, very steady flows and moderate vertical shear, associated with locations at or near the continental slope.

ii) flows which are relatively strong and steady (but less so than (i) in both senses) and which appear to have large vertical shear, associated with locations in the marginal trough.

iii) unsteady flows, with weak vertical shear and moderate energy, associated with stations located on the banks of the continental shelf.

iv) unsteady flows with high energy and moderate vertical shear, found at locations in saddles.

Group (i) comprises stations 5-3 and 7-3, group (ii) comprises stations 4-1, 5-1 and 7-1, group (iii) comprises stations 4-2, 4-3, 7-2, 9-1 and 10-1, and group (iv) comprises station 5-2. There are, of course, differences within each group, but on the basis of the above criteria of steadiness, energy and vertical shear, the definition of the groups is quite clear. Since the association is evident, the different flow regimes will be referred to by their bathymetric equivalents, i.e. as the slope, trough, bank or saddle regimes.

5.2 CURRENT METER DISTRIBUTIONS

On the basis of the averaged vector currents and mean speeds, four types of circulation categories were identified corresponding to particular bathymetric regimes: continental slope, marginal trough, banks and saddles. These categories can be examined further using the speed and directional distributions from each current meter record. In Figures 16 and 17, current roses are plotted for data sets collected at depths between 52 and 10 m and 143 and 203 m, respectively. Speed distributions for depths between 52 and 102 m are presented in Figure 18.

At the two stations located on or near the slope (5-3 and 7- 3), the directional distribution is dominated by a single prominent peak parallel to the local bathymetric contours. For the three complete records available between 102 and 202 m depth, at these two stations, over 80% of the current measurements fall within 35 degrees of the peak directional value. The strongest currents were found to occur along the preferred direction of flow while flows directed across the slope were markedly weaker. The speed distributions of the slope currents reflect the relatively strong flows encountered in this bathymetric regime; the histograms are shifted to noticeably higher speed levels in comparison with those obtained in other areas.

The strong, uni-directional flows associated with the slope regime extend over the outer edge of the continental shelf. This is clearly the case at station 5-3, located about 6 km from the shelf break, where the speed and directional distributions reveal currents associated with slope flows. In fact,

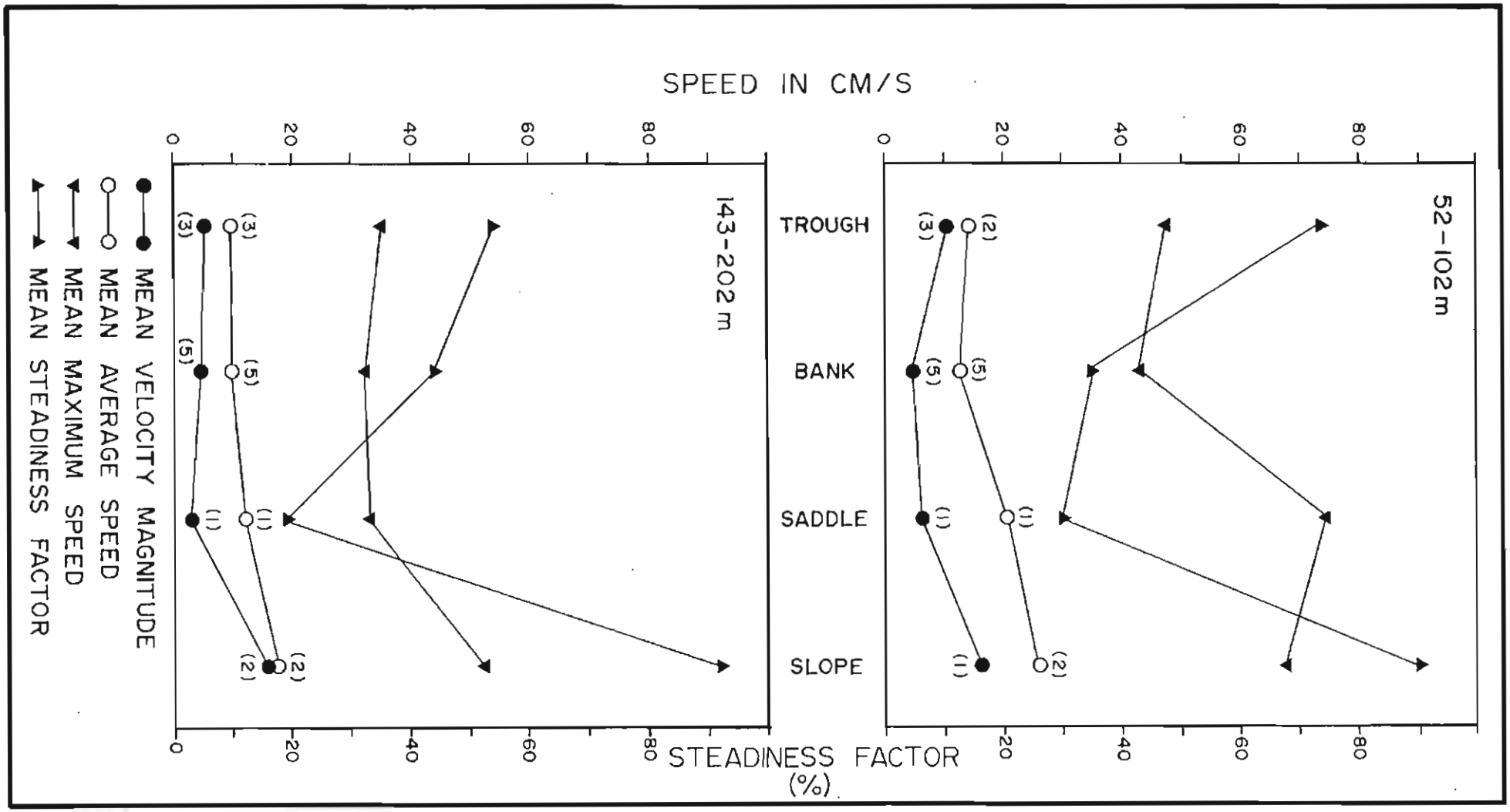

Figure 15: The velocity magnitude, mean speed, maximum speed and steadiness factor averaged according to type of bathymetric regime at measurement location. The values in parentheses indicate the number of data sets used to compute these quantities.

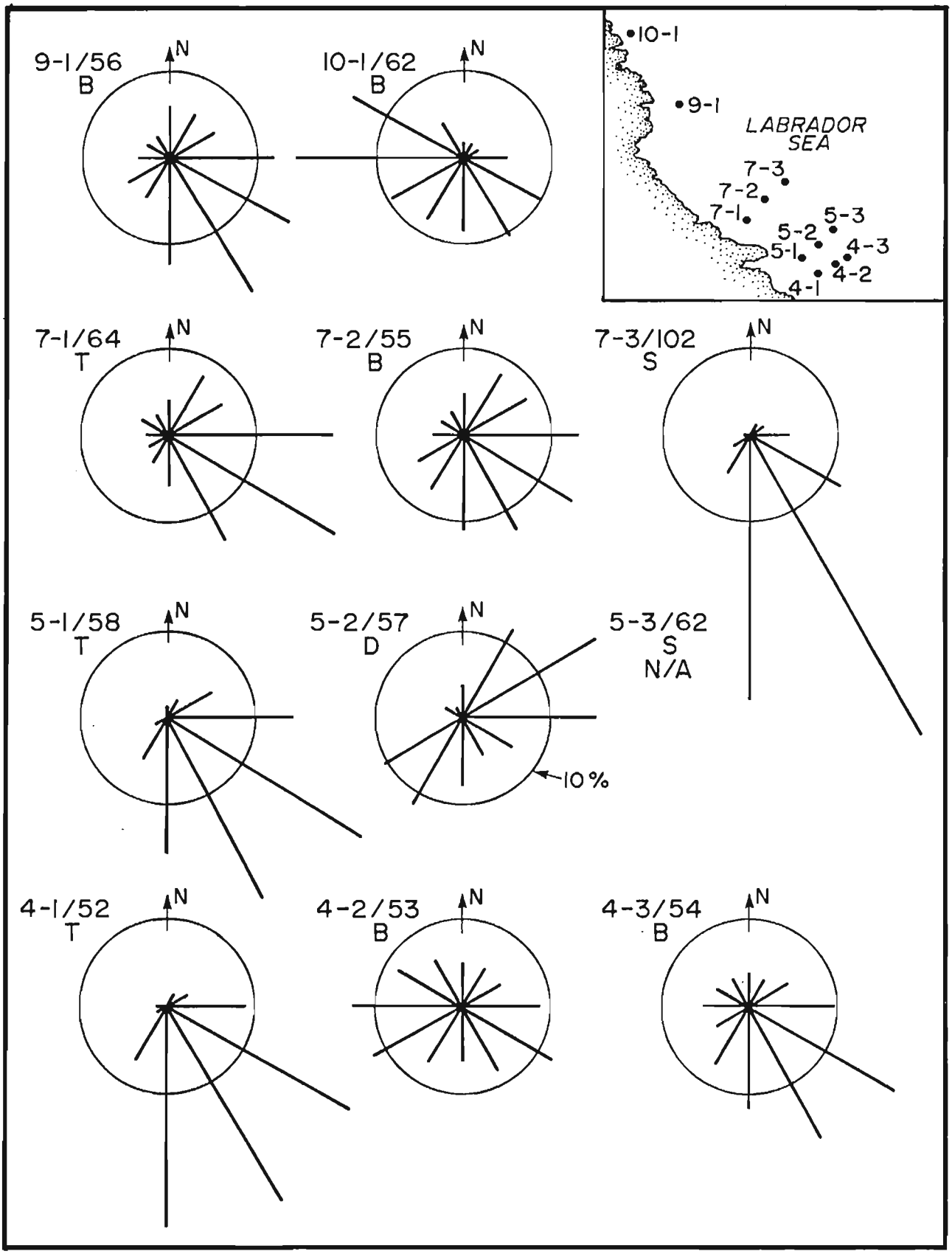

Figure 16: Directional distributions of current meter data obtained between 52 and 102 m depth.

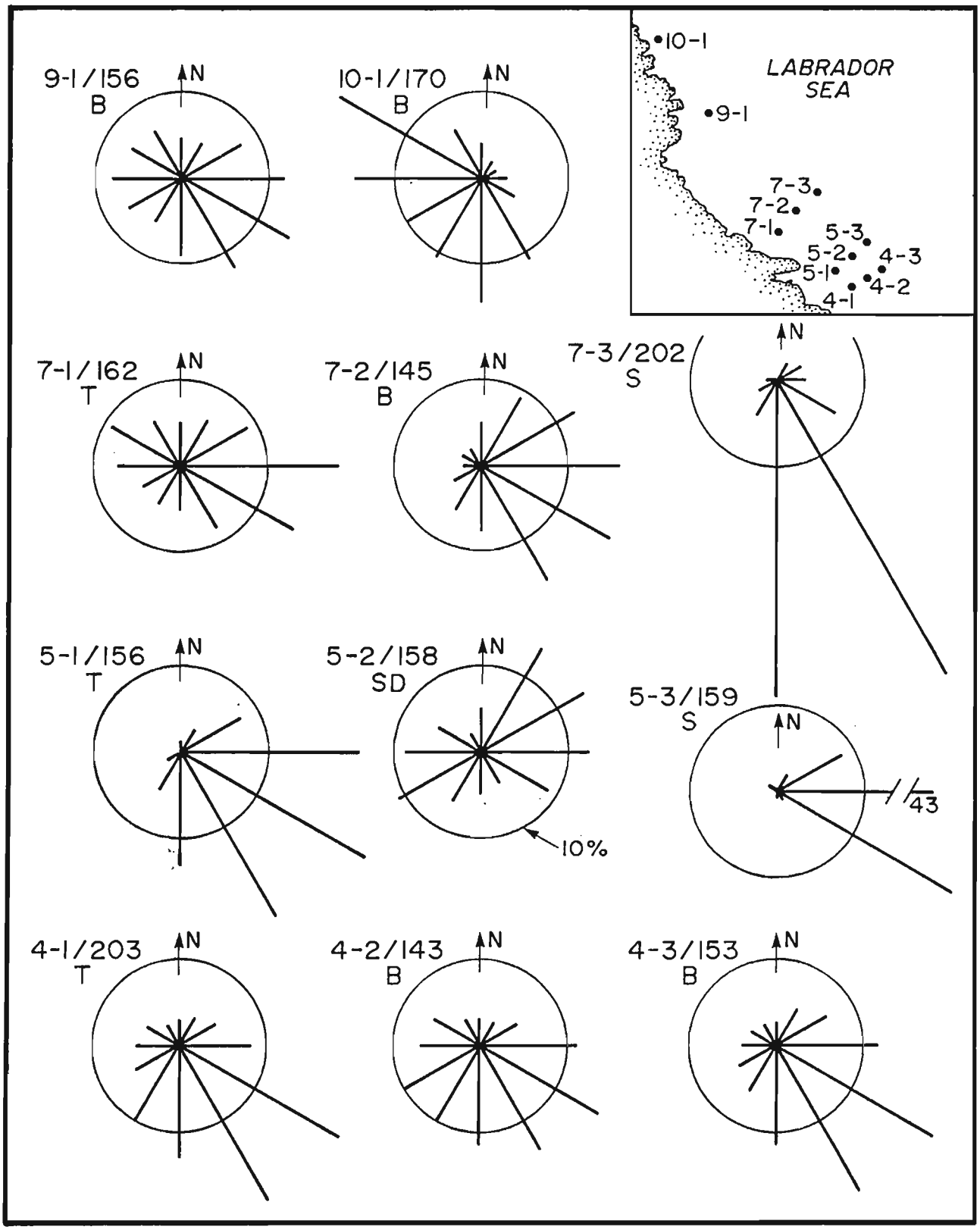

Figure 17: Directional distributions of current meter data obtained between 143 and 203 m depth.

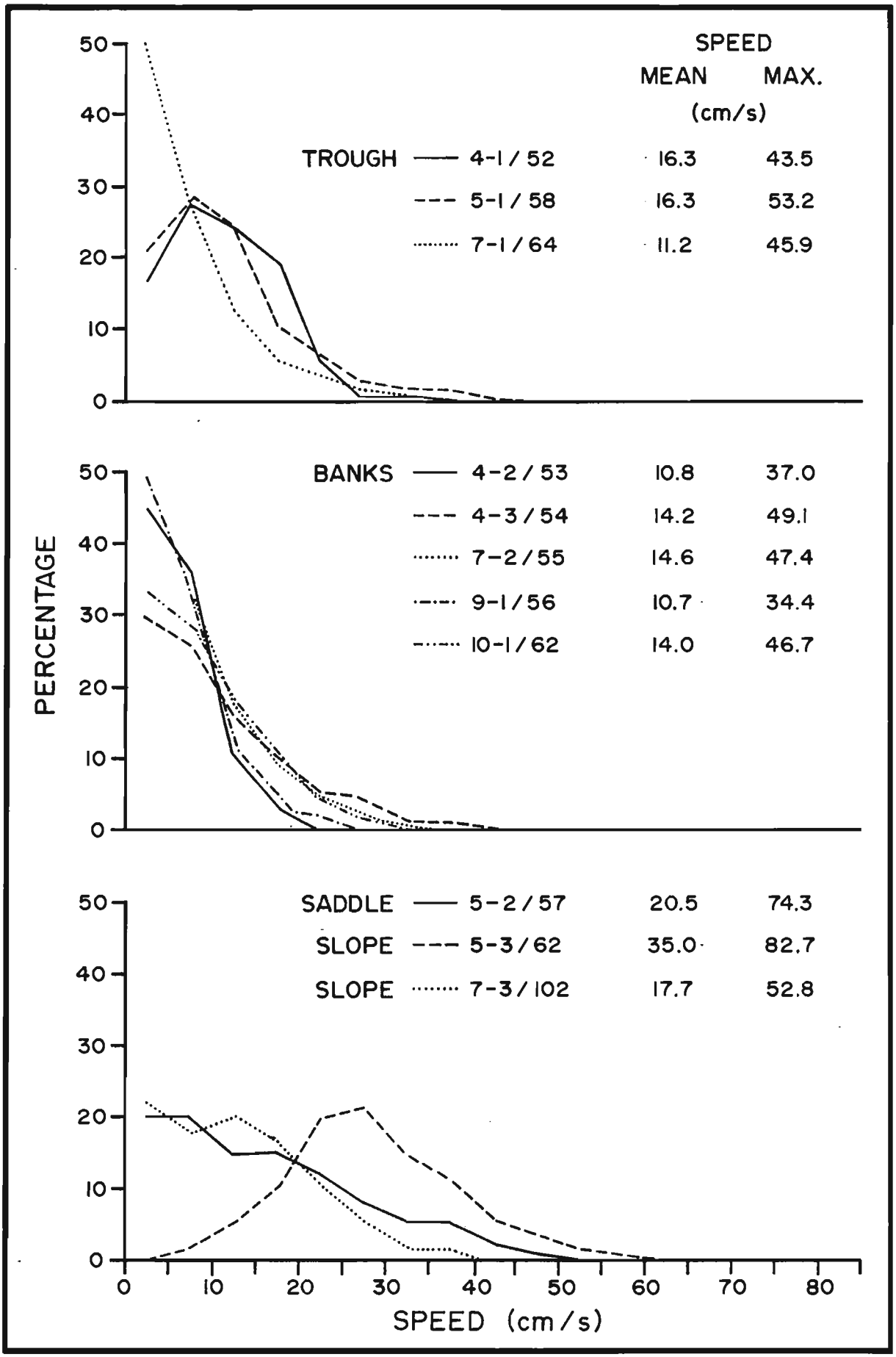

Figure 18: Speed distributions of current meter data obtained between 52 and 102 m depth.

the speeds at 62 m depth recorded at this location are consistently larger than those at any other measurement site (Figure 18).

Currents flowing over the marginal trough have a high degree of directional stability, although less so than currents over the continental slope. The directional distribution exhibits a single peak, somewhat broader than that of the slope regime. At stations 4-1 and 5-1, virtually no currents were found to flow against the preferred flow direction. However, at station 7-1, reversals did occur occasionally. The speeds measured at trough locations were consistently lower than those of the slope regime. While the strongest flows often followed the most common direction, this was not always the case. For example, at 4-1/52 while the directional distribution peak was at 180 degrees, and strong flows (43 cm/s) did occur in this direction, currents nearly as strong (40 cm/s) were measured with directions of 90 degrees.

At trough locations, the currents showed less of a tendency to follow local bathymetric contours than on the continental slope. Differences of about thirty degrees between the most common direction and the direction of the local bathymetry were found for all three trough stations at both the 50 and 150 m measurement levels.

Flows over the banks of the continental shelf exhibit a high degree of directional variability. The directional distributions (Figures 16 and 17) demonstrate that currents can occur in any direction. At some locations, however, a broad peak (or peaks) in the distribution indicates preferred flow directions. This is most evident at station 10-1 where westerly to northwesterly flows are prevalent, possibly reflecting the influence of an east-west trench immediately to the north of the measurement site. At three of the remaining four moorings located on banks (4-3, 7-2 and 9-1) more of the measured directions fell in the southeastern quadrant than in any other. The directions of the net velocity, though small, and of the largest measured currents also occur in the southeasterly quadrant. This weak southeasterly directional preference may reflect the influence of the Labrador Current, possibly as occasional meanders or eddies propagating onto the bank.

Current speeds over the banks are generally weaker than those observed at other continental shelf locations. At 50 m depth mean speeds range from 10 to 15 cm/s among the measurement locations, with maximum values of 35 to 50 cm/s. Mean speeds decrease relatively little with increasing depth: at 150 m depth, the average values range from 8 to 12 cm/s with corresponding maximum speeds of 24 to 38 cm/s.

At the one current meter station located in a saddle, the observed flows appear to have characteristics distinct from those of the other bathymetric regimes. The directions measured at station 5-2 in the Cartwright Saddle have a bi-modal distribution with peaks in the northeasterly and southwesterly directions at 31 and 57 m depth. At greater depths, the southwesterly peak is shifted to westerly with the northeasterly peak being largest at 158 m and the westerly peak dominant at 269 m. The local bathymetry in the vicinity of station 5-2 is complex with an overall north-south orientation through the saddle.

Speeds measured at the saddle location are variable. Occasionally the speeds are high with a maximum value of 74.3 cm/s at 57 m depth. However, the many occurrences of speeds less than 15 cm/s limit the average speed to 20 cm/s. Strong flows tend to occur along the preferred directions described above.

5.3 WATER PROPERTIES

With the exception of the near-surface layer, the waters of the Labrador coast may be divided into three distinct masses, each with a well-defined range of temperature and salinity. Figure 19(a) and (b) shows, respectively, cross sections of temperature and salinity at line 4 on Hamilton Bank, August 1 to 3. On the shelf, at depths less than 200 m and within 200 km of the shore, there is a large mass of uniformly cold water with essentially linear salinity stratification. This water, all at temperatures between 0 and -1.7°C (with the bulk of it being between -1.0°C and -1.5°C) has salinities between 32.60 and 33.70°/oo. It is overlain by a shallow (20-30 m) surface layer which is much warmer and fresher, being subjected to solar heating and run-off of fresh water. The majority of this cold water mass (called Shelf Water) is thought to originate in the Arctic regions and Baffin Bay, from whence it is carried south by the Baffin Current. Some additional input of cold, relatively fresh water from Hudson Bay is thought to join the Baffin Current via Hudson Strait (Smith, Soule and Mosby, 1937).

The zone beyond the continental slope (i.e. at stations 412 and 413 in Figure 19) is occupied by Labrador Sea water, which has temperatures between 3 and 4°C and salinities between 34.7 and 34.9°/oo. This water mass exists seaward and below the region of strong temperature gradient over the continental slope (stations 410, 411 and 412 in Figure 19(a)), down to the limit of measurements at 1000 m. As in the case of the Shelf Water, it too (seaward of the slope region) is overlain by a surface layer, which in this case is warmed by the sun, but is not significantly affected by fresh water input.

The Labrador Sea Water and the Shelf Water are separated by a transition zone, visible in Figure 19 as a region of strong gradient in both temperature and salinity which slopes upward and seaward away from the shelf break. The water in this zone (Slope Water) exhibits temperature and salinity properties which lie between those of the Labrador Sea Water and those of the Shelf Water. Figure 20(a), a composite plot of the temperature- salinity curves from stations located beyond the shelf break occupied during cruise A, illustrates the mixed nature of the Slope Water. The cluster of points near 3°C represents the Labrador Sea Water. Some Shelf Water is apparent at salinities less than 33.5°/oo, with temperatures between -0.5°C and -1.0°C. The Slope Water is represented by the envelope of points falling along a straight line between the Shelf and Labrador Sea Water. Figure 20(b), is the corresponding plot for stations up to the shelf break. It consists largely of Shelf Water, with some Slope Water visible. Envelopes defining the three water masses are shown in Figure 21.

At depth in the marginal trough (e.g. stations 403 and 404 in Figure 19), the water characteristics were too warm and too saline to be Shelf Water. It has the characteristics of Slope Water and was continuously present as may be seen from the time series measurements of temperature and salinity which are available from most of the current meters. Figure 22 shows the

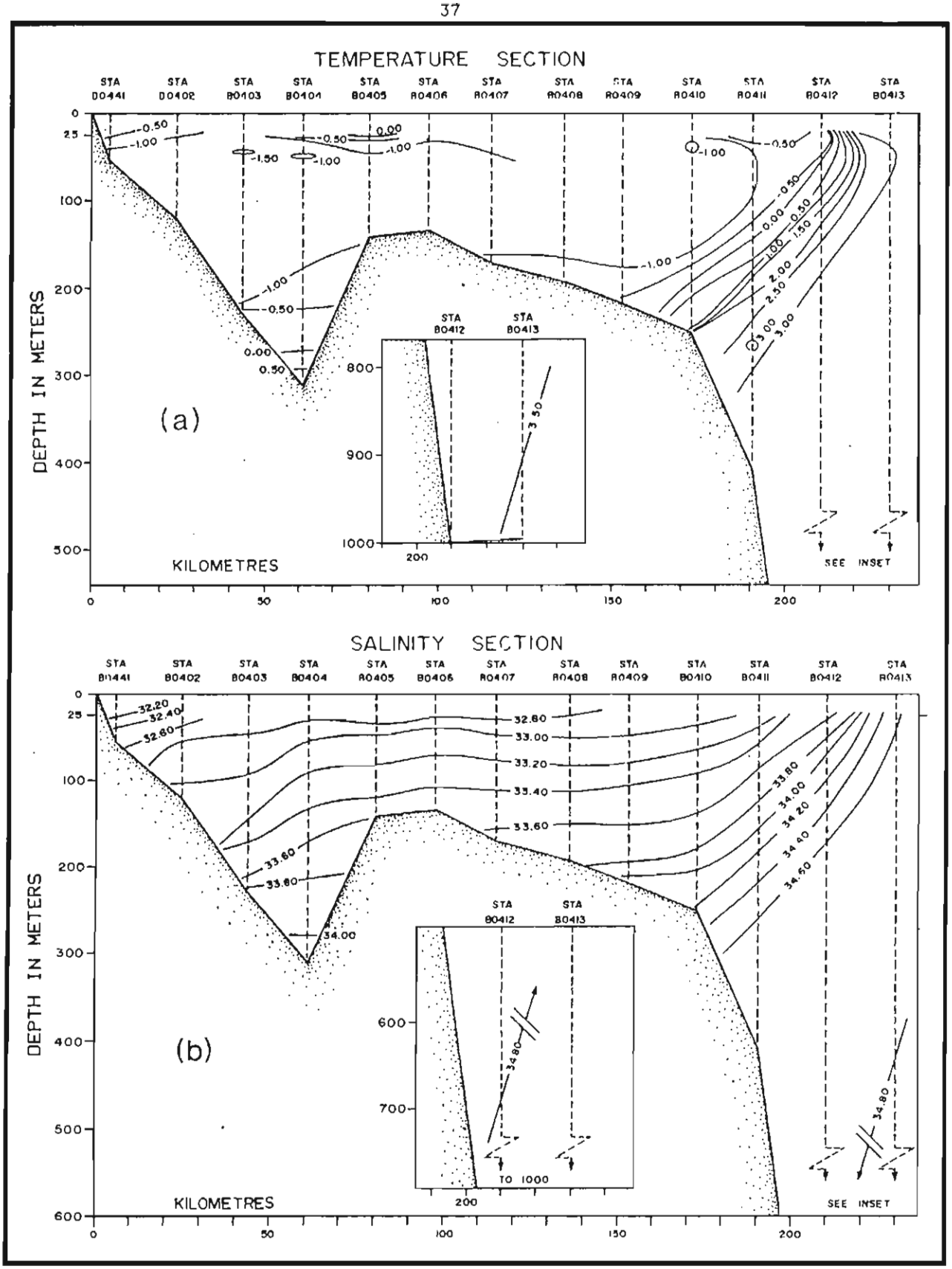

Figure 19: (a) Cross section of temperature, Hamilton Bank, August 1-3.
(b) Cross section of salinity, Hamilton Bank, August 1-3.

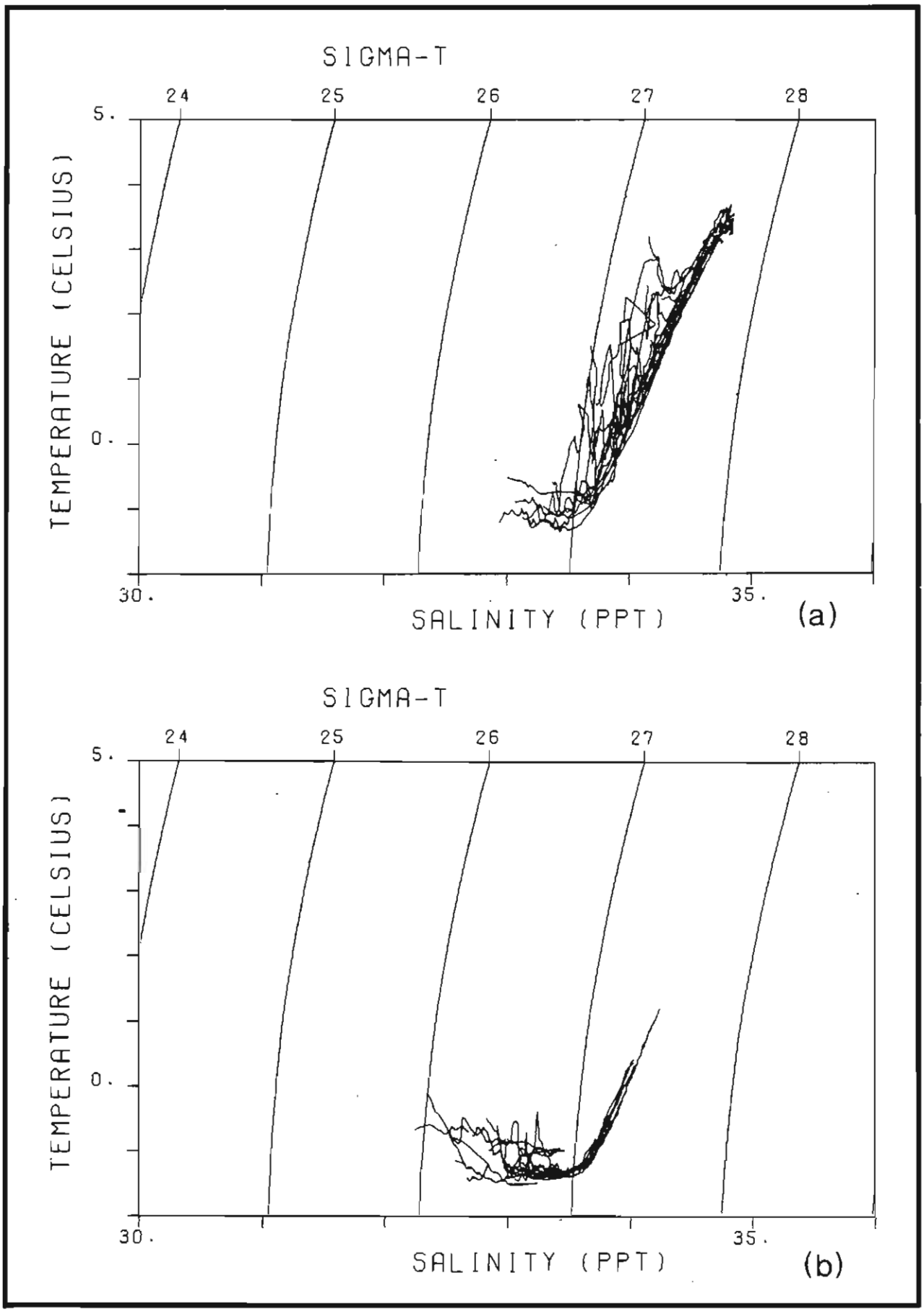

Figure 20: Temperature-salinity characteristics measured July 18-30 for (a) Slope and Labrador Sea regions (b) Shelf and Slope regions.

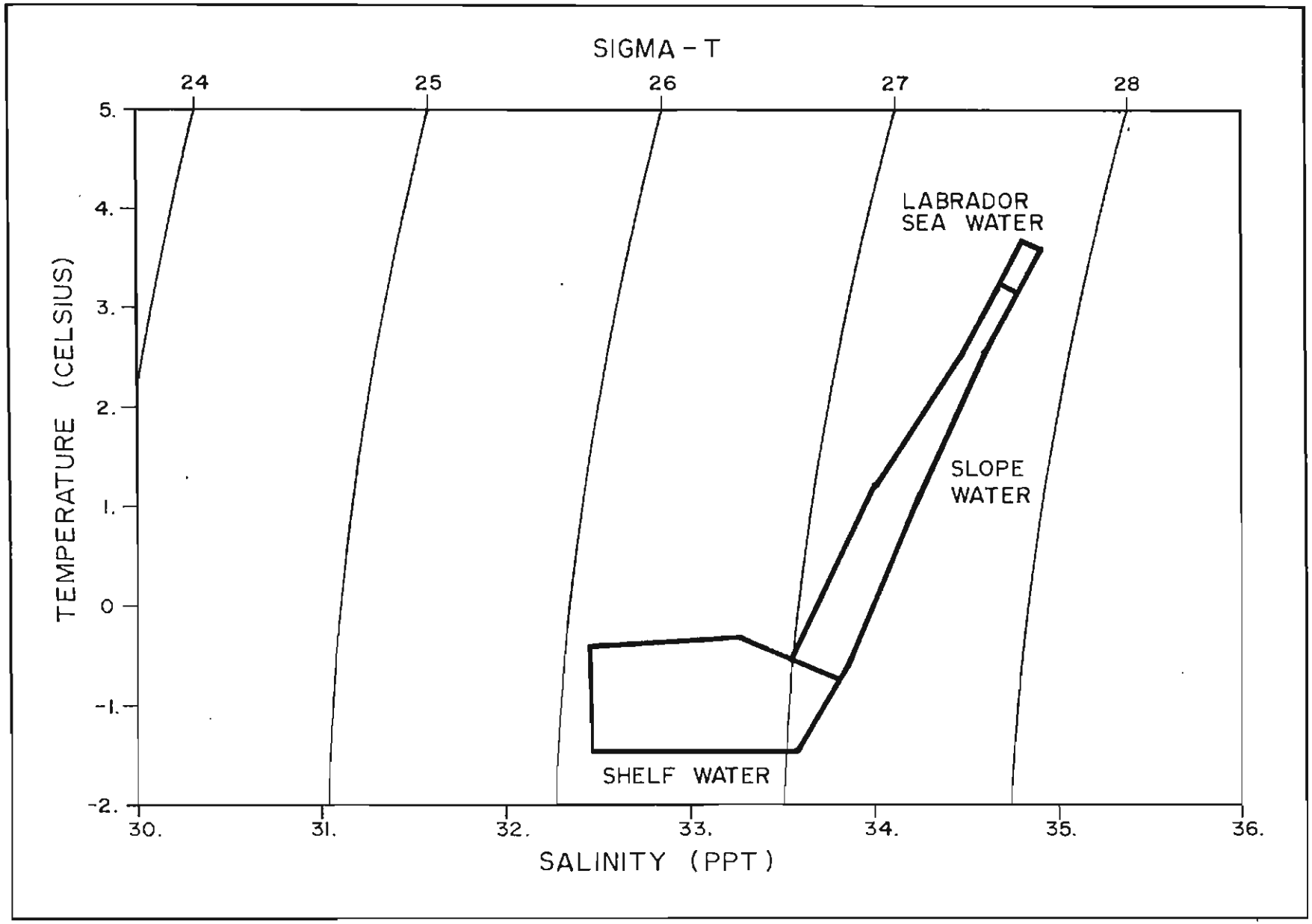

Figure 21: Schematic diagram of Labrador coast water masses.

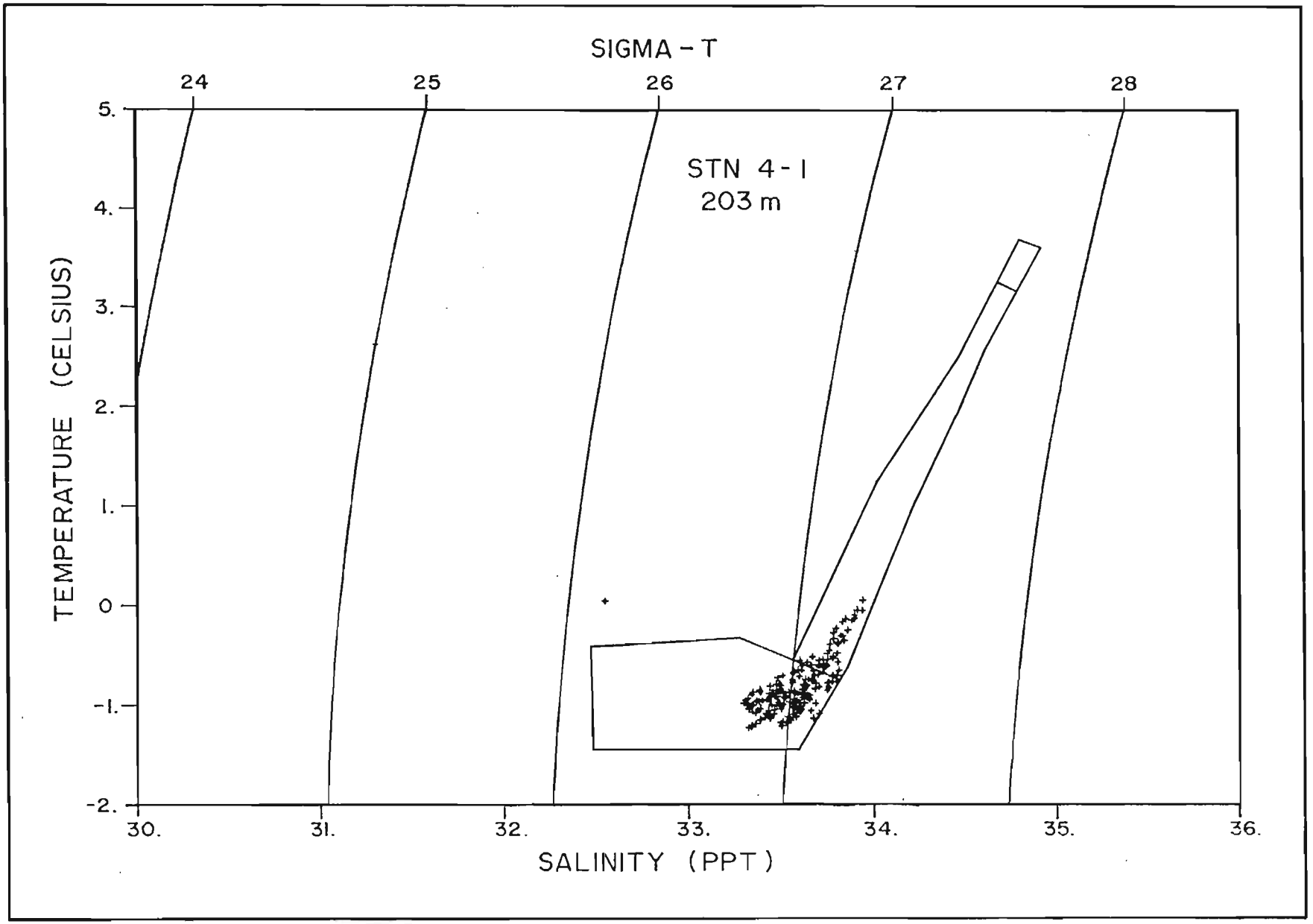

Figure 22: Temperature-salinity characteristics at 203 m depth at mooring 4-1.

temperature-salinity characteristics from the current meter at 203 m depth at mooring 4-1 (situated between CTD stations 403 and 404). Even at that relatively shallow depth, some Slope Water is apparent; the effect is even clearer at the 265 m instrument at station 7-1 (Figure 23). Slope Water is also present over a significant fraction of the water column in the saddles. Figures 24(a) and (b) show, respectively, cross-sections of temperature and salinity along line 5 through Cartwright Saddle, August 26 and 27. Water with temperatures between 0°C and 2.5°C, and salinities 34.0 to 34.6°/oo is present from 150 or 200 m to the bottom through the whole saddle, which suggests that Slope Water occupies all of the lower part of the water column in Cartwright Saddle. Figure 25, which is a plot of the temperature-salinity characteristics from 158 m at mooring 5-2 (coincident with CTD station 505) confirms that the water at depth in the saddle is indeed Slope Water. The same effect may be seen in Hopedale Saddle, in the temperature and salinity cross sections from line 8 (Figure 26(a) and (b)).

The horizontal distributions of temperature and salinity at 100 m (Figure 27(a) and (b) shows the August 19-28 case) also help to define the spatial distribution of the three water masses. At that depth, the Shelf Water is visible as a body of sub-zero temperature water, with little horizontal gradient in salinity. The Labrador Sea Water is apparent along the outside edge of the station pattern where the temperature is near 3°C and the salinity is above 34.6°/oo. The Slope Water can be seen as a zone of strong horizontal gradient in both temperature and salinity, which separates the Shelf and Labrador Sea Waters. An indication of the presence of the Slope Water in the saddles is shown by the shoreward displacement of the zone of temperature and salinity gradient at line 8 and, less clearly, at line 5.

The geographical distribution of the water masses present along the Labrador coast may be summarized as follows: With the exception of a near-surface layer, about 25 m deep, which is subject to the influence of solar radiation and runoff, the shallow waters of the shelf (in particular the banks and the upper 100 to 150 m of the water column in the saddles) consist of cold, low-salinity Shelf Water, chiefly of Arctic origin. Beyond the continental shelf, the upper 1000 m of the water column (again, with the exception of the near-surface layer) consists of Labrador Sea Water with a temperature near 3°C and salinities from 34.7 to 34.9°/oo. These two water masses are divided along the shelf break and the upper part of the continental slope by Slope Water, which exhibits a range of temperatures and salinities between those of the Shelf and Labrador Sea Waters, and appears to be formed from a mixture of them. Slope Water is also found at the bottom of the marginal trough, and in the lower half of the water column in the saddles.

5.4 GEOSTROPHIC CIRCULATION

In a highly variable area containing extensive regions of shallow water, computations of currents by the dynamic method, using an assumed level of no motion, are unlikely to yield accurate results. Over the shallow shelf area, a variety of influences, such as friction and accelerations caused by local winds may cause significant departures from geostrophic balance. It is also quite likely that significant barotropic currents arising from sea surface slopes (e.g. against the coastline) may be present. Since, with but a few exceptions, the stations in this program were taken in relatively shallow Shelf

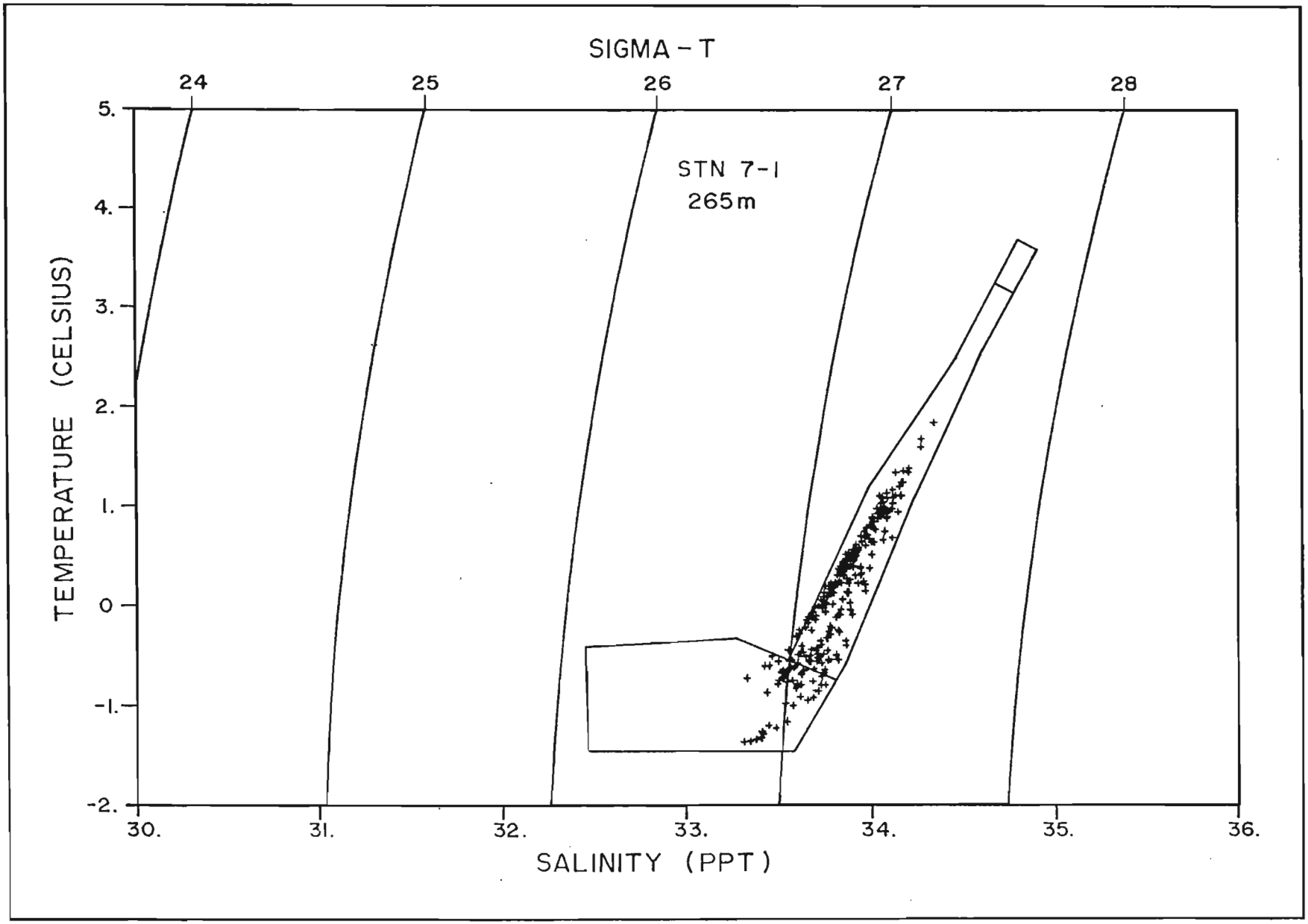

Figure 23: Temperature-salinity characteristics at 265 m depth at mooring 7-1.

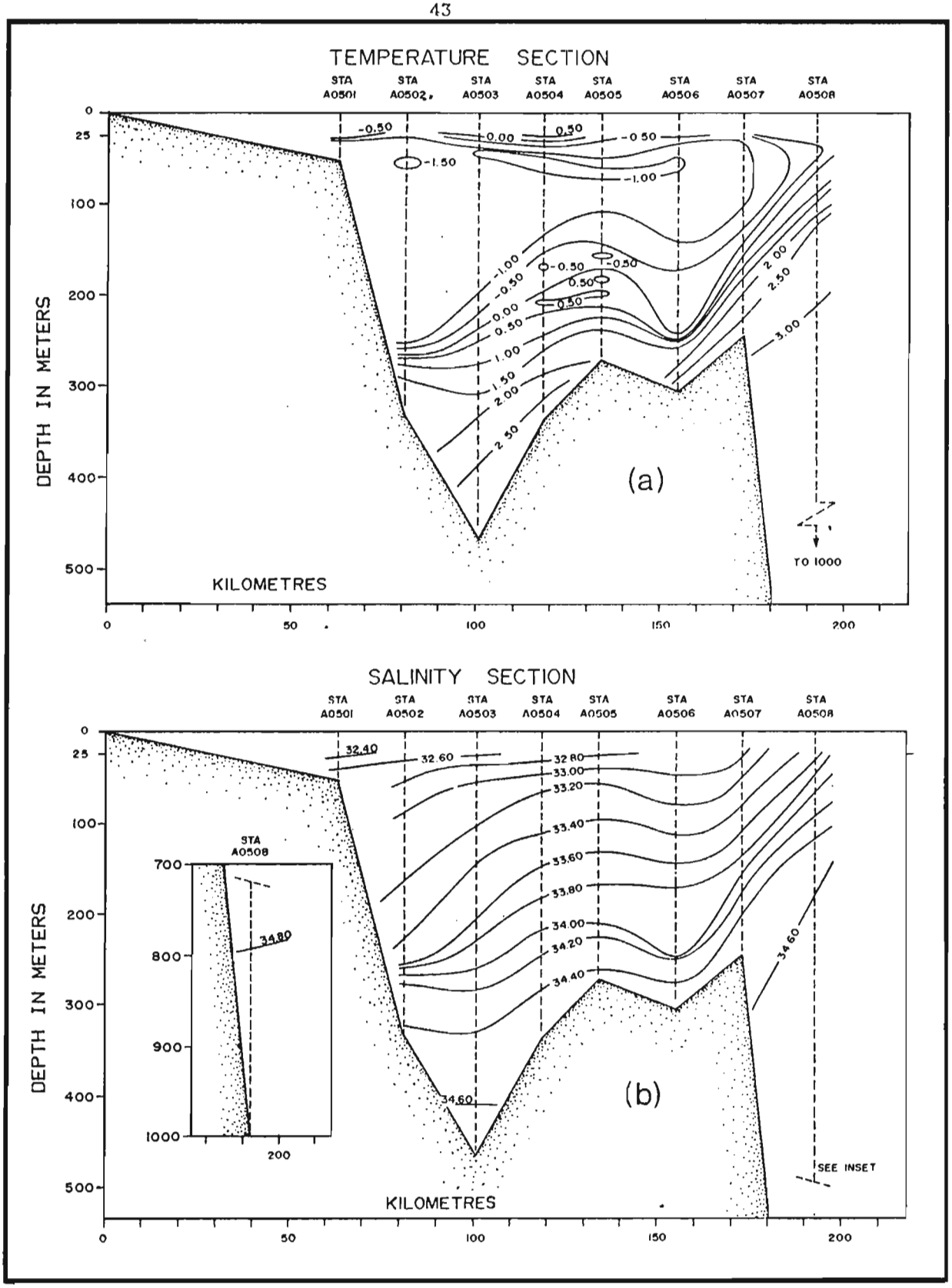

Figure 24: (a) Temperature cross section, through Cartwright Saddle (line 5), August 26-27. (b) Salinity cross section through Cartwright Saddle (line 5), August 26-27.

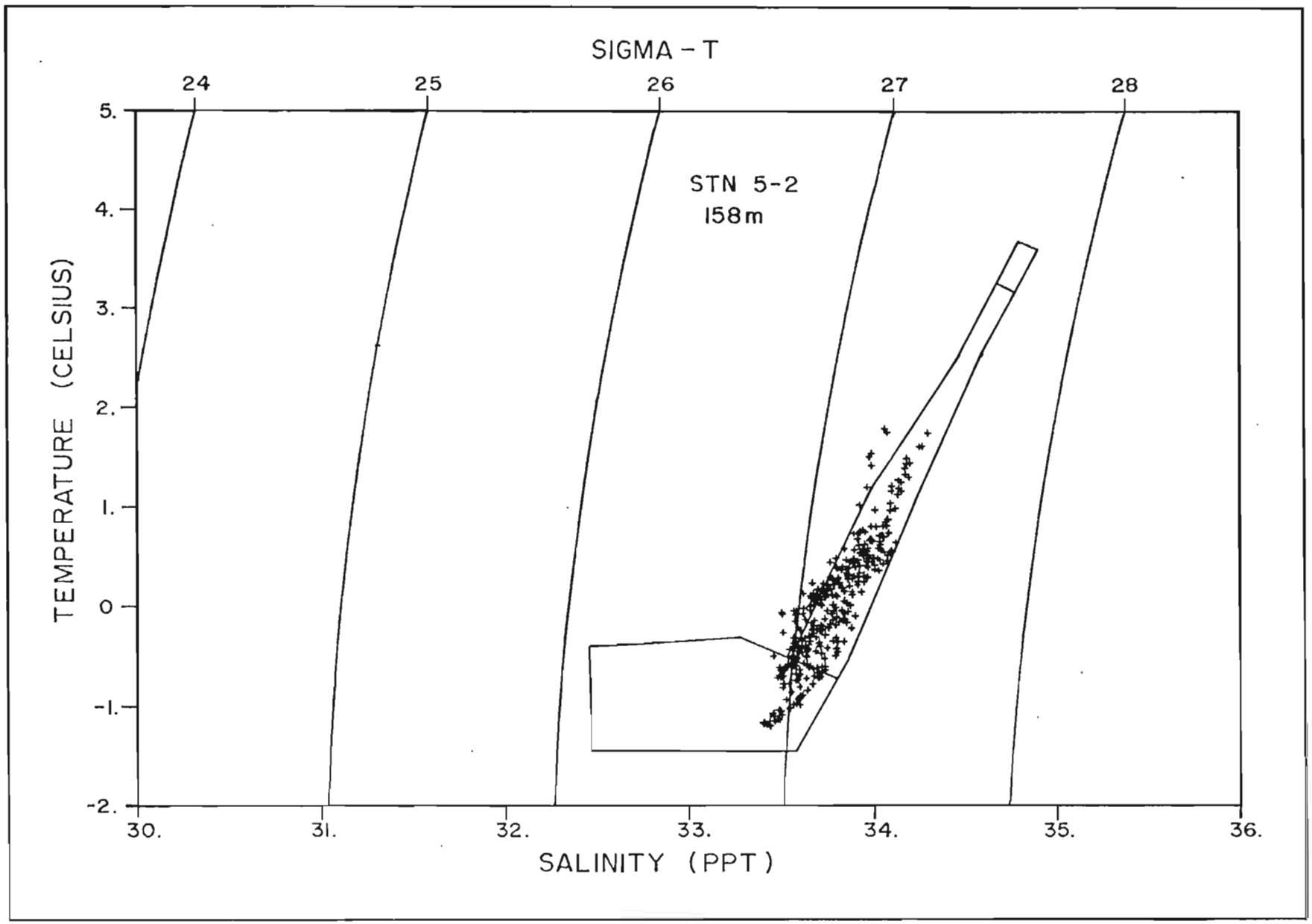

Figure 25: Temperature-salinity characteristics for 158 m depth at mooring 5-2.

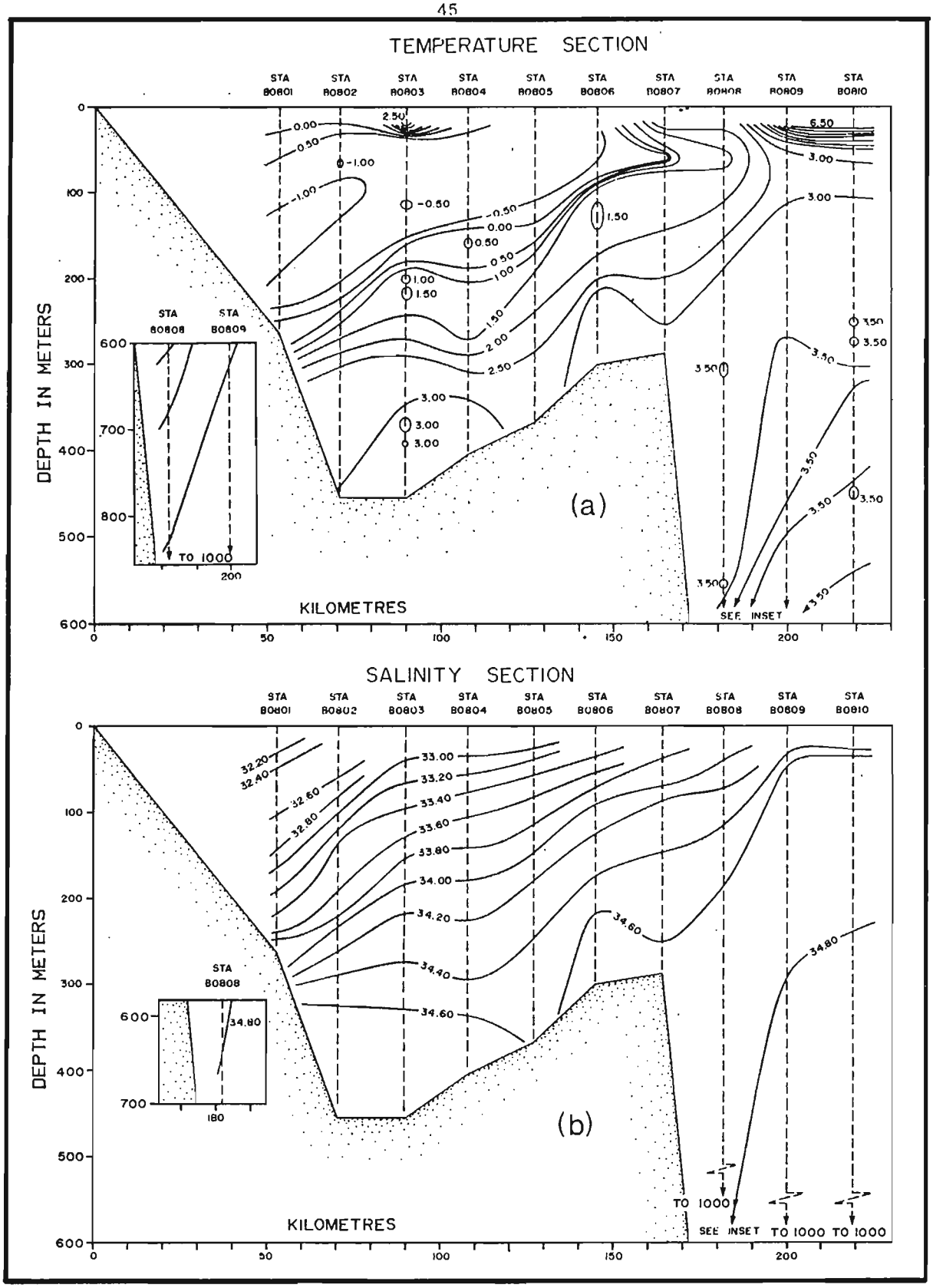

Figure 26: (a) Temperature cross section through Hopedale Saddle (line 8), August 5-6. (b) Salinity cross section through Hopedale Saddle (line 8), August 5-6.

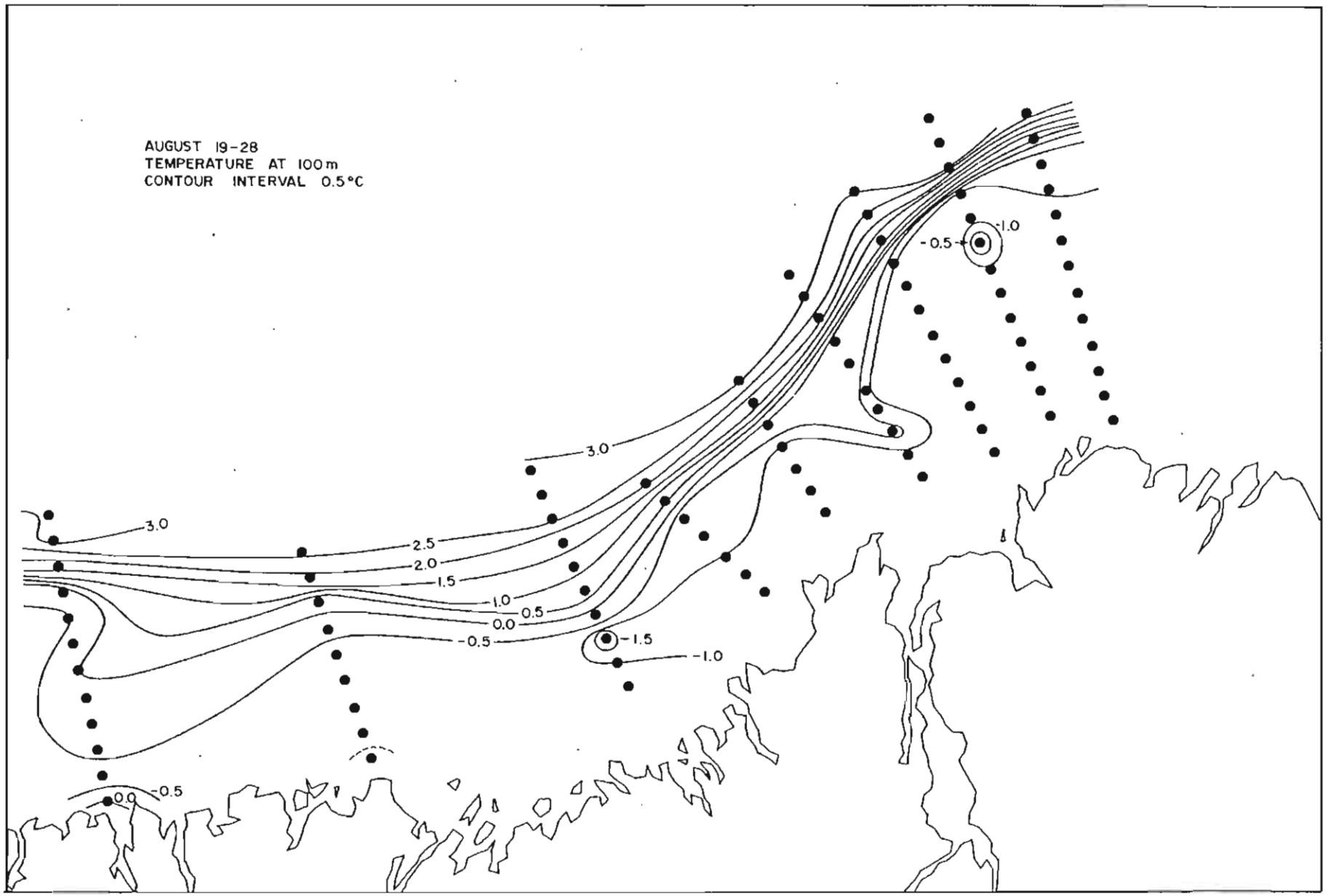

Figure 27a: Horizontal distribution of temperature at 100 m depth, August 19-28.

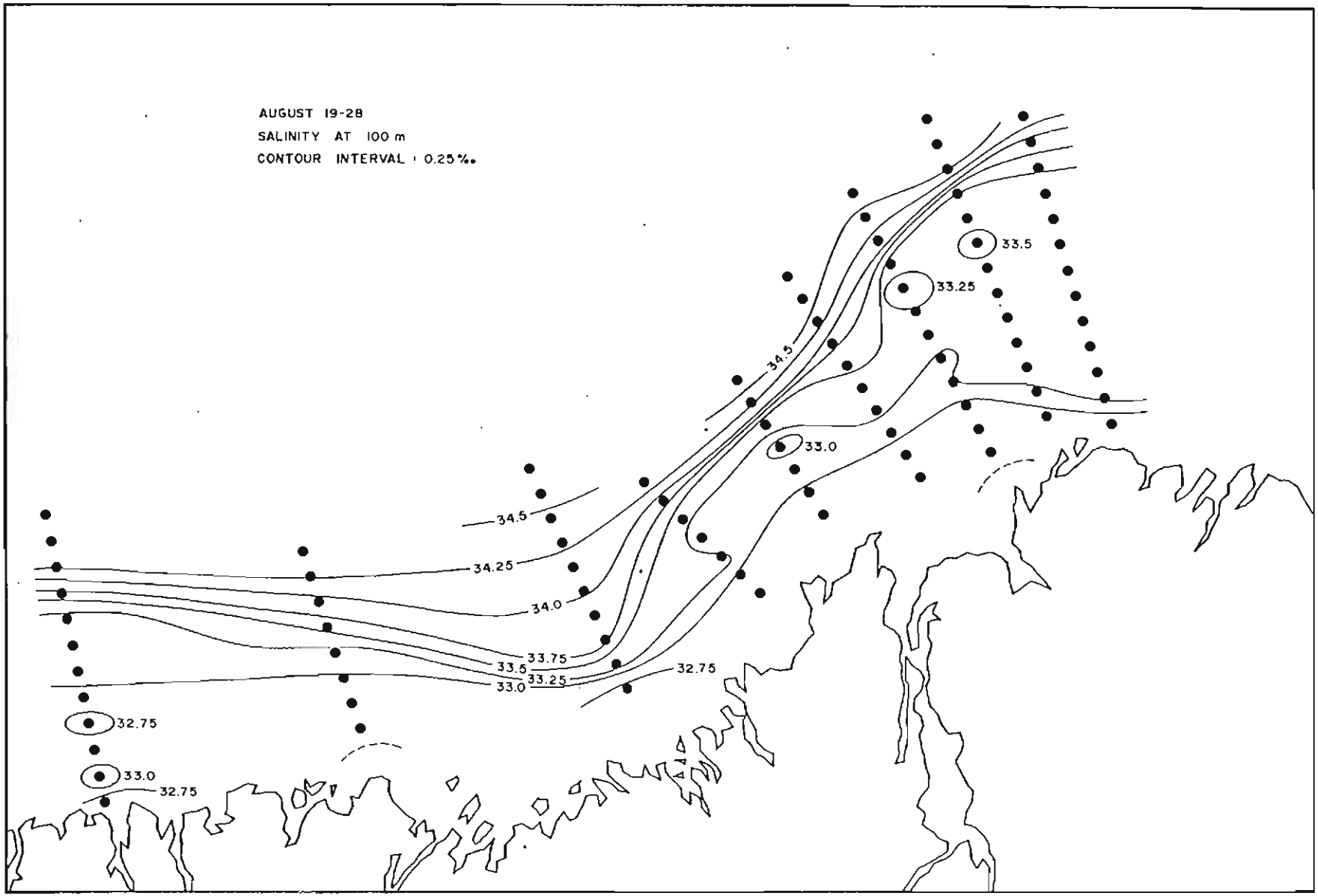

Figure 27b: Horizontal distribution of salinity at 100 m depth, August 19-28.

and Slope Waters, it is not likely that a level of no motion (if any existed) was reached, or, in the event that it was reached by the small number of offshore stations occupied, that sufficient points were occupied to allow extrapolation of the reference level into the shelf zone.

The data from the current meter moorings, however, provide an alternative approach. An arbitrary reference level may be chosen, to which the dynamic topography is referred, and then the flow at that level may be estimated from the current meter moorings. If the moorings were sufficiently dense to define the field of flow at the reference level, then both the barotropic and baroclinic portions of the mean flow can be defined. Before the separation can be done, however, a method for treating the current meter data to make them compatible with the CTD data must be found.

When making comparisons between current meter records and currents derived from CTD data, it is necessary to eliminate the higher-frequency fluctuations (e.g. tidal currents) in the record. Since only the baroclinic portion of the geostrophic flow can be deduced from CTD measurements (Pond and Pickard, 1978), the appropriate comparison is between parallel components of the vertical shear of the current as measured at a mooring and computed from a nearby pair of stations. If the current field is in geostrophic balance (or close to it), then there should be agreement between the measured and computed shears at some consistent averaging or low-pass filtering period for the current meter data.

The velocity time series were first passed through a digital low-pass filter, to remove variations at diurnal and higher frequencies. (The characteristics of the filters are described in Section 4.1.) All the moorings were placed in the lines of CTD stations; most were placed between a pair of stations, with the remainder being coincident with a station (see Figure 7). If the mooring was between two stations, comparisons were made between the measured shear and the shear computed from that pair; if the mooring was coincident with a station, the comparison was made with the two pairs formed by that station and its immediate neighbours.

In all cases, progressively longer averages of the component of the low-passed current perpendicular to the line of CTD stations were made, beginning at the time of occupation of the stations, and working backward in time. The corresponding averages of the component of shear normal to the CTD line were then computed, and the averaging times which produced the best agreement noted. Table 6 summarizes these times and the values of the shear derived from both data sets.

In most cases, the averaging times required to produce the closest agreement were quite consistent, and with some exceptions the agreement was within 30%. The average agreement time, for all cases where agreement was found, was 2 $\pm$1.5 days. Separating the moorings into their various topographic classes produced the following results:

a) Trough stations: 1.5 $\pm$0.8 days
b) Slope stations : 1.5 $\pm$1.1 days
c) Bank stations : 1.7 $\pm$1.1 days
d) Saddle stations: 3.0 $\pm$2.4 days

Table 6

Times of best agreement between measured and computed shears for all mooring sites. (Symbols are explained at the end of the table.)

STN	DATE	CM DEPTH RANGE (M)	1000 X MEASURED SHEAR (CM/S/M)	1000 X COMPUTED PR1 SHEAR (CM/S/M)	1000 X COMPUTED PR2 SHEAR (CM/S/M)	PR1 AVERAGE TIME (D)	PR2 AVERAGE TIME (D)
4-1	JUL.27	52-203	42	47	--	2.5	--
4-1	AUG.2	52-203	75	84	--	2.0	--
4-1	AUG.27	52-203	75	8	--	2.0	--
4-2	JUL.27	53-143	-27	35	-5	?	0.5
4-2	AUG.2	53-143	-14 to 21	27	-12	0.5	1.0
4-2	AUG.27	53-143	-28	-28	-46	1.0	?
4-3	JUL.27	54-153	5	41	--	2.0(?)	--
4-3	JUL.27	153-171	44	42	--	2.5	--
4-3	AUG.2/3	54-153	16	32	--	1.0	--
4-3	AUG.2/3	153-171	6 to -44	-4	--	0.5-1.0	--
4-3	AUG.28	54-153	-35	-38	--	3.0	--
4-3	AUG.28	153-171	6	8	--	1.5	--
5-1	JUL.25	58-156	26	58	52	3.0	3.0
5-1	AUG.11	58-156	19 to 35	26	88	2.0-2.5	?
5-1	AUG.27	58-156	94	92	38	1.5	?
5-2	JUL.25	30-57	-15	45	-15	?	3.0
5-2	JUL.25	57-158	-24	31	-28	?	1.5
5-2	JUL.25	158-269	73	30	-24	5	?
5-2	AUG.4	30-57	-11 to 133	10	5	?	?
5-2	AUG.4	57-158	21 to -18	35	8	?	1.0
5-2	AUG.4	158-269	22	29	27		0.5
5-2	AUG.27	30-57	167	65	30	?	?
5-2	AUG.27	57-158	86	21	68	?	5.5(?)
5-2	AUG.27	158-269	47	53	60	8(?)	8(?)
5-3	JUL.25	159-277	64	67	--	2.0	--
5-3	AUG.3	159-277	29	40	--	1.0	--
5-3	AUG.26	159-277	64	52	--	1.0	--
7-1	JUL.23	64-162	13	17	--	1.0	--
7-1	AUG.5	64-162	64	70	--	1.0	--
7-1	AUG.23	64-162	105	100	--	0.5	--
7-2	JUL.24	75-55	50	-7	60	?	2.0
7-2	JUL.24	55-145	18 , 54	20	63	2.5	1.5
7-2	AUG.5	25-55	-37 , 33	-37	33	0.5	2.0
7-2	AUG.5	55-145	-16 ,-27	-10	-41	1.0	2.0
7-2	AUG.23	25-55	-37 , 70	-37	90	5.0	1.5
7-2	AUG.23	55-145	-32	-28	60	2.5	?
7-3	JUL.24	102-202	18 (24)	30	--	3.5(6)	--
7-3	AUG.5	102-202	71	192	--	0.5	--
7-3	AUG.23	102-202	15	81	--	1.0(?)	--
9-1	JUL.22	56-156	34	30	16	2.0	?
9-1	AUG.8	56-156	7	37	57	1.0(?)	?
9-1	AUG.20	56-156	41	4	54	?	2.5
10-1	AUG.13	62-170	-10 , 59	-11	71	5.0	0.5
10-1	AUG.19	62-170	-48	-47	-62	1.0	?

Table 6 symbols: In the column headings, "COMPUTED PR1 SHEAR" and "COMPUTED PR2 SHEAR" refer to the current shear computed from pairs of CTD stations. If the current meter mooring was coincident with a CTD station, PR1 and PR2 refer to the station pairs formed by that station and its left- and right-hand neighbours, and the shear measured by the current meter mooring was compared with the shears computed from both CTD station pairs. If the mooring was between 2 CTD stations, the comparison was made only with that pair of stations. The computed value is entered in the PR1 column, and a dash (-) appears in the PR2 column. The averaging times which gave the best agreement are entered in the columns labelled "PR1 AVERAGE TIME" and "PR2 AVERAGE TIME". If no averaging time could be found which gave shears of the same sign, and that also agreed within 100%, a question mark appears. The shear values measured by the current meters are listed in the column head "MEASURED SHEAR". The values given are for the averaging times listed in the 2 right-hand columns of the table. If different times were found for cases where 2 CTD station pairs existed, the 2 values are shown separated by a comma. If the value changed dramatically when the averaging time was increased by 12 hours, the limits are given as a range of values.

Although all the above values fall within each other's error limits, the saddle stations appear to be different; as well as the larger mean period required to achieve agreement, there appears to be more scatter in the times required. The saddle stations also had the poorest agreement between the measured and computed shear, while the slope and trough stations had the best.

Dynamic height charts relative to 150 m were then drawn for each of the four occupations of the pattern of CTD stations, and are shown in Figures 28(a)-(d). Vectors representing the flow as measured at 150 m depth for each mooring site are also shown on the first three charts (all the moorings had been retrieved before the October occupation of the stations). The current velocity represented by each of the vectors was obtained by computing the vector average flow at that depth over the time which was required to produce agreement in the shears. (Almost all the moorings had a current meter within 10 m of 150 m depth; at those stations where there was no instrument at that depth, an interpolation was made.) Surface currents relative to 150 m may be computed from the charts in Figure 28 using the thermal wind relation. For the scale and contour interval used here, the surface current speed is:

$$V = 42/L$$

where V is the surface current speed in cm/s, and L is the separation of adjacent contours in millimetres (mm) as measured on the map. Current direction at any point is tangent to the contour lines. The 150 m flow vectors then are the corrections which must be added (in a vector sense) to the relative surface currents to find the true surface current. On the banks, which are generally between 150 and 200 m deep, the surface current relative to 150 m depth derived from the CTD data approximately corresponds to the baroclinic portion of the flow, while the 150 m flow vectors are roughly equivalent to the barotropic part, after elimination of the tides.

Corrected values for the surface current have been computed at each mooring site for each of the three station occupations, and are summarized in Table 7.

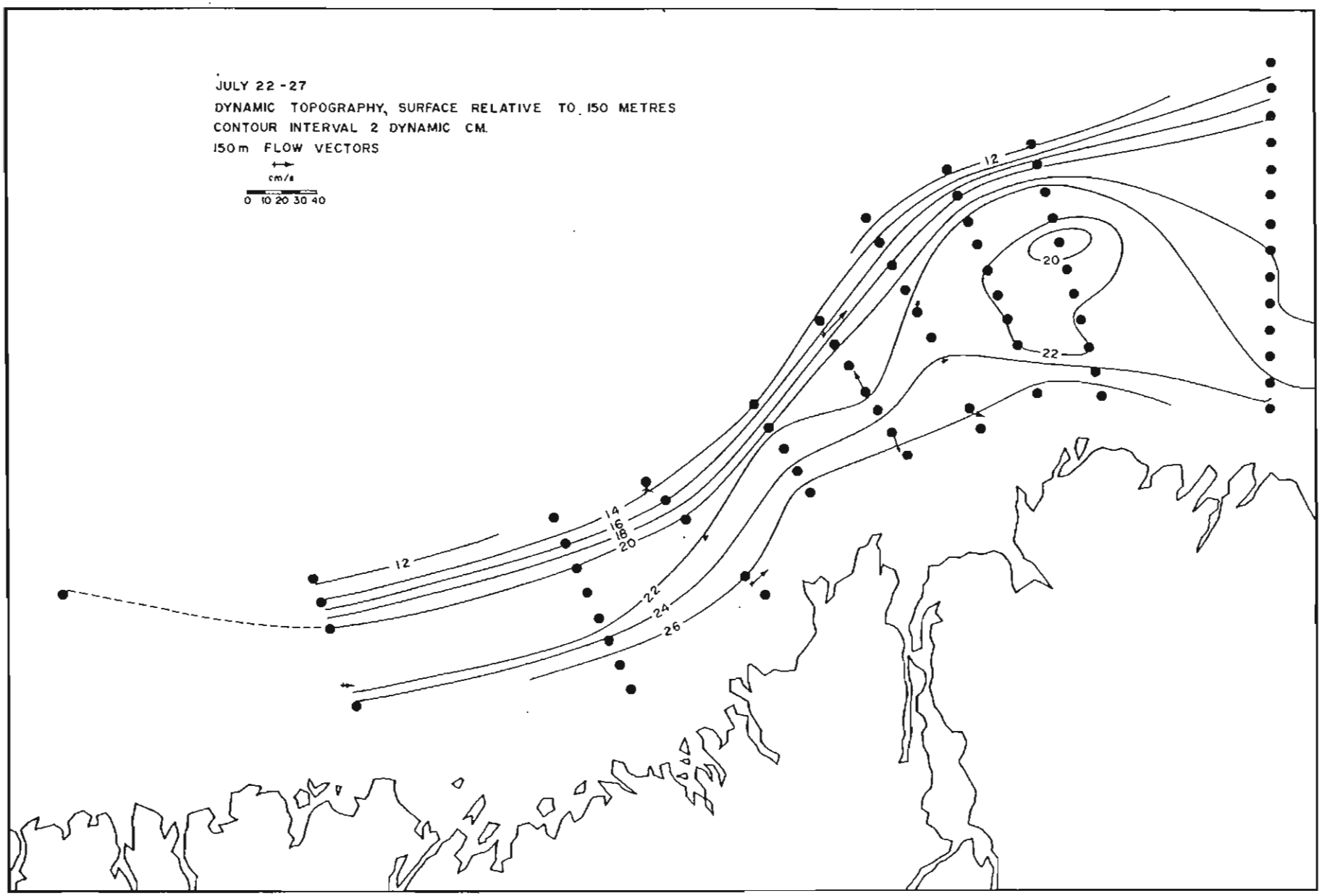

Figure 28a: Dynamic topography of the surface relative to 150 m, July 22-27.

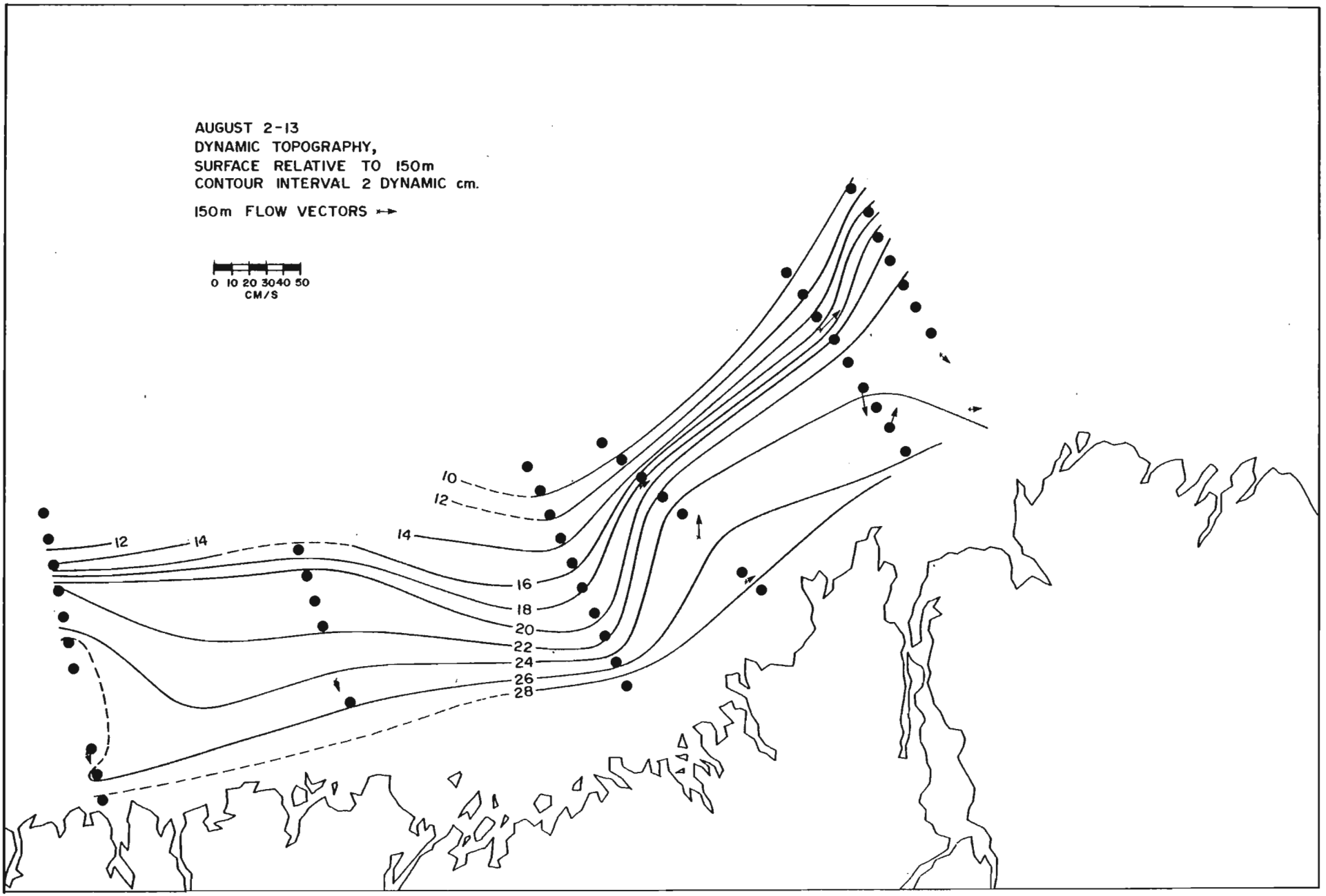

Figure 28b: Dynamic topography of the surface relative to 150 m, August 2-13.

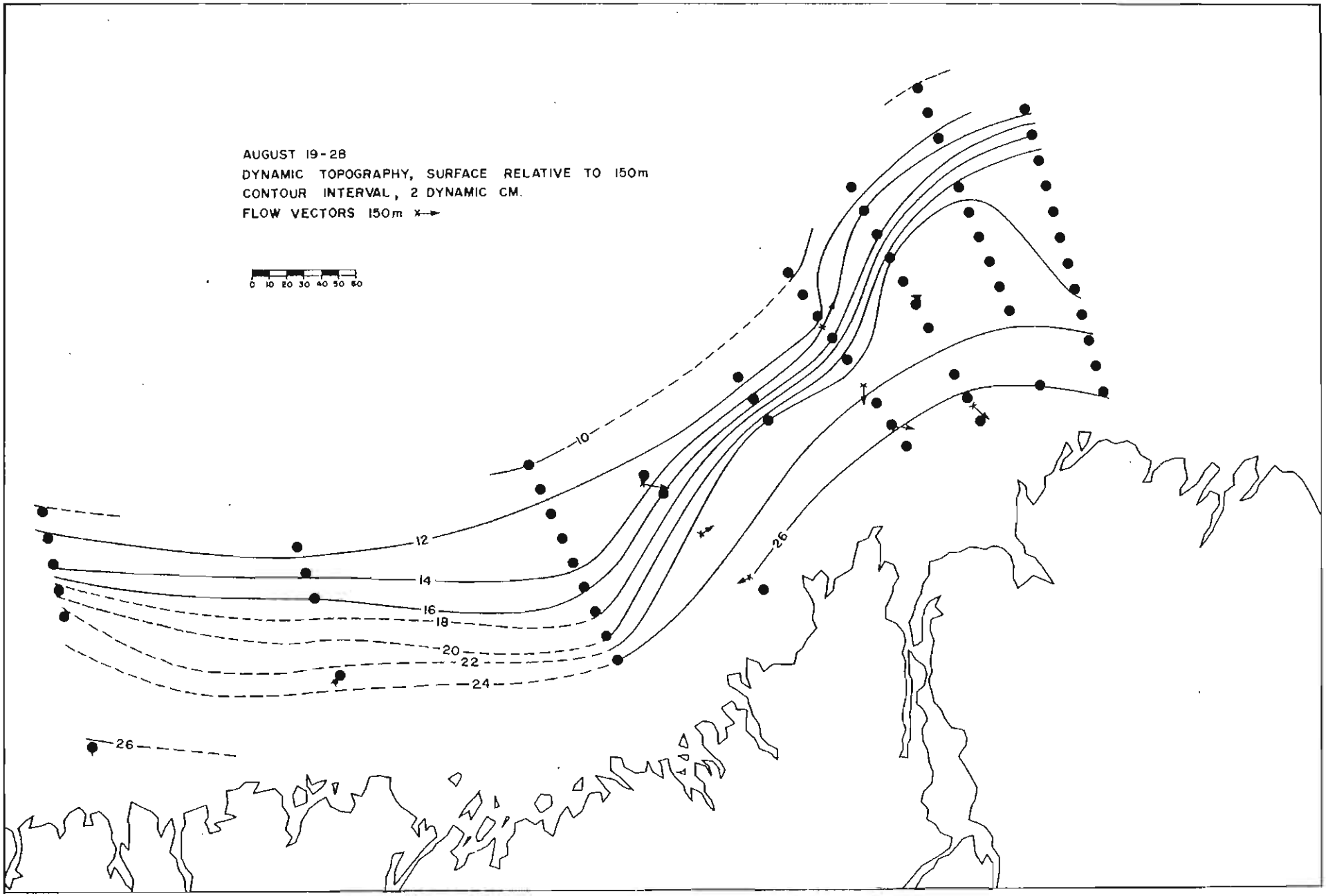

Figure 28c: Dynamic topography of the surface relative to 150 m, August 19-28.

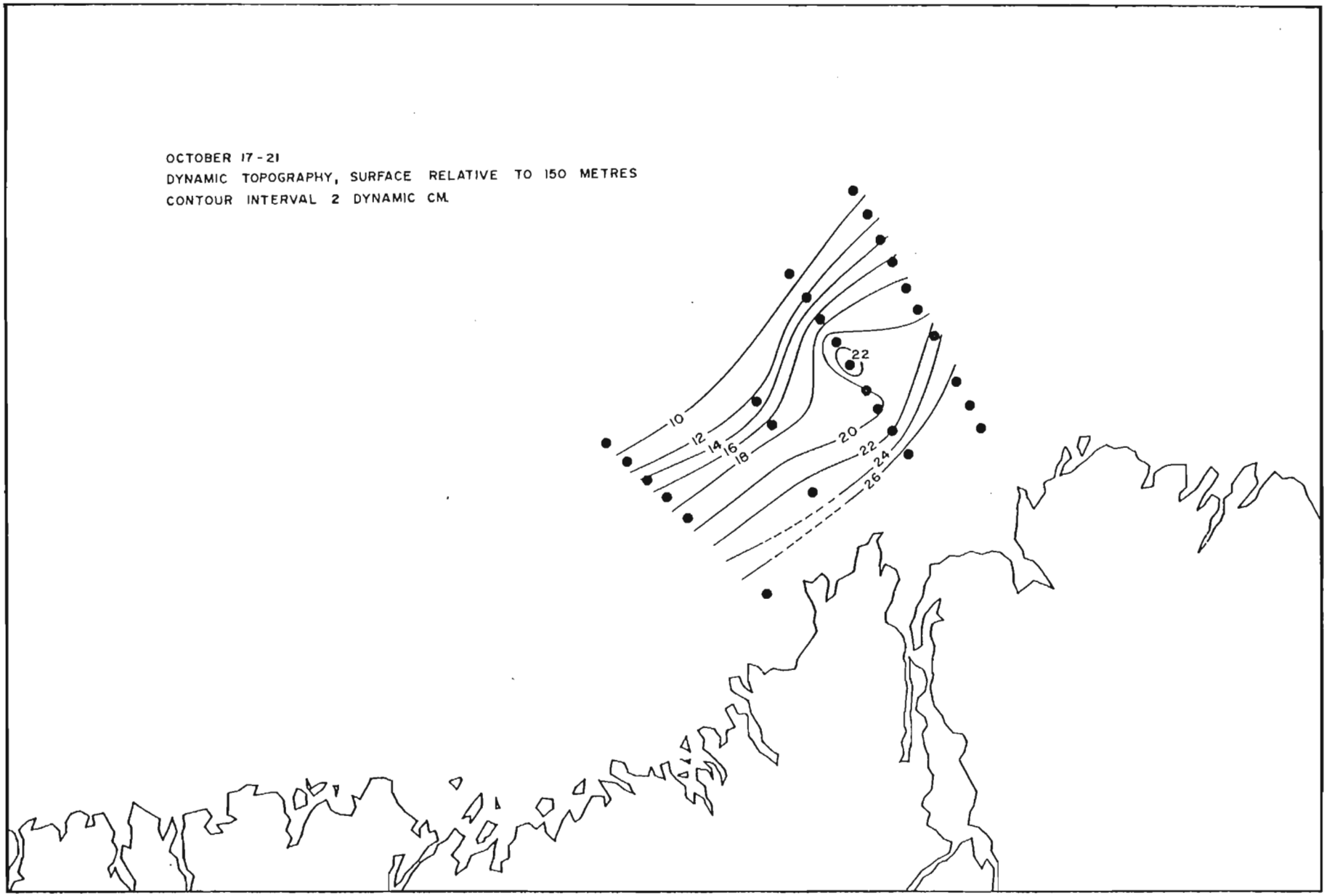

Figure 28d: Dynamic topography of the surface relative to 150 m, October 17-21.

Table 7

Surface flow relative to 150 m, computed flow at the 150 m reference level and resulting corrected surface currents.

STATION	DATE	COMPUTED SURFACE FLOW REL. 150 M (CM/S)	FLOW AT 150 M (CM/S)	CORRECTED SURFACE FLOW (CM/S)
4-1	JUL.27	9 @ 141°	6.5 @ 180°	14 @ 158°
4-1	AUG.2	9 @ 180°	8 @ 140°	16 @ 161°
4-1	AUG.27	6 @ 160°	11.5 @ 208°	16 @ 192°
4-2	JUL.27	4 @ 175°	4.5 @ 167°	8.5 @ 171°
4-2	AUG.2	1.5 @ 145°	6 @ 198°	7 @ 187°
4-2	AUG.27	*	*	*
4-3	JUL.27	8 @ 103°	1 @ 141°	9 @ 108°
4-3	AUG.2/3	4 @ 125°	3.5 @ 238°	3.5 @ 181°
4-3	AUG.28	2 @ 100°	2 @ 8°	3 @ 53°
5-1	JUL.25	8 @ 132°	12 @ 156°	20 @ 146°
5-1	AUG.11	8, - ~	13 @ 95°	~
5-1	AUG.27	5.5 @ 128°	14 @ 171°	18 @ 159°
5-2	JUL.25	8 @ 96°	15 @ 50°	21 @ 65°
5-2	AUG.4	5 @ 134°	15 @ 242°	14 @ 222°
5-2	AUG.27	9.5 @ 130°	9 @ 259°	8 @ 193°
5-3	JUL.25	19 @ 116°	20 @ 117°	39 @ 116°
5-3	AUG.3	23 @ 115°	21 @ 116°	44 @ 116°
5-3	AUG.26	28 @ 101°	17 @ 109°	45 @ 104°
7-1	JUL.23	4 @ 102°	13 @ 120°	17 @ 116°
7-1	AUG.5	7 @ 121°	5.5 @ 127°	13 @ 124°
7-1	AUG.26	9 @ 115°	9 @ 326°	4.5 @ 41°
7-2	JUL.24	10 @ 103°	6 @ 106°	16 @ 104°
7-2	AUG.5	4.5 @ 96°	14 @ 72°	18 @ 86°
7-2	AUG.23	5 @ 106°	9 @ 139°	13 @ 127°
7-3	JUL.24	14 @ 127°	5 @ 174°	18 @ 140°
7-3	AUG.5	29 @ 119°	7 @ 118°	36 @ 119°
7-3	AUG.23	9 @ 119°	14 @ 173°	21 @ 153°
9-1	JUL.22	4-28 @ 155°#	6 @ 152°	10-34 @ 154°
9-1	AUG.8	6 @ 149°	5 @ 238°	8 @ 189°
9-1	AUG.20	11 @ 159°	2 @ 96°	12 @ 151°
10-1	AUG.13	4-12 @ 280°#	7 @ 233°	10@250° to 18@263°
10-1	AUG.19	3-6 @ 170°#	3.5 @ 232°	5.5@203° to 8@192°

* No agreement in shear found.

~ Direction of surface flow uncertain, as a small eddy is shown centred on the mooring.

A range of values is shown, as the location of the dynamic height contours is more uncertain due to larger separation between CTD stations.

Over the slope, and in the marginal trough, the corrected surface velocities are quite constant from one occupation to another. On the banks and in the saddles, the corrected velocities are much more variable in both speed and direction. A major deflection of the main current branch (i.e. the branch over the continental slope) into Hopedale Saddle occurred at the beginning of August and appears to have persisted beyond the last set of measurements in that area at the end of August (Figures 28(b) and (c)). Other, smaller shifts in the position of the main branch of the current are also apparent between the four times when the station pattern was occupied. The time and space scales of these fluctuations cannot be determined precisely from the dynamic topographies, since they are almost certainly not fully resolved. At best, their upper bounds may be estimated as equivalent to the alongshore station spacing (approximately 70 km) and the interval between cruises (2 to 3 weeks).

In addition to the smaller-scale shifts observed in the position of the main branch of the current, occasional eddies were observed, both over the shallow banks and in Cartwright Saddle (Figure 28(a) and (d)). Figure 29 shows temperature and salinity cross sections through the eddy observed on southern Hamilton Bank (Figure 28(a)), July 28-29. The eddy, centred at station 208, is clearly visible as a dome in the isohalines which coincides with a column of significantly warmer water. A similar structure was observed on Nain Bank at line 9 in early August (Figure 30).

The 150 m reference currents defined above may also be used to construct cross sections of geostrophic velocity which show the vertical structure of the current. The reference currents were interpolated between current meter moorings, and extrapolated to the ends of the sections by one of three schemes:

i) the reference currents were assumed to be constant beyond the last mooring;

ii) the rate of change of the reference current was held constant beyond the last mooring;

iii) as for (ii) but with the sign of the rate of change reversed. (Equivalent to the assumption that the core of a symmetrical current lies centred on the outermost mooring. Figure 28 suggests that this may often be the case.)

This technique will produce a completely faithful representation of the current field only if the current meters are sufficiently closely spaced to resolve the spatial variability of the mean current field. The cross-spectral analyses of Section 5.9 show that, in general, the moorings were not sufficiently dense to accomplish that. As a result, spatial variations in the currents at the reference level are not fully resolved, nor are they as well resolved as the variations in the baroclinic portion of the flow, since the CTD stations were twice as dense as the current meter moorings. Although we cannot quantitatively estimate the errors in the current cross sections arising from insufficient resolution of the reference current field, we are confident that the sections following give a more realistic representation of the flow than would sections constructed using a level of no motion.

Figures 31 and 32 show two such cross sections for line 7 (Makkovik Bank). In both cases, the core of the main branch of the current flows over the

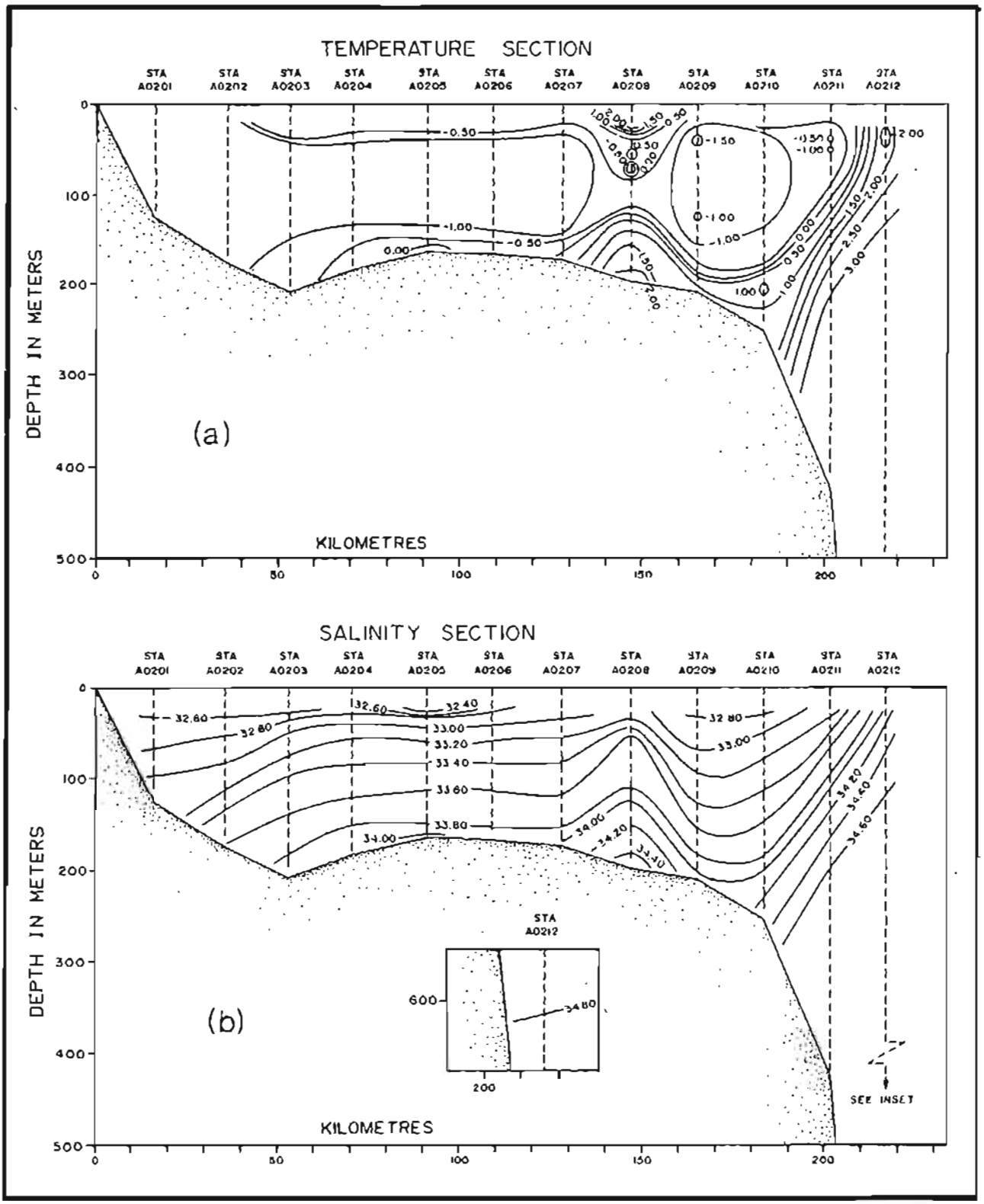

Figure 29: (a) Temperature cross section over Hamilton Bank (line 2), July 28-29. (b) Salinity cross section over Hamilton Bank (line 2), July 28-29.

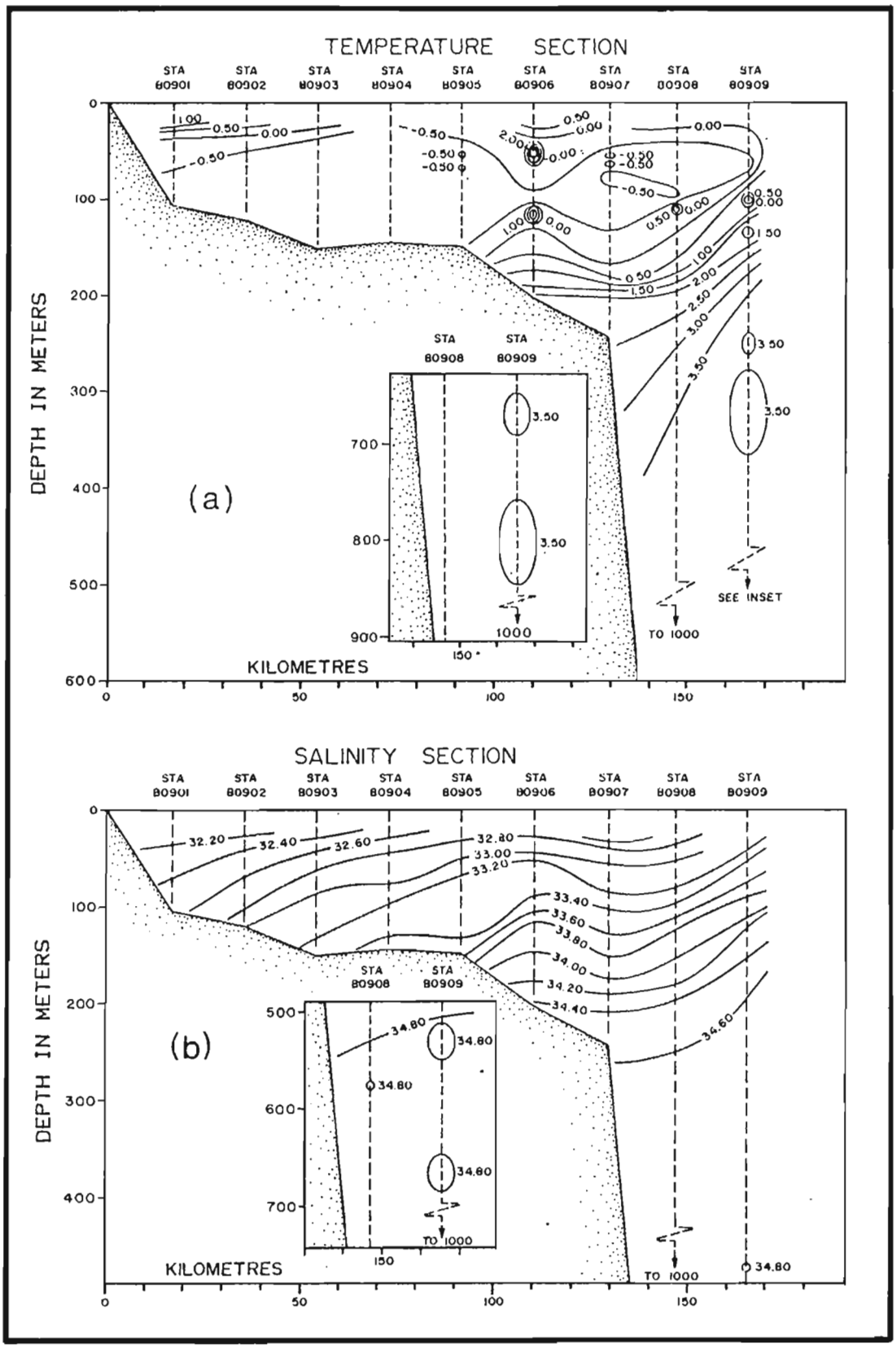

Figure 30: (a) Temperature cross section, over Nain Bank (line 2), August 8. (b) Salinity cross section over Nain Bank (line 9), August 8.

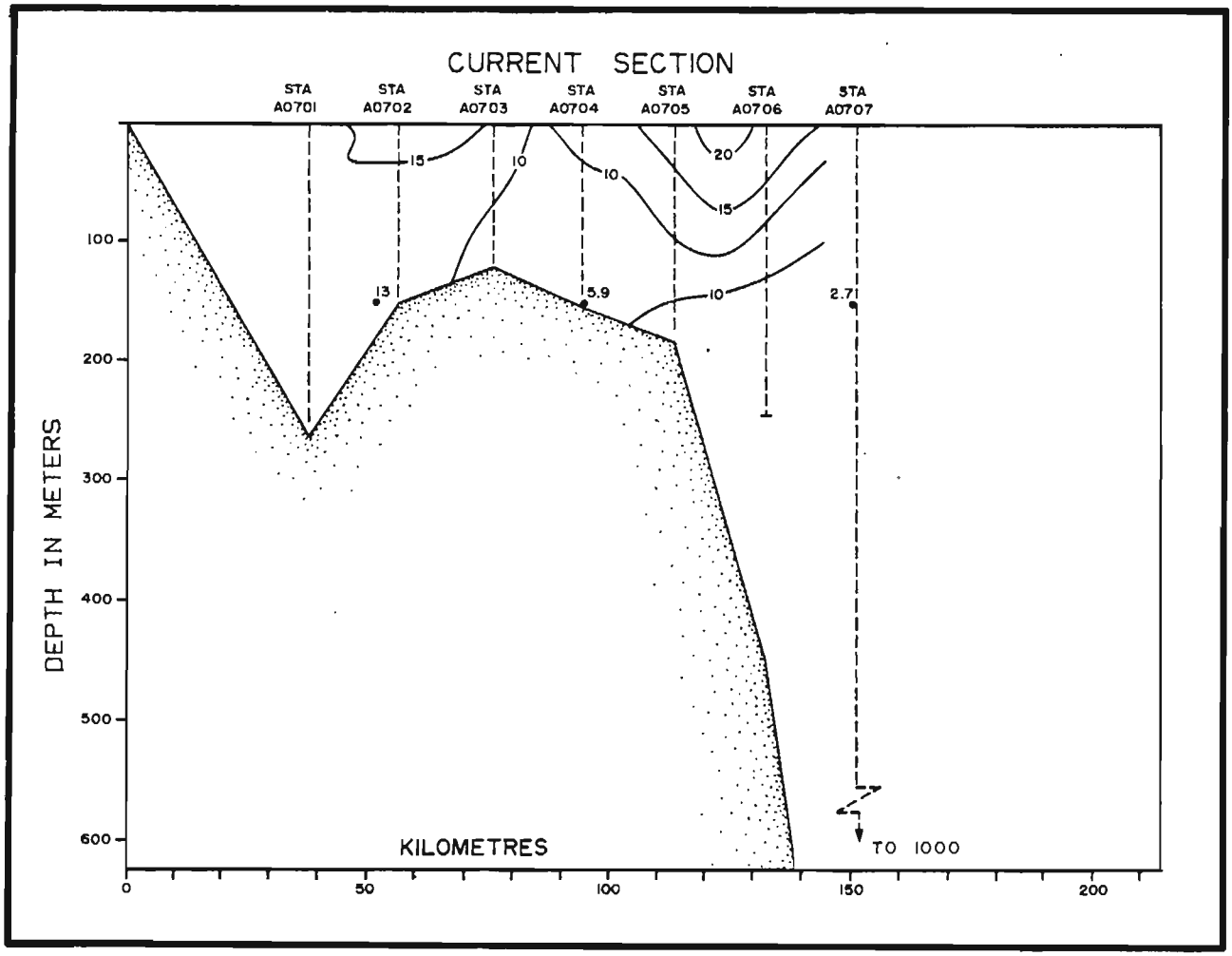

Figure 31: Cross section of geostrophic velocities over Makkovik Bank (line 7), July 23-24. Positive values indicate flow out of the page. Flow into the page is indicated by negative values and shading. The numbers beside the dots (.) are the reference current values derived from the current meter moorings.

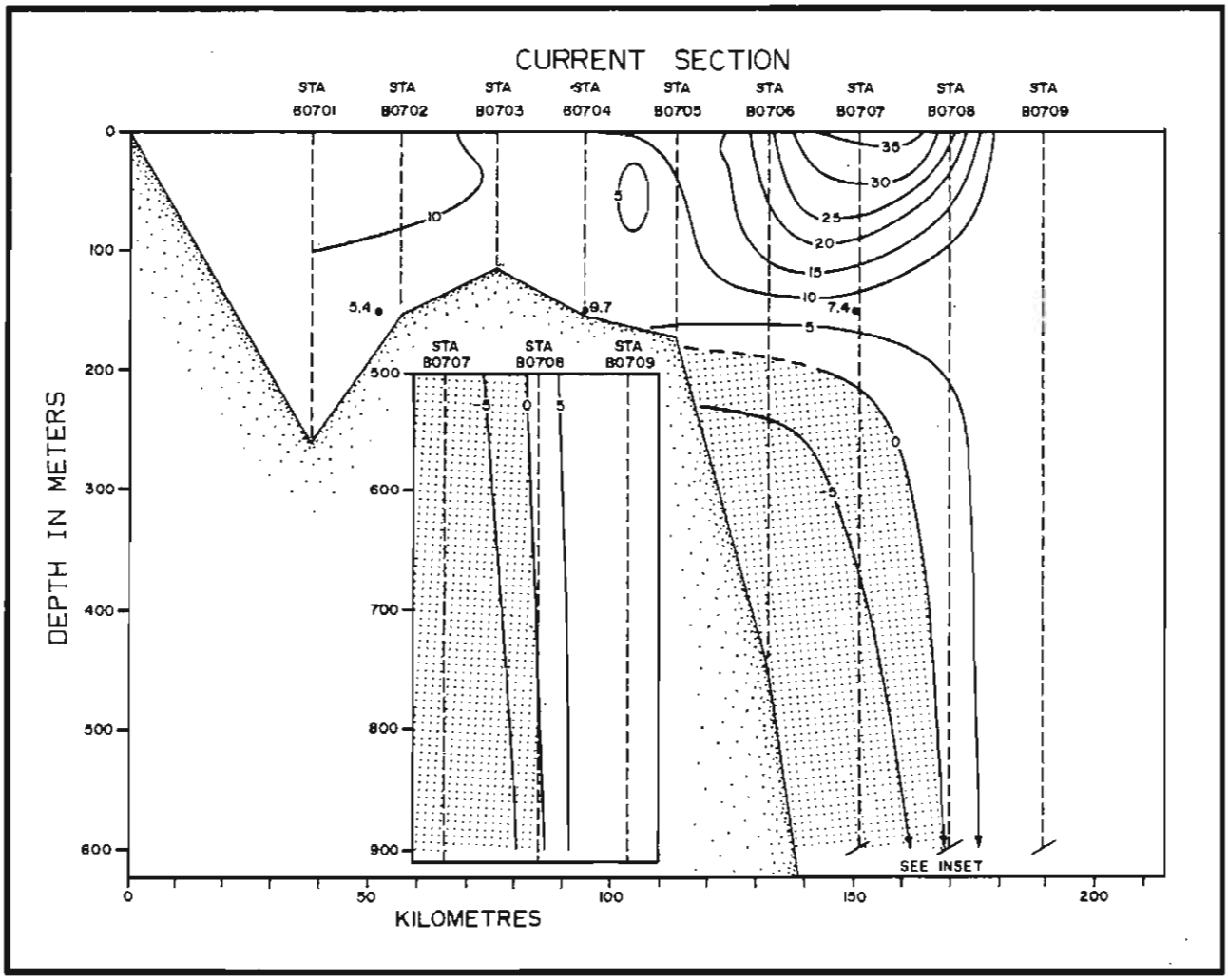

Figure 32: Cross section of geostrophic velocities over Makkovik Bank (line 7), August 5. Positive values indicate flow out of the page. Flow into the page is indicated by negative values and shading. The numbers beside the dots(.) are the reference current values derived from the current meter moorings.

continental slope, somewhat further offshore on August 5 than July 23-24, although in the latter case the two stations furthest offshore were not occupied. The highest speeds appear at the surface in both cases, although in August they are nearly twice what they were in July. There is a minimum in the flow over the banks, without much vertical shear, and then a second southward maximum (weaker than the offshore branch) over the trough. A reverse flow along the slope is shown below 200 m on August 5 (Figure 32). It is not apparent in Figure 31 (July 23-24), perhaps because the data did not extend to sufficient depth.

Similar cross sections on Hamilton Bank at line 4 are shown in Figure 33 (July 26-27), Figure 34 (August 2-3) and Figure 35 (August 27-28). The current meter moorings on line 4 extended only as far as station 409 in the offshore direction. It was not felt reasonable to extrapolate reference currents measured on the shelf into the slope zone where a different type of current structure clearly prevailed. Instead, the reference currents at station 5-3 were used to fix a 150 m reference current between station 410 and 411. Examination of the dynamic topographies in Figure 28 that mooring 5-3 and the midpoint of the line joining stations 410 and 411 occupy equivalent positions within the baroclinic portion of the main branch of the current. Two versions are shown for each cross section to demonstrate the effect of the different extrapolation schemes used at the offshore end of the sections. No great changes occur in the general pattern of the flow, although the different methods can shift the location of the core by 5 to 10 km and can alter the peak current values by approximately 25%. In all cases however, the main branch of the current is found over the slope, with its core between the surface and 150 m depth. Its highest speeds occur at or near the surface and are between 30 and 45 cm/s. A second southeastward flow is apparent in all three sections, located either over the centre of the marginal trough or over its eastern side. This second branch is considerably weaker, with peak speeds of 10 to 15 cm/s, and with its core between the surface and 50 m depth. It also seems to be less closely bound to the local topography than is the branch on the continental slope. The core of this second flow may be found anywhere from the centre of the trough to the edge of the banks bordering the offshore side of the trough, but it does not ever seem to occupy the western side. No obvious pattern to the position of the flow is apparent from the limited data available; it appears to wander back and forth more or less randomly.

As well as the trough flow there is in all cases an indication of a separate, fairly swift surface current (up to 30 cm/s) within 15 km of the coastline. The reference level could not be reliably extrapolated into that zone, however, and in any case the flow is not properly resolved by the available data. It is very likely that a nearshore coastal flow of some sort (perhaps driven by local runoff) does exist, even though we are not able to characterize it very precisely.

5.5 SCALES OF TEMPORAL VARIABILITY

The auto-spectra of all current meter measurements obtained at depths of 50 m or greater are presented in Figures 36, 37 and 38. In this presentation, the kinetic energy auto-spectra are computed as the sum of the auto-spectra of two orthogonal current components. In order to display the full range of resolvable frequencies (1 cycle in 28 days to 48 cycles per day for the Aanderaa

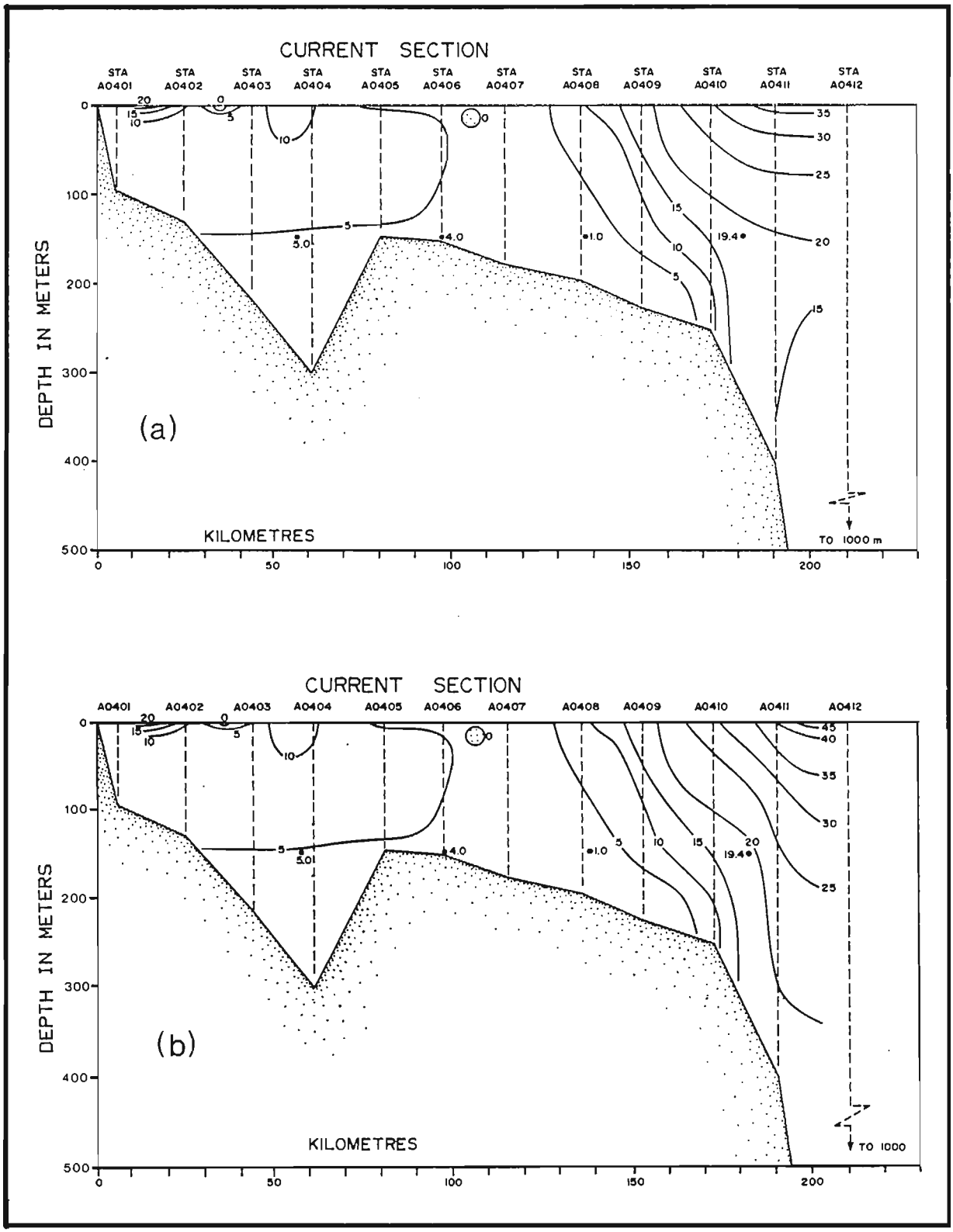

Figure 33: Cross section of geostrophic velocities over Hamilton Bank (line 4), July 26-27. (a) Extrapolation scheme (ii). (b) Extrapolation scheme (i). Positive values indicate flow out of the page. Flow into the page is indicated by negative values and shading. The numbers beside the dots(.) are the reference current values derived from the current meter moorings.

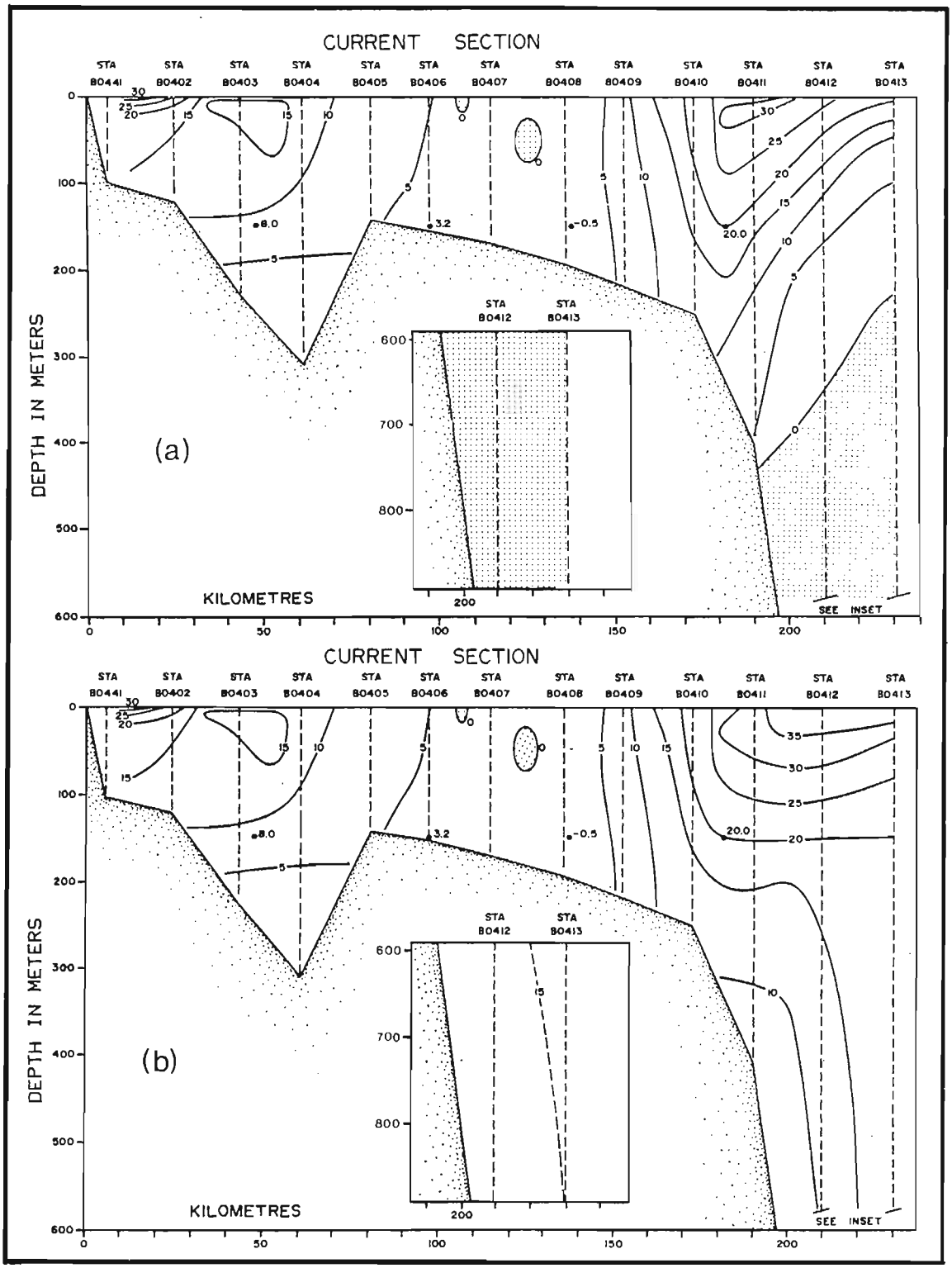

Figure 34: Cross section of geostrophic velocities over Makkovik Bank (line 7) July 23-24. Positive values indicate flow out of the page. Flow into the page is indicated by negative values and shading. The numbers beside the dots (.) are the reference current values derived from the current meter moorings.

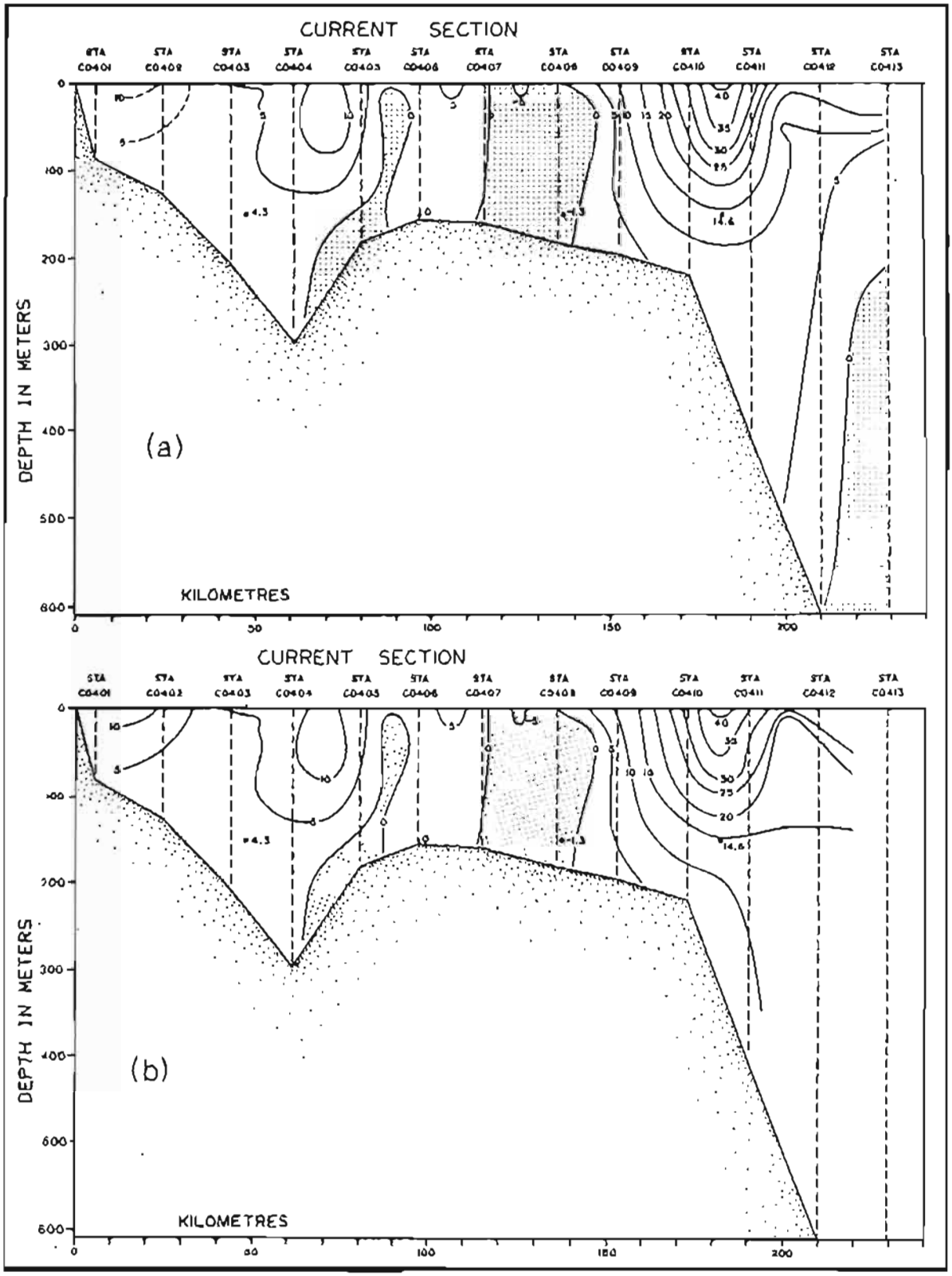

Figure 35: Cross section of geostrophic velocities over Hamilton Bank (line 4), August 27-28. (a) Extrapolation scheme (iii). (b) Extrapolation scheme (i). Positive values indicate flow out of the page. Flow into the page is indicated by negative values and shading. The numbers beside the dots(.) are the reference current values derived from the current meter moorings.

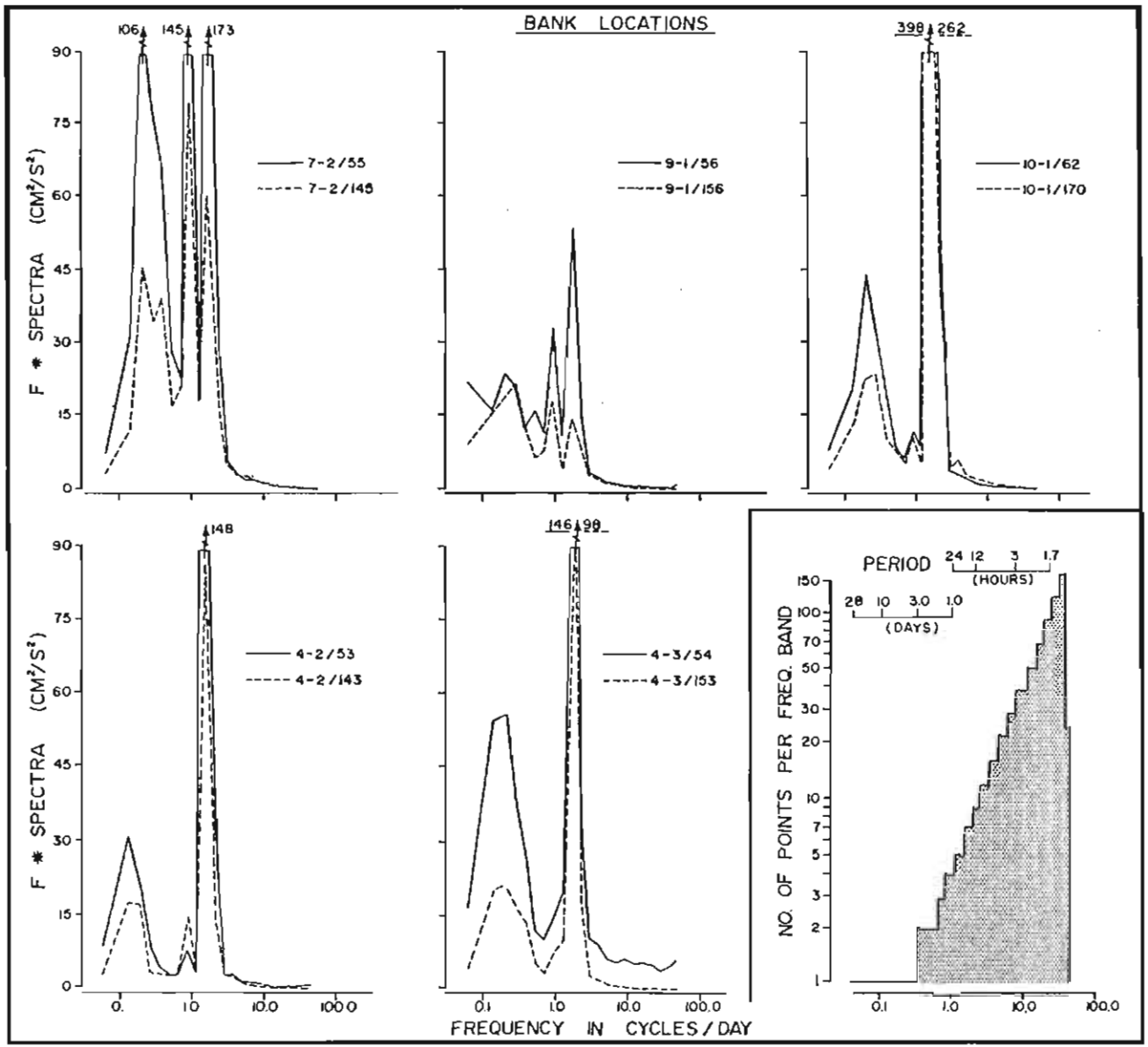

Figure 36: The kinetic energy auto-spectra of current meter data obtained at moorings located on banks. The amount of band averaging varies with frequency (see inset) in order that the number of spectral estimates remains constant on the logarithmic frequency scale.

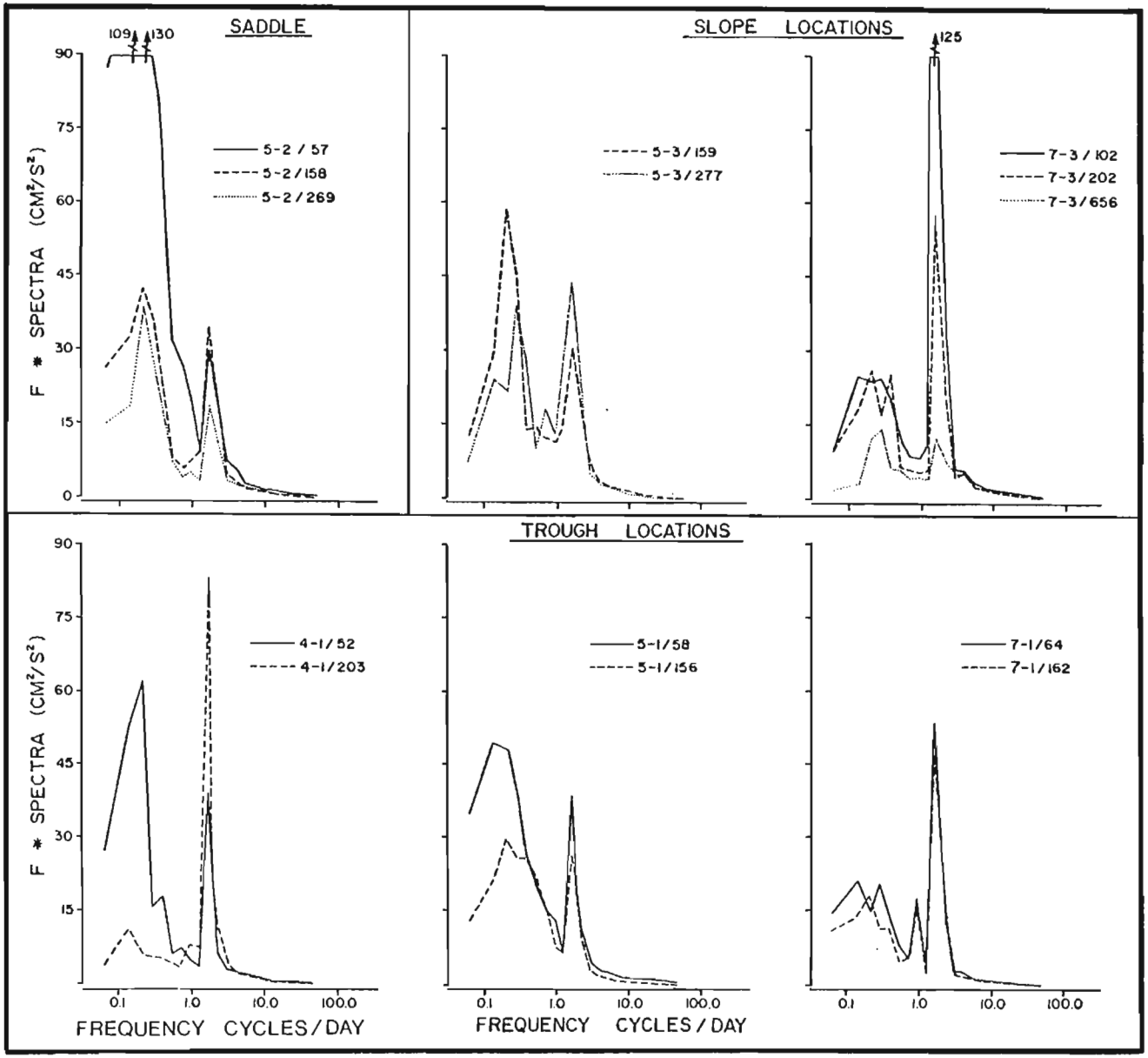

Figure 37: The kinetic energy auto-spectra of current meter data obtained at moorings in trough, slope and saddle locations.

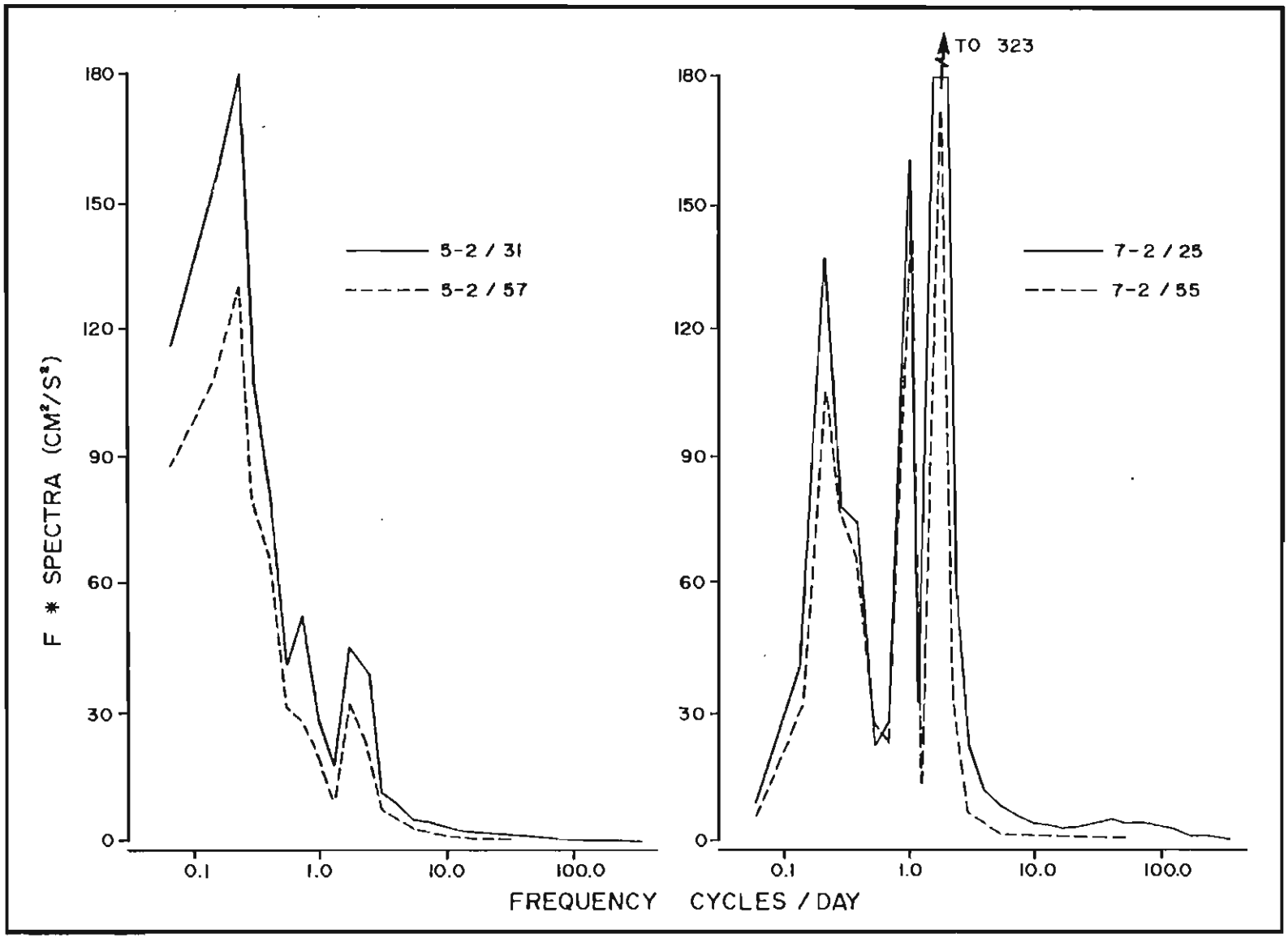

Figure 38: The kinetic energy auto-spectra of current meter data obtained at 25 m depth (station 7-2) and 31 m depth (station 5-2).

data), the spectral estimates are plotted on a logarithmic frequency scale. The estimates are band averaged in such a way as to produce approximately 10 spectral estimates per decade of frequency; the degree of band averaging varies from one raw estimate per band at the lowest frequency to 162 raw points per band at high frequencies (see insert in Figure 36). The ordinate used in the plots is the product of frequency and the spectral density in order that the area beneath any portion of the plotted curve is proportional to the variance (in this case, kinetic energy) of the velocity time series.

In the auto-spectral results, the largest spectral values are found in two broad ranges: the low frequency band and the tidal and inertial frequency band. In the low-frequency band there is usually either one broad peak covering a wide range of frequencies or two or more peaks with comparable levels that are seldom statistically significant. In most of the auto-spectra, the energy levels decrease between 0.5 and 0.9 cycles per day; this frequency range separates the low frequency band from the tidal and inertial frequency band.

The tidal and inertial band has a different spectral character: variations contributing to this band occur at a number of discrete frequencies. These frequencies include the diurnal and semi-diurnal tidal constituents (ranging from 0.83 to 1.11 cycles per day and 1.83 to 2.04 cycles per day, respectively) and the inertial frequency (ranging from 1.6 to 1.8 cycles per day, according to the latitude of the measurement). In the auto-spectra of Figures 36 to 38, the effects of inertial oscillation activity is included in the semi-diurnal frequency band and is not seen as a separate peak.

Above the semi-diurnal peak, the auto-spectral values decrease to very low levels. This range of frequencies, designated as the high frequency band, is generally featureless with no significant peaks. In all but a few of the auto-spectra, the contribution to the total variance from this range of frequencies is negligible. Those data sets with relatively more energy at high frequencies (4-2/53, 4-3/54 and 7-2/25) are analyzed further in Section 5.6.

A comparison of auto-spectra between locations categorized according to bathymetric regime suggests that the temporal variability of the currents varies from one regime to another. However, marked differences in the spectral character are also found between locations with similar bathymetries.

At nearly all locations, low frequency variations dominate the auto-spectra. Low frequency contributions to the variance are markedly larger than those of tidal and inertial origin at measurement sites on the inner marginal trough or continental slope. However, at locations on the banks the tidal contributions, particularly at the semi-diurnal frequency are enhanced and the low frequency variability is generally less than in other bathymetric regions. As a result there are comparable contributions to the variance from the low frequency and tidal bands at bank locations. At one location, station 10-1, the semi-diurnal tidal activity exceeds that of the low frequency band.

The largest low frequency spectral levels occur at the one mooring located in a saddle (station 5-2, in Cartwright Saddle) at depths of 31 and 57 m. Near 50 m depth, relatively large low frequency spectral levels are also found at stations 4-1 and 5-1 both located in the inner marginal trough. However, at the trough station 7-1, the low frequency spectral levels are much reduced.

Similarly, for the two slope stations, the low frequency spectral levels at station 5-3 are relatively large while those at station 7-3 are markedly lower. The fact that stations 4-1, 5-1, 5-2 and 5-3 (all in the vicinity of a saddle) have a higher degree of low frequency activity than stations 7-1 and 7-3 (located on either side of a bank) may be significant. At locations on the banks, the low frequency activity varies significantly from one site to another. At stations 4-3 and 7-2, the spectral levels are comparable to those computed for trough and slope stations while at stations 4-2, 9-1 and 10-1, the spectral levels are markedly lower.

Where larger low frequency spectral levels occur, the spectral activity decreases sharply at depths greater than 50 to 60 m. At stations 4-1 and 5-1 (trough), 5-2 (saddle), and 4-3 and 7-2 (banks), the spectral levels decrease by a factor of two or more between the nominal depths of 50 m and 150 m. At the two locations, 5-2 and 7-2, where time series current measurements were obtained at depths of less than 50 m, the auto-spectral results (Figure 38) indicate that markedly larger amplitude low frequency activity occurs nearer the surface than at 50 m depth.

The tidal and inertial frequency activity shows a general tendency to increase at locations on the banks. At all bank locations with the exception of station 9-1, the semi-diurnal peak value exceeds those computed for all other sites. The level of semi-diurnal activity varies considerably among the bank stations from a maximum at 10-1 to a minimum at 9-1. By comparison, activity at diurnal frequencies is more variable with location, ranging from levels comparable to semi-diurnal levels (at station 7-2) to negligible levels (station 4-3).

At non-bank locations, the semi-diurnal activity is always present but generally reduced from that observed on the banks. The diurnal activity is very small, without any significant peak at stations 4-1, 5-1, 5-2, 5-3 and 7-3.

A more detailed discussion of the variability at different frequency ranges is presented below. In Section 5.6, the high frequency activity is described, while tidal variations are analyzed in Section 5.7. Inertial oscillation activity described in Section 5.8 and low frequency variability is presented, in some detail, in Section 5.9.

5.6 HIGH FREQUENCY VARIATIONS

The auto-spectra of the measured currents indicate that at frequencies above semi-diurnal, the amplitude of current variations decreases rapidly with increasing frequency. Spectral levels are small and generally decrease monotonically out to the highest resolvable frequency of one-half the sampling rate (the Nyquist frequency).

In a few data sets, the high frequency spectral levels are larger than those in the remainder of the records. As an example consider the spectral densities at a frequency of 30 cpd. In most of the data sets (22 of 27), values for current components range from 2.7 - 11.5 x 10^{-3} cm^2/s^2-d with a median value of 6.2 x 10^{-3}. However, the remaining five data sets have spectral densities of 15.1 - 90.8 x 10^{-3} cm^2/s^2-d at this frequency. These data sets, and the corresponding spectral values are: 4- 2/53 (16.0 x 10^{-3}), 4-3/54 (79.9 x 10^{-3}),

5-2/31 (29.1×10^{-3}), 7-2/25 (90.8×10^{-3}), and 9-1/56 (15.1×10^{-3}). A measure of the significance of these levels can be obtained by considering the spectral levels expected from the least count noise resulting from the digital nature of the raw speed data. For the digital resolution of 0.2 cm/s of the Aanderaa current meters, the spectral level would be $(0.2/2)^2$ divided by the bandwidth of the spectral estimates (8.71 cpd at a frequency of 30 cpd), giving 1.2×10^{-3} cm^2/s^2-d. Thus, most of the spectral levels fall within an order of magnitude of least count noise level, but the five above mentioned records exceed this level by an order of magnitude or more.

The high frequency activity of data set 4-3/54 are likely fictitious. In this data set, the high frequency levels are relatively low until mid August; in the remainder of the record many isolated, large-amplitude values occur. Given the difficulties in removing all errors from this record and the associated uncertainties (Section 3.1), these data must be considered suspect and will not be considered further in this section.

The data sets having larger levels at high frequencies were measurements obtained in the upper 60 m of the water column. These data sets include the two Neil Brown current meter records at depths of 25 and 30 m as well three of the uppermost Aanderaa records.

The high frequency activity in these data sets were further examined by applying a high-pass digital filter to the data. The first of these filters passed variations with frequencies of 10 cpd (periods of 2.4 hours or less) up to the Nyquist frequency of 48 cpd for the Aanderaa data and 72 cpd for Neil Brown data, averaged over 10-minute intervals (see Figure 11 for a plot of the transfer function). The results of the filtering are plotted in Figures 39 and 40. The amplitudes of the high frequency variations are typically about 1.0 cm/s in data sets 4-2/53, 5- 2/30 and 9-1/56 and markedly higher at 2.5 cm/s at 7-2/25. The corresponding maximum amplitudes are 8.4, 10.5, 8.9 and 36.1 cm/s, respectively. The larger amplitude events appear to occur as isolated bursts of activity, with a typical duration of a few days. During these bursts, particularly large amplitudes often occur very abruptly, at intervals of once every 6 to 12 hours, with lower levels of activity in the interim. Particularly good examples of this pattern of activity are apparent at 4-2/53 from August 18-20, at 5-2/31 from August 28-30 and at 7-2/25 from August 24-31.

The Neil Brown current meter data, obtained at 2-minute intervals, offers much higher resolution than the 15-minute Aanderaa data. Another high pass digital filter (Figure 11) was designed for the Neil Brown data, which passed fluctuations from 75 cpd (19.2 minutes period) up to the Nyquist frequency of 360 cpd (period of 4 minutes). The level of variability in this frequency range is definitely higher at station 7-2 than at 5-2. The mean and maximum speeds are 1.7 and 34.8 cm/s at the former compared to 0.8 and 12.7 cm/s at the latter.

Segments of the very high frequency filtered time series are presented in Figures 41 and 42. These segments, which contain the maximum speed, reveal that times of pronounced activity at very high frequencies occur in clusters. Each cluster lasts about 2 to 4 hours and is separated from the other clusters by about 12 hours. A detailed examination of the largest event, observed at 7-2/25 on August 12, indicates that the individual readings change very abruptly. The speeds appear to reach minimums of less than 10 cm/s over periods of about 8

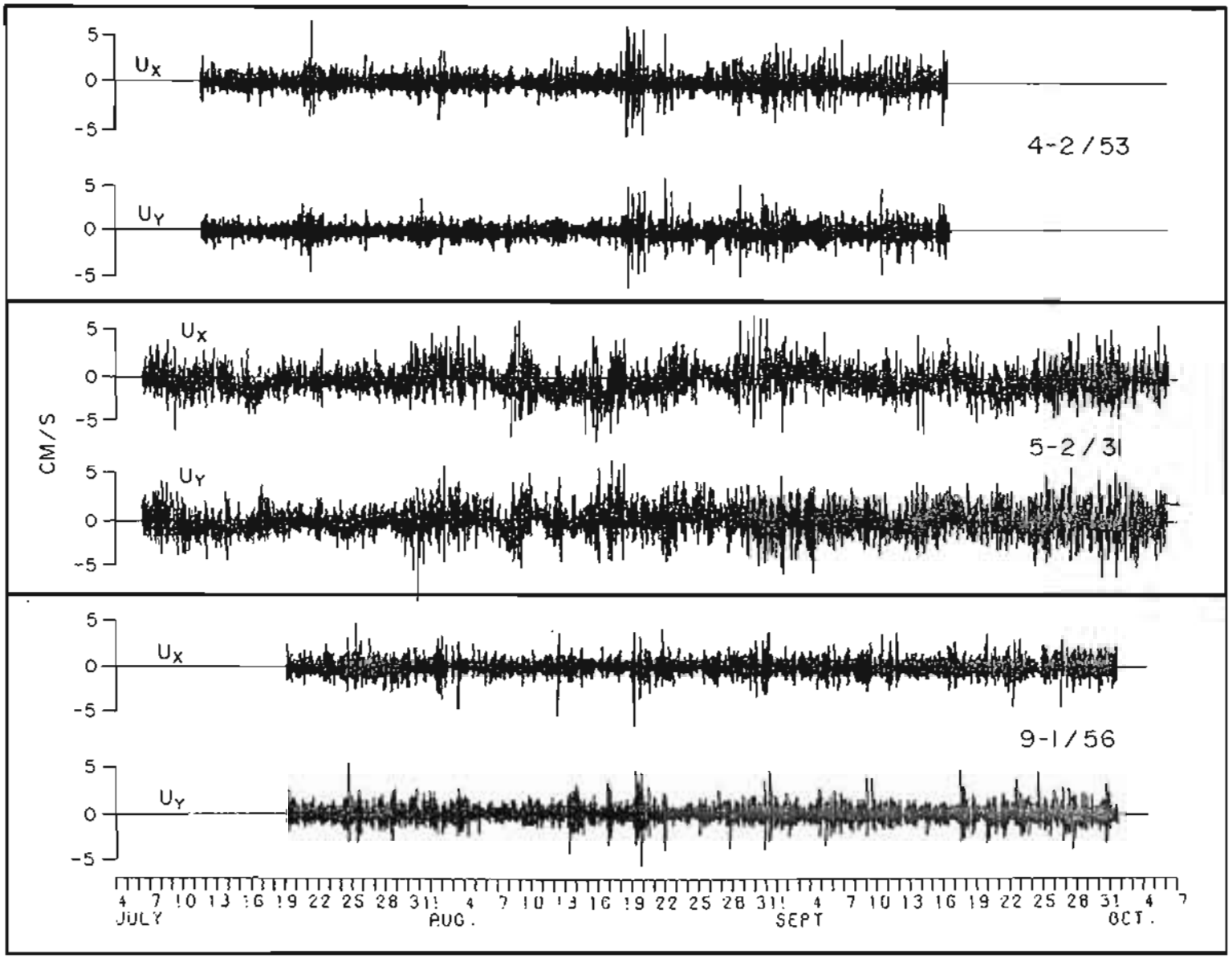

Figure 39: The high-pass filtered times series data of easterly (U_X) and northerly (U_Y) current components for records 4-2/53, 5-2/31 and 9-1/56. The digital filter passes current fluctuations from 10 cpd to the Nyquist frequency (48 cpd for 4-2/53 and 9-1/56; 72 cpd for 5-2/31) subsampled at 10 minutes).

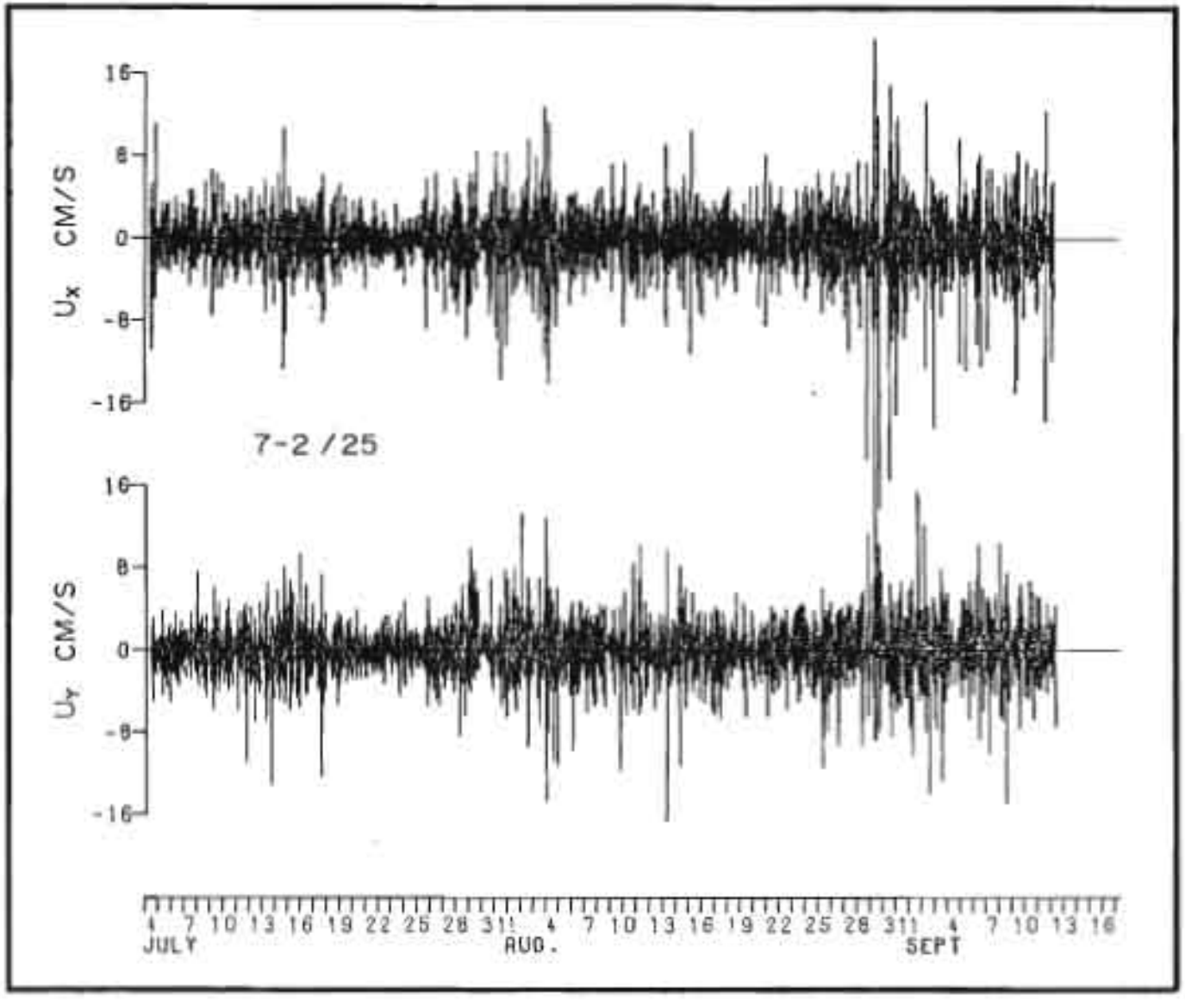

Figure 40: The high-pass filtered times series data of easterly (U_x) and northerly (U_y) current components for record 7-2/25, subsampled at 10 minutes. The digital filter passes current fluctuations from 10 to 72 cpd.

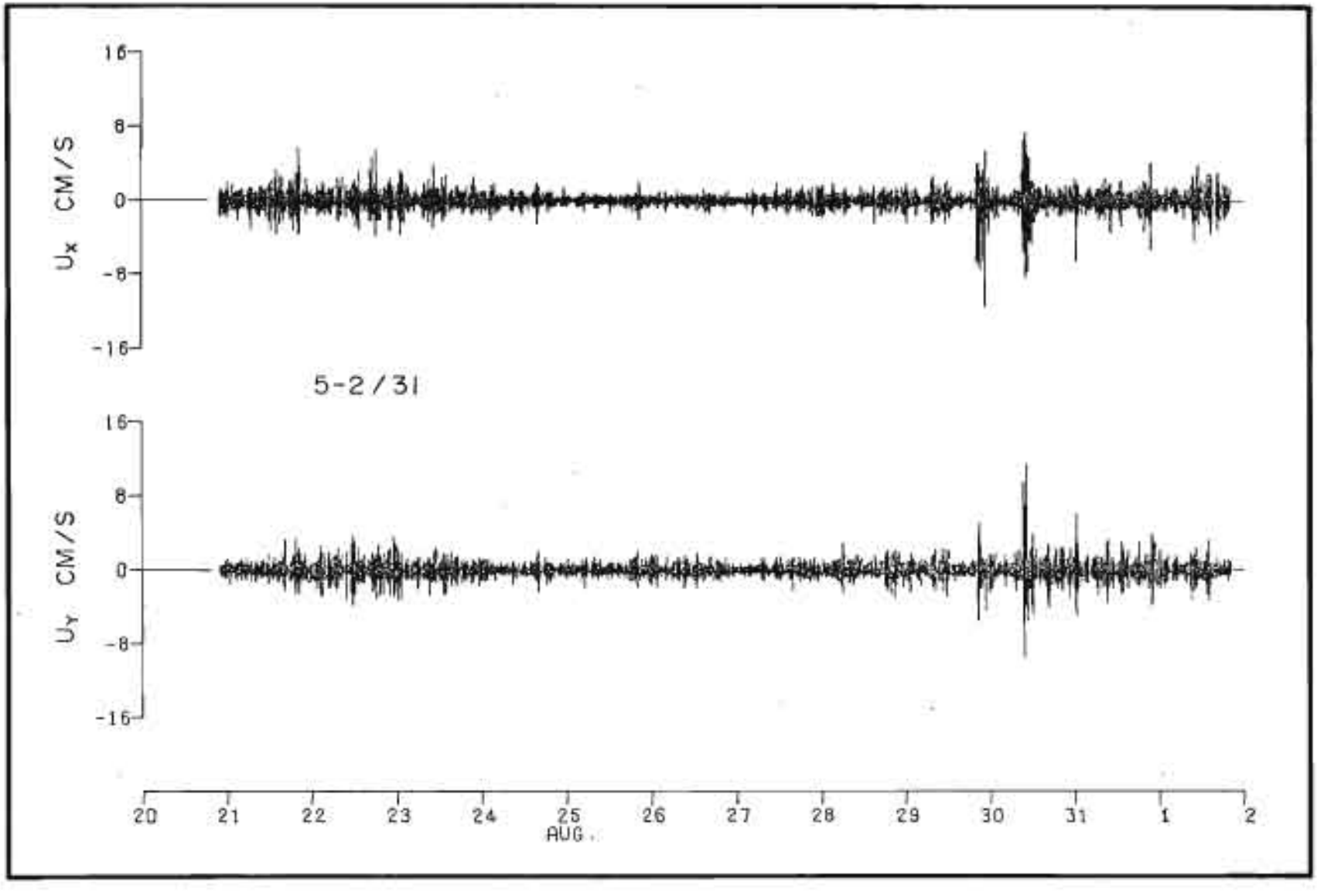

Figure 41: The very high-pass filtered time series data of easterly (U_x) and northerly (U_y) current components for record 5-2/31, August 20 - September 2, 1980. The digital filter passes fluctuations from 75 to 360 cpd.

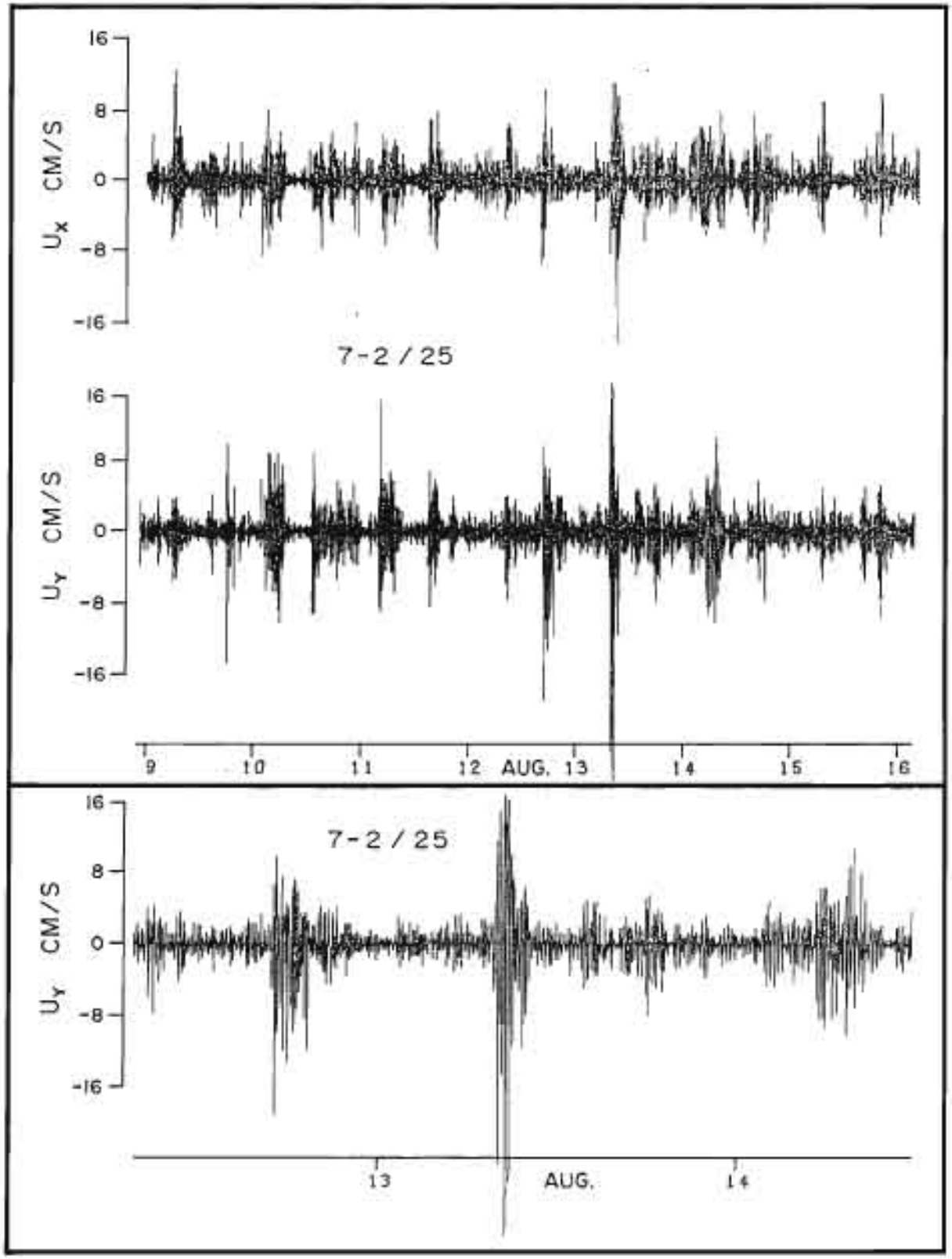

Figure 42: The very high-pass filtered time series data of easterly (U_x) and northerly (U_y) current components for record 7-2/25. The upper portion shows the variations from August 9-16, while the lower portion shows the maximum fluctuations (August 12-14) on an expanded time scale. The digital filter passes fluctuations from 75 to 360 cpd.

minutes. The high level of activity occurs first in the north-south direction, and about 1 hour later the peak speed of 19 cm/s occurs in the east-west component.

From the preliminary analysis of high frequency activity described above, it is evident that the variations with frequencies of 10 cpd or more are generally small, with typical values of less than 1.0 cm/s and maximum amplitudes of 6 cm/s or less. However, at a few stations within the upper 60 m of the water column, the amplitudes can be considerably larger. The overall maximum values were measured at station 7-2 at a depth of 25 m, where overall peak speeds of 36.1 cm/s were observed for frequencies between 10 and 72 cpd. In the same data set for higher frequencies ranging from 50 to 360 cpd, the largest amplitude was 34.8 cm/s.

5.7 TIDAL VARIATIONS

The tidal currents were deduced from the harmonic analyses of all current meter records containing valid data of 57 days duration or more. The largest tidal variations occur at semi-diurnal frequencies. The M_2 constituent has the largest amplitude of the resolvable semi-diurnal constituents in all of the time series analyzed. The amplitude of this constituent exceeds that of the next largest semi-diurnal constituent, the S_2, by more than a factor of two in 23 of the 27 data sets. The N_2 constituent, found to be the next largest semi-diurnal constituent in most of the records, has typical amplitudes of less than one-third of those of the M_2 constituent.

The tidal current ellipse parameters for the M_2 and S_2 constituents are summarized in Table 8 and the M_2 ellipses are shown in Figure 43 for two depth ranges of 52-102 m and 143- 203 m. The amplitude of the semi-diurnal currents varies markedly over the study area. For the M_2 constituent, the largest amplitudes occur at the northernmost station 10-1 on Saglek Bank (13.4 cm/s at 62 m depth). Relatively large values also occur in areas on and adjacent to Makkovik Bank (a range of 4.4 to 10.0 cm/s at stations 7-1, 7-2 and 7-3 above 202 m depth) and Hamilton Bank (a range of 3.8 to 7.4 cm/s at stations 4-1, 4-2 and 4-3 above 203 m depth). Markedly smaller M_2 amplitudes were observed at the three stations in the vicinity of Cartwright Saddle (a range of 1.9 to 3.3 cm/s at stations 5-1, 5-2 and 5-3) and at mooring 9-1 located on Nain Bank between Makkovik and Saglek Banks (3.9 and 1.9 cm/s amplitudes).

At locations with relatively large amplitude semi-diurnal tidal activity (4-2, 7-2, 7-3 and 10-1) the tidal ellipses tend to be broader and more circular than elsewhere. This characteristic indicates that the tidal flows are rotationally polarized. In all of these instances the flows rotate in a clockwise sense. At most locations, the degree of circular polarization is largest nearer the surface, at depths of 60 m or less, and decreases with increasing depth. In conjunction with the reduced degree of circular polarization, the amplitude of the tidal variations also decreases with increasing depth.

At some of the other locations where semi-diurnal tidal flows are not particularly large, the tendency is also for reduced circular polarization with increasing depth. While they do decrease at moorings 5-1 and 9-1, at mooring 7-1, the amplitudes are nearly equal at depths of 64 and 162 m. At the

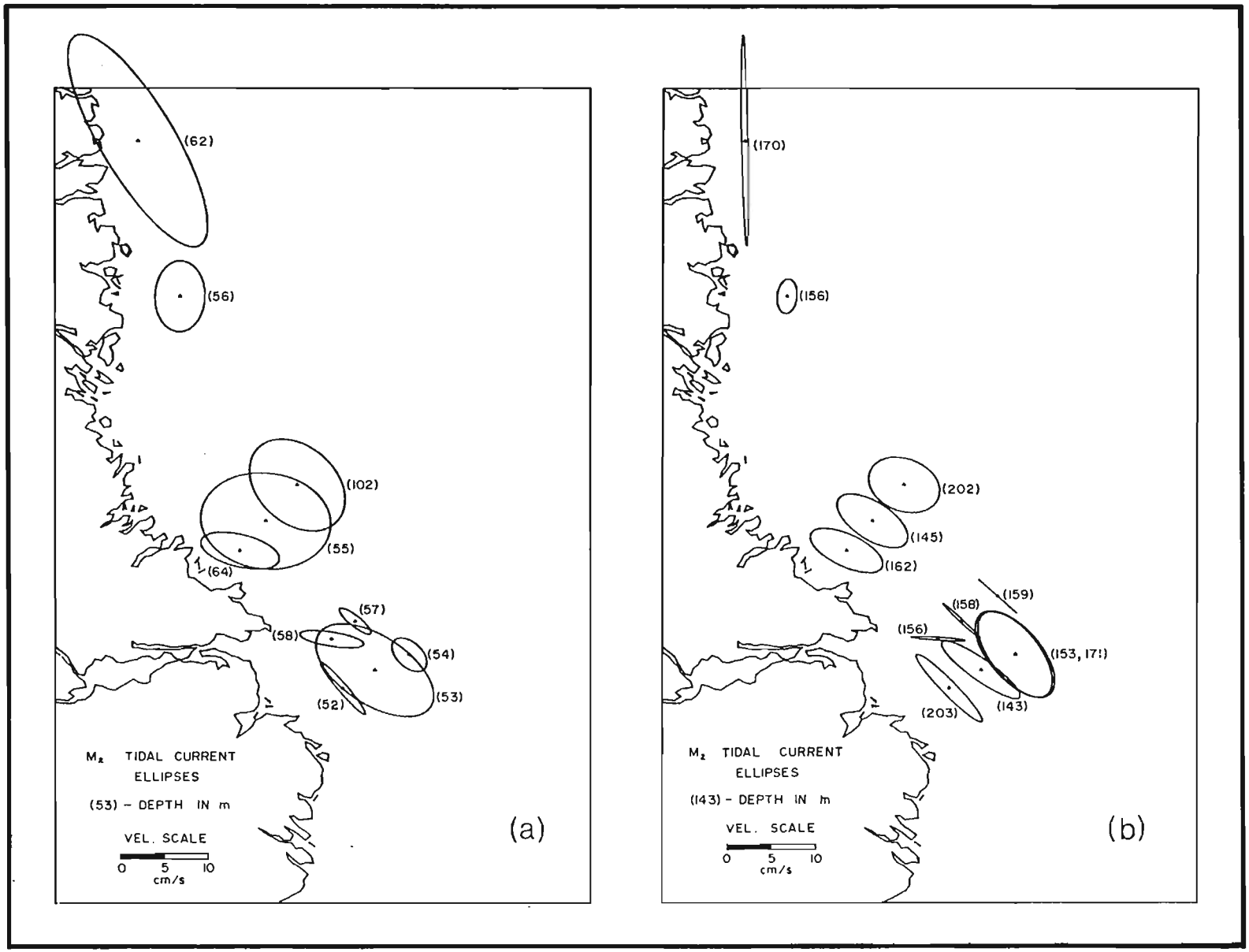

Figure 43: The M_2 tidal current ellipses computed from current meter data obtained at depth ranges of (a) 52 to 102 m and (b) 143 to 203 m.

Table 8

A summary of computed tidal current ellipse parameters for the M_2 and S_2 constituents. The values represented by A and B refer to the amplitudes of the semi-major and semi-minor axes of the tidal current ellipse. A negative value for B indicates a clockwise rotation of the tidal current.

Stn	Latitude	Longitude	Start Date	Stop Date	No Days	Depth (m)	M_2 A cm/s	M_2 B cm/s	M_2 Inc Degrees	M_2 Phse Degrees	S_2 A cm/s	S_2 B cm/s	S_2 Inc Degrees	S_2 Phse Degrees
4-1	54°10.0'	55°44.0'	11/07	10/09	61	52	3.8	-0.5	144	225	1.0	-0.3	152	266
4-1	54°10.0'	55°44.0'	11/07	10/09	61	203	5.2	-0.8	148	238	1.4	-0.2	156	285
4-2	54°25.2'	55°15.9'	11/07	16/09	67	53	7.4	-3.8	160	233	3.1	-2.1	169	276
4-2	54°25.2'	55°15.9'	11/07	16/09	67	143	5.3	-1.2	158	232	1.8	-0.7	174	281
4-3	54°39.1'	54°44.0'	11/07	5/10	86	54	2.3	-1.4	150	306	0.8	-0.2	166	348
4-3	54°39.1'	54°44.0'	11/07	5/10	86	153	5.7	-2.7	142	228	2.1	-1.3	150	275
4-3	54°39.1'	54°44.0'	11/07	5/10	86	171	5.9	-2.9	144	228	2.3	-1.4	151	267
5-1	54°37.4'	56° 7.7'	7/07	15/09	70	58	3.6	-0.8	5	101	0.9	-0.2	12	148
5-1	54°37.4'	56° 7.7'	7/07	15/09	70	156	3.0	-0.2	10	88	1.1	-0.5	20	129
5-2	54°51.7'	55°47.2'	6/07	5/10	91	31	1.9	0.8	174	248	1.9	0.8	174	248
5-2	54°51.4'	55°47.9'	7/07	5/10	90	57	2.2	0.6	155	229	0.8	-0.0	168	258
5-2	54°51.4'	55°47.9'	7/07	5/10	90	158	2.8	0.2	151	227	1.4	-0.4	166	285
5-2	54°51.4'	55°47.9'	7/07	5/10	90	269	2.6	0.3	145	216	1.1	-0.2	177	281
5-3	55°11.0'	55°16.1'	12/07	13/09	63	159	2.8	0.0	152	246	1.5	-0.1	16	155
5-3	55°11.0'	55°16.1'	12/07	13/09	63	277	3.4	-0.8	171	262	1.6	-0.9	166	293
7-1	55°15.0'	58° 5.9'	4/07	12/09	70	64	4.5	-1.8	2	74	1.8	-0.7	9	123
7-1	55°15.0'	58° 5.9'	4/07	12/09	70	162	4.4	-1.8	171	245	1.9	-0.9	166	296
7-2	55°36.6'	57°46.7'	4/07	12/09	70	25	10.0	-7.2	1	65	2.5	-1.5	175	296
7-2	55°36.5'	57°47.4'	4/07	12/09	70	55	7.3	-5.3	9	77	3.0	-2.1	0	118
7-2	55°36.5'	57°47.4'	4/07	12/09	70	145	4.5	-2.1	163	231	4.5	-2.1	163	231
7-3	56° 2.5'	57°24.2'	5/07	11/09	68	102	6.0	-4.3	154	272	1.8	-1.6	11	90
7-3	56° 2.5'	57°24.2'	5/07	11/09	68	202	4.1	-2.9	174	258	1.6	-1.1	45	75
7-3	56° 2.5'	57°24.2'	5/07	31/08	57	656	1.5	-0.4	133	185	0.3	-0.2	154	170
9-1	57°32.3'	60°28.3'	18/07	1/10	75	56	3.9	-2.8	105	330	1.4	-1.1	73	33
9-1	57°32.3'	60°28.3'	18/07	1/10	75	156	1.9	-1.1	101	319	1.9	-1.1	101	319
10-1	58°53.3'	62°10.3'	16/07	30/09	76	62	13.4	-4.1	140	318	4.4	-1.2	135	43
10-1	58°53.3'	62°10.3'	16/07	30/09	76	170	11.5	-0.4	110	319	3.6	0.2	108	23

remaining sites (4-1, 4-3, 5-2 and 5-3), semi-diurnal tidal amplitudes actually increase at greater depths.

In comparison with the semi-diurnal tidal currents, the amplitude of the diurnal flows is generally low (Figure 44 and Table 9). The form number (defined as the sum of the amplitudes of the two largest diurnal constituents, the K_1 and O_1, divided by the corresponding sum of the M_2 and S_2 amplitudes) ranges from 0.2 to 0.7 at all but three of the mooring sites. The exceptions occur at 5-2 where both semi-diurnal and diurnal tidal flows are small and at stations 7-2 and 9-1 as discussed below. At all locations excluding 7-2 and 9-1, the amplitude of the largest diurnal constituent, K_1, ranges from 0.3 to 2.5 cm/s, about a median value of 1.1 cm/s.

At mooring 7-2, the amplitude of the diurnal tidal flows is much larger. For the K_1 constituent, the semi-major value ranges from 6.1 to 4.2 cm/s according to depth. The amplitude of the O_1 constituent is nearly as large, ranging from 5.6 to 4.2 cm/s. In both constituents, the ellipses are nearly circular, illustrating the high degree of clockwise polarization of the tidal flows. The tidal flows change relatively little with depth, with respect to either amplitude or degree of circular polarization. At mooring 9-1, the diurnal tidal flows are about one-half the amplitude of those of 7-2. The degree of circular polarization is also reduced, although it remains clockwise.

Tidal currents can result from barotropic (surface) tides or from baroclinic (internal) tides. The spatial pattern of the barotropic tide is illustrated in the cotidal charts for the surface tidal elevations of the M_2 and K_1 tidal constituents (Figure 45) as computed from coastal water level measurements (Godin, 1980). The M_2 tidal height amplitudes range from 40 cm in the southern end of the area of interest, to more than 200 cm at the area's northern limit. The K_1 tidal heights are much smaller, 10 to 15 cm in amplitude, with the result that the surface tidal height variations are predominantly semi-diurnal throughout the area, particularly in the northern portion. The dominance of the semi-diurnal surface tidal activity can be seen in the coastal water level record from Nain, Labrador (Figure 46).

Based on the spatial pattern of the surface tide, the tidal currents would be expected to be predominantly semi-diurnal with the largest values occurring in the northern part of the study area. The relatively large semi-diurnal flows observed at station 10-1 on Saglek Bank are consistent with such a description. However, given the spatially irregular variations in the amplitudes of the semi-diurnal tidal currents throughout the region, both horizontally and vertically, the surface tide alone cannot account for the observed spatial variability. Thus, the possibility of internal tidal activity requires examination.

As a first step, a semi-diurnal band-pass digital filter was applied to selected current meter data sets, before and after the removal of the predicted tidal currents. The predicted tidal flows were removed by subtracting a time series, computed from all the resolvable tidal constituents, from the original time series data. The results are shown in Figures 47 and 48 for data sets 4-1/52, 4-2/53, 4-3/153, and 7-2/55. In each case, following removal of the predicted tidal currents, the amplitudes are markedly reduced. Also, the total

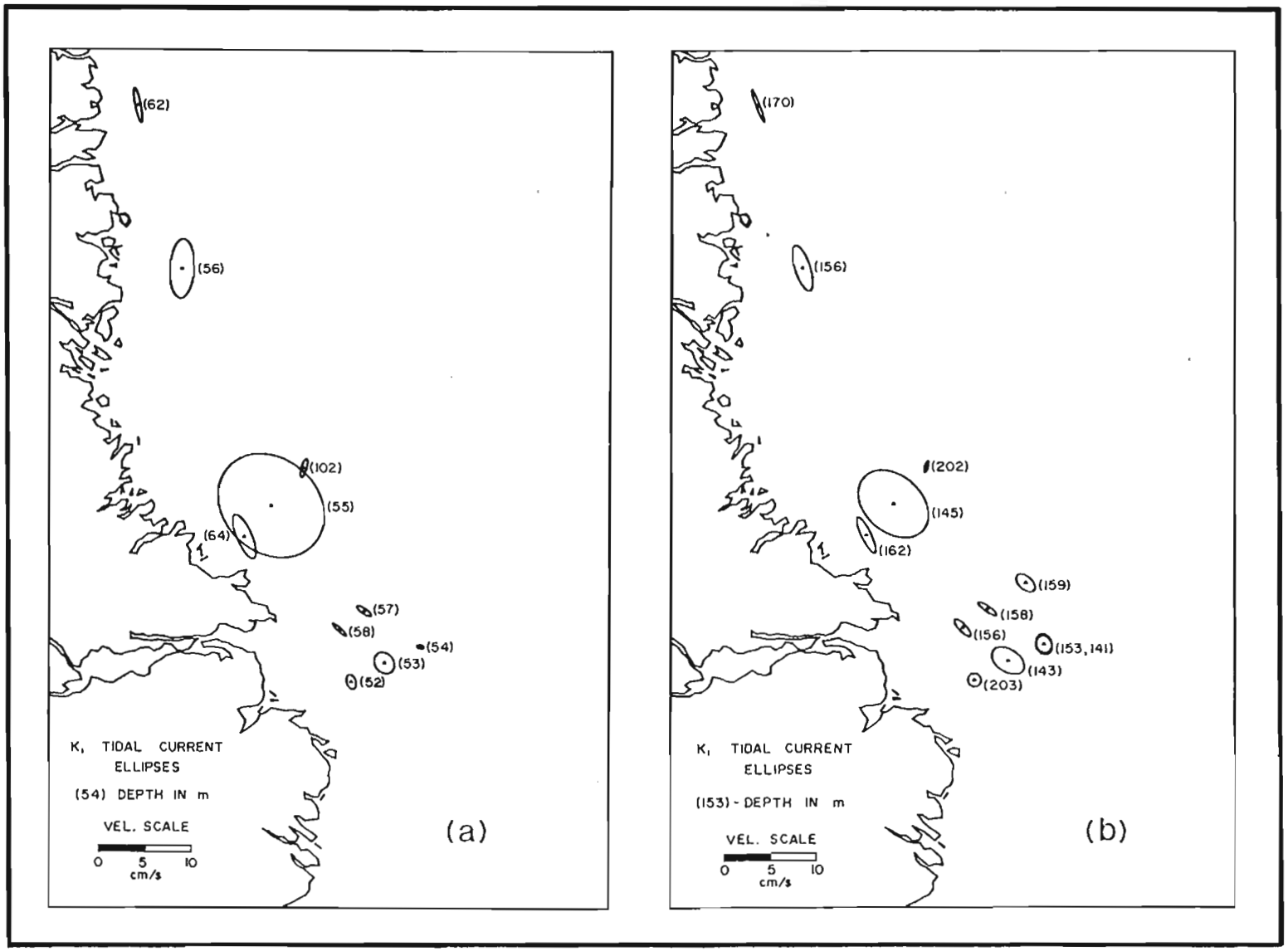

Figure 44: The K_1 tidal current ellipses computed from current meter data obtained at depth ranges of (a) 52 to 102 m and (b) 143 to 203 m.

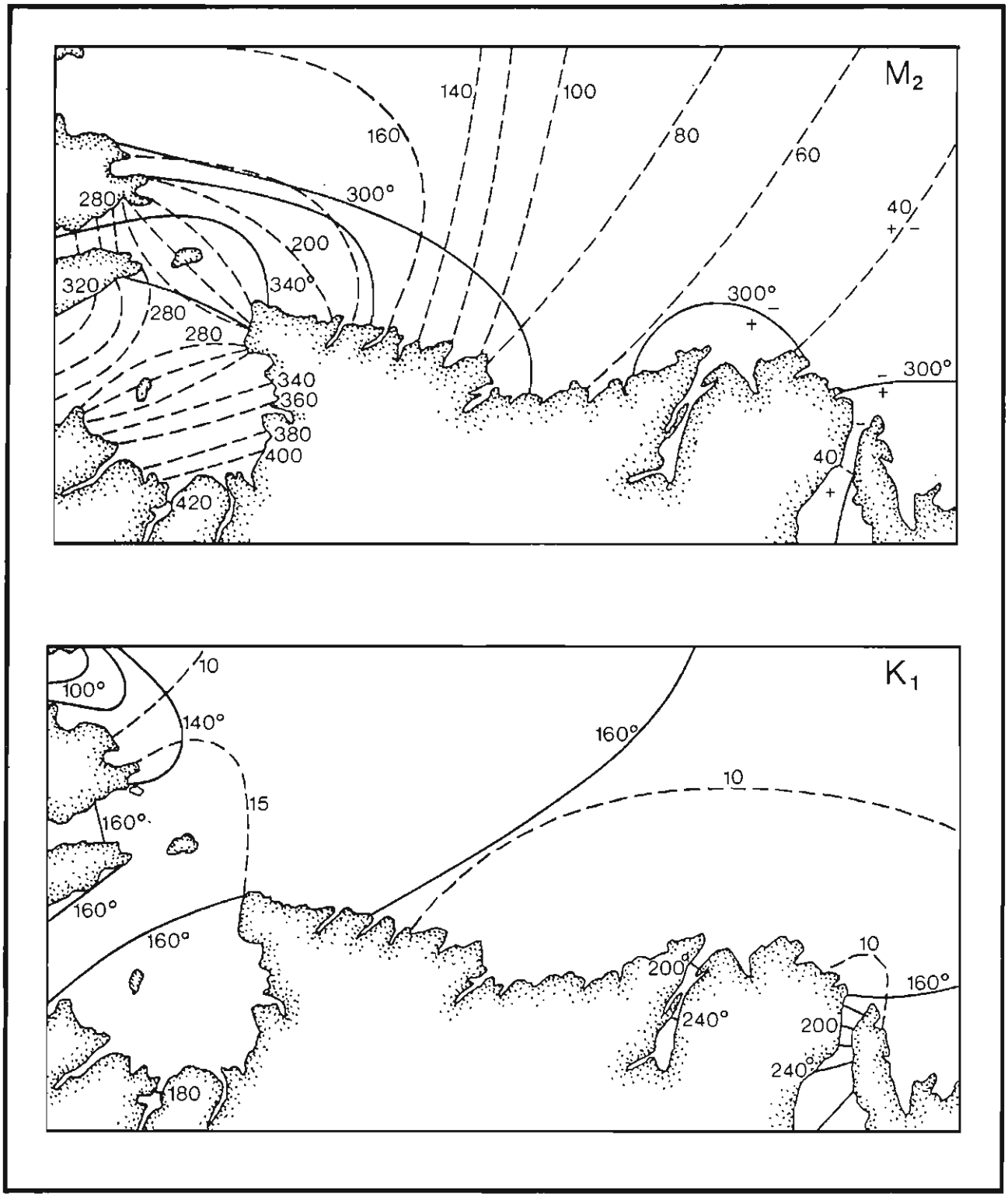

Figure 45: Cotidal charts of the surface tidal elevations for (a) the M_2 constituent and (b) the K_1 constituent (from Godin, 1980). The solid lines are contours of constant Greenwich phase in degrees; the dashed lines are contours of constant amplitude in centimetres.

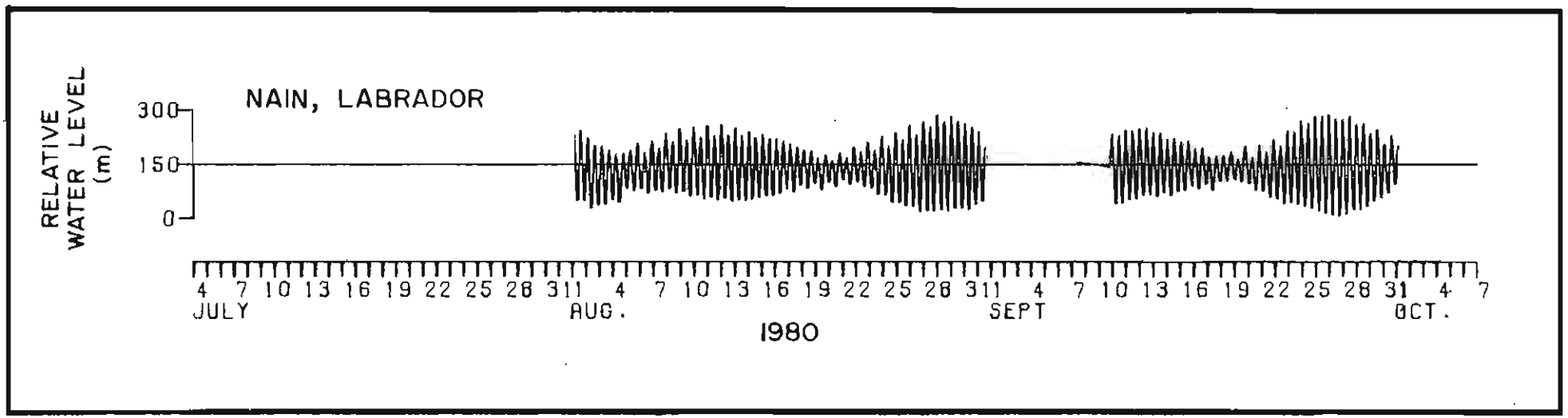

Figure 46: Water level data collected at Nain, Labrador by the Marine Environmental Data Service, for the period July-September, 1980.

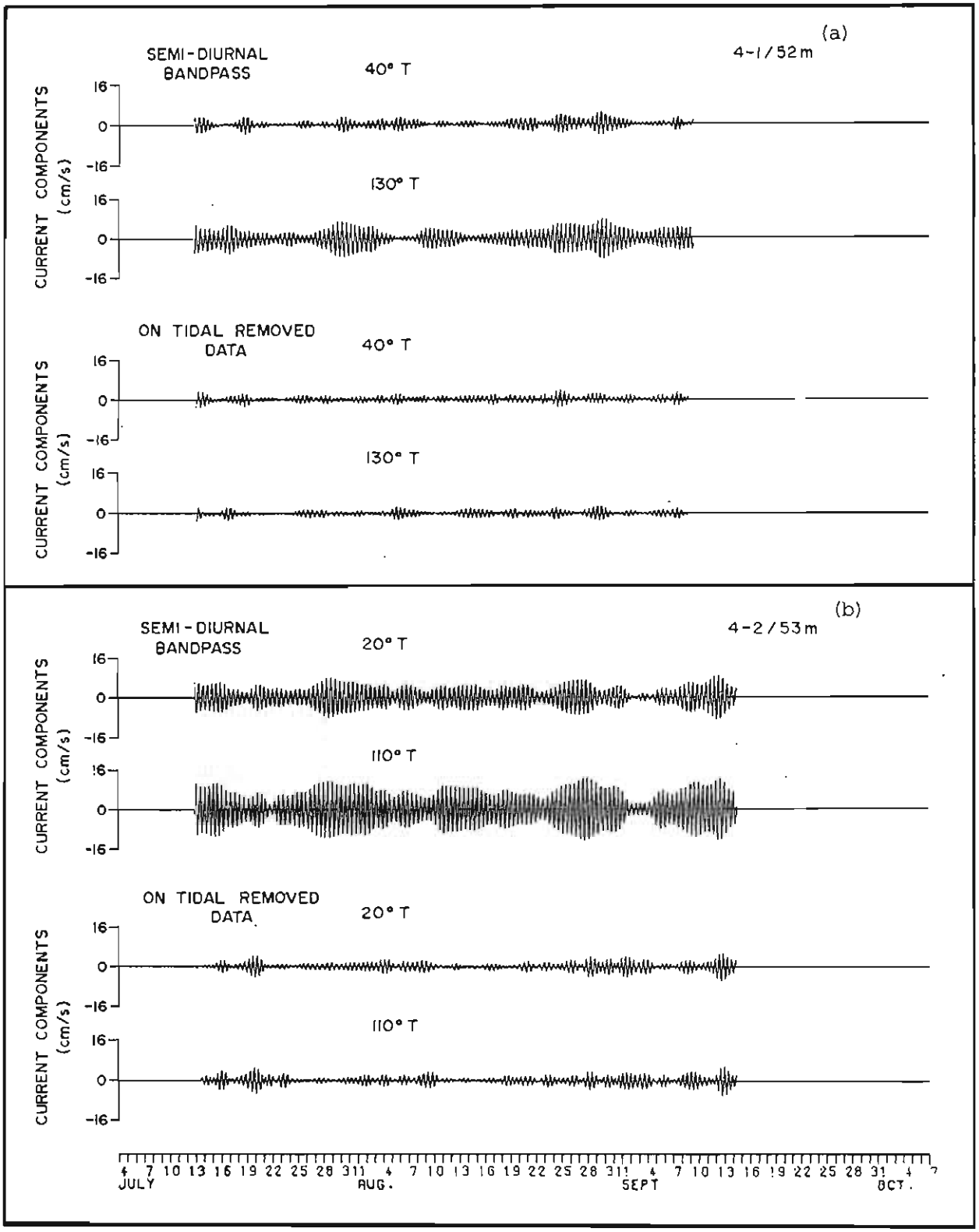

Figure 47: Semi-diurnal passed time series computed from hourly current data before and after removal of the predicted tidal currents. The results are given for data sets (a) 4-1/52 and (b) 4-2/53. The direction in degrees of each orthogonal current component is indicated by the number located above each time series plot.

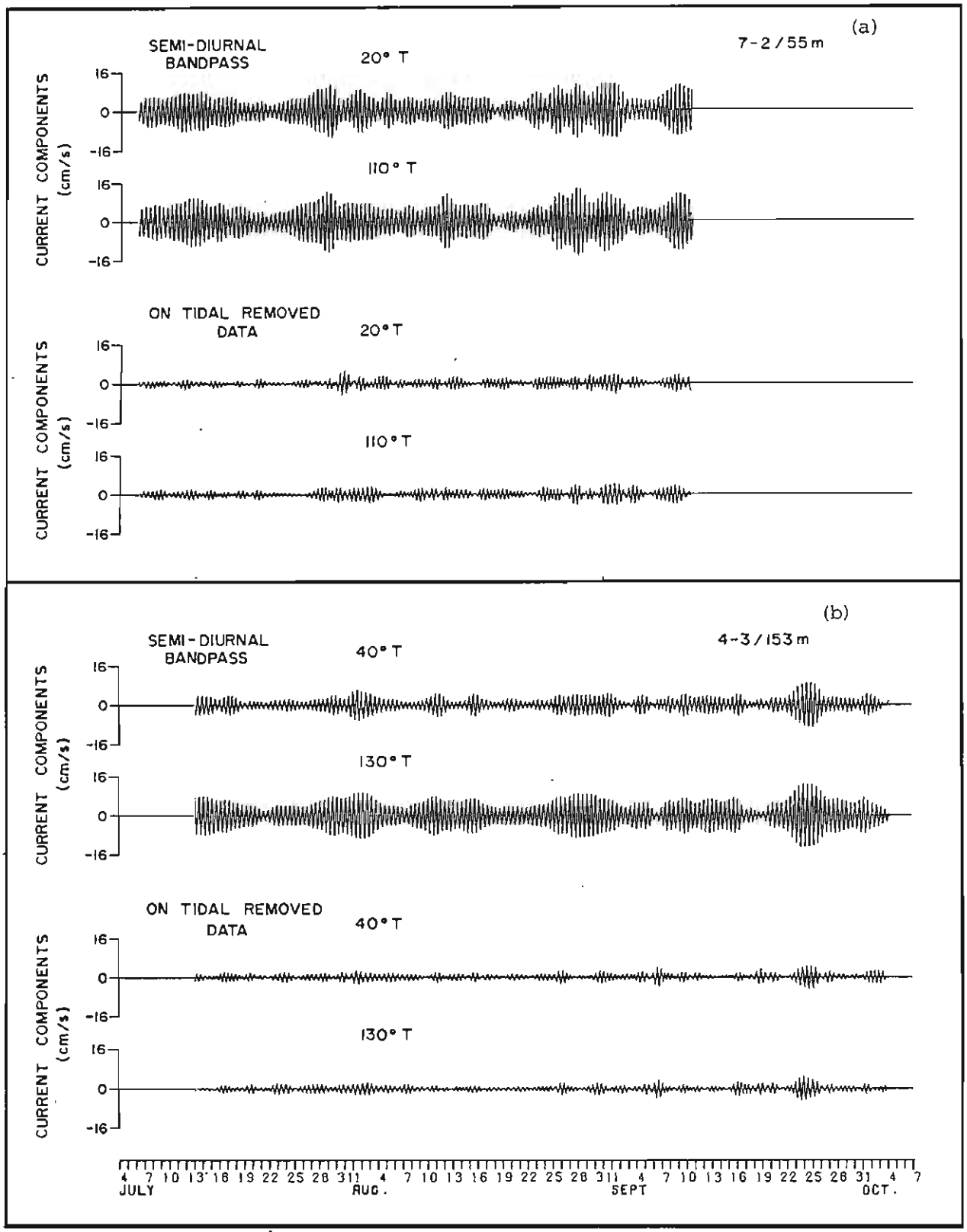

Figure 48: Semi-diurnal passed time series computed from averaged hourly current data before and after removal of the predicted tidal currents. The results are given for data sets (a) 7-2/55 and (b) 4-3/153. The direction in degrees of each orthogonal current component is indicated by the number located above each time series plot.

Table 9

A summary of computed tidal current ellipse parameters for the K_1 and O_1 constituents. The values represented by A and B refer to the amplitudes of the semi-major and semi-minor axes of the tidal current ellipse. A negative value of B indicates a clockwise rotation of the tidal current.

Stn	Latitude	Longitude	Start Date	Stop Date	No Days	Depth (m)	K_1 A cm/s	K_1 B cm/s	K_1 Inc Degrees	K_1 Phse Degrees	O_1 A cm/s	O_1 B cm/s	O_1 Inc Degrees	O_1 Phse Degrees
4-1	54°10.0'	55°44.0'	11/07	10/09	61	52	0.8	-0.5	121	255	0.9	-0.2	150	93
4-1	54°10.0'	55°44.0'	11/07	10/09	61	203	0.7	-0.7	124	282	1.5	-1.1	116	174
4-2	54°25.2'	55°15.9'	11/07	16/09	67	53	1.2	-1.0	143	251	1.4	-1.1	113	183
4-2	54°25.2'	55°15.9'	11/07	16/09	67	143	1.9	-1.2	161	258	2.1	-1.4	150	168
4-3	54°39.1'	54°44.0'	11/07	5/10	86	54	0.4	0.2	8	165	0.9	-0.4	129	148
4-3	54°39.1'	54°44.0'	11/07	5/10	86	153	0.9	-0.8	133	274	1.2	-0.7	141	169
4-3	54°39.1'	54°44.0'	11/07	5/10	86	171	1.1	-0.9	122	289	0.9	-0.6	173	145
5-1	54°37.4'	56° 7.7'	7/07	15/09	70	58	1.0	-0.2	152	263	0.9	-0.6	121	168
5-1	54°37.4'	56° 7.7'	7/07	15/09	70	156	1.2	0.4	147	257	0.9	0.1	130	154
5-2	54°51.7'	55°47.2'	6/07	5/10	91	31	1.3	-0.7	166	215	1.6	-0.5	153	135
5-2	54°51.4'	55°47.9'	7/07	5/10	90	57	0.9	-0.3	161	238	1.6	-0.5	152	158
5-2	54°51.4'	55°47.9'	7/07	5/10	90	158	1.2	-0.3	159	221	1.3	-0.6	153	148
5-2	54°51.4'	55°47.9'	7/07	5/10	90	269	1.0	-0.3	176	226	0.7	-0.1	159	158
5-3	55°11.0'	55°16.1'	12/07	13/09	63	159	1.2	-0.7	153	154	1.2	-0.7	153	154
5-3	55°11.0'	55°16.1'	12/07	13/09	63	277	1.1	-0.8	65	331	1.1	-0.7	153	186
7-1	55°15.0'	58° 5.9'	4/07	12/09	70	64	2.5	-0.8	129	176	1.9	-0.8	127	95
7-1	55°15.0'	58° 5.9'	4/07	12/09	70	162	2.1	-0.5	131	194	2.0	-0.2	128	111
7-2	55°36.6'	57°46.7'	4/07	12/09	70	25	5.9	-4.8	150	178	5.6	-4.0	147	99
7-2	55°36.5'	57°47.4'	4/07	12/09	70	55	6.1	-5.0	156	181	4.7	-3.5	143	116
7-2	55°36.5'	57°47.4'	4/07	12/09	70	145	4.2	-3.0	154	203	4.2	-3.7	148	120
7-3	56° 2.5'	57°24.2'	5/07	11/09	68	102	1.0	-0.3	88	238	0.9	-0.5	45	238
7-3	56° 2.5'	57°24.2'	5/07	11/09	68	202	0.6	-0.2	86	240	0.5	-0.4	8	262
7-3	56° 2.5'	57°24.2'	5/07	31/08	57	656	0.3	0.0	10	335	0.3	-0.1	66	339
9-1	57°32.3'	60°28.3'	18/07	1/10	75	56	3.1	-1.3	104	127	2.8	-1.0	102	52
9-1	57°32.3'	60°28.3'	18/07	1/10	75	156	2.5	-0.8	125	134	2.2	-0.6	132	52
10-1	58°53.3'	62°10.3'	16/07	30/09	76	62	1.8	-0.3	120	53	1.6	-0.3	120	330
10-1	58°53.3'	62°10.3'	16/07	30/09	76	170	1.8	-0.2	130	74	1.6	-0.2	133	356

standard deviation, mean and maximum speed values are all reduced by factors of two to three.

The semi-diurnal variations remaining after removal of the predicted tidal currents can be largely associated with the phase varying portion of the internal tide. Tidal variation due to the surface tide and the phase invariant portion of the internal tide (over periods of 57 to 90 days) would be contained in the predicted tidal currents and thus removed from the residual semi- diurnal time series. These phase varying internal tidal currents generally occur as individual events which have durations from a few to several days, and typical amplitudes of 2 cm/s or less.

Given the large spatial variations of the predicted tidal ellipse parameters, it appears that internal tidal activity accounts for much of this variability. The internal tidal currents resolved in the tidal analysis are, in large part, phase-invariant over the record lengths of 57 to 90 days. A more detailed analysis of the internal tidal currents based on these data can be found in Martec (1982).

5.8 INERTIAL OSCILLATIONS

Current fluctuations occurring at or near the inertial frequency are an ubiquitous feature of the world's oceans. The amplitude of inertial oscillations is usually largest in the near-surface layer, resulting primarily from fluctuations in the surface wind (Pollard, 1970). At greater depths, inertial oscillations can also occur (Fu, 1980). The inertial frequency, f_I, varies with latitude ($\emptyset$) as:

$$f_I = 2 \sin \emptyset / (1 \text{ sidereal day})$$

where one sidereal day is 23.94 hours. Over the range of current meter mooring locations, the local inertial frequency varies from 1.626 to 1.717 cpd (Figure 49).

The velocity vector associated with inertial oscillations is nearly circularly polarized, rotating clockwise in the northern hemisphere. As a first step in delineating inertial oscillation activity in the current meter observations, the rotary auto- spectral results were examined. The clockwise spectral levels were found to be consistently larger than the counterclockwise values (Table 10) at frequencies between 1.39 and 1.82 cpd, with the single exception of the deepest current meter record (7- 3/656. At depths of less than 300 m, clockwise spectral densities in the band containing the inertial frequency were typically an order of magnitude larger than those of the counterclockwise frequencies, with the ratio ranging from 3 (7- 1/64) to 81.4 (4-1/203).

While the level of clockwise activity is markedly greater than that of counterclockwise activity, the spectral peaks occurring at or near inertial frequencies were small relative to those of the semi-diurnal tidal currents and low frequency variations. With the exception of a few time series records where the semi-diurnal activity was particularly low (7-3/656, 9-1/156 and all four levels at station 5-2), the spectral peaks at or near inertial frequencies were generally about an order of magnitude lower than the semi-diurnal tidal peak.

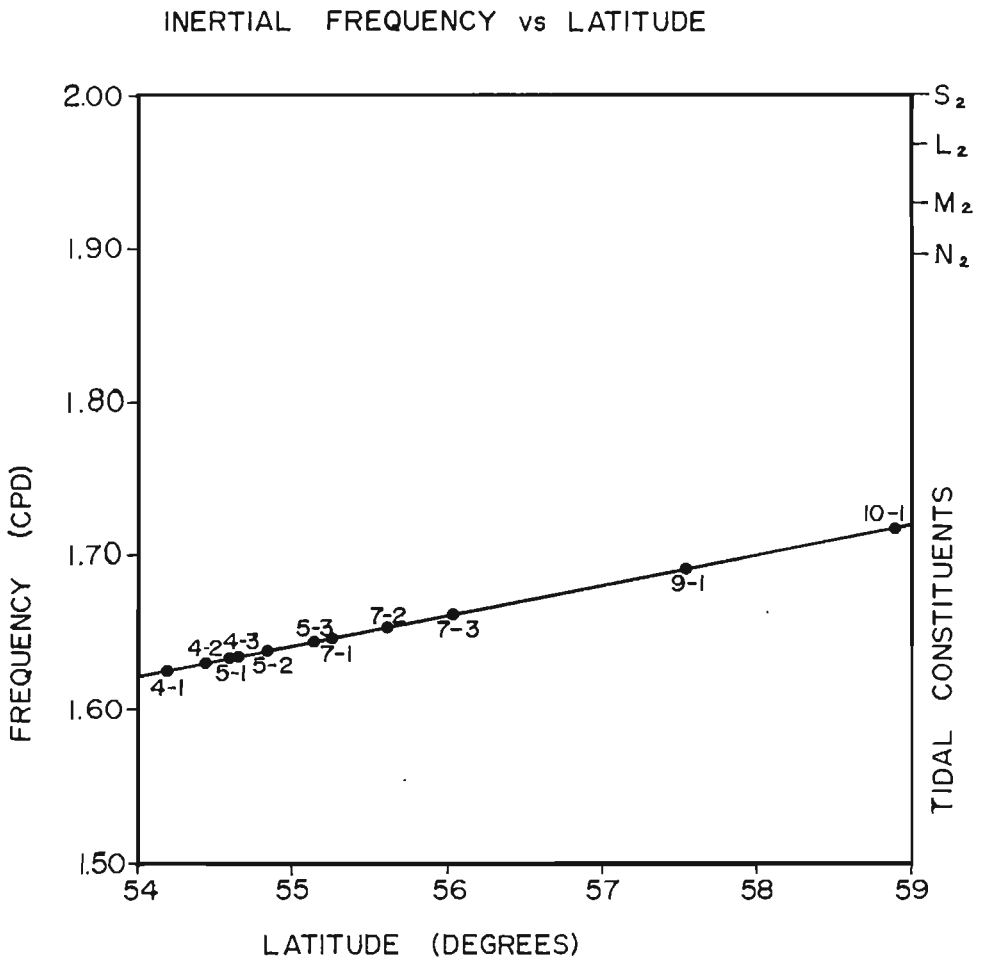

Figure 49: The inertial frequency as function of latitude. The dots indicate the value for each mooring station, while the frequency of semi-diurnal tidal constituents are shown on the right-hand border.

Table 10

The rotary auto-spectral densities of vector currents, clockwise (cw) and counterclockwise (ccw) for frequencies near the inertial frequency (f_I). The spectral bandwidth is 0.0714 cpd. Spectral densities are in $(cm/s)^2/cpd$.

Station	Depth (m)	f_I	Spectral Density cw	Spectral Density ccw	Peak?	Other Spectral Peaks Density (frequency)
4-1	52	1.626	4.4	0.3	N	12.0 (1.57)
4-1	203	1.626	40.7	0.5	Y	--
4-2	53	1.631	23.6	0.7	Y	24.0 (1.79)
4-2	143	1.631	11.6	0.3	N	12.1 (1.50), 28.9 (1.71)
4-3	54	1.635	22.5	1.1	N	28.8 (1.50), 28.4 (1.17)
4-3	153	1.635	11.6	0.9	N	23.5 (1.50)
4-3	171	1.635	13.7	0.5	N	19.8 (1.50)
5-1	58	1.635	8.1	1.4	N	10.7 (1.57), 15.0 (1.79)
5-1	156	1.635	5.8	1.7	N	8.9 (1.71)
5-2	31	1.640	32.7	4.6	Y	--
5-2	57	1.640	12.8	3.6	Y	14.9 (1.50)
5-2	158	1.640	10.7	0.5	N	11.8 (1.57), 13.4 (1.71)
5-2	269	1.640	2.2	0.4	N	--
5-3	159	1.646	6.5	1.7	N	20.6 (1.57)
5-3	277	1.646	20.3	2.2	N	23.3 (1.71)
7-1	64	1.647	3.4	1.3	N	10.2 (1.71)
7-1	162	1.647	5.5	0.8	Y	--
7-2	25	1.655	14.7	1.8	N	39.1 (1.54), 76.5 (1.79)
7-2	55	1.655	15.5	3.1	N	17.8 (1.57)
7-2	145	1.655	13.0	1.6	Y	--
7-3	102	1.663	6.9	1.1	N	9.4 (1.50)
7-3	202	1.663	4.9	1.1	N	6.4 (1.71)
7-3	656	1.663	0.8	0.7	N	5.9 (1.57)
9-1	56	1.692	13.1	0.9	Y	10.9 (1.57)
9-1	156	1.692	6.2	0.5	Y	--
10-1	62	1.717	19.8	0.8	N	24.8 (1.64)
10-1	170	1.717	12.8	2.0	N	--

The peaks in the clockwise auto-spectra in many cases do not coincide with the spectral band containing the inertial frequency. Of the 27 time series records available for rotary auto-spectral analysis, only eight exhibited peaks in the frequency band containing f_I (centred at 1.64 cpd for mooring locations 4-1 to 7-3, 1.71 cpd for mooring locations 9-1 and 10- 1). Of the remaining time series records, nine had the largest near-inertial spectral levels occurring at subinertial frequencies (centred on 1.50, 1.57 or 1.64 cpd) while eight of the records exhibited peaks in frequency bands (1.71 and 1.79 cpd) above the inertial frequency. In two of the records, 5- 2/269 and 10-1/170, no peaks were present near the inertial frequency. In 8 of the 27 time series records, two or more peaks were found at near-inertial frequencies (Table 10).

Previous studies of inertial oscillations (Thomson and Huggett, 1981; Kundu, 1976) reveal peak spectral frequencies of inertial oscillations deviating by as much as $\pm$20% from the local inertial frequency. Such deviations and broadening of the inertial spectral peak can result from a variety of causes. In the absence of a mean flow or a horizontal density gradient, inertial oscillations resulting from a downward flux of wind- generated energy in a stratified fluid are shifted to frequencies above the local inertial frequency. An alternative explanation links the higher observed frequencies to southward wave propagation in the presence of a meridionally variable f_I (see Thomson and Huggett, 1981). In either of these explanations, the shift will be toward higher frequencies since the wave frequencies theoretically lie in the range between the inertial and Brunt-Vaisala frequencies. However, inertial oscillations in the presence of a mean flow can be Doppler shifted resulting in frequency shifts of either sign according to the orientation of the mean current and direction of inertial wave propagation.

The rotary clockwise auto-spectral levels computed near the inertial frequency vary markedly with both location and depth. Not unexpectedly two of the four records with peak clockwise spectral densities in excess of 25 $(cm/s)^2$/day were the data sets collected with Neil Brown current meters at 25 m (station 7-2) and 30 m (station 5-2). At these near-surface depths, the amplitude of wind-generated inertial oscillations would be expected to be larger than for the remaining data sets. More surprisingly, the remaining two data sets with spectral densities exceeding 25 $(cm/s)^2$/cpd were near-bottom measurements taken at station 4-1, 203 m depth and 4-2, 143 m depth. In both cases, the peak values exceeded those computed for the data set obtained at 50-60 m at the same site. However, at the remaining sites where data were collected 9 m above the bottom (4-3/171, 5-2/269, 7-2/145, 9-1/156 and 10-1/170), the clockwise near-inertial peak spectral levels were less than those calculated from the uppermost current meter records.

To examine the amplitudes and temporal variations of inertial oscillations, a few selected data sets were subjected to a bandpass digital filter. The transfer function of the filter is provided in Figure 11. In order to reduce possible contamination through inclusion of semi-diurnal tidal currents, the predicted tidal currents computed from harmonic analysis were subtracted from the time series data prior to application of the digital filter. The resulting time series may still contain some contributions from the random phase portion of the internal tidal currents, but these are too small in amplitude to seriously contaminate the results.

The results of the digital filtering for the two near- surface Neil Brown current meter time series data are shown in Figure 50. At both locations, the inertial oscillations occur as intermittent events with durations from two to seven days. The largest current amplitudes for each record are 11 cm/s at 5-2/31 (Oct. 2) and 10 cm/s at 7-2/25 (Aug. 31). Typical amplitudes for individual events are 5 to 10 cm/s.

A visual comparison between the inertial oscillation activity and the available wind time series data (Figure 51) indicates that the coupling between surface winds and inertial oscillations is not simple. Of the two major inertial events in August, (August 16-21 and August 27-31), the second does not appear to be associated with any particularly prominent shift in the local winds; the winds at station 5-2 were generally weak from August 22-28. The August 16-21 event may be associated with the occurrence of moderate northerly to westerly winds from August 16-18 which reached peak speeds of 17 m/s. Interestingly a series of pronounced wind changes in early September with magnitudes greater than the changes in the winds observed in August were accompanied by relatively low inertial activity. The largest inertial event of the season which occurred from October 1-4 was preceded on September 30 by a sharp change from moderate southerly winds to strong (30 m/s) northwesterly winds.

It is difficult to study the correspondence between inertial activity and surface winds at 7-2/25 since no wind time series data are available at the site for the period of current measurements. A comparison of the currents at stations 5-2 and 7-2 (both band-passed) with the the nearest available wind data at 5-2, suggests that the horizontal coherence of inertial activity is low for these two sites, separated by 300 km.

The lack of a good correspondence between inertial activity and the wind is not unexpected. The vertical coherence scale for inertial motion is typically tens of metres in the upper layer of the ocean (Pollard, 1980). During the July to September period, both of the near-surface current meter data sets were obtained within the seasonal pycnocline. Indeed, the available CTD profiles collected near both measurement sites suggest that until September the most intense part of the pycnocline was usually between depths of 10 and 25 m. As a result, most of the wind generated inertial activity would be confined to depths nearer the surface. Within the pycnocline, the amplitude of inertial oscillations would be reduced and the coherence with the surface winds lessened. By mid-October the seasonal pycnocline was greatly reduced. Based on the abrupt warming observed from the temperature data in late September at 5-2/31, the apparent weakening of the pycnocline may account for the larger inertial activity observed on October 1-4 in this record.

Two other time series data sets, 4-1/52 and 4-1/203, were subjected to bandpass digital filtering (see Figure 52). As noted previously, the near-bottom currents at this site exhibited a very prominent inertial spectral peak, markedly larger than the corresponding peak for the 52 m time series record. The amplitudes in both records reveal the same intermittency apparent in the near-surface currents discussed above. The peak amplitude at 203 m depth is 8 cm/s as compared to 6 cm/s at 52 m depth. There appears to be no coherence in the inertial activity between the two levels. The cause of the enhanced inertial activity in the near-bottom currents at station 4-1 (and at 4-2, as

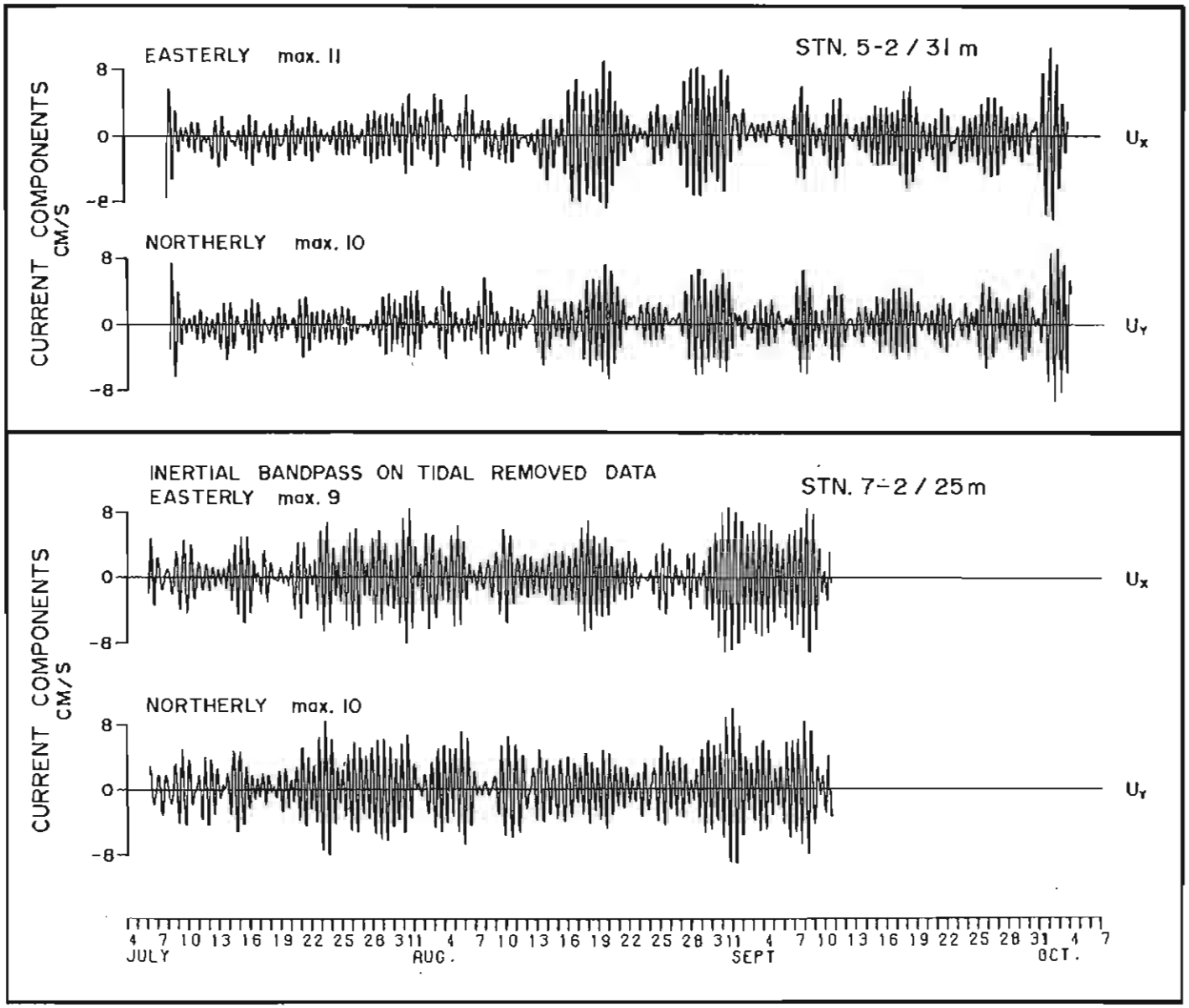

Figure 50: Current components for records 5-2/31 and 7-2/25 following removal of predicted tidal currents and the application of a digital band-pass filter, passing near-inertial frequencies.

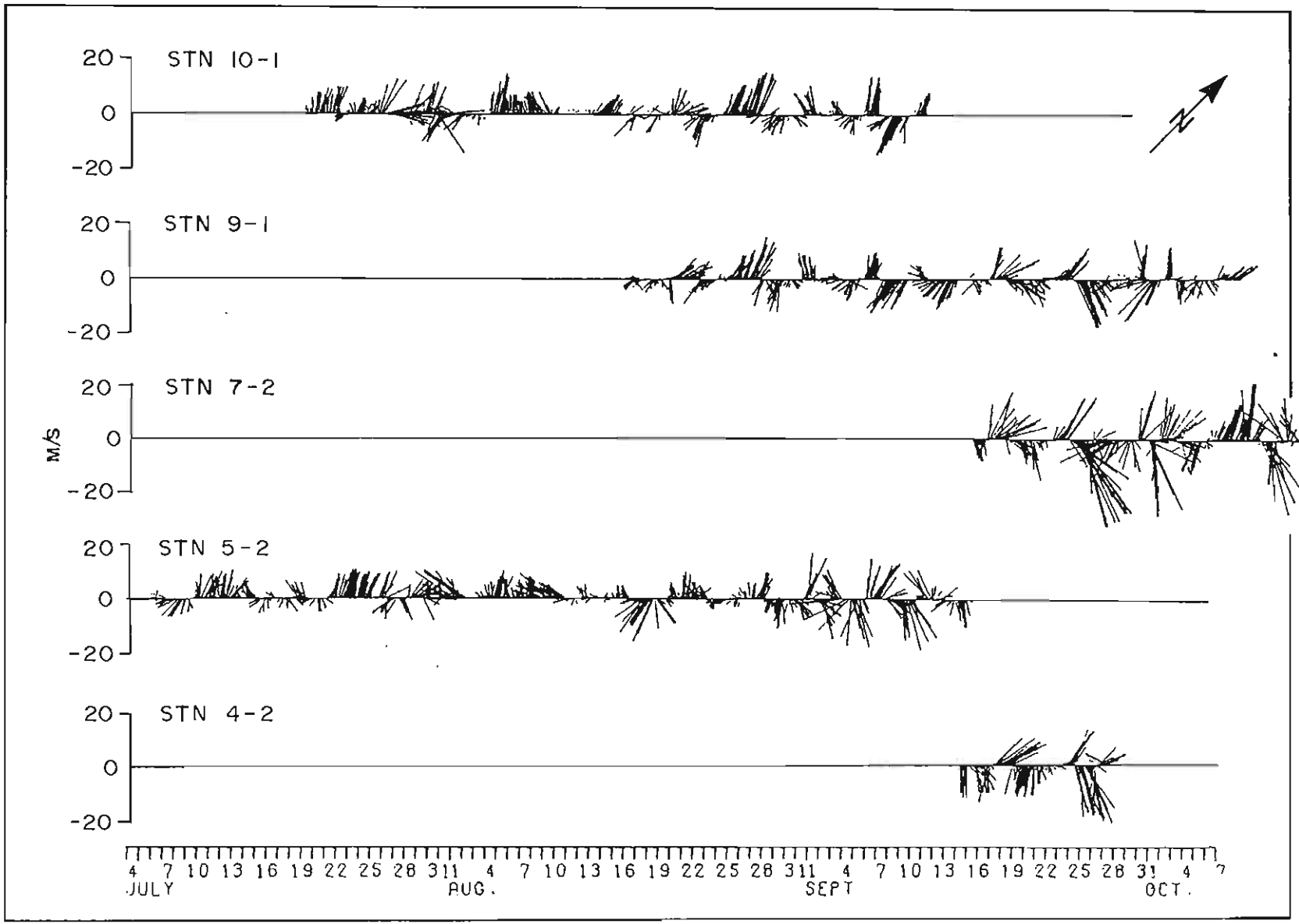

Figure 51: The vector wind time series data obtained from drillships. The vectors are oriented in the direction that the wind blows toward, relative to geographic north as indicated by the arrow.

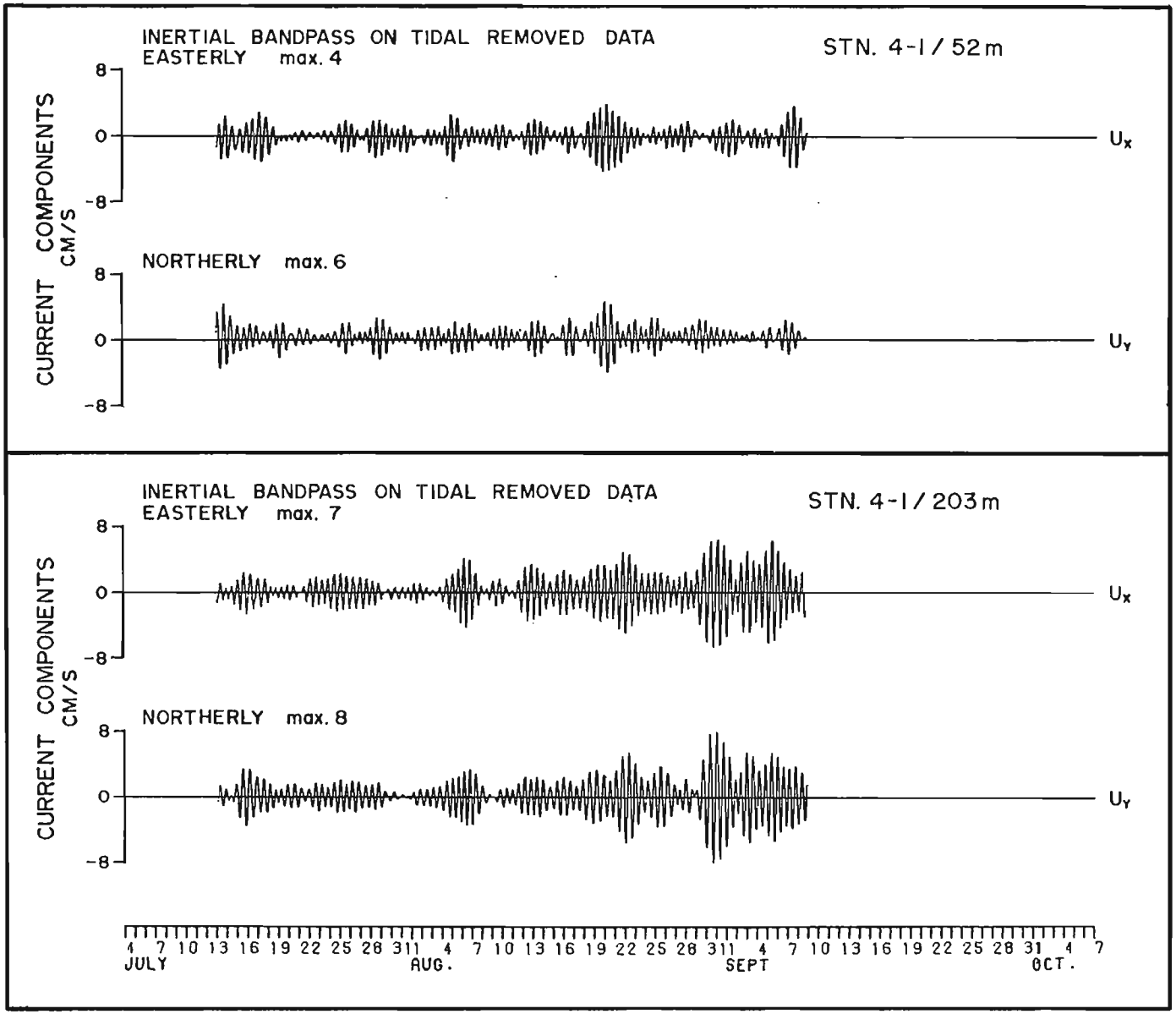

Figure 52: Current components for records 4-1/52 and 4-1/203 following removal of predicted tidal currents and the application of a digital band-pass filter, passing near-inertial frequencies.

deduced from the auto-spectral results) is not clear. An examination of the low frequency currents from the same time series indicates that the periods of relatively large inertial oscillations do not coincide with stronger net flows. Indeed, the inertial activity tends to occur at times of relatively weaker currents directed towards the north, opposite to the stronger southerly flows which occur at other times.

5.9 SUB-TIDAL VARIABILITY

Low Frequency Auto-Spectra

The variability of the currents is dominated by low frequency fluctuations with frequencies below 0.8 cpd (periods greater than 1.2 days) as shown in Figures 36, 37 and 38. To better define the time scales of the low frequency variations, auto-spectra of current components were computed over four to six 14-day blocks. With no band averaging, the frequency resolution is 0.0714 cpd. The lowest frequency band encompasses frequencies from .0357 to 0.107 cpd (periods of 28 to 9.3 days). The spectral values are displayed up to frequencies of .79 cpd. For each frequency band the results are presented as the total auto- spectral level, consisting of the sum of the auto-spectral values for the two orthogonal current components.

The results (Figure 53) show that most of the low frequency activity occurs at or near the lowest resolvable frequencies. In all cases, the largest spectral levels are found to occur in one of the three lowest frequency bands centred at .071, 0.014 or 0.21 cpd (periods of 14, 7 or 5 days). At higher frequencies, the spectral levels decrease markedly. The spectral densities at frequencies of 0.6 to 0.8 cpd are generally reduced by one to two orders of magnitude from the densities computed for frequencies of 0.0357 to 0.2 cpd.

The level of low frequency activity decreased with increasing depth. In Figure 54, the cumulative spectral densities for each record computed over frequencies from 0.0357 to 0.82 cpd are plotted as a function of measurement depth. The cumulative spectral density at 150 m is typically reduced by a factor of two to four from the levels at 50 m depth.

Among the measurement locations, the low frequency activity varies markedly. The highest spectral levels occur at station 5- 2 located in the Cartwright Saddle. Here, at depths of 30 and 50 m, the cumulative low frequency spectral density exceeds that computed at any other station by at least a factor of two. Other locations with relatively large low frequency spectral levels include: station 7-2 located on Makkovik Bank, station 5-3 located near the continental slope and station 5-1 located in the marginal trough. Locations with relatively small low frequency spectral levels are: station 4-2 located on Hamilton Bank, station 7-1 located in the marginal trough, and stations 9-1 and 10-1 located on Nain and Saglek Banks. Low frequency spectral activity at stations 4-1 and 4-3, located on either side of Hamilton Bank, had intermediate levels at 50 m depth, but was relatively low at depths greater than 150 m. Conversely, at station 7-3 located on the continental slope, the low frequency activity was relatively constant with increasing depth with the result that the spectral levels were relatively high at 20 m depth but low at 100 m depth.

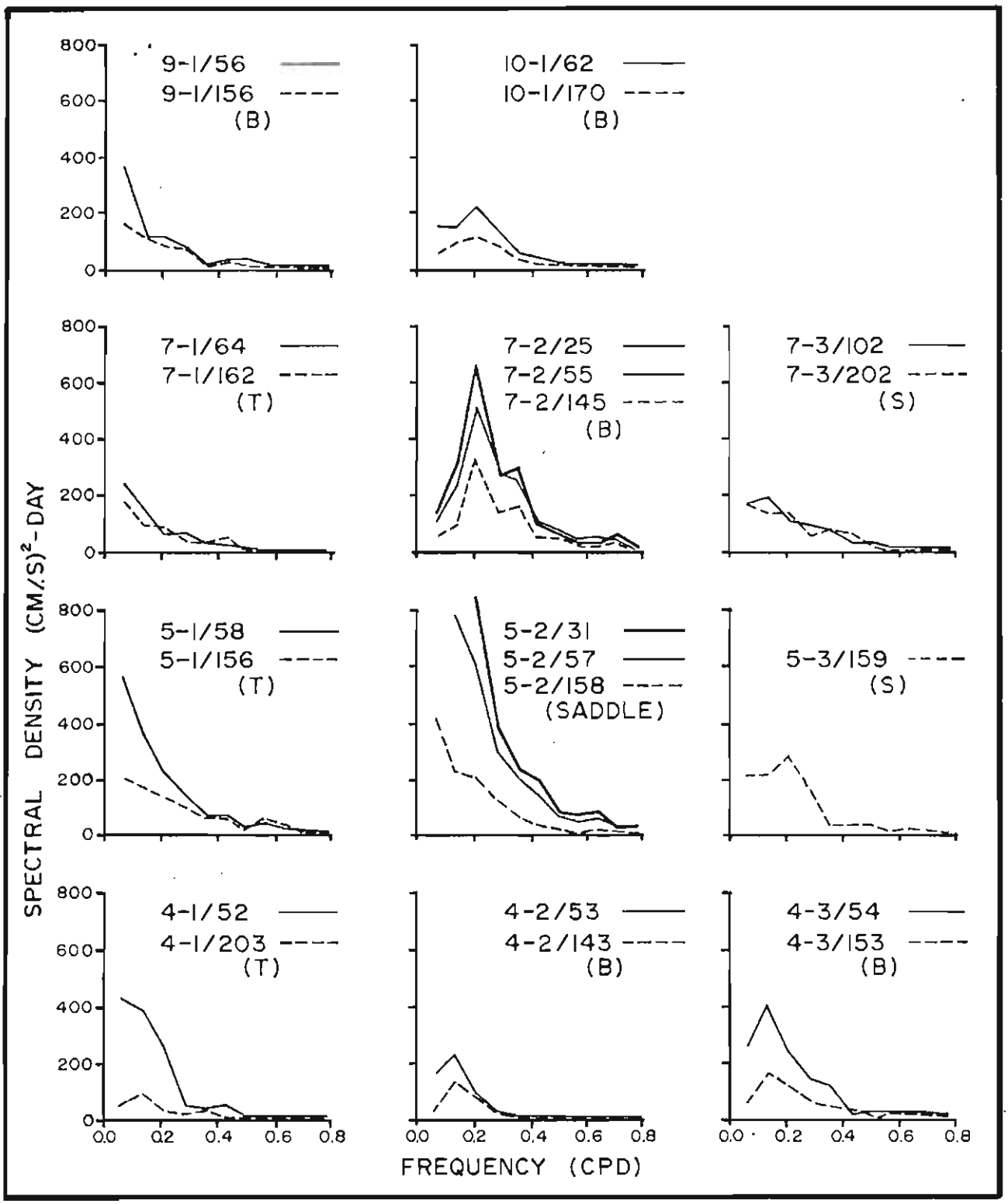

Figure 53: The low frequency auto-spectra densities of the vector current time series. The bandwidth for each spectral estimate is 0.0714 cpd. Bathymetric regimes are indicated as: (T) trough, (B) bank), (S) slope, and (Saddle).

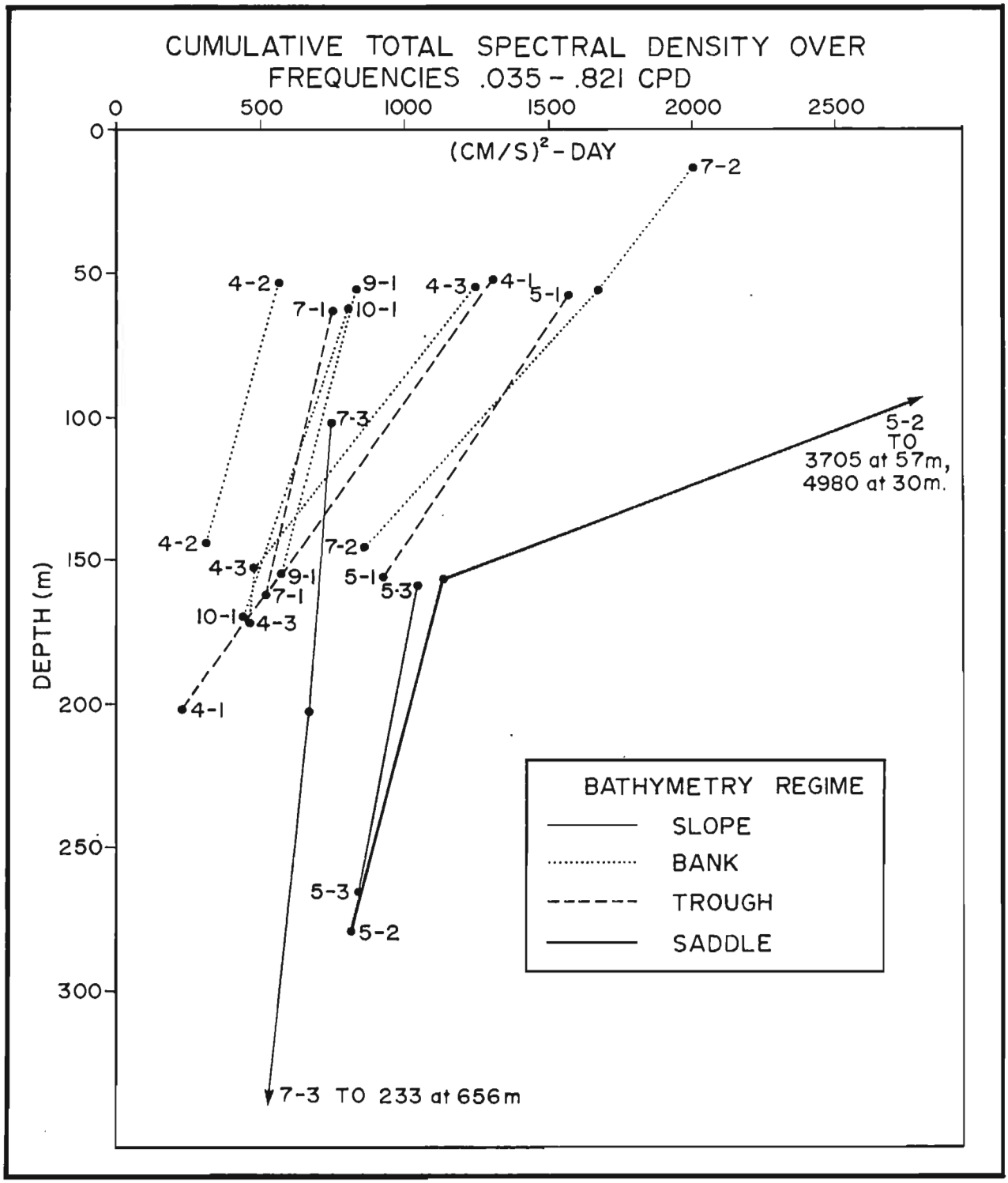

Figure 54: The cumulative spectral density of vector currents, computed over frequencies from 0.035 to 0.821 cpd, plotted as a function of depth.

Given the large differences of spectral levels among the various locations, the amplitude of low frequency activity appears to vary markedly among locations within the same bathymetric regime. This is particularly evident for the currents measured at locations over banks. For example, at 50 m depth the cumulative spectral density varies from 1683 $(cm/s)^2$- day at station 7-2 to 560 $(cm/s)^2$-day at station 4-2. Similarly, for the sites located over the marginal trough, the spectral values range from 1573 $(cm/s)^2$-day at 5-1 to 658 $(cm/s)^2$-day at 7-1 for depths near 50 m.

While the spectral levels differ substantially within bathymetric regimes, the frequency distribution of low frequency activity appears to be more consistent. Variations at the lowest resolvable frequencies (from 0.0357 to 0.107 cpd or periods of 28 to 9.3 days) dominate the spectra for currents measured over the marginal trough and in Cartwright Saddle (Figures 53 and 55). Over the continental slope, the contributions from the three lowest frequency bands, spanning frequencies of 0.035 to 0.25 cpd (periods of 28 to 4 days) are nearly equal.

The distribution of low frequency activity is more variable over the banks, with a tendency for peaks to occur at higher frequencies (Figure 55). This tendency is most evident at station 7-2, where a well defined spectral peak occurs in the third lowest frequency band, (centred at 0.21 cpd (4.7 days). At station 10-1, the peak spectral level occurs at the same frequency, although the magnitude of the peak is considerably reduced. At stations 4-2 and 4-3, the peak spectral values are found in the second lowest frequency band, spanning frequencies from 0.107 to 0.179 cpd centred on 0.143 cpd (periods from 9.3 to 5.6 days, centred on 7.0 days). The spectra for station 9-1, also located on a bank, are somewhat anomalous with peak levels occurring in the lowest frequency band.

With increasing depth, the spectral levels decrease more rapidly in the lowest resolvable frequency band than in other bands. From depths of 50 to 150 m, the relative contribution from the lowest frequency band (centred at 14 days) decreased at all locations but one. (The one exception was station 7-3, located over the continental slope, where the lowest band contributions were very nearly equal at depths of 102 and 202 m.) This decreasing trend appears to continue with increasing depths at stations 5-2, 5-3 and 7-3 (see Figure 56).

Very Low Frequency Auto-Spectra

In view of the relatively high levels of spectral densities found in the lowest frequency band for many of the current meter records, the auto-spectral analysis was extended to lower frequencies. This was accomplished by computing spectral densities over blocks of 28 days rather than 14. By doing so, the lowest resolvable frequency band is centred at 0.036 cpd (28 days) extending from 0.018 cpd (56 days) to 0.054 (18.7 days). However, for most of the records, only two 28 day blocks could be used, which reduced the statistical confidence of the auto- spectral estimates (at station 4-3 and 5-2, the records were of sufficient duration to use three blocks for auto-spectral computations).

The results of the very low frequency auto-spectral analyses are presented in Figures 57 and 58, as the total spectral densities for the seven lowest frequency bands, from 0.018 to 0.27 cpd. At depths near 50 m, relatively large

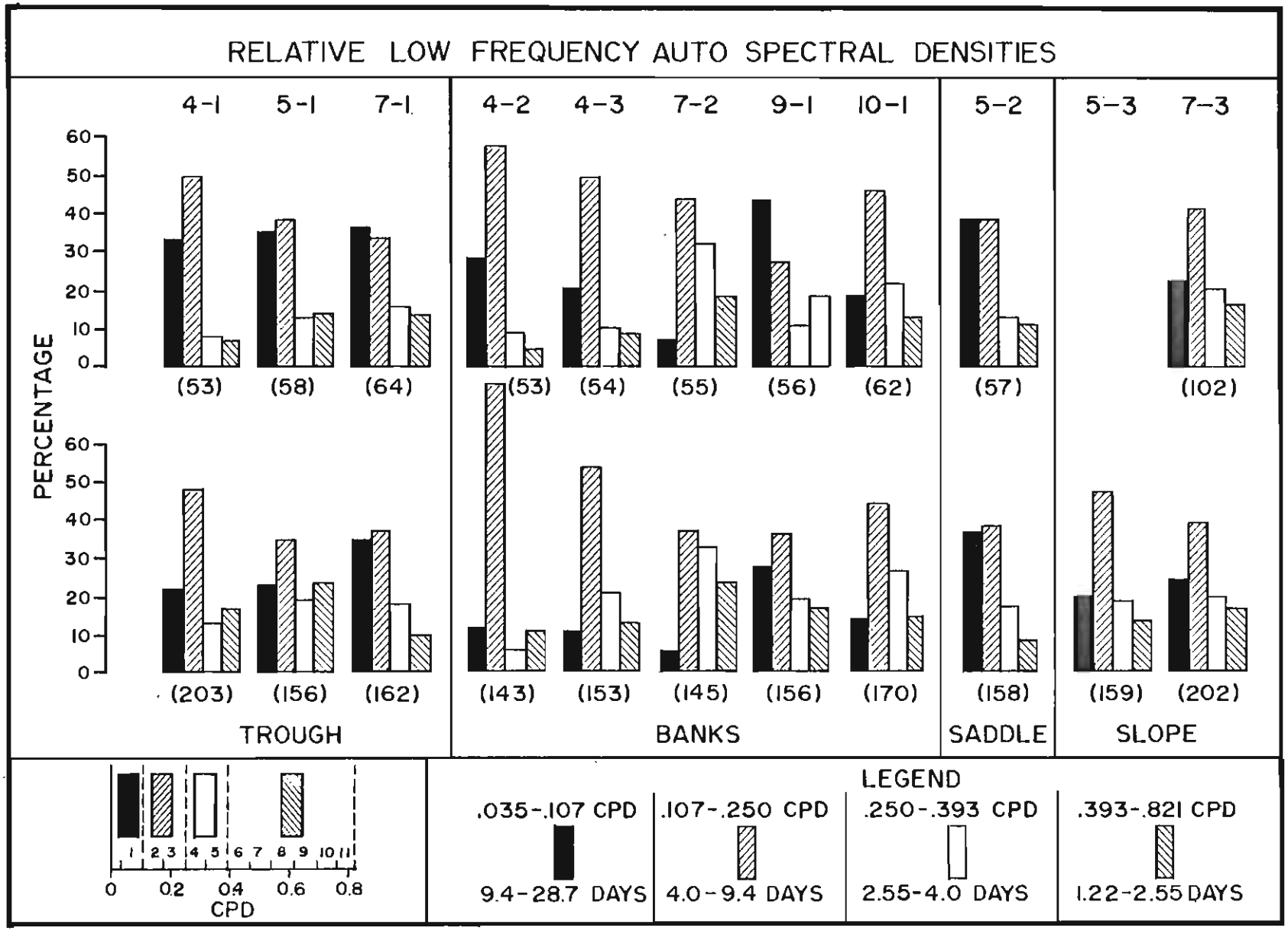

Figure 55: Relative auto-spectral density levels of vector currents over frequencies of 0.035 to 0.821 cpd. The relative contributions are provided for four individual bands for depths of 52 to 203 m.

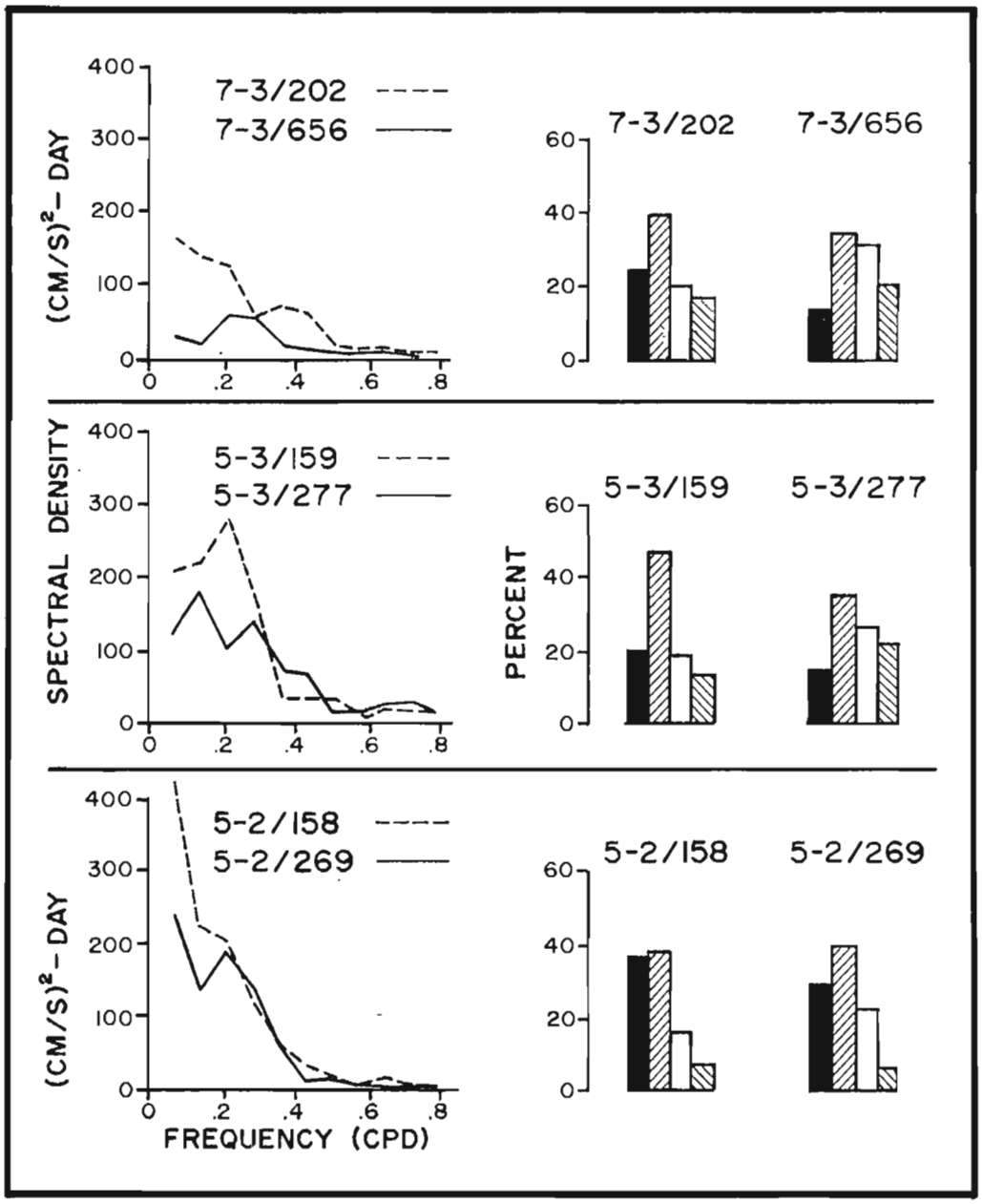

Figure 56: The low frequency auto-spectral densities and the relative auto-spectral density levels for vector currents obtained at depths greater than 250 m.

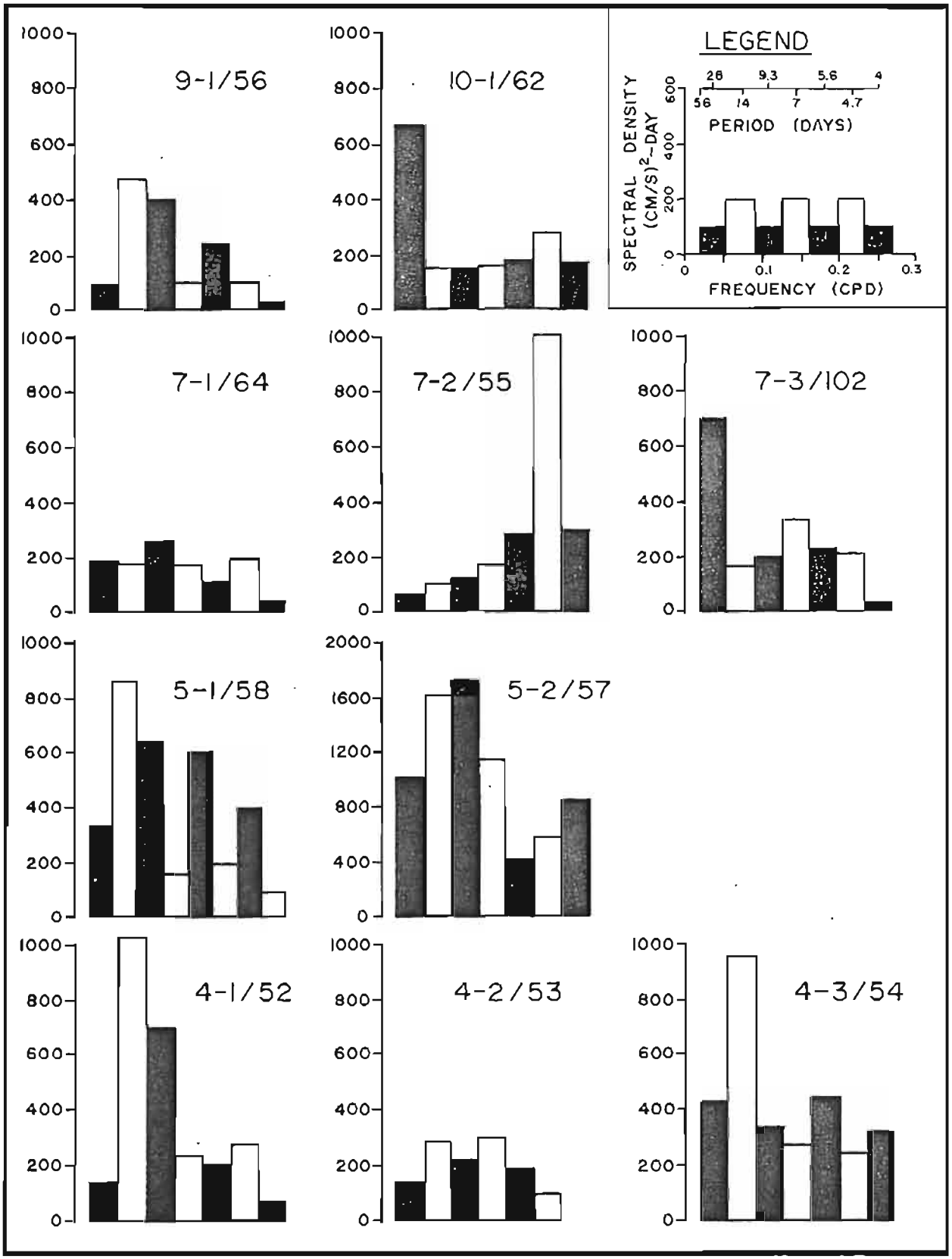

Figure 57: The auto-spectral densities of vector currents at depths of 52 to 102 m for very low frequencies computed from 28 day blocks. The number of blocks was two, except at stations 4-3 and 5-2 where three blocks were used.

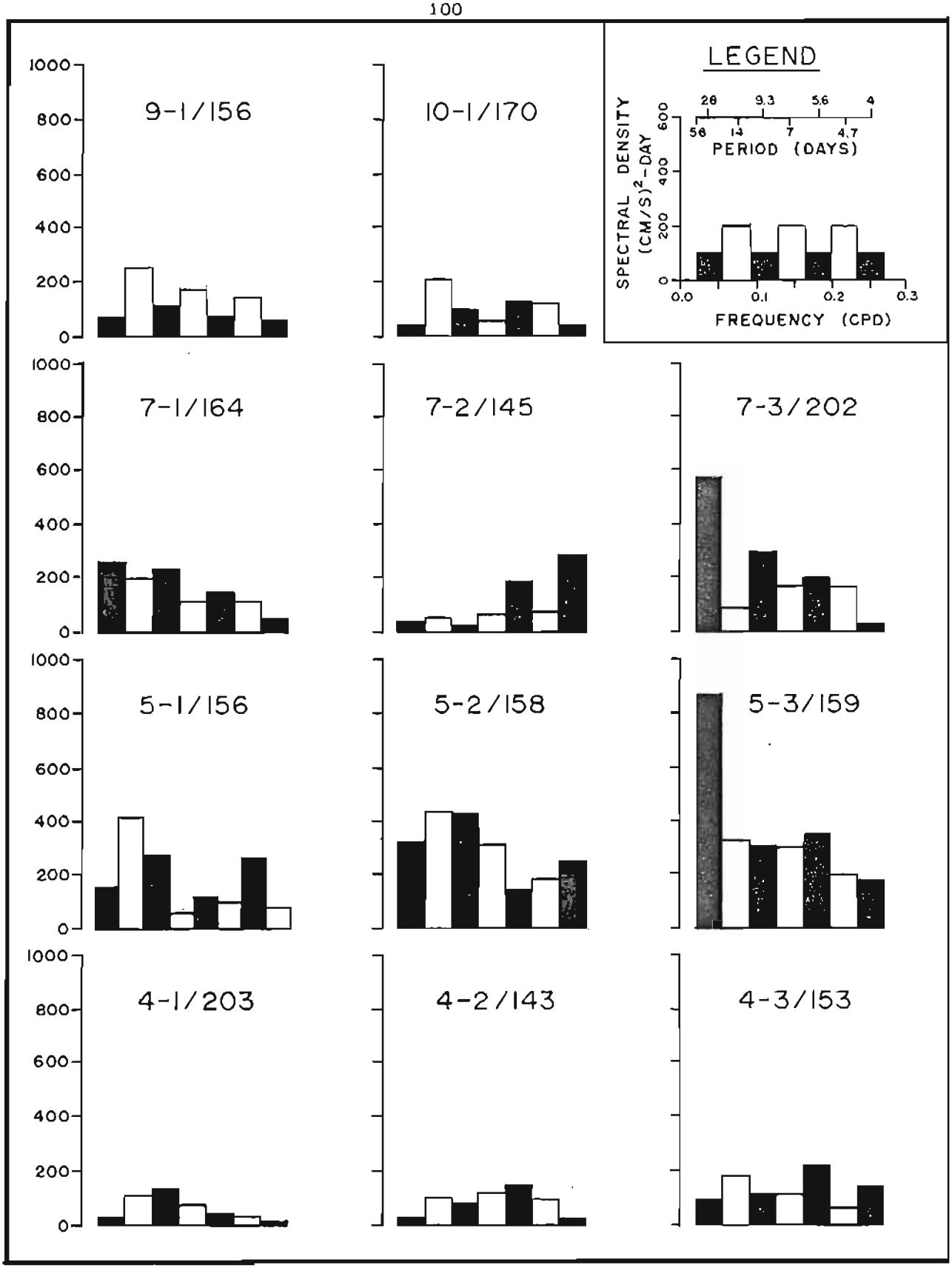

Figure 58: The auto-spectral densities at depths of 143 to 203 m for very low frequencies computed from 28 day blocks. The number of blocks was two in most cases, except at stations 4-3 and 5-2 where three blocks were used.

spectral levels occur in either or both of the two lowest frequency bands, centred at 28 and 14 day periods for all locations but one (station 7-2).

Very low frequency activity appears to be most pronounced at the slope stations 5-3 and 7-3. Here, the 28 day peaks exceed by a factor of two or more spectral levels computed for any other frequencies. A broad secondary peak occurs at both sites over periods of 5 to 7 days.

The very low frequency activity on the banks varies markedly among locations. At station 10-1, a large peak is found in the 28-day band at 62 m depth, but is not present at 170 m depth. Similarly, at station 4-3 a large 14 day peak present at 54 m depth is much reduced in relative amplitude at 153 and 171 m. At station 9-1, a peak at 14 days also occurs at 56 m depth but remains present at 156 m depth as well. At all bank locations, the very low frequency auto-spectra show enhanced spectral levels at periods of 4 to 7 days, with the activity at these periods being dominant at stations 4-2 and 7-2.

At the trough (4-1, 5-1 and 7-1) and saddle (5-2) locations, the spectral levels in the 28 day band are generally lower than those computed for the 14 and 7 day bands. These latter two bands appear to contain most of the low frequency activity. However, smaller but non-negligible spectral levels do occur at shorter periods (4 to 6 days) in nearly all of the saddle and trough location records.

Rotational Versus Rectangular Auto-Spectra

The auto-spectra of the current vector time series data were computed both as rotary components (clockwise and anticlockwise) and as orthogonal geographic components (along the major and minor components of the current record). The cumulative values for each representation, over frequencies from 0.036 to 0.821 cpd (period of 28 to 1.22 days) are displayed in Figures 59 and 60. The same values are tabulated in Tables 11 and 12 along with the spectral levels for the three lowest frequency bands, centred at periods of 14, 7 and 4.7 days.

The results indicate that at measurement locations over the banks, the degree of circular polarization exceeds that of geographical component polarization for the low frequency current variations. At all bank locations, the level of clockwise rotational activity exceeds that of anticlockwise activities. This clockwise polarization is largest at stations 4-2, 7-2 and 10-1 where the cumulative clockwise spectral densities exceed the corresponding anticlockwise values by more than a factor of two at 50 m depth. Enhanced levels of clockwise activity are also found at bank stations 4-3 and 9-1, although the ratios are reduced.

At the remaining measurement locations, the degree of circular polarization tends to be less than the ratio of spectral levels between the major and minor current components. At the slope (5-3 and 7-3) and saddle (5-2) locations, the low-frequency activity is concentrated along the direction of the major current component. The ratio of major to minor component spectral densities reaches values of 5 to 7 at station 7-3, 3 to 5 at station 5-3 and 2 to 3 at station 5-2. While the degree of circular polarization is much smaller (on the order of 30% differences) a preference is indicated for anticlockwise activity at station 5-2 and 5-3, and clockwise activity at station 7-3.

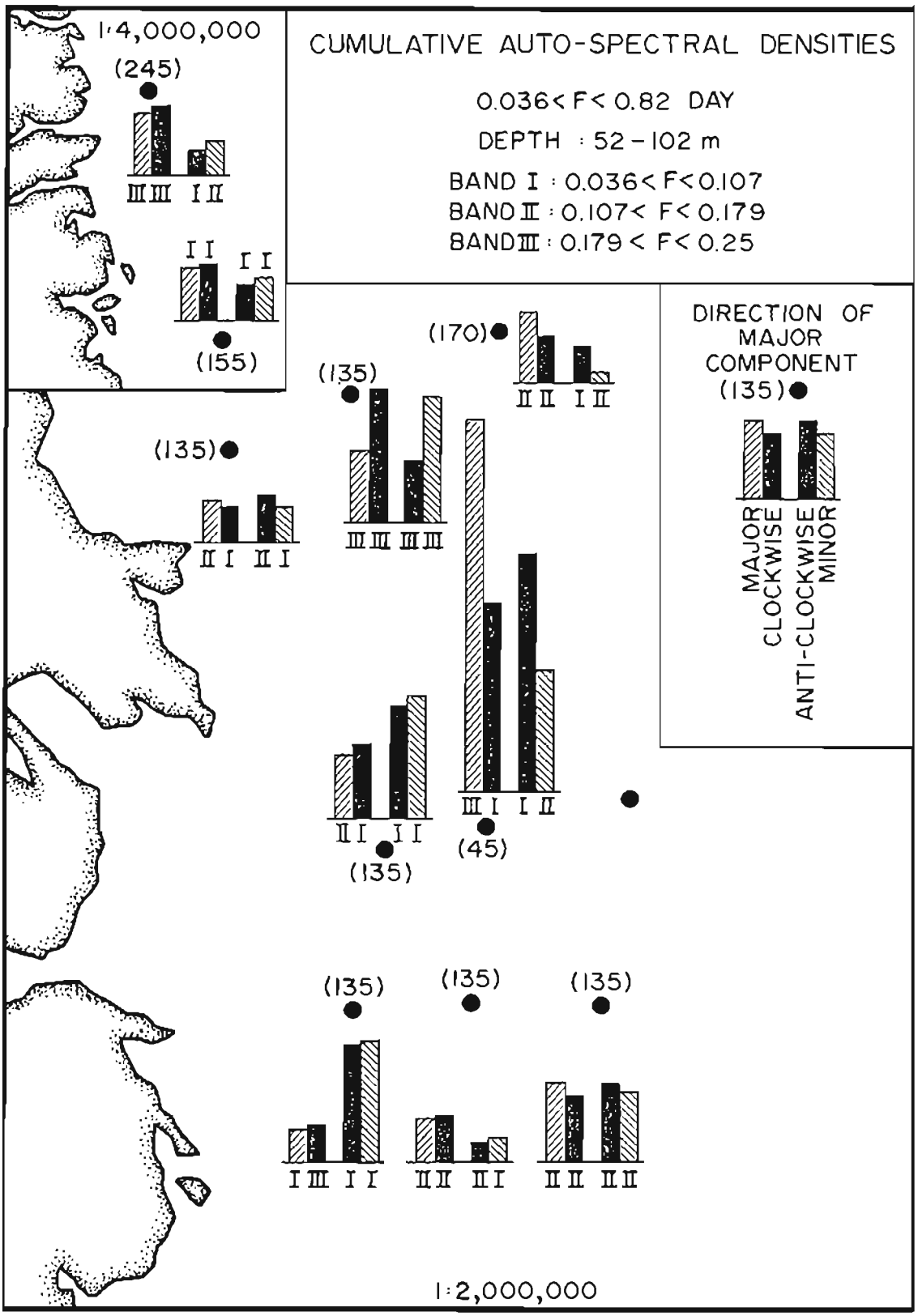

Figure 59: The auto-spectral density of vector currents over frequencies of 0.035 to 0.82 cpd for rotational (clockwise and anticlockwise) and rectangular (major and minor) current components at depths of 52 to 102 m.

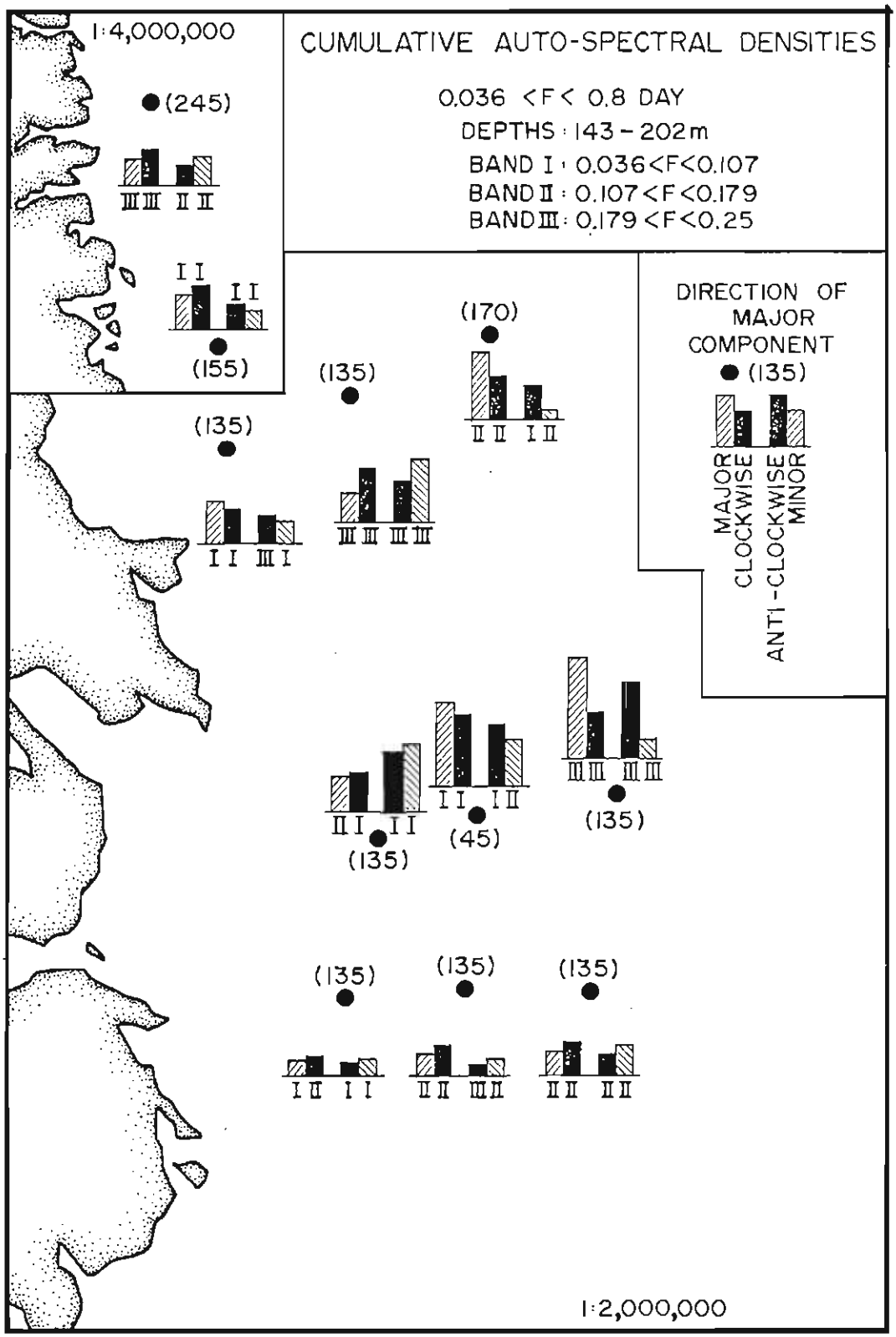

Figure 60: The auto-spectral density of vector currents over frequencies of 0.035 to 0.82 cpd for rotational (clockwise and anticlockwise) and rectangular (major and minor) current components at depths of 143 to 202 m. The roman numeral under each bar indicates the band in which the maximum spectral level occurred.

Table 11

The low frequency auto-spectral densities of vector currents for rotational components. Values are given for the three lowest frequency bands (bandwidths of 0.0714 cpd) centred at 0.07, 0.14 and 0.21 cpd (periods of 14, 7 and 4.7 days). Also given are the cumulative component totals over frequencies of 0.035 to 0.821 cpd, and the ratio between the cumulative totals.

		CLOCKWISE Frequencies				ANTICLOCKWISE Frequencies				
STATION	DEPTH (M)	.07 cpd	.14 cpd	.21 cpd	CUMU-LATIVE	.07 cpd	.14 cpd	.21 cpd	CUMU-LATIVE	RATIO
		$(cm/s)^2$-day				$(cm/s)^2$-day				
4-1	52	56	96	99	331	373	290	198	988	0.34
4-1	203	16	67	17	144	35	19	12	93	1.55
4-2	53	113	178	63	403	45	52	31	157	2.57
4-2	143	31	114	65	243	4	16	19	58	4.19
4-3	54	72	201	77	580	189	198	165	683	0.85
4-3	153	32	95	54	307	25	61	53	179	1.72
4-3	171	37	82	50	292	17	67	43	164	1.78
5-1	58	227	181	90	628	330	182	138	946	0.66
5-1	156	98	86	63	390	113	86	82	524	0.74
5-2	31	850	418	264	2067	1020	711	581	2913	0.71
5-2	57	630	350	219	1628	787	439	399	2066	0.79
5-2	158	215	98	123	606	205	134	82	531	1.14
5-2	269	127	86	116	503	111	54	73	322	1.56
5-3	159	69	90	120	409	142	129	156	644	0.64
5-3	277	64	66	47	353	63	116	58	465	0.76
7-1	64	157	40	27	287	84	116	40	370	0.78
7-1	162	133	57	34	286	48	41	59	233	1.23
7-2	25	101	222	480	1430	37	93	180	571	2.50
7-2	55	75	162	368	1161	30	72	135	522	2.22
7-2	145	46	41	62	496	8	53	160	361	1.37
7-3	102	89	113	84	433	80	79	29	324	1.34
7-3	202	74	76	69	351	88	62	55	318	1.10
9-1	56	216	48	68	498	147	68	45	336	1.48
9-1	156	86	76	67	384	70	39	23	178	2.16
10-1	62	98	104	201	578	56	48	17	229	2.52
10-1	170	37	56	69	278	25	40	39	175	1.59

Table 12

The low frequency auto-spectral densities of vector currents for rectangular components. Value are given for the three lowest frequency bands (bandwidths of 0.0714 cpd) centred at 0.07, 0.14 and 0.21 cpd (periods of 14, 7 and 4.7 days). Also given are the cumulative component totals over frequencies of 0.035 to 0.821 cpd, and the ratio between the cumulative totals.

		MAJOR COMPONENT					MINOR COMPONENT				
		Frequencies					Frequencies				
STATION	DEPTH (M)	DIR'N	.07 cpd $(cm/s)^2$-day	.14 cpd	.21 cpd	CUMU-LATIVE	DIR'N	.07 cpd $(cm/s)^2$-day	.14 cpd	.21 cpd	CUMU-LATIVE	RATIO
4-1	52	135	98	79	56	286	225	331	307	242	1034	0.28
4-1	203	135	26	45	13	120	225	25	41	16	117	1.02
4-2	53	135	69	183	75	375	225	89	48	19	186	2.02
4-2	143	135	16	88	61	196	225	20	42	23	107	1.83
4-3	54	135	197	226	120	655	225	64	173	122	609	1.08
4-3	153	135	34	75	55	224	225	22	80	52	261	0.86
4-3	171	135	37	78	43	217	225	17	72	50	238	0.91
5-1	58	135	143	169	25	529	225	415	194	203	1046	0.51
5-1	156	135	71	89	11	346	225	140	83	234	569	0.61
5-2	31	45	1580	782	638	3688	135	304	347	214	1304	2.82
5-2	57	45	1180	499	448	2656	135	242	290	168	1030	2.58
5-2	158	45	340	141	121	737	135	81	92	84	401	1.84
5-2	269	45	173	74	131	501	135	64	67	58	323	1.55
5-3	159	135	186	198	244	872	225	24	21	32	189	4.84
5-3	277	135	104	147	80	610	225	22	35	25	208	2.93
7-1	64	135	142	82	40	353	225	100	74	27	304	1.16
7-1	162	135	148	64	54	336	225	33	33	38	182	1.85
7-2	25	135	53	175	222	717	225	86	140	439	1289	0.56
7-2	55	135	45	150	199	606	225	60	84	304	1077	0.56
7-2	145	135	22	51	60	288	225	33	43	162	571	0.50
7-3	102	170	154	172	92	637	260	15	38	21	120	5.31
7-3	202	170	153	129	105	587	260	9	9	20	80	7.34
9-1	56	155	212	56	93	469	245	152	58	19	366	1.28
9-1	156	155	97	65	58	335	245	59	50	32	227	1.48
10-1	62	245	110	75	148	516	155	44	76	70	291	1.77
10-1	170	245	10	42	63	233	155	52	54	45	220	1.06

At stations 4-1 and 5-1 (both located over the marginal trough) the auto-spectral densities indicate that the degrees of rotational and geographic component polarization are comparable. At both sites, the spectral level in the minor current component is markedly larger than that of the major current component by factors of 4 and 2 at station 4-1 and 5-1 at 50 m depth. The same records reveal anti-clockwise spectral densities exceeding clockwise spectral values by a factor of 3 (station 4-1) and 1.5 (station 5-1).

At station 7-1, also located in the marginal trough, the degree of either circular or geographical component polarization is much smaller. At 64 m depth, the currents were polarized in an anti-clockwise sense (ratio of 1.28). However, unlike stations 4-1 and 5-1, the major current component variations exceed those of the minor current component (ratio of 1.16).

Summary - Low Frequency Auto-Spectra

The auto-spectra computed for the subsurface current meter records indicated that the largest variations occur at low frequencies, less than 0.8 cpd (1.25 days period). The variations occur over a wide range of periods, extending to at least 30 days.

Given the broad-banded nature of the low frequency variability, it appears useful to divide the low frequencies into three ranges: periods exceeding 7 days, periods of 4 to 7 days and shorter periods, 1.25 to 4 days. The largest amplitude variations occur in the lowest two ranges, although appreciable relative contributions to the low frequency variance can occur at the third range of frequencies, particularly at some locations over the banks and at depths in excess of 100 m (Figures 55 and 56).

At locations over the marginal trough, the saddle and the continental slope, the dominant low frequency variations occur at periods in excess of 7 days. Over the continental slope, the peak amplitudes are at the lowest resolvable frequencies, greater than 20 days. Over the trough and saddle, the peak periods range from 7 to 14 days. At all of these types of locations, significant motions do occur at periods of 4 to 7 days, although with smaller amplitudes than those of the longer periods.

Over the banks, relatively more activity occurs at periods of 4 to 7 days. Indeed, at some locations (4-2 and 7-2), these periods dominate the low frequency activity. At other locations, the longer period is more active (station 9-1) or comparable (stations 4-3 and 10-1).

At bank locations, the activity at periods of 4 to 7 days has a pronounced clockwise circular polarization. At locations in other bathymetric regimes, the degree of circular polarization is generally less than the difference between the energy levels of the major and minor current components. Where any degree of circular polarization is evident, it tends to be directed anticlockwise at these locations.

Cross-Spectra Between Vertically Separated Current Pairs

Pairs of current meter records obtained at the same locations were subjected to cross-spectral analysis. The results (Tables 13 and 14) indicate

that low frequency motions are generally coherent at statistically significant levels in the upper 300 m of the water column.

Between depths near 50 and 150 m, for all pairs of current meter records, there were some frequency bands where the coherence levels were statistically significant at the 95% level. In those bands with high coherence levels, the phase angles were generally small, typically within $\pm$30 degrees, indicating that the low frequency motions are highly correlated.

The highest vertical coherence levels were found at station 5-2 in Cartwright Saddle for the major component of current. Here, the coherence values for the lowest frequency band (centred on 0.14 cpd) ranged from 0.90 to 0.998 among depths of 30, 57, 158 and 269 m.

Peak coherence levels of 0.9 or more for depth pairs of 50 and 150 m were also computed for stations 4-2, 5-1, 5-3, 7-3 and 9-1. The peak coherence levels at stations 4-1, 4-3, 7-1 and 7-2 were somewhat lower, but still above the 95% significance level.

The lowest vertical coherence levels were computed for station 10-1, between depths of 62 and 170. Here in the frequency band with the largest auto-spectral levels (0.14 cpd clockwise) the coherence value was only 0.64, just significant at the 80% level.

Cross-Spectral Analysis Between Horizontally-Separated Pairs of Current Meter Records

Cross-spectral analyses were carried out on pairs of horizontally separated current meter records to examine the spatial scales of low frequency current variability. The hourly data for each record were divided into consecutive blocks of 14 days length. For the data from current meter moorings 4-1 to 7-3, inclusive, four blocks were used to compute the cross-spectral values, with the first block beginning at 2300 GMT July 11, 1980. The cross-spectral values between pairs of current meter records at stations 9-1 and 10-1 were computed over five blocks, commencing at 0000 GMT July 21, 1980.

Cross-spectral computations were made for both rotational and rectangular component representations of current variations. The cross-spectral results for the three lowest frequency bands, centred at 0.07, 0.14 and 0.21 cpd (periods of 14, 7 and 4.7 days) are illustrated schematically in Figures 61 (rotary) and 62 (rectangular). Coherence and phase values are given only if the coherence estimates exceed the 80% significance level (0.64 for four blocks, 0.58 for five blocks). Cross-spectral analyses were carried out on all adjacent pairs of current meter records. In addition, the innermost and outermost pair of stations on lines 4, 5 and 7 were also subjected to cross-spectral analysis.

The results, for depths of 53 to 102 m, indicate that horizontal coherences are generally low. There were 108 possible coherences which could be computed from the 18 pairs of current meter records for both rotary and rectangular components. In the rotary case, only 18 had coherence levels exceeding the 80% significance level. The cross-spectral analyses for the rectangular component variations yielded 21 coherence values significant at the 80% level, again out of a possible 108 pairs. The number of pairs of 80% significant coherence

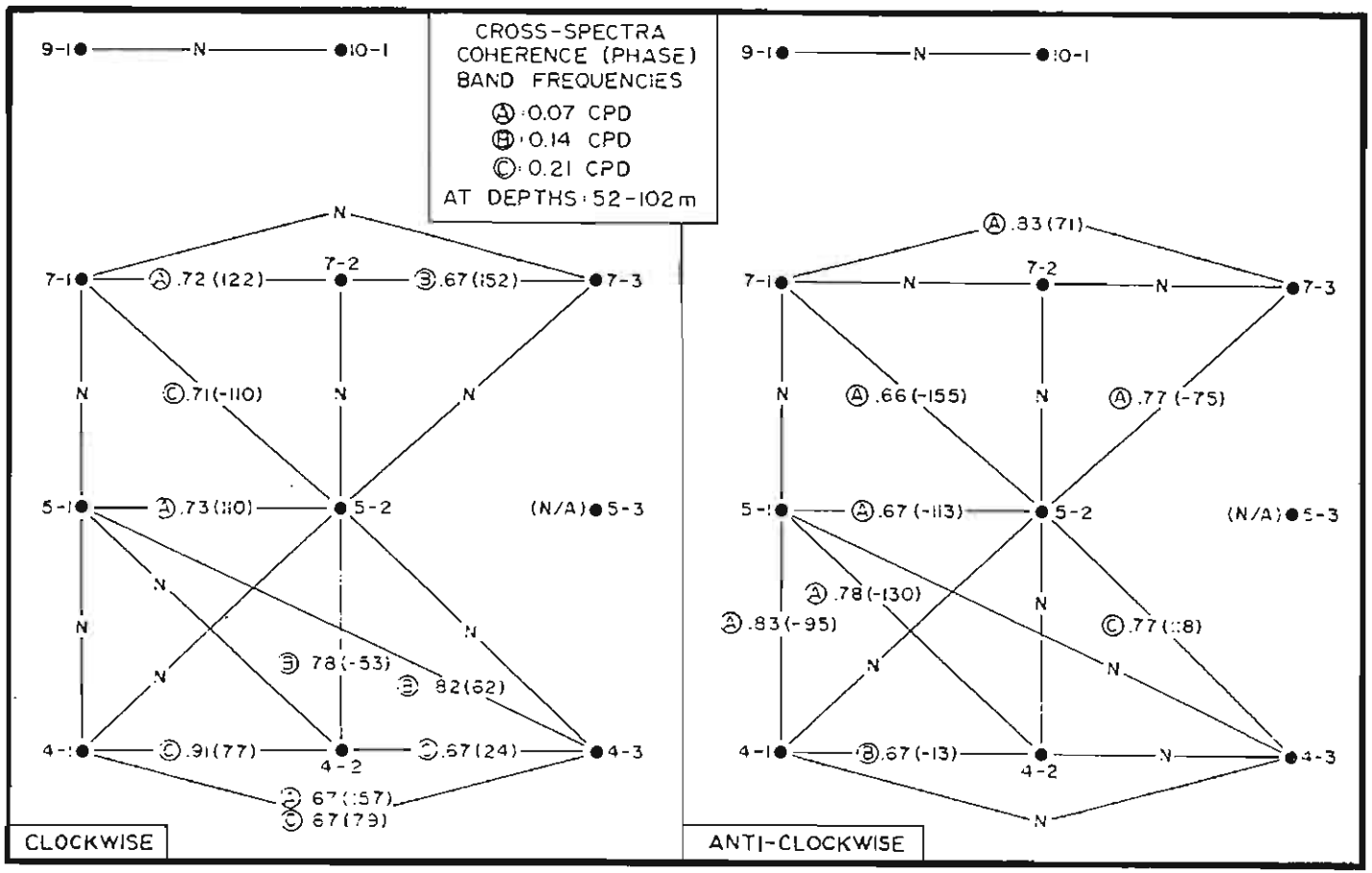

Figure 61: The low frequency coherence and phase values computed for horizontally separated pairs of current meter data obtained at depths of 52 to 102 m. The values are computed for rotational components at frequency bands centred at (A) 0.07 (B) 0.14 and (C) 0.21 cpd. Coherence and phase values are given only if the coherence exceeds the 80% significance level. The symbol "N" denotes no significant coherence for any of the three frequency bands.

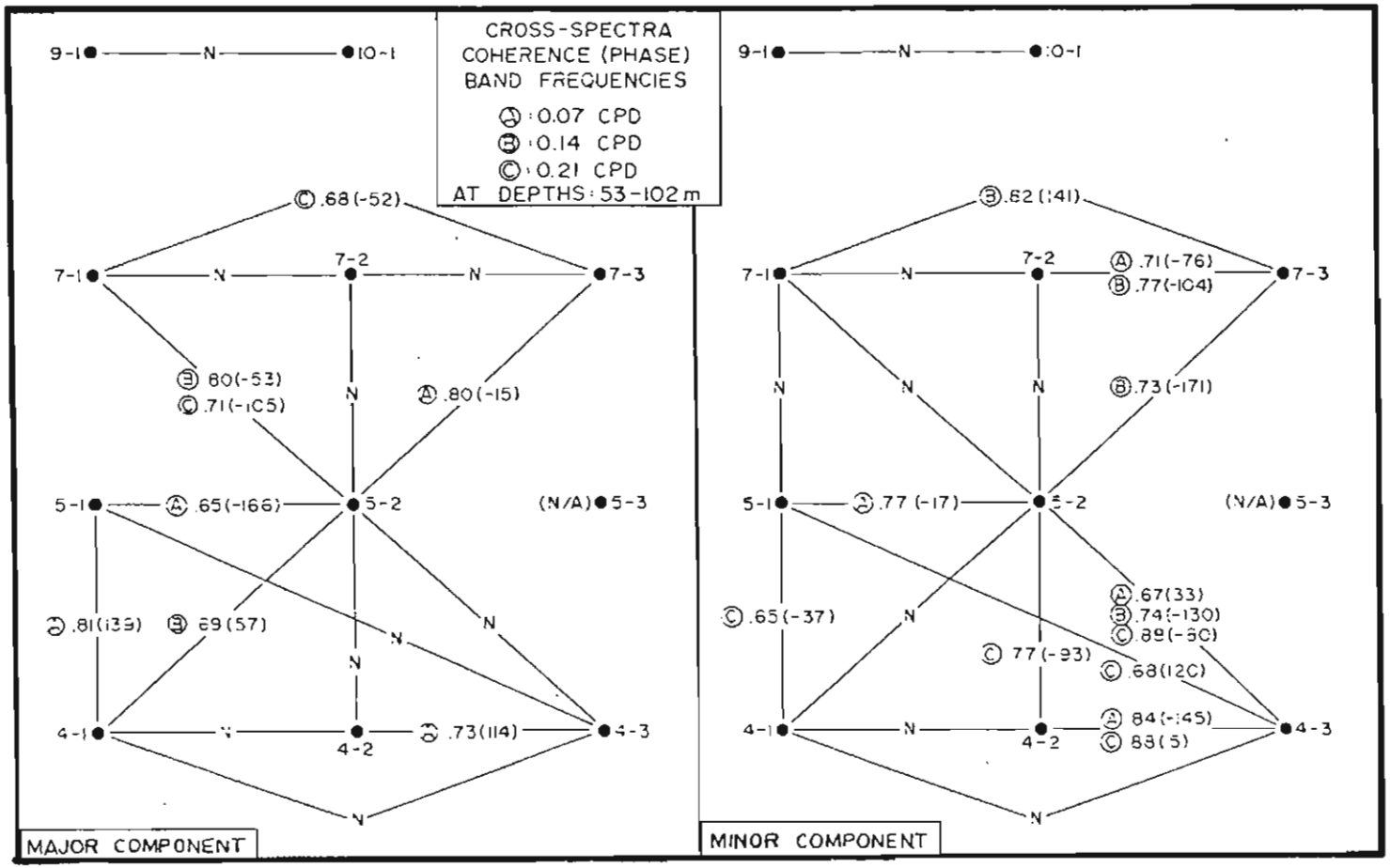

Figure 62: The low frequency coherence and phase values computed for horizontally separated pairs of current meter data obtained at depths of 52 to 102 m. The values are computed for rectangular components at frequency bands centred at (A) 0.07 (B) 0.14 and (C) 0.21 cpd. Coherence and phase values are given only if the coherence exceeds the 80% significance level. The symbol "N" denotes no significant coherence for any of the three frequency bands.

Table 13

Cross-spectral results for vertically separated pairs of current records in terms of rotational components. The coherence (and phase) values are presented for the three lowest resolvable frequency bands (bandwidth of 0.0714 cpd) at frequencies centred on 0.07, 0.14 and 0.21 cpd (periods of 14, 7 and 4.7 days). Coherence and phase values are given only if the coherence exceeds the 80% significance levels.

				Coherence (Phase) Values					
				Clockwise			Anticlockwise		
	Depth	Depth	# of	*******Frequencies*******			******Frequencies*******		
Stn	(1) (m)	(2) (m)	Blocks	0.07	0.14	0.21	0.07	0.14	0.21
4-1	52	202	4	---	0.71(7)	0.66(25)	0.90(-43)	---	0.91(-48)
4-2	53	143	4	0.92(+10)	0.96(14)	0.96(14)	---	0.94(+12)	0.96((3)
4-3	54	153	6	---	0.78(+33)	0.70(0)	0.75(-17)	---	0.71(-40)
	54	171	6	---	0.75(+31)	0.56(-3)	---	0.53(-61)	0.64(-36)
	153	171	6	0.94(-8)	0.98(-1)	0.96(1)	0.89(-12)	0.99(-11)	0.98(4)
5-1	58	156	5	0.94(-17)	0.92(-34)	0.93(-19)	0.93(-2)	0.83(-5)	0.92(+18)
5-2	31	57	6	1.0(+3)	1.0(+6)	0.97(-1)	1.0(+4)	0.99(+5)	0.98(3)
	31	158	6	0.96(+23)	0.82(+12)	0.83(-10)	0.94(+9)	0.86(+9)	0.74(6)
	31	269	6	0.88(+33)	0.62(-13)	0.86(-12)	0.74(+9)	0.07(-78)	---
	57	158	6	0.97(+19)	0.84(+7)	0.89(-7)	0.95(+5)	0.88(+4)	0.80(2)
	57	269	6	0.88(+28)	0.63(-18)	0.89(-8)	0.76(+4)	---	0.61(-17)
	158	269	6	0.93(+11)	0.70(-28)	0.89(2)	0.85(-6)	---	0.82(-11)
5-3	159	277	4	0.69(-10)	0.91(+7)	0.93(-13)	0.75(-34)	0.90(-31)	0.93(38)
7-1	64	162	4	0.89(+12)	0.77(9)	0.70(-2)	---	---	0.73(-20)
7-2	25	55	4	0.97(-6)	0.98(-14)	0.99(6)	0.94(+6)	0.98(-18)	0.96(-9)
	25	145	4	0.67(-7)	0.83(19)	0.71(36)	---	0.85(1)	0.92(-31)
	55	145	4	0.72(+6)	0.87(4)	---	0.92(17)	0.96(-23)	---
7-3	102	202	4	0.97(-3)	0.93(-5)	0.96(-11)	0.92(+2)	0.87(-12)	0.70(4)
	102	656	4	---	---	---	---	---	0.80(-144)
	202	656	4	0.67(+13)	0.72(22)	---	---	---	---
9-1	56	156	5	0.93(+2)	0.80(-7)	0.90(-4)	0.92(-11)	0.68(-45)	0.78(-9)
10-1	62	170	5	0.68(+5)	0.65(30)	0.72(13)	0.64(-54)	---	---

Table 14

Cross-spectral results for vertically separated pairs of current records in terms of rectangular components. The coherence (and phase) values are presented for the three lowest resolvable frequency bands (bandwidth of 0.0714 cpd) at frequencies centred on 0.07, 0.14 and 0.21 cpd (periods of 14, 7 and 4.7 days). Coherence and phase values are given only if the coherence exceeds the 80% significance levels.

				Coherence (Phase) Values					
				Clockwise			Anticlockwise		
	Depth	Depth	# of	******Frequencies*******			******Frequencies*******		
Stn	(1) (m)	(2) (m)	Blocks	0.07	0.14	0.21	0.07	0.14	0.21
4-1	52	202	4	0.72(70)	---	---	0.82(31)	0.88(23)	0.90(34)
4-2	53	143	4	0.79(1)	0.98(1)	0.96(11)	0.88(14)	0.88(-10)	0.90(2)
4-3	54	153	6	---	0.72(50)	---	0.73(-19)	0.69(22)	0.81(27)
	54	171	6	---	0.67(53)	---	---	0.06(30)	0.73(22)
	153	171	6	0.95(4)	0.98(0)	0.98(3)	0.84(-10)	0.98(8)	0.97(-8)
5-1	58	156	5	0.91(-18)	0.87(-14)	0.92(-15)	0.94(-1)	0.79(-18)	0.92(-19)
5-2	31	57	6	1.0(-1)	1.9(-1)	0.98(-3)	0.98(0)	0.96(0)	0.97(-2)
	31	158	6	0.96(8)	0.84(0)	0.84(-13)	0.72(-2)	0.81(-3)	0.62(7)
	31	269	6	0.90(16)	---	0.77(-12)	---	---	---
	57	158	6	0.97(9)	0.86(2)	0.90(-8)	0.81(-3)	0.87(-2)	0.69(4(
	57	269	6	0.91(16)	---	0.85(69)	---	---	---
	158	269	6	0.93(10)	---	0.90(-2)	0.76(2)	0.56(6)	0.84(-1)
5-3	159	277	4	0.76(10)	0.90(21)	0.97(13)	---	0.80(27)	---
7-1	64	162	4	0.70(8)	---	0.69(11)	0.93(-6)	0.64(34)	0.73(12)
7-2	25	55	4	0.97(-4)	0.98(-15)	0.98(-9)	0.97(-7)	0.98(15)	0.99(5)
	25	145	4	---	0.86(-1)	0.85(-5)	0.77(-8)	0.77(-27)	0.79(50)
	55	145	4	---	0.91(-14)	0.81(-13)	0.75(-4)	0.81(9)	0.83(45)
7-3	102	202	4	0.96(10)	0.92(4)	0.94(1)	0.92(7)	0.77(13)	0.90(21)
	102	656	4	---	---	---	---	---	---
	202	656	4	---	---	---	---	0.76(14)	---
9-1	56	156	5	0.93(9)	0.63(3)	0.89(3)	0.92(0)	0.71(27)	0.83(-10)
10-1	62	170	5	0.70(33)	---	0.70(-27)	0.83(12)	---	0.72(44)

levels expected as a result of random current variations would be 20%, or about 22 out of 108. On this basis, the cross-spectral results indicate that the general level of horizontal coherences in the measured currents are comparable to those expected from random motions alone.

Examination of individual pairs of current records, having significant coherence levels, shows that, in may cases, one or both records have relatively low spectral density levels. For example, the largest computed coherence of 0.91 occurred for clockwise rotations at frequencies of 0.21 cpd between records 4- 1/52 and 4-2/53. However, the clockwise auto-spectral levels for this frequency are low for record 4-1/52 and low to moderate for record 4-2/53 (Table 11). Thus, the amount of the variance common to the two records is low despite the relatively high computed coherence value.

In a few record pairs, significant coherence levels do occur in frequency bands with substantial spectral density values. One such pair is 5-2/57 and 7-3/102 where, for the lowest frequency band, large amplitude variations of the major components at both sites are coherent (0.80) and nearly in phase. A visual comparison of the two records indicates that while there is some similarity, the two records exhibit marked differences in low frequency flows, as well.

The cross-spectral analysis results (not shown) for horizontally separated current pairs at depths of 143 to 202 m reveal similar generally low coherence levels. Over this range of depths, 25 pairs of current records were analyzed, including data from station 5-3, where no data were available at the 53- 102 m levels. For the lowest three frequency bands, of a total of 150 cross-spectral estimates, only 31 of the pairs of rectangular components had coherences exceeding the 80% level. The corresponding total for rotary components was 33 out of 150. Such numbers of pairs are consistent with those expected from random variability alone.

Based on the low levels of horizontal coherence in the currents, the length scales of current variability would appear to be less than the station separations of the present study. Spacing between adjacent stations ranges from 35 to 50 km within lines. Adjacent stations in lines 4 and 5 are separated by about 60 km, while lines 5 and 7 are separated by 140 km and stations 9 and 10 are separated by 155 km.

The varying nature of the bathymetric regime among adjacent stations (trough, banks, saddle, slope) results in differences in the temporal distribution and energy levels of low frequency flow variability. Such differences among the measurement sites may also contribute to the relatively low levels of horizontal coherence.

Based on these results, reduced separations between current meter mooring locations would be advisable in future studies. Given the immense size of the study area, this approach would lend itself to more detailed studies involving several current meter moorings concentrated on one bathymetric regime.

Time Series of Water Properties and Their Correlations with Velocity

The lack of horizontal coherence in the velocity field means that velocity fluctuations at different points cannot be directly related to each other. Changes in water properties associated with the velocity fluctuations can assist in deducing their nature, however. The presence of slope water on the outer sides of some of the banks, in the saddles and in the bottom of the marginal trough was described in Section 5.3. Examination of selected temperature and salinity measurements in Figures 63 and 64 shows that the slope water occurred as intermittent bursts which alternated warm, saline slope water with cool, fresh shelf water. The fluctuations in water properties at each measurement site which resulted from the appearance of the bursts of slope water had some fairly well-defined characteristics which varied according to bathymetric regime.

The 159 m record from station 5-3 (Figure 63) provides an example from the slope region. Two periodicities are visually evident, one at 3 to 5 days, the second at approximately 20 days. They are most apparent in the temperature and salinity, but may also be perceived in the velocity plot. The velocity signal was separated into along-slope and across-slope components, and a cross-spectral analysis was performed with the temperature. (No cross-spectra were computed for salinity since the temperature and salinity signals are very similar in form.) Significant coherences with temperature were found at the 3 to 5 day period for both components, but only for the along-slope component at 20 days. (For the raw spectral estimates computed over four blocks, each of 14 days duration, coherences above 0.8 are significant at the 95% level [Table 4].)

At periods between 3 and 5 days, a coherence of 0.9 was computed between the temperature and the along-slope velocity component, with the temperature lagging the speed by approximately 80°. The same coherence was found for the across-slope component, with the temperature lagging by 50 to 80°. The longer period (approximately 20 days) oscillations fall into the lowest frequency band in the spectra (centred at .0714 cpd), and consequently are not fully resolved. There is significant coherence (0.9) between the temperature and the along-slope component, but because of the lack of resolution the phase relationship is not defined. Strengthening of the along-slope flow, however, does seem to be associated with colder, fresher water at the mooring site. Coherence levels between the temperature and the across-slope component at this period were smaller (0.64), and just barely significant at the 80% level.

Coincident variations in velocity and water properties also occurred in the saddle regions. Figure 63(b) shows the 158 m temperature, salinity and velocity records from station 5-2 in Cartwright Saddle. Periods of approximately 20 days and of 4 to 7 days can be visually detected in temperature and salinity, but not as clearly in velocity. Although significant low-frequency energy is present in the velocity, the two periods (20 and 4-7 days) cannot be clearly resolved in the autospectrum (see discussion above concerning very low-frequency auto-spectra).

Cross-spectra between the temperature and components of velocity along and across the saddle were computed as for the slope site described above. In this case, however, coherences greater than 0.67 were significant at the 95% confidence level because 6 blocks of data were available rather than four

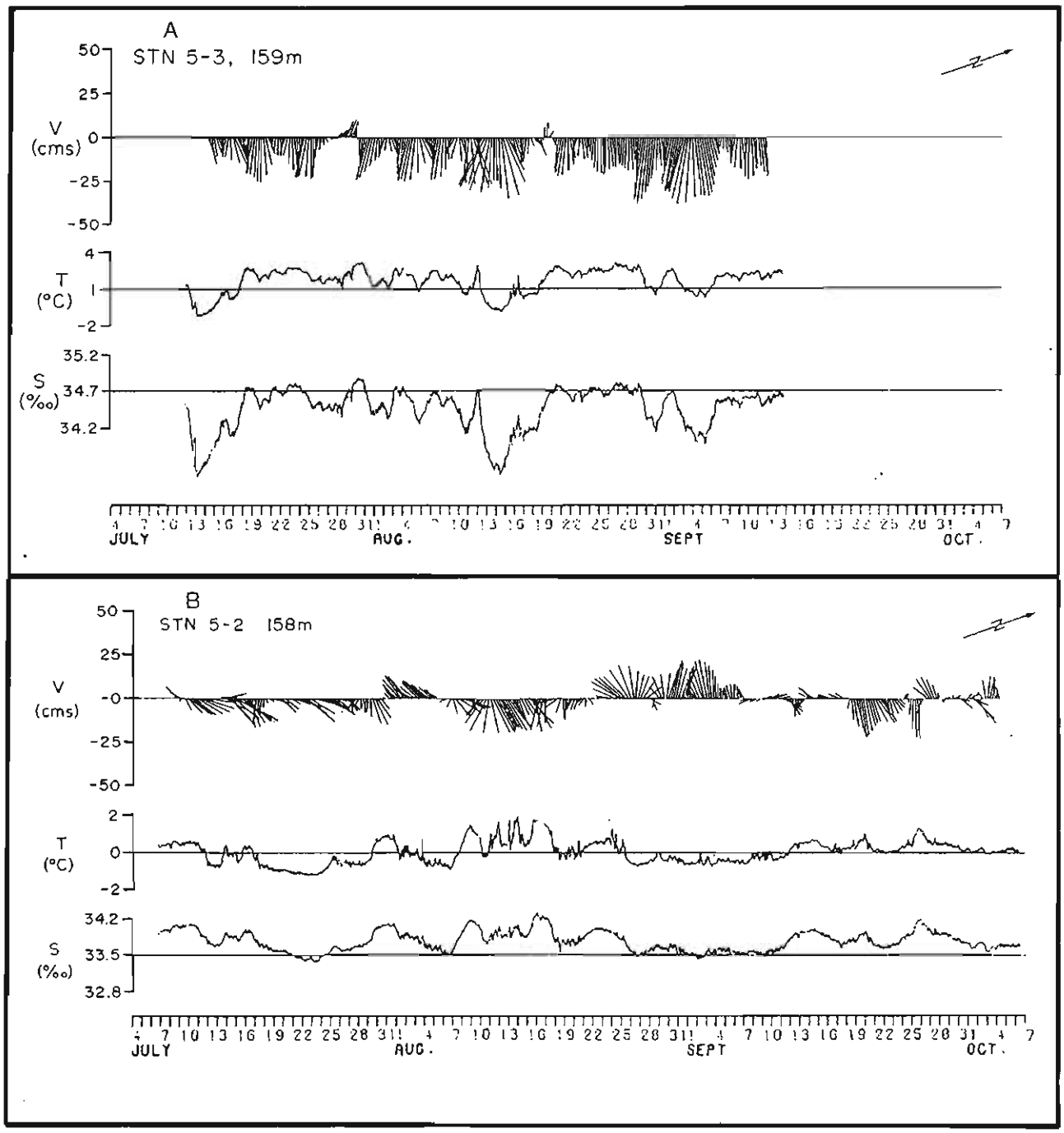

Figure 63: Low-passed records of velocity, temperature and salinity at mid-depth. (a) mooring 5-3 (b) mooring 5-2.

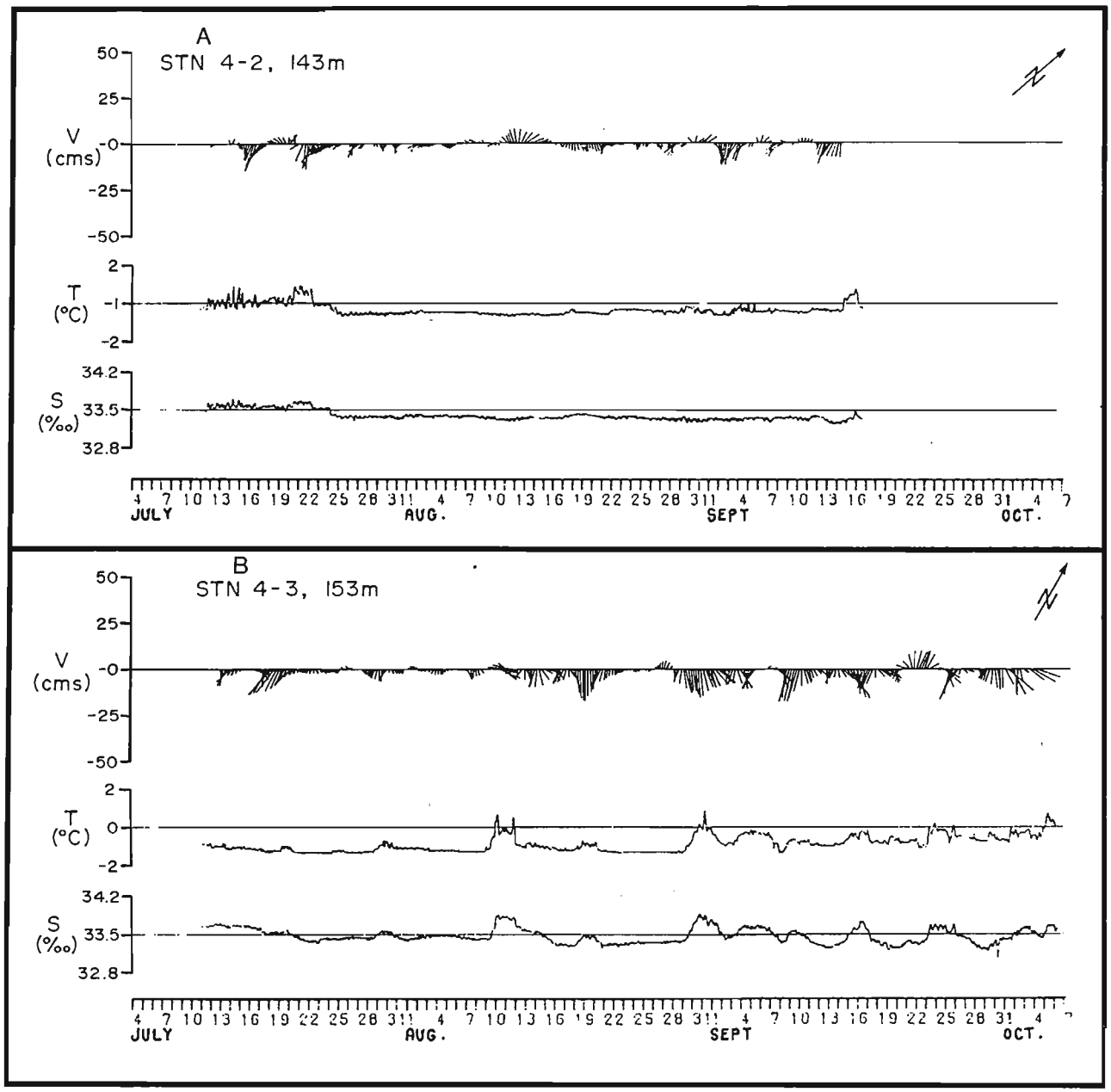

Figure 64: Low-passed records of velocity, temperature and salinity at mid-depth. (a) mooring 4-3 (b) mooring 4-2.

(Table 4). A significant coherence (0.7 to 0.8) was found at periods between 4.6 and 7 days between the temperature and the cross-saddle velocity component, with the temperature leading the velocity by 65° to 85° (note that the phase relationship here is opposite to that found at mooring 5-3). No significant coherence was found between the temperature and the along-saddle velocity component.

The situation in the trough is less clear. Short bursts (1 to 2 days duration) of warmer, more saline (than ambient) water were observed at station 5-1 at 156 m, but not at 514 m. At station 4-1, longer episodes of warmer, more saline water were observed. In neither case was there any obvious correlation with the velocity record.

Velocity fluctuations of an approximately 5-day period were also observed on the banks (see discussion above of low-frequency autospectra). The velocity fluctuations were sometimes accompanied by coincident fluctuations in temperature and salinity. At 143 m at station 4-2, (Figure 64(a)) little activity was apparent in the temperature and salinity records, with no evidence of slope water present. Significant low- frequency velocity fluctuations (between 4 and 9 days period) were present throughout the record, with a strong clockwise polarization (see the discussion above on rotational auto-spectra).

At 153 m at station 4-3 (Figure 64(b)) the situation differs from that nearer the centre of the bank at station 4-2. The activity in the velocity record was still present, but was only slightly clockwise polarized. Incursions of slope water of approximately 5 days duration were observed with increasing frequency in September. The incursions were sometimes associated with distinct events in the velocity record. For example, at station 4-3, the temperature and salinity pulse observed August 8 to 12 was accompanied by a strong, counterclockwise-rotating current event.

Other stations placed near the centres of banks showed little activity in temperature or salinity. The most striking example is perhaps at station 7-2, where, despite a very high degree of clockwise-polarized velocity fluctuations throughout the water column, no accompanying fluctuations in temperature or salinity were observed.

5.10 SEASONAL VARIATIONS OF WATER MASS DISTRIBUTIONS

The last occupation of the CTD stations took place in mid- October, which was sufficiently far into the autumn to show evidence of some large-scale changes. Figure 65 shows temperature and salinity cross sections at line 7 on Makkovik Bank during late August. Cold, (<0°C), low-salinity (<33.2°/oo) Shelf Water is evident over the bank and trough region, from the surface to 200 m. Figure 66 shows temperature and salinity cross sections taken at the same location two months later in October. With the exception of the water below 150 m in the trough, no subzero water appears anywhere in the section. Over the shelf, the bulk of the water column is between 0.5 and 1.5°C. The temperature of the surface layer (depth <25 m), which was 5 to 7°C in August, did not exceed 2°C in October. (The surface layers are not shown in Figures 65 and 66.) Vertical mixing by autumn storms would appear to be one possible cause for the warming of the water column. However, the amount of heat contained in the upper layer, if mixed throughout the upper 100 m of the water column, is sufficient

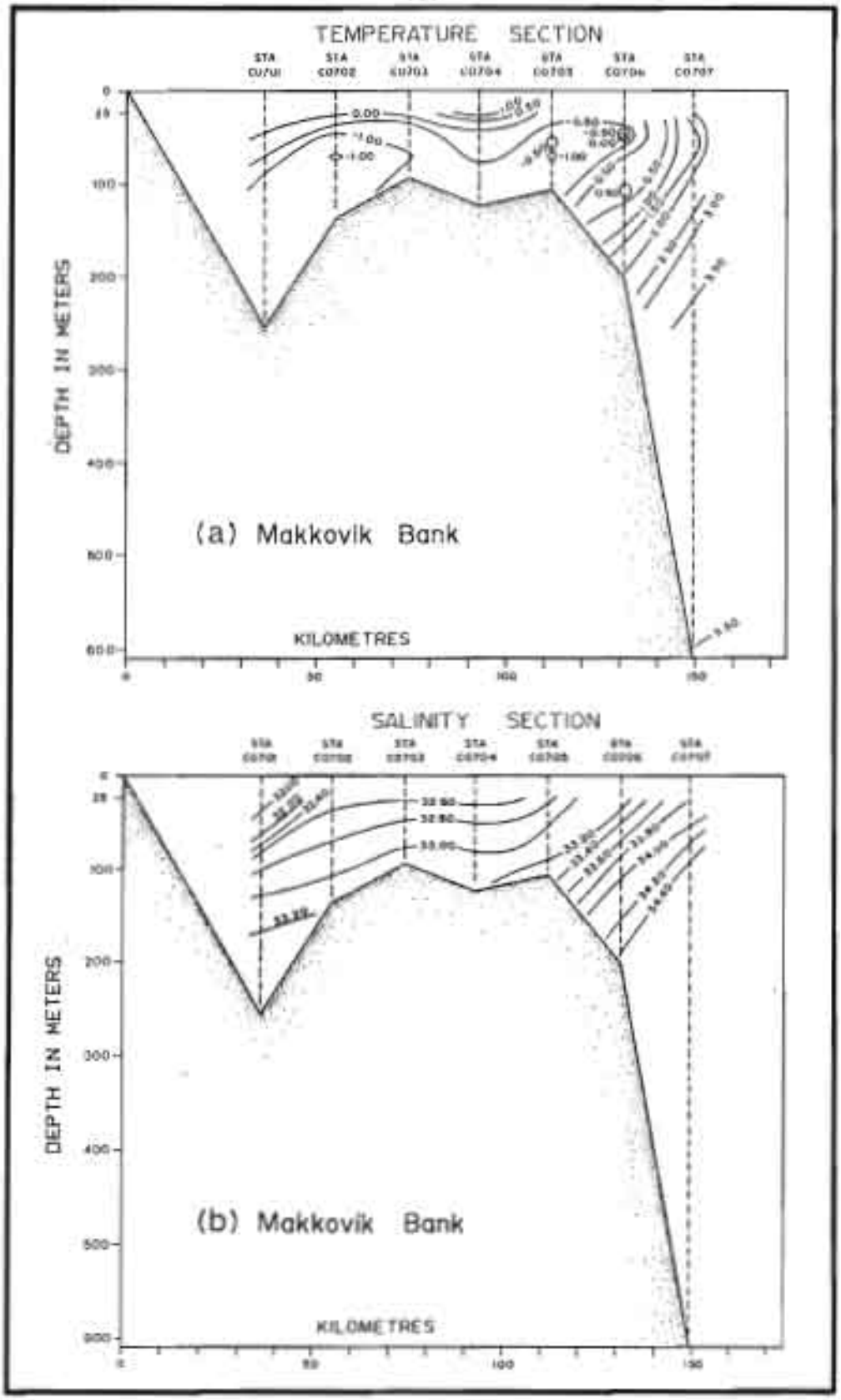

Figure 65: (a) Temperature cross section, line 7, August 23.
(b) Salinity cross section, line 7, August 23.

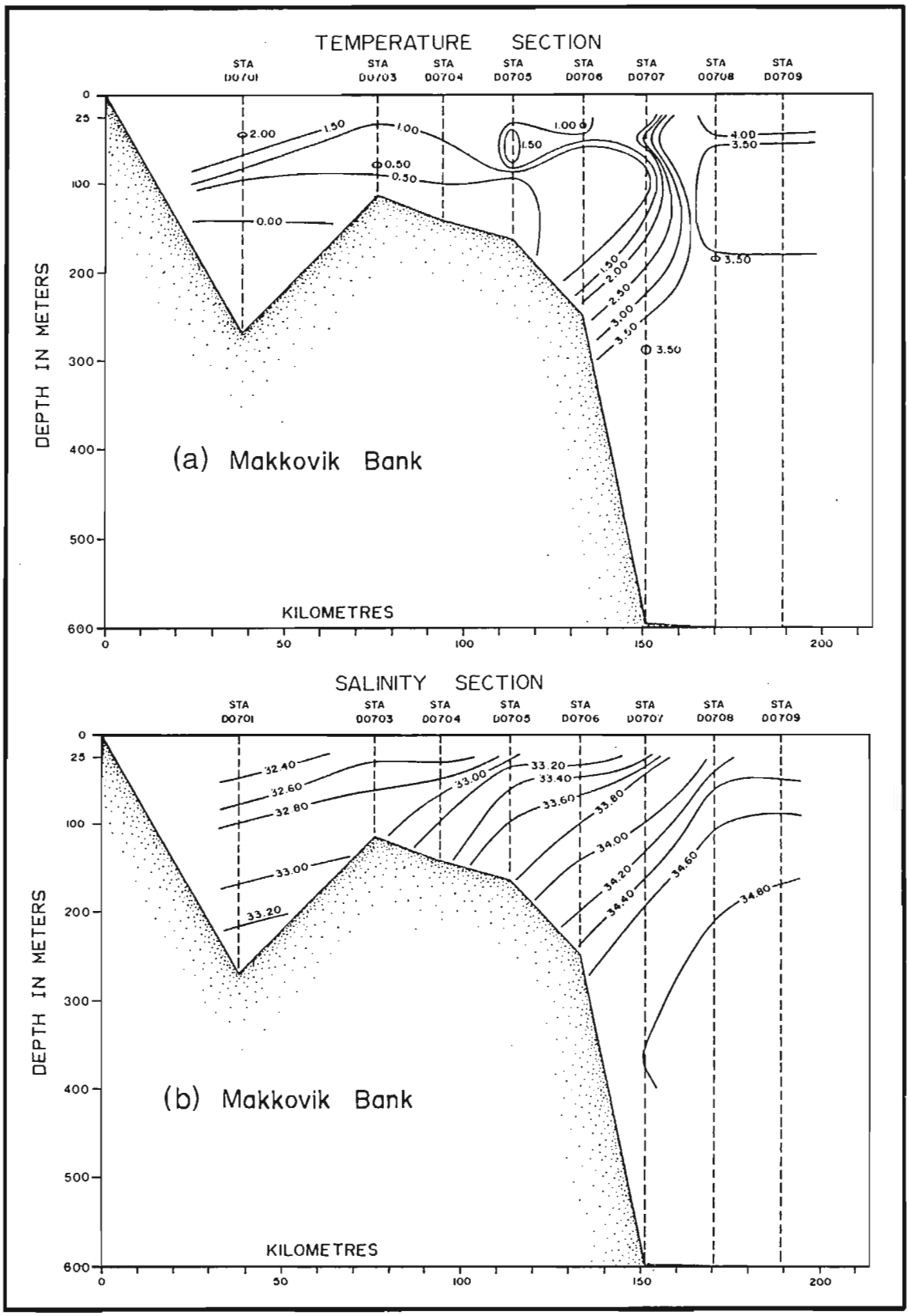

Figure 66: (a) Temperature cross section, line 7, October 17-18.
(b) Salinity cross section, line 7, October 17-18.

to raise its average temperature only to 0.5°C instead of 1°C. In addition, vertical mixing alone would produce a decrease in salinity near the bottom, while a significant increase is observed (Figures 65(b) and 66(b)). Advection of warmer, saltier water at depth must therefore be at least partially responsible for the October warming of the water over the shelf.

Examination of sections taken further south (line 4, over Hamilton Bank) at the same times show the effect more clearly. Temperature and salinity sections taken at line 4 in late August (Figure 67) show essentially the same structure as on Makkovik Bank, with cold, lower-salinity, uniformly stratified Shelf Water occupying the area over the shelf, except in the bottom of the marginal trough. Figure 68 shows sections taken at the same location in late October. Significant warming of the entire water column over the shelf had occurred; only traces of water colder than -1°C remain, and water below -0.5°C is confined to the upper part of the marginal trough. Surface temperatures (not shown in Figures 67 and 68) declined from about 8°C in August to 1.5 to 2.5°C in October.

Over Hamilton Bank proper in October, a relatively narrow mid-depth temperature minimum (with temperatures between 0 and - 0.5°C) remained between 100 and 150 m depth, except near the shelf break, where it rose toward the surface. Warming occurred both above and below this minimum. However inspection of Figure 68(b) shows that freshening occurred above the cold core, especially on the inner side of the bank, while beneath the cold core, particularly on the outer side of the bank, there was an increase in salinity. It would appear, then, that the increase in temperature and salinity below the temperature minimum was caused by advection of slope water onto the bank, while the warming and freshening above the cold core was most likely caused by mixing down of the warm surface layer. The two effects were not so clearly separated on Makkovik Bank (line 7) presumably because it is both smaller and shallower than Hamilton Bank.

Lazier (1982), working with averages of historical data, has noted the same autumn increase in temperature and salinity below a temperature minimum on the shelf, and attributed it to a breakdown of the horizontal density gradient across the slope, which allowed warmer, more saline water from offshore to flow onto the shelf along isopycnal surfaces. Cross sections of sigma-t observed at line 4 on Hamilton Bank in late August and October are shown in Figure 69(a) and (b), respectively. A definite weakening of the horizontal gradient over the slope is apparent, with isopycnal surfaces connecting offshore near- surface waters with near-bottom water in the centre of the banks. The change in horizontal density gradient illustrated by Figure 69, appears to be an instance of the process described by Lazier (1982), but the cause of the breakdown in horizontal density gradient is not clear. The most likely possibility would seem to be a combination of a decrease in the supply of cold, low-salinity water to the shelf region, and wind mixing by autumn storms.

5.11 WIND-CURRENT COUPLING

Wind data were collected from drillships operating near some of the current meter locations (Figure 70). The strongest winds occurred from the latter half of September until the end of the observations in mid-October. The most common wind direction was southeasterly to southerly; however, the strongest winds were

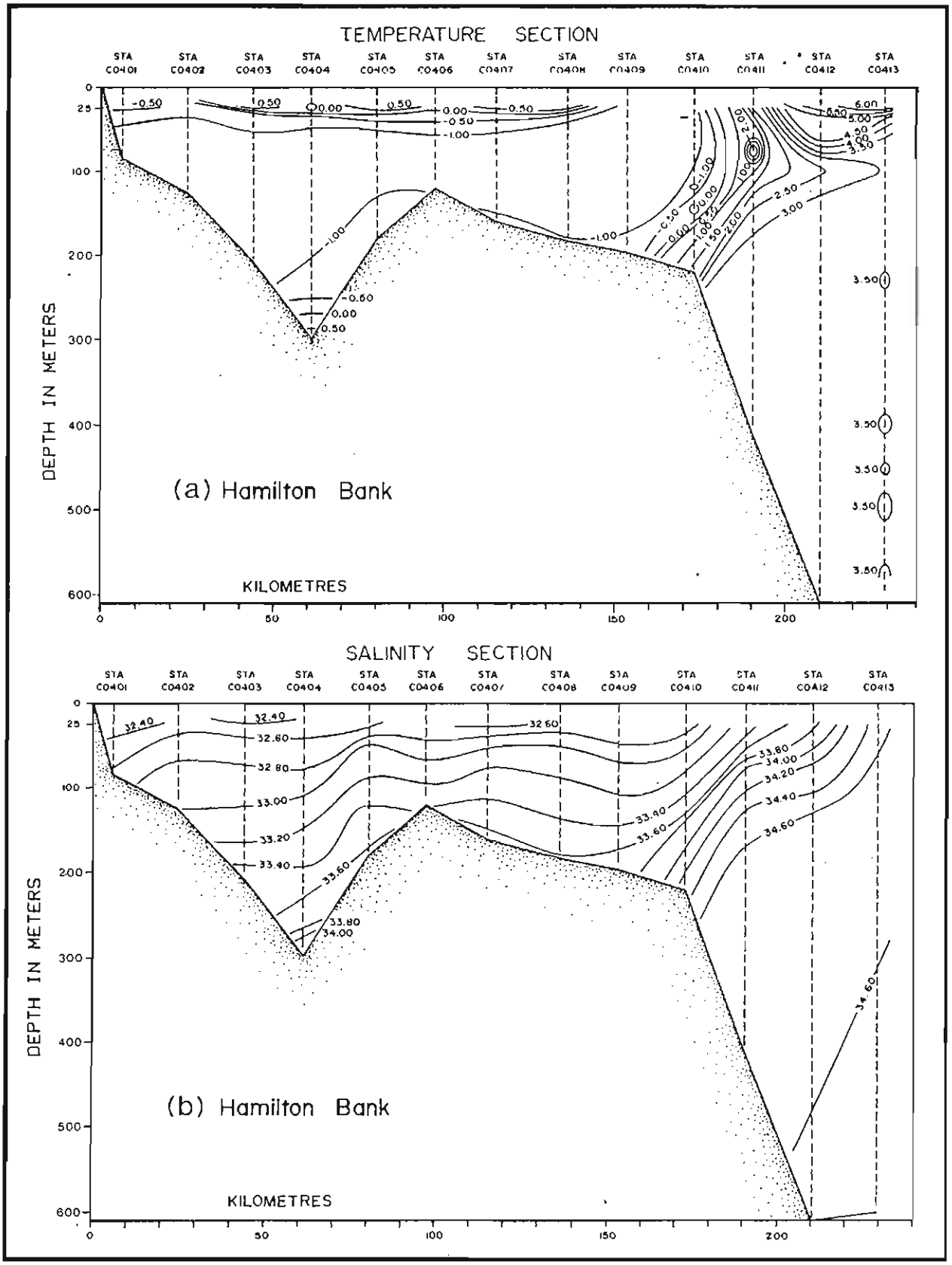

Figure 67: (a) Temperature cross section, line 4, August 27-28.
(b) Salinity cross section, line 4, August 27-28.

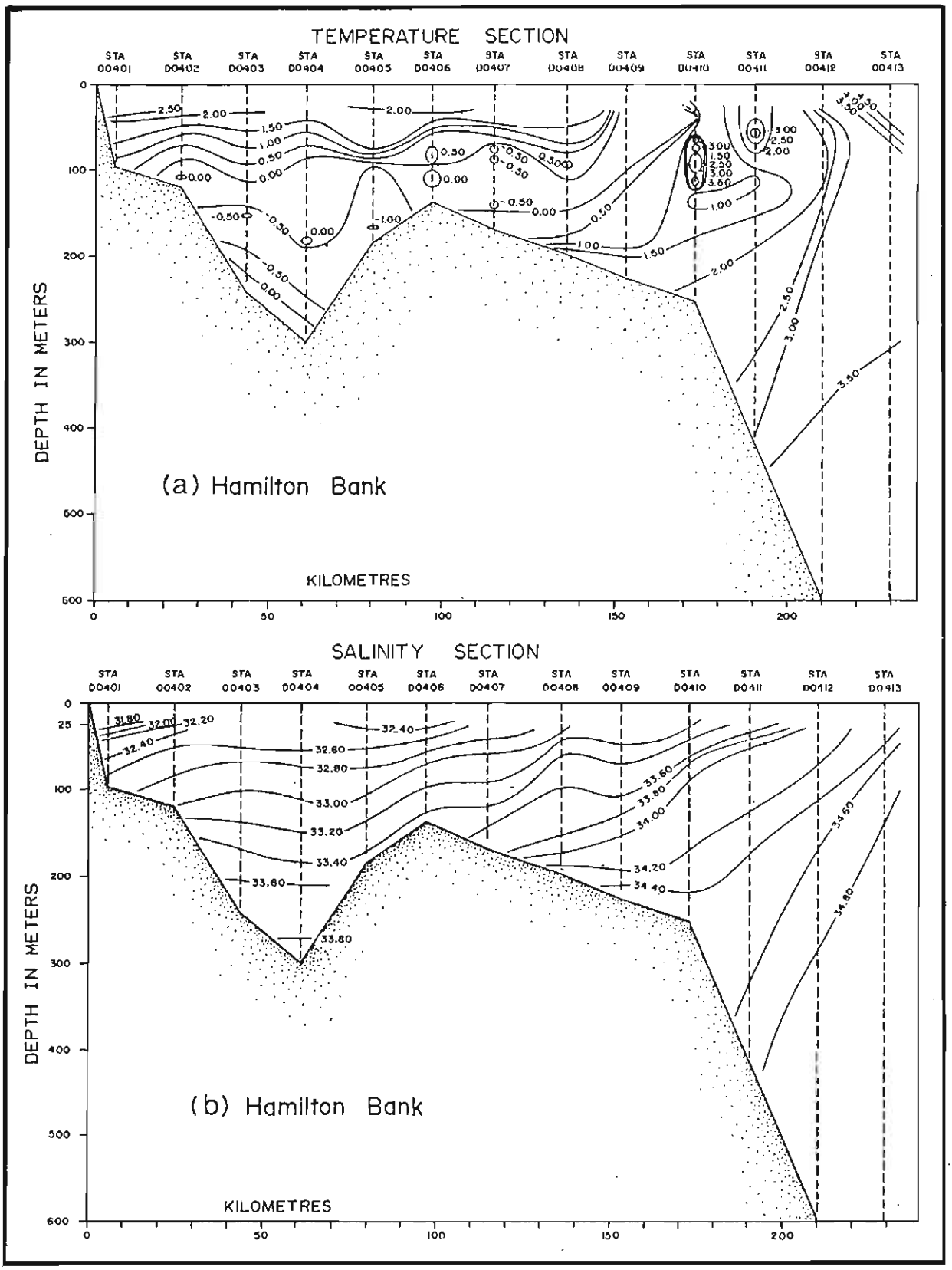

Figure 68: (a) Temperature cross section, line 4, October 21.
(b) Salinity cross section, line 4, October 21.

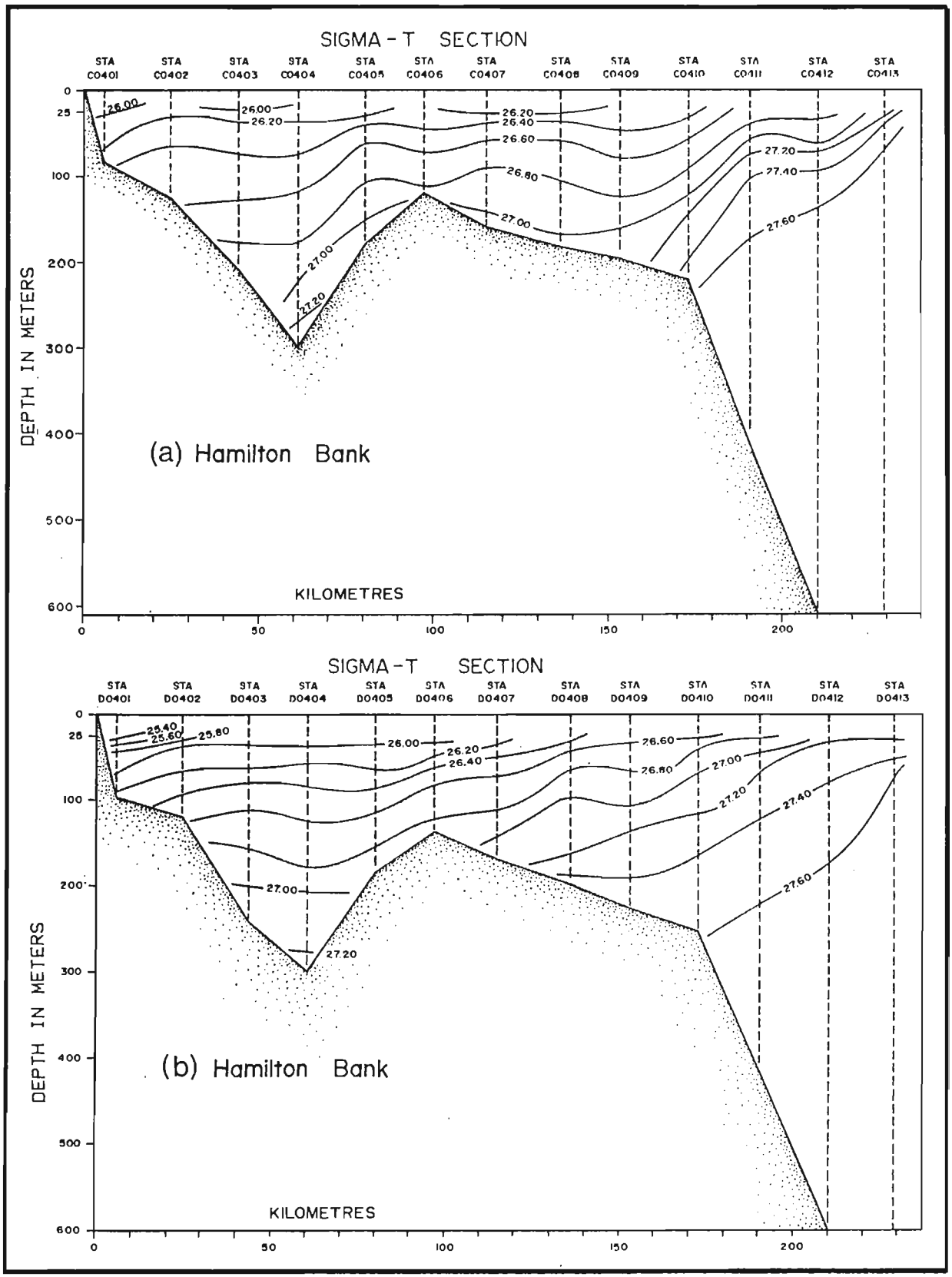

Figure 69: (a) σ_t cross section, line 4, August 27-28.
(b) σ_t cross section, line 4, October 21.

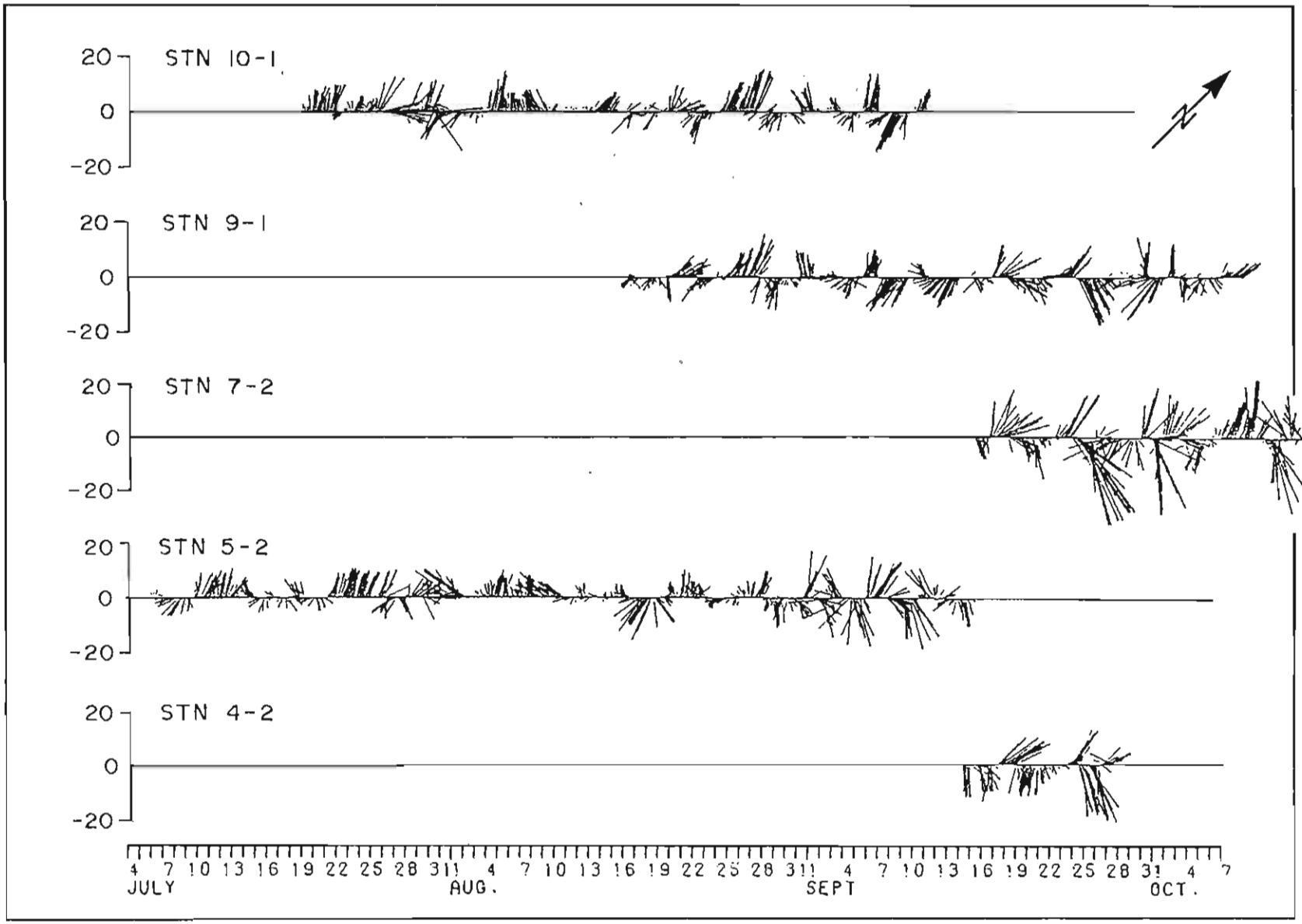

Figure 70: The vector winds time series data obtained from drillships. The vectors are oriented in the direction that the wind blows towards, relative to geographic north as indicated by the arrow.

westerly to northwesterly. The maximum wind speed observed was 33.5 m/s (65 knots) blowing from the northwest on September 25 at station 7-2. For the purposes of cross-spectral analysis, the major component of the wind was taken along the northwesterly- southeasterly axis, with winds blowing from the northwest being positive. The minor component of the wind vector was chosen as positive when blowing from the northeast.

The auto-spectra of the two wind components (Figure 71) indicate that nearly all of the resolvable variances occur at frequencies less than 0.5 cpd (periods in excess of 2 days). For the major (northwesterly) wind component, large spectral levels are found over a wide range of frequencies from 0.036 to 0.5 cpd (periods of 2 to 28 days) with individual peaks at periods of 7, 3.5 and 2.3 days. In the minor component, a spectral peak occurred at 7 days but at higher frequencies (or shorter periods of 3.5 to 2 days). The minor component spectral levels were significantly reduced from those of the major component.

Cross-spectra between parallel wind and current components were computed. The longest available time series of wind data, obtained near station 5-2, were used along with the uppermost current meter measurements available from stations 4-1, 4-2, 4-3, 5-1 and 5-2 over a 56-day period, July 12 to September 4, 1980 (see Table 15). For each pair of wind and current data the current measurements were obtained within 75 km of the wind measurement location.

Based on the cross-spectral results (Table 15), the low frequency current variations appear to be dissimilar to wind variations at the same frequencies. For nearly all frequency bands, the coherence levels were below the 80% level of statistical confidence in each wind-current pair. Even in the few cases where some of the coherence levels were statistically significant, they tended to occur at frequencies where the auto- spectral levels were low in either the wind or current signal. (For example, at station 4-2/53 where coherence levels of 0.7 to 0.85 were computed, the higher coherence values occurred in frequency bands ranging from 0.32 to 0.5 cpd where the auto- spectral levels of the current components are low.)

Cross-spectra were also computed over shorter 42-day periods for other times and locations of wind measurements (Table 16). Again, the coherence levels were generally low and not statistically significant, indicating little or no direct coupling of low frequency current variations at depths of 25 to 62 m, with the local surface wind fluctuations at the same frequencies.

Cross-spectra were also computed between perpendicular components of winds from station 5-2 and nearby upper current meter measurements. As indicated by the generally low, non- statistically significant coherence levels, on- or offshore transports induced by alongshore wind variations are small in terms of accounting for the total low frequency variability of currents at depths of 31 and 58 m.

5.12 FRESH WATER INFLUENCE

Fresh water input from local and remote sources has an important effect on the composition of the Shelf Water. The effect of fresh water discharge from Hamilton Inlet can clearly be seen in the plot of surface salinity shown in Figure 72. Runoff from Hamilton Inlet constitutes almost half the run-off from

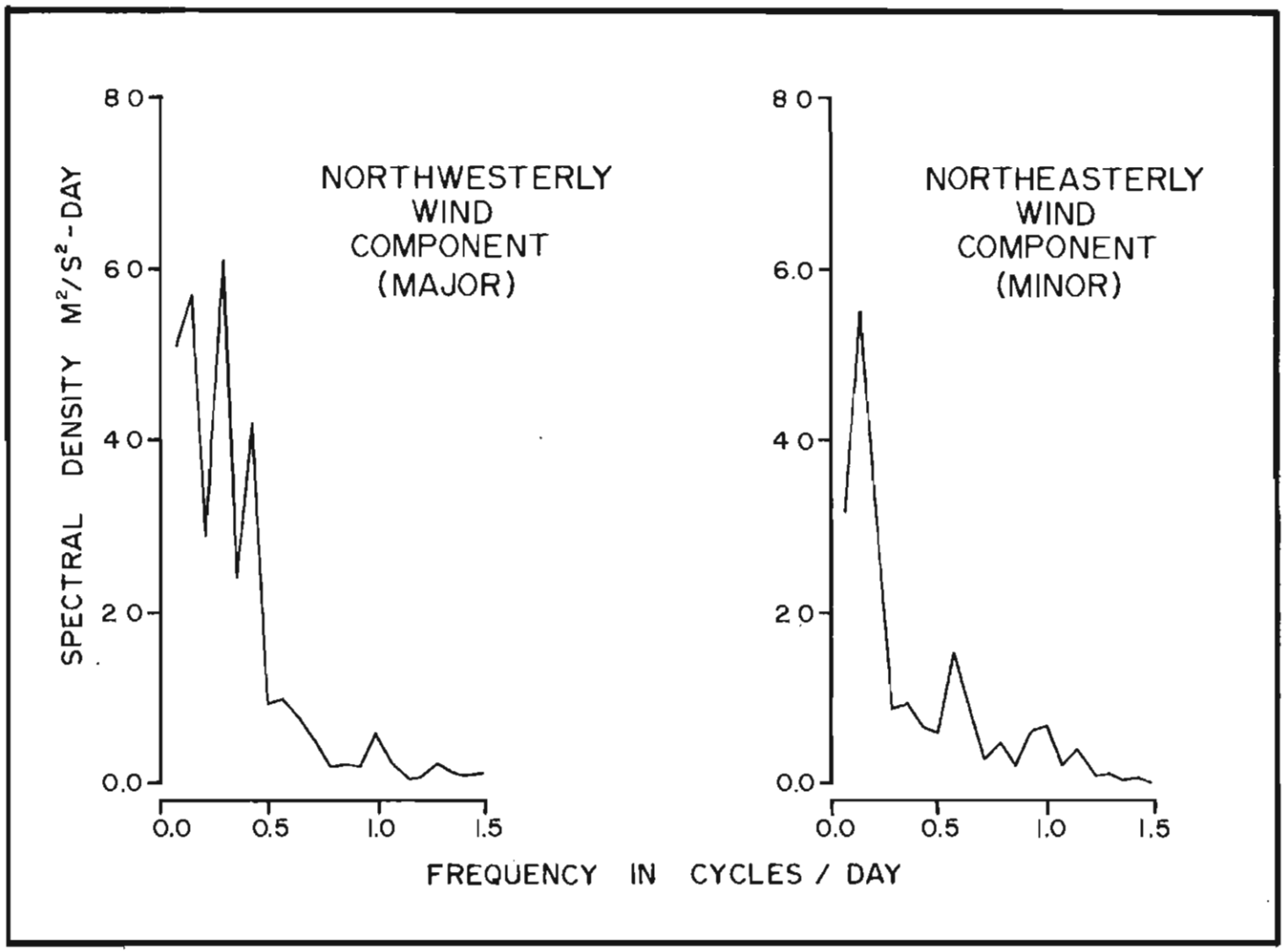

Figure 71: The auto-spectra of components of wind time series collected near station 5-2, from July 12 to September 4, 1980.

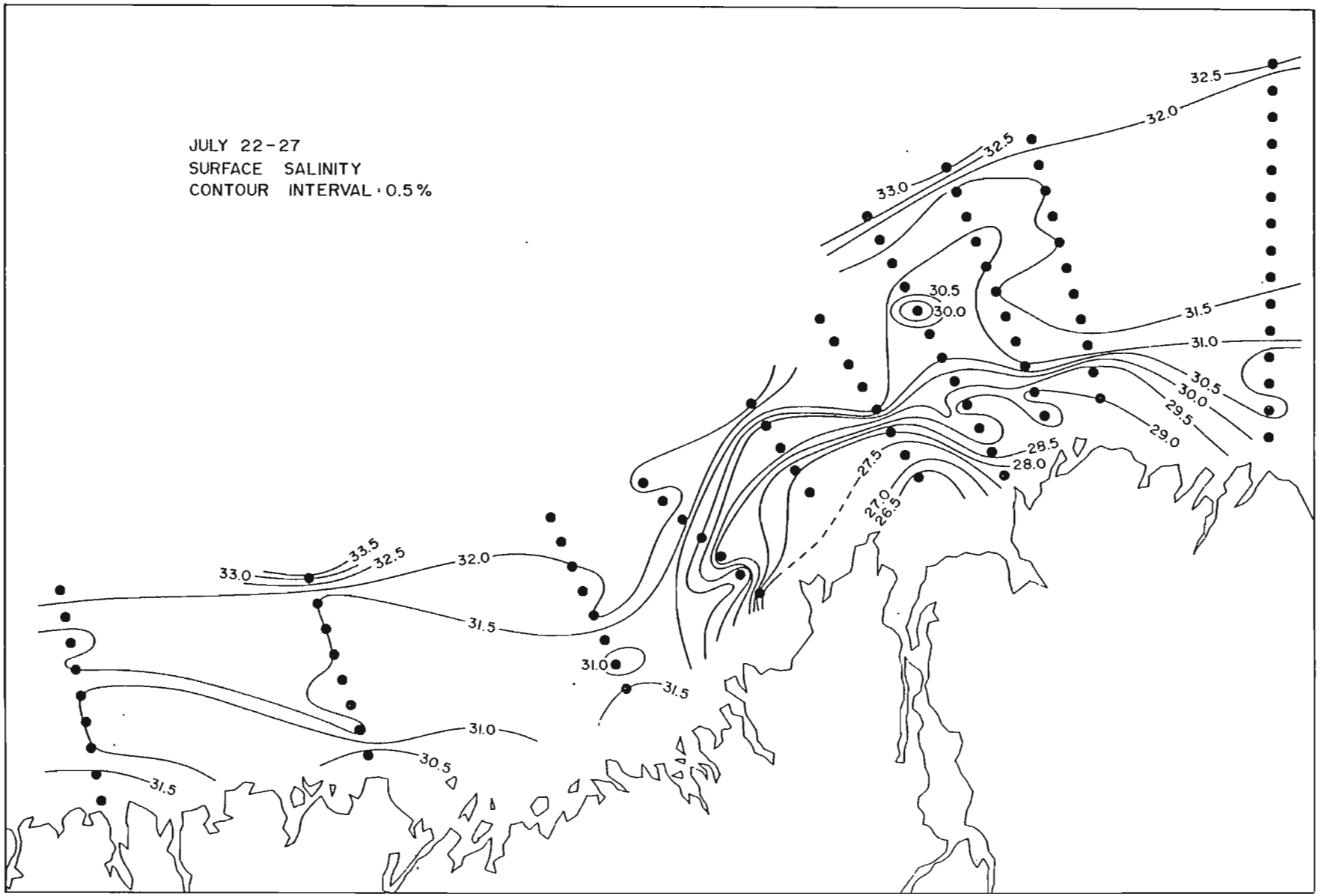

Figure 72: Surface salinity distribution, July 22-27.

Table 15

Summary of cross-spectral results between parallel components of wind and currents for frequencies from 0.035 to 0.5 cpd. The wind data were collected near station 5-2, over a 56-day period from July 12 to September 4, 1980. Results are given only if the computed coherence level exceeds the 80% level of confidence (0.64). Entries in the tables are provided as coherence values followed, in parentheses, by the phase differences.

(a) Major Component - Positive Toward 135°

Current	Centre Period of Frequency Band (days)					
	14.0	7.0	4.7	3.5	2.8	2.3
5-2/31	.94 (-4)	---	---	---	---	---
5-2/57	.94 (0)	---	---	---	---	---
4-1/52	---	---	---	---	---	---
4-2/53	---	---	---	.74 (70)	.70 (80)	.85 (68)
4-3/54	---	---	---	---	---	---
5-1/58	---	---	---	---	---	---

(b) Minor Component - Positive Toward 275°

Current	Centre Period of Frequency Band (days)					
	14.0	7.0	4.7	3.5	2.8	2.3
5-2/31	---	---	---	.65 (42)	---	---
5-2/57	---	---	---	---	---	---
4-1/52	.74(-162)	---	---	.68 (-6)	---	---
4-2/53	---	---	.71(64)	---	---	---
4-3/54	---	---	---	---	.78 (62)	---
5-1/58	---	.78(53)	---	---	---	---

Table 16

Summary of cross-spectral results between parallel components of wind and currents for frequencies from 0.035 to 0.5 cpd. The wind data, collected over a 42-day period, are from stations 5-2, 9-1 and 10-1. Results are given only if the computed coherence level exceeds the 80% level of confidence (0.74). Entries in the table are provided as coherence values followed, in parentheses, by the phase differences.

(a) Major Component - Positive Toward 135°

Current	Centre Period of Frequency Band (days)					
	14.0	**7.0**	**4.7**	**3.5**	**2.8**	**2.3**
		(5-2 Wind: July 12 to August 23)				
7-2/25	---	---	---	---	---	.78 (55)
		(9-1 Wind: August 18 to September 29)				
9-1/56	---	---	.81 (19)	---	---	.93 (43)
		(10-1 Wind: July 26 to September 6)				
10-1/62	---	.74 (151)	.89(-16)	---	---	---
9-1/56	.80 (-30)	---	.79 (-6)	---	---	.88 (00)
7-2/25	---	---	---	---	---	---

(b) Minor Component - Positive Toward 225°

Current	Centre Period of Frequency Band (days)					
	14.0	**7.0**	**4.7**	**3.5**	**2.8**	**2.3**
		(5-2 Wind: July 12 to August 23)				
7-2/25	---	.91 (32)	---	---	.81 (7)	---
		(9-1 Wind: August 18 to September 29)				
9-1/56	.82 (13)	---	---	---	---	.83 (31)
		(10-1 Wind: July 26 to September 6)				
10-1/62	---	---	---	---	---	---
9-1/56	---	.79 (-22)	---	---	---	---
7-2/25	.91 (40)	.88 (3)	---	---	---	---

Labrador (see Figure 73), but is still minor in relation to other sources of fresh water which influence the Labrador coast (Vandall, 1978). The other sources are the Baffin Current, and the outflow from Hudson Strait, which combines the runoff and icemelt from Hudson Bay with that from Ungava Bay. Because of its very large drainage area, Hudson Bay dominates the other sources (Jordan, 1976). The effect of fresh water input to the Labrador Current is apparent as a decrease in the salinity of the upper layers. In particular, the arrival of the leading edge of the Hudson Bay fresh water is observed as a sharp drop in salinity in the upper 100 m (Jordan, 1976). The upper layer salinity then continues to decrease slowly to a winter minimum. The initial decrease is observed, on average, in late August off the southern Newfoundland coast (Keeley, 1981). Note that this is somewhat earlier than the total discharge shown in Figure 73 for Battle Harbour would indicate. We have no explanation for the discrepancy, except to point out that Figure 73 is based on estimates of volumes and transit times which are imperfectly known, while the results at station 27 are an average of 10 years of observations.

No evidence of such a sharp drop in upper layer salinity is evident in any of the CTD data or the time series salinity measurements from the various current meter moorings. The leading edge of the Hudson Bay fresh water was observed at station 27 (47°33'N, 52°35'W) off the southern Newfoundland coast on August 18, 1980 (B. Petrie, Bedford Institute, personal communication), somewhat earlier than its usual arrival at the end of August. Since no sign of the pulse was seen at any of the moorings on line 4, it must already have passed them by the time they were deployed on July 4. If it is assumed that the leading edge of the pulse passed line 4 one or two days before deployment, its net southerly speed was 20 km/day (23 cm/s), which compares favourably with the usual transit time of 1 month from the Strait of Belle Isle to Station 27 (B. Petrie, personal communication). It seems almost certain, therefore, that the leading edge of the Hudson Strait freshwater discharge passed through the study area before measurements were begun.

The fact that the leading edge of the Hudson Bay fresh water had passed the southern limit of measurements at least 3 weeks before the start of the program may account for the fact that the lowest subsurface temperatures were always measured at the southern end of the shelf (e.g. Figure 53a). With the exception of the October measurements this was always the case, with only slight changes observed over the summer. (For example, at 100 m the -1.0°C isotherm moved 120 km south between the end of July and the third week of August). Such a distribution of temperature is plausible if, as seems likely, the initial part of the fresh water discharge is the coldest.

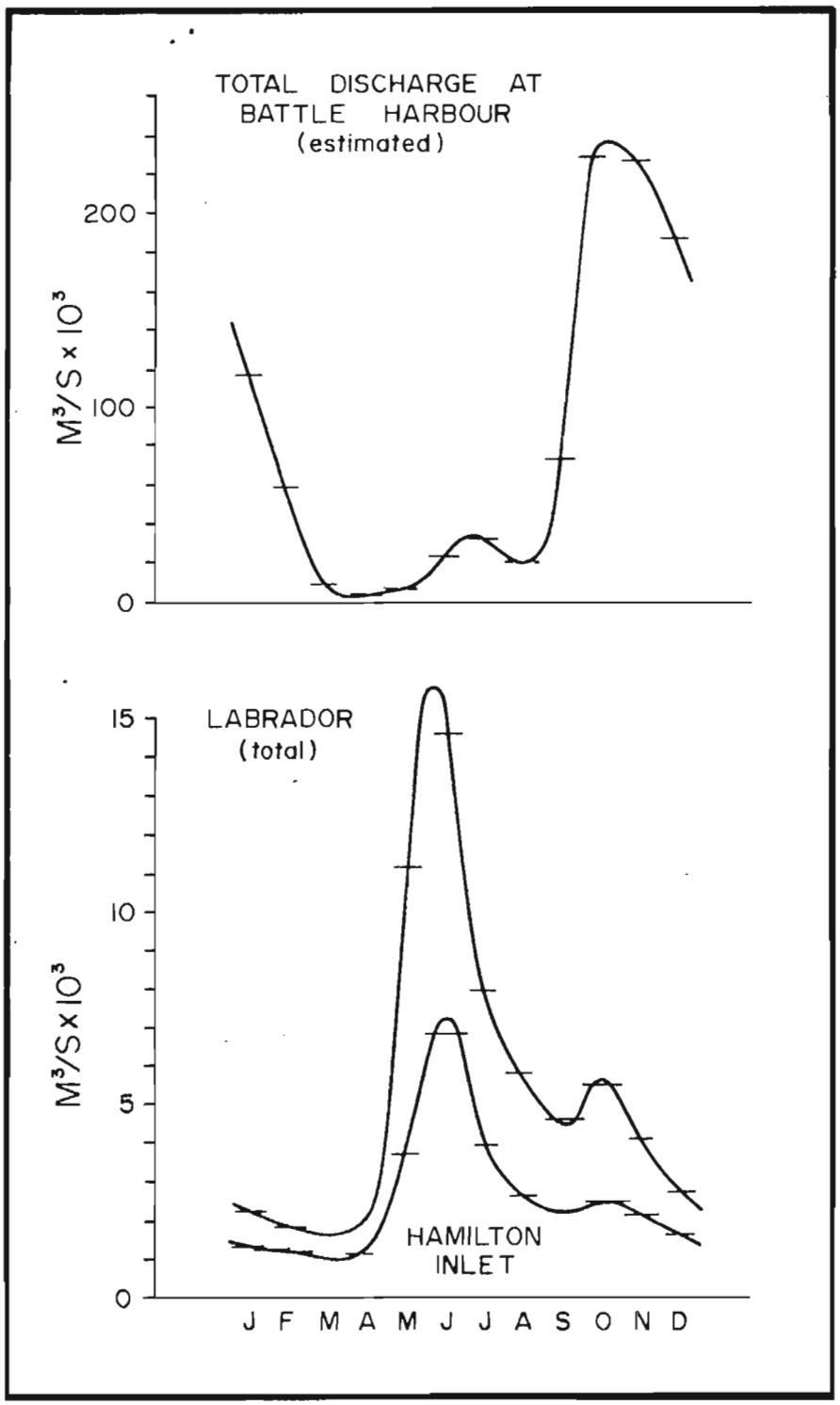

Figure 73: Monthly variation of fresh water discharge passing Battle Harbour (from Vandall, 1978). The upper figure represents the total discharge while the lower curves represent the portion originating in Hamilton Inlet and from all sources entering from the Labrador coast.

6. SUMMARY AND DISCUSSION

In this report, an analysis has been carried out on the extensive set of current meter and CTD data collected over the Labrador continental shelf and slope in the summer of 1980. The results reveal that the circulation and water property distribution in the area are complex and highly variable, both in time and in space. Because the measurement program consisted of wide areal coverage combined with extended time series data collected at several locations, a great deal of new information has been added to the existing knowledge of the spatial and temporal variability of the region's circulation.

On average, the regional circulation is best described as consisting of the two southeastward-flowing cores of the Labrador Current, the main and stronger one following the edge of the continental shelf, the other, slightly weaker, located over the seaward half of the marginal trough. Near-surface speeds in the main core average 30 to 40 cm/s, with peak speeds near 80 cm/s, while in the inner core the average is 15 to 20 cm/s, with peaks near 50 cm/s. These two cores are separated by a zone of more variable, but not less energetic, flow. The net drift in this latter zone is still to the southeast. In addition to these two main cores, there is some evidence for a third southeasterly flow found within 15 km of the coastline and confined to the near- surface layer.

The largest tidal flows within the study area occurred over the banks, with amplitudes of up to 13 cm/s for the major semi- diurnal (M_2) tidal constituent. At these locations, the tidal current rotated in a clockwise manner. Over other types of bathymetry, the tidal flows were weaker, ranging from 2 to 6 cm/s and exhibited a reduced degree of clockwise polarization. The diurnal tidal currents had amplitudes of 3 cm/s or less with the exception of a measurement location over Makkovik Bank, where the currents were 6 cm/s in amplitude and also had a high degree of clockwise polarization. The semi-diurnal tidal currents exhibited pronounced spatial gradients, both vertically and horizontally. These variations are believed to originate largely from phase-locked internal tidal activity, as discussed in a companion report (Martec, 1982).

In most of the current meter records, some activity was evident at the inertial frequency, but the typical amplitudes associated with these intermittent events were about 5 cm/s. The largest inertial oscillations were observed in the shallowest current meter records, at depths of 25 and 31 m, having peak amplitudes of 11 cm/s. Even at these levels, relatively close to the surface but still within the seasonal pycnocline, there was little correlation between changes in the surface and the occurrence of inertial oscillations.

At higher frequencies (greater than two cycles per day), the variations observed in most current meter data sets were small, with mean amplitudes of less than 1 cm/s and maximum values of less than 6 cm/s. The levels of high frequency activity tended to be larger nearer the surface. For the current meter data obtained nearest the surface (25 m depth), the mean amplitudes were 2.5 cm/s with a maximum value of 36 cm/s.

The main core of the Labrador Current is in approximate geostrophic balance and forms the boundary between the relatively warm, saline water of the Labrador Sea and the relatively cold, fresh Shelf Water which occupies the majority of

the water column over the shelf and marginal trough. The water in the main current core itself is a mixture of Shelf Water and Labrador Sea Water called Slope Water. Slope Water is also found in the saddles and at the bottom of the marginal trough. Its presence there does not seem to be the result of any steady flow of Slope Water from the continental slope into those areas, but appears to be a result of fluctuations in the currents. Significant, long- term deflections of the main core of the current into the saddles were observed during the summer; at no time, however, did they appear to have penetrated more than halfway into the saddles.

With the exception of the tides, the major part of the temporal variability of the currents occurs at periods greater than two days. Differences in the nature of the low-frequency variations seem to be strongly dependent on the bathymetry. The flow was divided into four different bathymetrically-defined regimes on the basis of that correlation: the slope, saddle, bank and trough regimes.

At locations over the marginal trough, the saddle and the continental slope, the low frequency variability in the currents is dominated by fluctuations with periods in excess of 7 days. The longest resolvable velocity variations, having periods between 28 and 50 days, were most important at locations near and over the continental slope. Over the trough and saddle, the peak periods range from 7 to 14 days. At all of these types of locations, significant motions do occur at periods of 4 to 7 days, although with smaller amplitudes than those of the longer period.

Over the banks, relatively more activity occurs at periods of 4 to 7 days and at some locations (sites 4-2 and 7-2), these periods are dominant. The 4 to 7 day variations in the current over the banks have a pronounced clockwise circular polarization. At locations in other bathymetric regimes, the degree of circular polarization is generally less pronounced. Where any such polarization is evident, it tends to be directed anticlockwise at these locations.

Despite the general similarity of the flow within each regime, cross-spectral analyses between horizontally-separated pairs of current records did not reveal significant coherences beyond those that would be expected to arise at random. The scale of spatial variability of currents over the Labrador continental shelf is therefore less than the minimum mooring spacing of 35 to 40 km. Significant vertical coherence in the low-frequency fluctuations was found in the upper 300 m, however.

The lack of horizontal coherence in the velocity field suggested examination of the relationship between fluctuations in water properties and current velocity as a means of gaining some insight into the nature of the variability of the flow. Three characteristic types of fluctuations were found. The first type consisted of variations with a period of 4 to 7 days in which temperature was significantly correlated with velocity and lagged it by about 80°. They were observed at the shelf break (i.e. in the main current core, towards its inner edge) and in the saddle. At the outer edge of the banks, bursts of slope water were occasionally observed to coincide with 4 to 7 day fluctuations in velocity. Similar velocity fluctuations without accompanying temperature variations formed the second type. They were observed on the banks.

The third type was longer-period (20 days or more) fluctuations which were observed only over the slope. In this case, temperature was correlated only with the along- slope component of velocity. The available record was too short to define a clear phase relationship, but increases in speed seemed to be associated with decreases in temperature.

Fluctuations of the first type at slope locations are consistent with the formation of meanders on the inner side of the main current core. Advection of the meander past a current meter near the inner edge of the current core would produce an increase in the speed of both components, followed by an increase in temperature, i.e. the speed and temperature variations would be in quadrature with temperature lagging. Such meanders could form warm-cored eddies spun off the inner edge of the main core of the current. They might then form a mechanism for the transport of Slope Water into the saddles, and eventually into the marginal trough. The frequency with which such eddies might be produced, and the distance to which they might penetrate over the shelf is not yet understood (see, for example Huthnance, 1981). Neither is it clear whether the fluctuations of the first type observed in the saddles are necessarily related to those observed at the slope, as the phase relationship of temperature and velocity observed in the saddles was opposite to that observed at the slope. The structures observed in the temperature and salinity sections in Figures 20 and 30 are strongly suggestive of warm-core eddies shed from the inner side of the main current core, as is the velocity and temperature event of August 7-10 at mooring 4-3 (Figure 64b).

The fluctuations of the second type, observed over the banks, are of unexplained origin. The most likely explanation for them would seem to be meteorological forcing of some sort; however, no correlation was found between currents and the available wind data.

The third type of fluctuation is consistent with a strengthening of the main core of the Labrador Current without change of position. If the flow were to strengthen, but remain in geostrophic balance, the slope of the isopycnals in the current would increase. If there were no lateral displacement of the current core, a mooring situated towards its inner edge would find itself in water of more Shelf-like properties, as well as in a stronger flow.

Changes of seasonal period also occur in the Labrador Current. From an analysis of historical data, Lazier (1982) has suggested that an autumnal breakdown of the interface between the Shelf Water and the Labrador Sea Water leads to a general warming of the waters over the shelf. That hypothesis is supported by the data analyzed here. It therefore seems likely that the fall and winter circulation along the Labrador coast may differ significantly from that observed in the summer. Winter measurements of currents along the coast would be necessary to determine the nature of any such changes.

The Labrador Current is a complex, highly variable system of currents flowing over an equally complex bathymetry. At least some of the spatial and temporal variability of the flow appears to be linked to the bathymetry. The remainder must arise from a variety of sources such as inherent dynamical instabilities of the currents themselves, and through meteorological forcing. Separation of these causes will require detailed study of the dynamics of the whole system.

7. REFERENCES

Aanderaa Instruments Ltd., 1978. Operating Manual for Recording Current Meter Model 4. Technical Description 119. Bergen, Norway.

Allen, A.A., 1979. Current variability at the offshore edge of the Labrador Current. M.Sc. Thesis. Dalhousie University, Halifax. 164 p.

Bendat, J.S. and A.G. Piersol, 1971. Random Data. Wiley- Interscience, New York. 407 p.

Bennett, A.S., 1976. Conversion of in situ measurements of conductivity to salinity. Deep-Sea Research 23: 157-165.

Dobson, D. and F. Jordan, 1978. The Labrador Sea - A Bibliography of Physical Oceanography. Bedford Institute of Oceanography Data Series B1-D-78-5. Dartmouth, N.S. 25 p.

Dunbar, M.J., 1951. Eastern Arctic Waters. Fisheries Research Board of Canada. Bulletin No. 88, Ottawa. 131 p.

Fenco, 1981. Ice and Environmental Surveillance Offshore Labrador 1980. Operations Report. Drilling Vessel Pelerin and Towing Vessels. Report submitted to Petro-Canada by Fenco (Nfld.) Limited. 58 p.

Fissel, D.B. and G.R. Wilton, 1980. Subsurface current measurements in western Baffin Bay and Lancaster Sound. Report prepared for Petro-Canada by Arctic Sciences Ltd., April 1980. [Available from Pallister Resource Management Ltd., 700-6 Ave. S.W., Calgary, Alberta.]

Fofonoff, N.P., 1962. Physical Properties of Sea Water. The Sea, Vol. 1, ed. M. Hill, Intersciences Publishers, New York: 3-28.

Foreman, M.G.G., 1978. Manual for Tidal Currents Analysis and Prediction. Unpublished manuscript. Pacific Marine Science Report 78-6, Institute of Ocean Sciences, Sidney, B.C. 70 pp.

Fu, L., 1980. Observations and models of inertial waves in the deep ocean. Ph.D. Thesis, Woods Hole Oceanographic Institution, WHOI-80-11, 202 p.

Godin, G., 1972. The Analysis of Tides. University of Toronto Press, Toronto. 264 pp.

Godin, G., 1980. Cotidal Charts for Canada. Manuscript Report Series No. 55. Marine Sciences and Information Directorate, Department of Fisheries and Oceans, Ottawa. 93 pp.

Groves, G.W. and E.J. Hannan, 1968. Time series regression of sea level on weather. Reviews of Geophysics, 6(2), pp. 129- 174.

Holden, B.J., 1973. Braincon current meter data, Dawson Cruise, Saglek, 1972. Data Report, Memorial University, St. John's, Nfld.

Huthnance, J.M. 1981. Waves and currents near the continental shelf edge. Progress in Oceanography, 10, pp. 193-226.

Jenkins, J.M. and D.G. Watts, 1968. Spectral Analysis. Holden- Day, San Francisco, 325 p.

Jordan, F., 1976. Canadian Runoff Contribution to the Labrador Current. Bedford Institute of Oceanography, Dartmouth, N.S. (unpublished manuscript).

Keeley, J.R., 1981. Temperature, salinity and sigma-t at station 27 (47°33'N, 52°35'W): an analysis of historical data. Marine Environmental Data Service, Technical Report No. 8, Canada, Dept. of Fisheries and Oceans, Ottawa.

Knight, D.N. and Fissel, D.B., 1981. A calibration report for Petro-Canada's current meters. Report prepared for Petro- Canada by Arctic Sciences Ltd. 28 p. plus unnumbered appendices.

Kundu, P.K., 1976. An analysis of inertial oscillations observed near the Oregon coast. J. Phys. Oceanogr., 6: 879-893.

Lazier, J.R.N., 1973. The renewal of Labrador seawater. Deep Sea Res., 20: 341-353.

Lazier, J.R.N., 1979. Moored current meter data from the Labrador Sea (1977-78). BIO Data Report BI-D-79-3, Bedford Institute of Oceanography, Dartmouth, N.S.

Lazier, J.R.N., 1982. Seasonal variability of temperature and salinity in the Labrador Current. Journal of Marine Research, 40: 341-356.

MacLaren Marex Inc., 1980. Appendices of environmental observations on Pelerin, offshore Labrador, summer 1979. Report to Total Eastcan Exploration Ltd., Marine Science and Engineering, St. John's, Nfld.

Martec, 1982. Internal wave activity at tidal frequency on the Labrador Shelf. Report prepared for Petro-Canada by Martec Ltd.

McCullough, J.R., 1980. Survey of techniques for measuring currents near the ocean surface. In Air-Sea Interaction, Instruments and Methods. F. Dobson, L. Hasse and R. Davis, eds. Plenum Press, New York: 105-126.

Mountain, D.G., 1980. Direct measurements in the Labrador Current. J. Geophys. Res. 85: 4097-4100.

Neil Brown Instrument Systems, 1979. Acoustic current meter model ACM-2, operation and maintenance manual. September, 1979.

NORDCO, 1980. Offshore Labrador initial environmental assessment - physical environment component - final report. Report to Petro-Canada, 68-80. St. John's, Nfld. 83 pp.

NORDCO, 1981. Current and CTD profiles on the Labrador Shelf; data report for the 1980 Labrador physical oceanography programs. Report to Petro-Canada Explorations, Inc. by NORDCO Ltd., June 19, 1981 (unpublished manuscript).

Petro-Canada, 1982. Offshore Labrador - Initial Environmental Assessment. Calgary, Alberta. 548 pp.

Plansearch, 1981a. Environmental Observations, Summer 1980, D.S. Neddrill II. Appendix V. Report submitted to Petro-Canada. Plansearch-Lavalin.

Plansearch, 1981b. Environmental Observations, Summer 1980, D.S. Pelican. Appendix II. Report submitted to Petro-Canada. Plansearch-Lavalin.

Pollard, R.J., 1970. On the generation of inertial waves in the ocean. Deep Sea Res. 17: 795-812.

Pollard, R.J., 1980. Properties of near-surface inertial oscillations. J. Phys. Oceanogr., 10: 385-393.

Pond, S. and G.L. Pickard, 1978. Introductory Dynamic Oceanography. Pergamon Press, Oxford. 241 pp.

Ramster, J.W., D.B. Hughes and G.K. Jurnes, 1978. A steadiness factor for estimating the variability of residual drift in current meter records. Dt. Hydr. Z., 31, 230-236.

Scobie, R.W., 1972. A comparison of current velocity determined by dynamic methods with direct current measurement in the Labrador Current. M. Sc. Thesis, Florida State Univ. Tallahassee, Florida.

Singleton, R.C., 1969. An algorithm for computing the mixed radix Fast Fourier Transform. IEEE Transactions on Audio and Electroacoustics, 17(2), pp. 93-103.

Smith, E.H., F.M. Soule and O. Mosby, 1937. The Marion and General Greene Expeditions to Davis Strait and the Labrador Sea. Bull. U.S. Coast Guard, 19, 1-259.

Swallow, J.C. and L.V. Worthington, 1969. Deep Currents, Labrador Sea. Deep-Sea Res., 16: 77-84.

Thomson, R.E. and W.S. Huggett, 1981. Wind-driven inertial oscillations of large spatial coherence. Atmosphere-Ocean, 19: 281-306.

Vandall, Jr., P.E., 1978. Physical oceanographic interest on the Labrador shelf at the Atlantic Oceanographic Laboratory (BIO), in: Workshop on Coastal Research and Planning in Labrador, Bedford Institute Report Series BI-R-77-12, March 1978. Bedford Institute of Oceanography, Dartmouth, N.S.